NATÁLIA DANIELE DORIGHELLO CARARETO

SOLID-LIQUID EQUILIBRIUM AND FLASH POINT OF FATTY MIXTURES

EQUILÍBRIO SÓLIDO-LÍQUIDO E PONTO DE FULGOR DE MISTURAS GRAXAS

CAMPINAS

2014

University of Campinas
Faculty of Food Engineering

University of Pau and the Adour Region
Doctoral School of Exact Sciences and Their Applications

NATÁLIA DANIELE DORIGHELLO CARARETO

SOLID-LIQUID EQUILIBRIUM AND FLASH POINT OF FATTY MIXTURES

Prof. Antonio José de Almeida Meirelles
Supervisor (Faculty of Food Engineering / University of Campinas)

Prof. Dr. Jérôme Pauly
Supervisor (University of Pau and the Adour Region)

Prof. Mariana Conceição da Costa
Co-supervisor (School of Applied Sciences / University of Campinas)

Doctorate thesis presented to the Food Engineering Graduate Programme of the Faculty of Food Engineering of the University of Campinas to obtain the PhD grade in Food Engineering and to the Doctoral School of Exact Sciences and Their Applications of the University of Pau and the Adour Region to obtain the PhD grade in Physical Chemistry according to the agreement signed by both Universities governing the Jointly-Awarded Degree.

THIS COPY CORRESPONDS TO THE FINAL VERSION OF THE THESIS DEFENDED BY NATÁLIA DANIELE DORIGHELLO CARARETO AND SUPERVISED BY PROF. ANTONIO J. A. MEIRELLES AND PROF. JÉRÔME PAULY

_____ _____

Antonio José de Almeida Meirelles **Jérôme Pauly**

CAMPINAS

2014

Ficha catalográfica
Universidade Estadual de Campinas
Biblioteca da Faculdade de Engenharia de Alimentos
Márcia Regina Garbelini Sevillano - CRB 8/3647

C176s

Carareto, Natália Daniele Dorighello, 1984-
Solid-liquid equilibrium and flash point of fatty mixtures / Natália Daniele Dorighello Carareto. – Campinas, SP: [s.n.], 2014.

Orientador: Antonio José de Almeida Meirelles e Jérôme Pauly.
Coorientador: Mariana Conceição da Costa.
Tese (doutorado) – Universidade Estadual de Campinas, Faculdade de Engenharia de Alimentos.

1. Equilíbrio sólido-líquido. 2. Ponto de fulgor. 3. Ácidos graxos. 4. Álcoois graxos. 5. Biodiesel. I. Meirelles, Antonio José de Almeida. II. Pauly, Jérôme. III. Costa, Mariana Conceição da. IV. Universidade Estadual de Campinas. Faculdade de Engenharia de Alimentos. V. Título.

Informações para Biblioteca Digital

Título em outro idioma: Equilíbrio sólido-líquido e ponto de fulgor de misturas graxas
Palavras-chave em inglês:
Solid-liquid equilibrium
Flash point
Fatty alcohols
Fatty acids
Biodiesel fuels
Área de concentração: Engenharia de Alimentos
Titulação: Doutora em Engenharia de Alimentos
Banca examinadora:
Antonio José de Almeida Meirelles [Orientador]
Jean-Luc Daridon
João Araújo Pereira Coutinho
Moisés Teles dos Santos
Simão Pedro de Almeida Pinho
Data de defesa: 18-03-2014
Programa de Pós-Graduação: Engenharia de Alimentos

Universidade Estadual de Campinas
Faculdade de Engenharia de Alimentos

Universidade de Pau e da Região do Adour
Escola Doutoral de Ciências Exatas e suas Aplicações

NATÁLIA DANIELE DORIGHELLO CARARETO

EQUILÍBRIO SÓLIDO-LÍQUIDO E PONTO DE FULGOR DE MISTURAS GRAXAS

Prof. Antonio José de Almeida Meirelles
Orientador (Faculdade de Engenharia de Alimentos /Universidade Estadual de Campinas)

Prof. Dr. Jérôme Pauly
Orientador (Universidade de Pau e da Região do Adour)

Prof. Mariana Conceição da Costa
Co-orientadora (Faculdade de Ciências Aplicadas / Universidade Estadual de Campinas)

Tese de doutorado apresentada ao Programa de Pós Graduação em Engenharia de Alimentos da Faculdade de Engenharia de Alimentos da Universidade Estadual de Campinas para obtenção do título de Doutora em Engenharia de Alimentos e para a Escola Doutoral de Ciências Exatas e suas Aplicações da Universidade de Pau e da Região do Adour para a obtenção do título de Doutora em Físico-Química, de acordo com parceria assinada pelas duas Universidades que regula a atribuição de Diploma de Doutorado em regime de co-tutela.

ESTE EXEMPLAR CORRESPONDE À VERSÃO FINAL DA TESE DEFENDIDA POR NATÁLIA DANIELE DORIGHELLO CARARETO E ORIENTADA PELOS PROFESSORES ANTONIO JOSÉ DE ALMEIDA MEIRELLES E JÉRÔME PAULY.

_____ _____

Antonio José de Almeida Meirelles **Jérôme Pauly**

CAMPINAS

2014

Examination Committee / Banca Examinadora

_____
Prof. Antonio José de Almeida Meirelles
Supervisor/*Orientador*

_____
Prof. Jérôme Pauly
Supervisor/*Orientador*

_____
Prof. Jean-Luc Daridon
Titular Member / *Membro Titular da Banca Julgadora*

_____
Prof. João Araújo Pereira Coutinho
Titular Member / *Membro Titular da Banca Julgadora*

_____
Dr. Moisés Teles dos Santos
Titular Member / *Membro Titular da Banca Julgadora*

_____
Prof. Simão Pedro de Almeida Pinho
Titular Member / *Membro Titular da Banca Julgadora*

_____
Prof. Vania Regina Nicoletti Telis
Substitute Member / *Membro Suplente da Banca Julgadora*

_____
Prof. Roberta Ceriani
Substitute Member / *Membro Suplente da Banca Julgadora*

_____
Prof. Charlles Rubber de Almeida Abreu
Substitute Member / *Membro Suplente da Banca Julgadora*

Abstract

The study on the physicochemical properties of fatty materials has acquired a growing importance, mainly due to the incentive of their use in energy and nutrition. The efficient production and use of fatty compounds requires a good knowledge of their properties and phase behavior that are necessary for development of processes, especially in production steps such as extraction and refining, but also during storage of the final products. Solid-liquid equilibrium data can be used to improve or propose new separation processes. Also the flash point is an important property that must be considered during storage, transportation and production of flammable compounds, such as biodiesel. This work aimed to study the solid-liquid equilibrium of binary mixtures consisting of fatty alcohols, fatty esters or fatty acids, and to evaluate the flash point of mixtures of ethyl esters, the major constituents of biodiesels, and ethanol, also present in biodiesel in residual levels. Flash points of ethyl esters, and also of the binary mixtures of ethyl esters with ethanol were determined experimentally. An empirical model for predicting the flash point of biodiesels as a function of composition and ethanol content was proposed. The solid-liquid phase diagrams of binary mixtures of fatty alcohol + fatty alcohol or fatty alcohols + fatty acid were determined experimentally by differential scanning calorimetry (DSC), using a linear heating rate, or by a stepscan DSC method, with the aim of investigating the occurrence of the eutectic, peritectic and metatectic reactions. X-ray diffraction and optical microscopy with temperature control techniques were applied to complement the understanding of the phase diagrams. The effect of pressure on the solid-liquid equilibrium was investigated for the binary mixtures of ethyl esters or fatty alcohols using an optical microscope coupled to a high pressure cell which allows the pressure increase up to 80 MPa. Margules 2 and 3-suffix and NRTL thermodynamic models were used for describing the liquidus line of the systems that presented peritectic point, and a predictive thermodynamic model was used to model the ESL function of pressure, which in both cases, gave a satisfactory fit compared to the experimental data.

Keywords: Flash point, solid-liquid equilibrium, fatty acids, fatty alcohols, ethyl esters.

Resumo

O estudo das propriedades físico-químicas de materiais graxos é uma demanda mundial crescente, principalmente devido ao incentivo do seu uso como fonte de energia e para a alimentação. Faz-se importante estudar e compreender todas as condições de equilíbrio que podem ser observadas durante o processamento de compostos graxos, por exemplo, óleos vegetais e biodieseis, desde a sua extração, refino e estocagem. Dados de equilíbrio sólido-líquido podem ser usados para melhorar ou propor novos processos de separação. Já o ponto de fulgor é uma propriedade importante que deve ser observada no armazenamento, transporte e produção de compostos inflamáveis, como o biodiesel. Este trabalho teve como objetivos estudar o equilíbrio sólido-líquido de misturas binárias graxas formadas por álcoois graxos, ésteres graxos ou ácidos graxos, e avaliar o ponto de fulgor de misturas de ésteres etílicos, que são constituintes principais de biodieseis, e etanol, presente em teores residuais. Os pontos de fulgor de ésteres etílicos, e também de misturas binárias destes ésteres com etanol foram determinados experimentalmente e a partir dos resultados foi proposto um modelo empírico para a predição do ponto de fulgor de biodieseis em função da sua composição e teor de etanol. Os diagramas de equilíbrio sólido-líquido de sistemas binários formados por ácidos + álcoois graxos ou formados por álcoois + álcoois graxos foram determinados experimentalmente através de calorimetria exploratória diferencial (DSC) com a intenção de melhor compreender as reações eutética, peritética e metatética que aparecem nos diagramas de equilíbrio tanto com taxas de aquecimento linear ou via o uso da ferramenta de *stepscan* DSC. Para complementar o estudo foram usadas técnicas de difração de Raios-X e microscopia óptica com controle de temperatura. O efeito da pressão sobre o equilíbrio sólido-líquido foi avaliado para misturas binárias de ésteres etílicos ou de álcoois graxos utilizando-se microscopia ótica acoplada a um aparato experimental que permite o aumento da pressão até 80 MPa. Foram utilizados os modelos termodinâmicos para coeficiente de atividade Margules 2 e 3-sufixos e NRTL para descrever a linha liquidus dos sistemas que apresentaram ponto peritético, e um modelo termodinâmico preditivo foi aplicado para modelar o ESL em função da pressão e, em ambos os casos, obteve-se um ajuste satisfatório em comparação aos dados experimentais.

Palavras-chave: Ponto de fulgor, equilíbrio sólido-líquido, ácidos graxos, álcoois graxos, ésteres etílicos.

Résumé

L’étude des propriétés physico-chimiques des matières grasses constitue une demande mondiale croissante liée à l’augmentation constante de leur utilisation comme source d'énergie et pour l'alimentation. Une bonne connaissance de leurs propriétés thermophysiques et de leur comportement de phases est nécessaire pour la production, l'utilisation efficace de ces matières grasses et le développement des processus d'extraction au niveau du raffinage et du stockage. Des données d'équilibre solide-liquide peuvent être utilisées pour améliorer les procédés existants, et également pour le développement des nouveaux procédés de séparation. Ainsi, le point d'éclair est une propriété importante qui doit être observée pendant le stockage, le transport et la production de composés inflammables, tels que le biodiesel. Ce travail vise à étudier l'équilibre solide-liquide de mélanges binaires constitués d'alcools gras, d’acides gras et d’esters éthyliques. Il porte aussi sur l'évaluation du point d’éclair de mélanges d'esters éthyliques, constituants majoritaires du biodiesel, et de l'éthanol, présent à des niveaux résiduels dans le biodiesel. Les points d’éclair des esters éthyliques mais également des mélanges binaires d'esters éthyliques et d’éthanol, ont été déterminés expérimentalement. Un modèle empirique de prédiction des points d’éclair des biodiesels en fonction de leur composition et de leur teneur en éthanol a été proposé. Les diagrammes de phases solide-liquide des mélanges binaires d'alcool gras + alcool gras ou d’alcools gras + acide gras ont été déterminés expérimentalement par analyse calorimétrique différentielle (DSC). Cette étude permet de caractériser les réactions eutectique, péritectique et métatectique, en utilisant une vitesse de chauffe linéaire ou une méthode de Stepscan DSC. Des mesures de diffraction rayons X et de microscopie optique de contrôle de la température ont été appliquées pour compléter la compréhension des diagrammes de phases. L'effet de la pression sur l'équilibre solide-liquide a aussi été mesuré pour les mélanges binaires d’esters éthyliques ou d'alcools gras en utilisant un microscope optique couplé à une cellule à haute pression qui permet d’augmenter la pression jusqu'à 80 MPa sur une large gamme de température. Les modèles thermodynamiques Margules 2 et 3-suffix et NRTL ont été utilisés pour décrire la ligne du liquidus des systèmes présentant un point péritectique, alors qu’un modèle thermodynamique prédictif a permis de modéliser l'ESL en fonction de la pression. Dans les deux cas, on a observé un ajustement satisfaisant par rapport aux données expérimentales.

Mots-clés: Point d'éclair, équilibre solide-liquide, acides gras, alcools gras, esters éthyliques.

Sumário

Outras vezes agitava-me. Ia às gavetas entornava as cartas antigas, dos amigos, dos parentes, das namoradas, e abria-as todas, lia-as uma a uma, e recompunha o pretérito... Leitor ignaro, se não guardas as cartas da juventude, não conhecerás um dia a filosofia das folhas velhas, não gostarás o prazer de verte, ao longe, na penumbra, com um chapéu de três bicos, botas de sete léguas e longas barbas assírias, a bailar ao som de uma gaita anacreôntica.

Guarda as tuas cartas da juventude!

Memórias póstumas de Brás Cubas, Machado de Assis

Agradecimentos

Esta tese é o resultado de uma longa jornada, uma sucessão perpétua dos momentos de euforia e profundos questionamentos. Sua conclusão teria sido seriamente comprometida sem o apoio científico e emocional que tive a sorte de ter.

Por isso gostaria de agradecer, primeiramente aos meus orientadores, Prof. Tonzé e Prof. Jérôme, por ter confiado na minha capacidade, por todos os ensinamentos e oportunidades proporcionadas. E à Profa. Mariana por tudo que tem me ensinado e por toda a sua ajuda no meu trabalho.

Aos membros da banca examinadora por todas as sugestões que enriqueceram o trabalho apresentado na minha tese.

Aos meus amigos do EXTRAE e aos funcionários da FEA e aos colegas do LFC por toda a ajuda e apoio.

À minha querida Profa. de francês Marisa por ter me apresentado ao idioma.

Às minhas melhores amigas e companheiras Florence, Janine e Julien por serem tão especiais e essenciais na minha vida.

A todos meus amigos que fiz em Pau que se tornaram minha família *paloise*, Carol, Gislane, Krisztina, José, Gustavo, Ulysse, Felipe, Lucas, Ralitza, Adilson, Bia e Fernando.

Um agradecimento mais do que especial à família Bourda-Couhet, que me acolheu como parte dela: minhas queridas Morgane e Ana Paula e meus queridos Bruno e Laurent.

Aos órgãos brasileiros de fomento à pesquisa, FAPESP, CNPQ, CAPES, FAEPEX/UNICAMP pelo investimento financeiro.

E acima de tudo aos meus pais por terem me apoiado incondicionalmente nas escolhas do meu caminho e a minha família por ser aquilo por quem sempre vou viver e lutar.

Capítulo 1. Introdução Geral

O Brasil é um dos grandes produtores mundiais de grãos, possuindo uma área plantada de 52,7 milhões de hectares em 2013. Segundo o IBGE[1], a estimativa de safra nacional para o ano de 2013 de cereais, leguminosas e oleaginosas (caroço de algodão, amendoim, arroz, feijão, mamona, milho, soja, aveia, centeio, cevada, girassol, sorgo, trigo e triticale) é da ordem de 187,0 milhões de toneladas, superior em 15,5% à obtida em 2012 (161,9 milhões de toneladas). Uma parte destes produtos é destinada para a produção em grande escala de óleos vegetais visando o seu uso alimentício e à fabricação de biocombustíveis. Conhecer as propriedades físico-químicas dos componentes da cadeia produtiva é fundamental para o estabelecimento dos parâmetros de processo e de segurança.

Duas propriedades físico-químicas ainda pouco investigadas são aquelas vinculadas ao equilíbrio sólido-líquido e ao ponto de fulgor de misturas graxas de interesse industrial. O ponto de fulgor é uma propriedade físico-química fundamental para o estabelecimento de temperatura de armazenamento e escoamento de substâncias inflamáveis. É uma propriedade que está bem estabelecida para uma vasta gama de compostos puros, mas para misturas multicomponentes ainda é pouco explorada. O biodiesel, produto da reação de transesterificação de óleos vegetais com álcoois de cadeia curta como metanol ou etanol, tem um ponto de fulgor que pode variar em função do óleo vegetal utilizado na sua produção assim como em função do etanol residual em sua composição. O crescimento da produção de biodiesel aumenta a necessidade do conhecimento desta propriedade e do desenvolvimento de métodos de correlação e de predição da mesma, métodos estes que empregam os conceitos do equilíbrio de fases.

O estudo do equilíbrio sólido-líquido (ESL) de sistemas multicomponentes, por exemplo, é importante para verificar a perda de carga em tubulações devido ao processo de precipitação de compostos. Além disso, o ESL é indispensável para realizar o dimensionamento de equipamentos de purificação de compostos através da cristalização. Mais recentemente tem-se destacado a capacidade dos compostos graxos de formar redes

[1] Instituto Brasileiro de Geografia e Estatística. **Em setembro, IBGE prevê safra de grãos 15,5% maior que a safra de 2012**. 2013. Disponível em: < http://cod.ibge.gov.br/1YAGX>. Acesso em: 10/26/2013.

de cristais com características muito distintas, o que afeta a estabilidade e textura de uma vasta lista de produtos como margarinas e embutidos.

Este trabalho teve como objetivo principal o estudo do ponto de fulgor de ésteres etílicos e do ESL para misturas formadas por compostos graxos. A tese foi realizada em regime de co-tutela entre a Universidade Estadual de Campinas e a *Université de Pau et des Pays de l'Adour* (França). Este Capítulo 1, redigido em língua portuguesa e também em língua francesa, explica ao leitor a estrutura da tese. O Capítulo 2, intitulado Revisão Bibliográfica, apresentado somente em português, contextualiza para o leitor alguns dos conceitos importantes necessários para o desenvolvimento do trabalho. A apresentação dos resultados foi organizada em cinco artigos, todos eles redigidos em língua inglesa, que individualmente abrangem cada um dos objetivos estabelecidos.

O Capítulo 3 traz o artigo intitulado "*Flash points of mixtures containing ethyl esters or ethylic biodiesel and ethanol*", que apresenta dados experimentais de ponto de fulgor para misturas de ésteres etílicos (FAEEs) e etanol. Os dados experimentais foram correlacionados por um modelo baseado na equação NRTL e na suposição que tanto as interações energéticas entre etanol e os FAEEs, como o próprio ponto de fulgor dos ésteres puros, apresentam dependência do tamanho da cadeia carbônica e do número de duplas ligações dos ésteres etílicos. A partir do modelo empírico é possível predizer o ponto de fulgor de misturas biodiesel-etanol, se considerado que as interações entre diferentes ésteres etílicos são ideais. Os resultados provenientes do modelo preditivo foram comparados com dados experimentais para o ponto de fulgor da mistura biodiesel de palma-etanol.

No Capítulo 4 está apresentado o artigo intitulado "*The binary solid-liquid phase diagrams of caprylic or capric acid + 1-octanol or 1-decanol*". Neste trabalho os dados de ESL para quatro misturas binárias de ácidos graxos + álcoois graxos foram determinados utilizando-se a técnica de DSC. De forma geral, os quatro sistemas apresentam um diagrama de equilíbrio com pontos eutético e peritético. No caso dos sistemas ácido caprílico + 1-decanol e ácido cáprico + 1-octanol as leituras das análises de DSC para diferentes composições do sistema apresentaram transições de fases endotérmicas e exotérmicas durante o aquecimento das amostras. As transições endotérmicas estão relacionadas, na maior parte dos casos, às transições de fase que ocorrem na mistura, porém

as transições exotérmicas estão relacionadas às transições de caráter cinético devido às taxas de aquecimento utilizadas nas análises de DSC. Por isso, para estes dois sistemas, ácido caprílico + 1-decanol e ácido cáprico + 1-octanol, foi proposta a utilização de uma ferramenta de análise do DSC chamada *stepscan*. As análises de *stepscan* DSC permitiram a deconvolução das curvas térmicas em duas respostas, uma reversível ou termodinâmica e outra não reversível ou cinética. Também foi realizada a modelagem termodinâmica dos sistemas binários utilizando-se o modelo de coeficiente de atividade da fase sólida proposto por Slaughter e Doherty[2] (1995) para sistemas que apresentam reação peritética.

O artigo descrito no capítulo 5, intitulado "*On the solid-liquid phase diagrams of binary mixtures of even saturated fatty alcohols: systems exhibiting peritectic reaction*" apresenta quatro diagramas de fases para os sistemas binários de álcoois graxos saturados: 1-octanol + 1-decanol, 1-decanol + 1-dodecanol, 1-dodecanol + 1-hexadecanol e 1-tetradecanol + 1-octadecanol. Os diagramas foram determinados por análises de DSC, e para dois sistemas, 1-dodecanol + 1-hexadecanol e 1-tetradecanol + 1-octadecanol, a ferramenta de *stepscan* DSC foi testada para verificar como a técnica se comporta para outras misturas além dos sistemas apresentados no capítulo 4. Microscopia ótica com controle de temperatura e análises de difração de raios-X também foram utilizadas para a caracterização do ESL. Os sistemas apresentaram miscibilidade parcial dos componentes no estado sólido, além de reação eutética, peritética e, em alguns dos sistemas, também reação metatética. Os diagramas foram discutidos individualmente devido às características particulares de cada um.

O artigo descrito no Capítulo 6, intitulado "*High pressure solid–liquid equilibrium of fatty acid ethyl esters binary systems*" apresenta os resultados de ESL para sistemas binários formados por laurato de etila, miristato de etila e palmitato de etila. As análises experimentais foram realizadas em microscópio ótico, que opera a altas pressões (no trabalho em questão com medidas sendo realizadas a 0,1, 20, 40, 60 e 80 MPa), assim foi possível verificar a influência da pressão do sistema sobre o ESL e a estabilidade do pontos eutéticos dos sistemas. Foi realizada a modelagem termodinâmica dos sistemas binários

[2] SLAUGHTER, D. W.; DOHERTY, M. F. Calculation of Solid-Liquid Equilibrium and Crystallization Paths for Melt Crystallization Processes. **Chemical Engineering Science,** v. 50, n. 11, p. 1679-1694, 1995.

utilizando-se um modelo preditivo já testado para sistemas formados por alcanos e também por ácidos graxos.

No Capítulo 7 é exposto o artigo intitulado "*High pressure solid–liquid equilibrium of fatty alcohols binary systems*". No artigo são apresentados os resultados de ESL para seis sistemas binários formados pelos seguintes álcoois graxos saturados: 1-dodecanol, 1-tetradecanol, 1-hexadecanol e 1-octadecanol. Em uma primeira parte do trabalho são discutidos os efeitos da pressão sobre o ponto de fusão dos álcoois puros. Em seguida, os resultados experimentais obtidos são discutidos especificamente para cada um dos sistemas em função do aumento da pressão, já que os sistemas binários apresentam diferentes tipos de diagramas de fases em comparação com os resultados de DSC anteriormente medidos.

O Capítulo 8 (Conclusões gerais), apresentado em língua portuguesa e francesa, discorre sobre os principais resultados obtidos em cada um dos artigos e também expõe sugestões sobre trabalhos futuros acerca dos temas apresentados nesta tese.

Chapitre 1. Introduction

Le Brésil est l'un des principaux producteurs mondials de céréales avec une surface cultivée de 52.700.000 hectares (2013). Selon l'IBGE[1] (*Instituto Brasileiro de Geografia e Estatística*), la récolte de céréales, de légumineuses et de graines oléagineuses (graines de coton, arachides, riz, haricots, graines de ricin, maïs, soja, avoine, seigle, orge, tournesol, sorgho, blé et triticale) pour l'année de 2013, est estimée à environ 187 millions de tonnes, soit une hausse de 15,5% par rapport aux résultats obtenus en 2012 (161,9 millions tonnes). Une partie de la récolte est destinée à la production à grande échelle d'huiles végétales pour l'utilisation dans l'industrie alimentaire et la production de biocarburants. Ainsi, connaître les propriétés physico-chimiques des composants de toute la chaîne d'approvisionnement est important pour une définition plus précise des paramètres de processus et de sécurité.

Parmi ces propriétés thermophysiques, deux sont encore peu étudiées pour les systèmes gras, celles liées à l'équilibre solide-liquide et celle liée au point d'éclair des mélanges de graisses d'intérêt industriel. Le présent travail porte donc sur l'étude de l'équilibre solide-liquide (ESL) des mélanges contenant des alcools gras, des acides gras et des esters éthyliques et du point d'éclair de mélanges contenant des esters éthyliques et d'éthanol.

Le point d'éclair est une propriété physico-chimique essentielle pour le contrôle de la température de stockage des corps combustibles. C'est une propriété qui est bien établie pour une large gamme de composés purs, mais encore peu explorée pour les mélanges multi-composants. Le biodiesel, produit de la transestérification d'huiles végétales avec des alcools inférieurs, tels que le méthanol ou l'éthanol, a un point d'éclair qui varie en fonction de l'huile végétale utilisée dans la production mais aussi en fonction de la quantité d'éthanol résiduel. La croissance de la production de biodiesel augmente la nécessité de mieux connaitre cette propriété par le développement de méthodes de corrélation et de prédiction. De telles méthodes peuvent être basée sur une approche similaire à celle utilisée dans la modélisation des équilibres de phase.

L'étude de l'ESL des systèmes multi-composants peut revetir un caractère important pour la vérification de la perte de charge dans les tuyaux due aux phénomènes de

[1] IBGE. Em setembro, IBGE prevê safra de grãos 15,5% maior que a safra de 2012. 2013. Disponible dans: < http://cod.ibge.gov.br/1YAGX >. Consultée: 10/26/2013.

précipitation de certains composés. En outre, l'ESL est aussi nécessaire pour effectuer la mise à l'échelle des équipements de purification par voie de cristallisation. Plus récemment, on a mis en évidence la capacité des composés gras à former des cristaux de caractéristique très particulière. Cette propriété affecte la stabilité et la texture d'une vaste gamme de produits tels que par exemple la margarine.

Le but de ce travail était d'étudier le point d'éclair d'esters éthyliques et l'ESL pour les mélanges des composés gras. La thèse a été réalisée sous cotutelle de thèse entre l'«*Universidade Estadual de Campinas*» (Brésil) et l'Université de Pau et des Pays de l'Adour. Ce Chapitre 1, rédigé en français et aussi en portugais, explique au lecteur la structure de la thèse. Le Chapitre 2 intitulé « *Revisão Bibliográfica* » (Analyse de la Littérature), présenté uniquement en portugais, présente au lecteur les concepts importants nécessaires au développement de ce travail. La présentation des résultats est organisée autour de cinq articles, tous écrits en anglais, qui couvrent individuellement chacun des objectifs fixés.

Le Chapitre 3 est construit autour de l'article intitulé « *Flash points of mixtures containing ethyl esters or ethylic biodiesel and ethanol* », qui présente les points d'éclair pour les mélanges d'esters éthyliques (FAEEs) et de l'éthanol. Les données expérimentales ont été ajustées à un modèle empirique pour le calcul des paramètres d'interaction thermodynamiques du modèle NRTL entre le FAEEs et l'éthanol en fonction de la taille de la chaîne de carbone et du nombre de doubles liaisons des esters éthyliques. A partir du modèle empirique, on peut estimer le point d'éclair des mélanges de biodiesel et d'éthanol, en admettant l'hypothèse que les interactions esters-esters sont idéales. Les résultats du modèle prédictif ont été comparés avec les données expérimentales du point d'éclair du mélange de biodiesel éthylique de palme + éthanol.

Dans le Chapitre 4, l'article intitulé « *The binary solid-liquid phase diagrams of caprylic or capric acid + 1-octanol or 1-decanol* » est présenté. Dans ce travail, l'ESL de quatre mélanges binaires d'alcools gras + acides gras a été déterminé par une technique de DSC. En général, les quatre systèmes présentent un diagramme d'équilibre avec des points eutectiques et péritectiques. Pour les systèmes acide caprylique + 1-décanol et acide caprique + 1-octanol, l'analyse des mesures DSC pour différentes compositions a montré

des transitions endothermiques et exothermiques au cours du rechauffement des échantillons. Les transitions endothermiques sont associées, dans la plupart des cas, aux transitions de phase qui se produisent dans le mélange alors que les transitions exothermiques sont liées à des transitions de caractère cinétique dues aux vitesses de réchauffement utilisées pour l'analyse DSC. Par conséquent, pour ces deux systèmes, acide caprylique + 1-décanol et acide caprique + 1-octanol, un outil d'analyse de DSC appelé Stepscan a été utilisé. Il permet la déconvolution de courbes thermiques DSC en deux réponses, une réversible (thermodynamique) et une autre non réversible (cinétique). La modélisation thermodynamique des systèmes binaires a également été réalisée en utilisant le modèle de coefficient d'activité proposé par Slaughter et Doherty[2] (1997) pour les systèmes qui présentent en phase solide une réaction péritectique.

L'article décrit dans le Chapitre 5, intitulé « *On the solid-liquid phase diagrams of binary mixtures of even saturated fatty alcohols: systems exhibiting peritectic reaction* », présente quatre diagrammes de phases pour les systèmes binaires d'alcools gras saturés: 1-octanol + 1-décanol , 1-décanol + 1-dodécanol, 1-dodécanol + 1-hexadécanol et 1-tétradécanol + 1 -octadécanol. Ces diagrammes de phases ont été déterminés par analyse DSC, et pour deux systèmes, 1-dodécanol + 1-hexadécanol et tétradécanol + 1-octadécanol, l'outil DSC Stepscan a été utilisé pour tester le comportement de la technique pour des mélanges autres que ceux présentés dans le Chapitre 4. La microscopie optique avec contrôle de la température et une technique de diffraction des rayons X ont été également utilisées pour caractériser l'ESL. Les systèmes présentaient une miscibilité partielle des composants à l'état solide, ainsi que des réactions eutectiques, péritectiques, et métathétiques. Les diagrammes ont été examinés individuellement en fonction des caractéristiques de chacun.

L'article décrit au Chapitre 6, intitulé « *High pressure solid–liquid equilibrium of fatty acid ethyl esters binary systems* », présente les résultats d'ESL pour les systèmes binaires formés par l'ethyl laurate, l'ethyl myristate et l'ethyl palmitate. Les expériences

[2] SLAUGHTER, D. W.; DOHERTY, M. F. Calculation of Solid-Liquid Equilibrium and Crystallization Paths for Melt Crystallization Processes. **Chemical Engineering Science,** v. 50, n. 11, p. 1679-1694, 1995.

ont été réalisées au moyen d'un microscope haute pression (mesures effectuée à 0,1, 20, 40, 60 et 80 MPa) ce qui a permis de vérifier l'influence de la pression sur l'ESL et sur la stabilité du point eutectique des systèmes. La modélisation thermodynamique des systèmes binaires a été réalisée à l'aide d'un modèle prédictif proposé pour des systèmes constitués d'alcanes et déjà testé pour des systèmes constitués d'acides gras.

L'article intitulé « *High pressure solid–liquid equilibrium of fatty alcohols binary systems* » est exposé dans le Chapitre 7. L'ESL pour six systèmes binaires formés par les alcools gras saturés suivants sont présentés dans l'article: 1-dodécanol, 1-tétradécanol, 1-hexadécanol et 1-octadécanol. Les effets de la pression sur les températures de fusion d'alcools purs ont été examinés. Par la suite, les résultats expérimentaux obtenus sont discutés spécifiquement pour chaque système en fonction de l'augmentation de la pression puisque les systèmes binaires présentent différents types de diagrammes de phase, d'après les résultats précédemment obtenus par DSC.

Le Chapitre 8 (Conclusions), rédigé en français et en portugais, résume les principaux résultats pour chacun des articles présentés dans ce travail de thèse et expose les suggestions pour des travaux futurs.

Capítulo 2. Revisão Bibliográfica

Neste capítulo são apresentados aspectos necessários para o desenvolvimento e compreensão deste trabalho, bem como alguns conceitos básicos sobre o assunto e os resultados dos trabalhos e investigações já existentes na literatura.

2.1. Compostos graxos

Embora não exista nenhuma definição comumente aceita para compostos graxos ou compostos lipídicos, eles podem ser considerados como substâncias orgânicas de origem vegetal, animal ou mineral que em regra são solúveis em solventes orgânicos e insolúveis em água (GUNSTONE e PADLEY, 1997). São geralmente classificados como compostos graxos: gorduras (triacilglicerídeos), mono e diglicerídios, esteróis, ácidos graxos, álcoois graxos, ésteres de cadeia longa, entre outros e são compostos vastamente utilizadas em produtos alimentícios, na indústria química e farmacêutica (DIJKSTRA e SEGERS, 2007).

O Equilíbrio Sólido-Líquido (ESL) de misturas de ácidos e álcoois graxos, assim como de ésteres etílicos e o ponto de fulgor de ésteres etílicos e etanol foram o objeto de estudo deste trabalho. Desta forma, nesta revisão bibliográfica será feita uma discussão sobre os trabalhos já publicados acerca destes tópicos, mas o capítulo terá início pela definição e caracterização dos compostos graxos de interesse, assim como por uma breve discussão acerca de suas principais aplicações industriais.

2.1.1. Ácidos graxos

Ácidos graxos são constituídos por uma cadeia de hidrocarbonetos alifáticos e um grupo carboxila terminal, são classificados de acordo com seu comprimento de cadeia, a existência de ligações duplas, e a presença de ramificações ou por outros grupos presentes (HARWOOD e SCRIMGEOUR, 2007). A notação geralmente usada em ácidos graxos relaciona o tamanho da cadeia carbônica (d) e o número de insaturações das moléculas (g) (Cd:g), assim para o ácido cáprico, ácido graxo com dez átomos de carbono e saturado, por exemplo, a notação usada para identifica-lo é C10:0.

Ácidos graxos são usados na fabricação de vários produtos da indústria química, entre os quais se podem mencionar tintas e detergentes (JOHNSON, 1988). Na indústria farmacêutica são amplamente utilizados na formulação de cosméticos e, por serem constituintes dos óleos e gorduras, são importantes para a indústria alimentícia, conferindo a muitos alimentos propriedades físicas como, por exemplo, a textura. Os ácidos graxos são encontrados em abundância na natureza como principal constituinte de lipídios complexos, tais como óleos e gorduras, fosfolipídios, glicolipídios, entre outras várias fontes (GURR e JAMES, 1971). Existem estudos na literatura relacionando as propriedades físicas ou mesmo o comportamento de fases de compostos lipídicos com a sua função biológica nos organismos vivos (BLOOM et al., 1991), por exemplo, sobre os efeitos de ácidos graxos na agregação de plaquetas e diminuição nas taxas de colesterol do sangue (TAN et al., 2014), assim como ácidos graxos ômega-3 e 6 que mostraram ter efeitos anti- e pró-prevenção de doenças inflamatórias e auto-imunes (PALMQUIST, 2009).

A maioria dos lipídios complexos possui diferentes espécies de ácidos graxos, e a combinação destas espécies determina as propriedades físicas das misturas resultantes. Por exemplo, óleos vegetais cuja composição seja rica em ácidos graxos saturados de cadeia curta e/ou em ácidos graxos insaturados apresentam baixa temperatura de fusão, como os óleos de babaçu, coco ou canola (INOUE et al., 2004a). Por outro lado, gorduras animais são formadas principalmente por ácidos graxos saturados de cadeia longa, razão pela qual as gorduras têm uma temperatura de fusão elevada. A temperatura de fusão dos óleos e gorduras alimentares é criticamente importante para o seu papel em organismos vivos (INOUE et al., 2004a).

Os ácidos graxos saturados com 4 a 10 átomos de carbono em suas cadeias são encontrados principalmente em gorduras do leite, óleos de coco e de dendê. Estes ácidos graxos de cadeia curta são líquidos à temperatura ambiente. O ácido butírico (C4:0) tem o menor número de átomos de carbono de todos os ácidos graxos encontrados em gorduras e óleos. A gordura do leite de vaca contém cerca de 4% de ácido butírico, o que contribui para o sabor característico de manteiga, e quantidades menores de ácido capróico (C6:0), ácido caprílico (C8:0) e ácido cáprico (C10:0). Estes ácidos graxos também proporcionam o sabor de ranço de manteiga a partir da hidrólise dos triacilgliceróis (O'BRIEN, 2008).

Ácido láurico (C12:0) é um dos três ácidos graxos saturados mais encontrados na natureza, os outros dois são o ácido palmítico (C16:0) e o ácido esteárico (C18:0). As fontes mais ricas e comuns de ácido láurico são óleos de coco e de palmiste, chegando a ter de 40 a 50% do mesmo. O ácido mirístico (C14:0) é também encontrado na maior parte das gorduras e óleos, como por exemplo o óleo de coco, o óleo de palmiste e a gordura de leite, todos contendo quantidades apreciáveis de ácido mirístico - tipicamente 18,1, 16,2, e 10,8%, respectivamente. Já as principais fontes de ácido palmítico são o óleo de palma, a banha de porco, sebo e o óleo de semente de algodão, com teores aproximados de 44, 26, 24 e 21,5%, respectivamente. A manteiga de cacau, sebo, banha de porco e manteiga têm grandes teores de ácido esteárico (C18:0), com aproximadamente 34, 18,6, 13,5 e 12,1% respectivamente. Nos óleos vegetais, o ácido esteárico é, normalmente, o resultado da hidrogenação de ácidos insaturados de 18 átomos de carbono (O'BRIEN, 2008).

A maioria dos triacilgliceróis (TAGs) possuem diferentes espécies de ácidos graxos na molécula e a combinação dos diferentes ácidos faz variar as propriedades físicas de moléculas lipídicas. O estudo do comportamento dos ácidos graxos constituintes das moléculas de TAGs é importante para compreender as propriedades físicas de lipídios e suas misturas e permitir o desenvolvimento de inovações para as indústrias químicas, farmacêuticas e alimentícias por serem responsáveis por algumas características, como por exemplo, a textura de cosméticos e gorduras (INOUE et al., 2004a).

2.1.2. Álcoois graxos

São classificados como graxos os álcoois de cadeia carbônica alifática longa de, no mínimo, seis átomos de carbono (FISK et al., 2009). Possuem predominantemente cadeia linear, podendo ser saturada ou ter uma ou mais ligações duplas. Álcoois com cadeia de carbono acima de 22 são citados como sendo álcoois presentes em ceras (JOHNSON, 1988). As propriedades de um álcool graxo (sendo primário ou secundário, linear ou de cadeia ramificada, saturado ou insaturado) são determinadas pelo processo de fabricação e pelas matérias-primas utilizadas. Produtos naturais, tais como gorduras, óleos e ceras, produzem geralmente álcoois lineares, primários, e com cadeia carbônica de número par, e

podendo apresentar também álcoois graxos insaturados. No entanto, processos industriais geram misturas de álcoois mais complexas, como no caso do processo Oxo em que são produzidos 20-60% de álcoois graxos ramificados e também alguns de cadeia carbônica ímpar, a dimerização Guerbet que resulta em álcoois de cadeias ramificadas ou a oxidação Bashkirov produzindo álcoois graxos secundários (NOWECK e GRAFAHREND, 2000).

Dependendo das matérias-primas utilizadas, álcoois graxos podem ser classificados como naturais ou sintéticos. Álcoois graxos naturais baseiam-se em recursos renováveis, tais como gorduras, óleos e ceras de origem vegetal ou animal, enquanto que os álcoois graxos sintéticos são produzidos a partir de produtos petroquímicos tais como olefinas e parafinas. Em 2005, a capacidade mundial de produção nominal de álcoois graxos foi estimada em 2,5 x 10^6 t/ano, sendo quase que igualmente dividida entre matérias-primas naturais e de origem petroquímica (NOWECK e GRAFAHREND, 2000).

Álcoois graxos são utilizados como emulsificantes, emolientes e espessantes na indústria de alimentos e de cosméticos (JOHNSON, 1988; KOGAN e GARTI, 2006; PERNETTI et al., 2007). Também podem ser usados como surfactantes não-iônicos empregados em detergentes e como solventes industriais, além de ainda serem empregados como biocombustíveis (JOHNSON, 1988; CANOIRA et al., 2006). Novos estudos indicam que álcoois graxos são excelentes estruturadores das cadeias cristalinas dos óleos, substituindo os ácidos graxos saturados e tornando, por exemplo, os alimentos mais saudáveis (SCHAINK et al., 2007).

Álcoois graxos estão entre as substâncias químicas mais importantes utilizadas para fins cosméticos e na indústria farmacêutica. No seu processo de fabricação, ao invés de utilizar matéria-prima de origem fóssil, podem ser sintetizados a partir de óleos vegetais refinados, que são primeiramente convertidos em ésteres de ácidos graxos, obtidos a partir da reação de transesterificação, mais conhecida pela produção de biodiesel. Em seguida, os ésteres etílicos são convertidos à álcoois graxos por meio de um processo de hidrogenação (NOWECK e GRAFAHREND, 2000), com uma etapa subsequente de destilação.

Álcoois graxos saturados de cadeia par e até 12 átomos de carbono são incolores e líquidos à temperatura ambiente. A partir de 14 átomos de carbono possuem uma consistência de cera. A maior parte dos álcoois graxos saturados cristaliza numa estrutura

estável ortorrômbica (MOSSELMAN, 1981) e, no geral, possuem uma densidade específica inferior à da água. Aqueles com cadeia curta têm odor característico e os álcoois graxos superiores são inodoros (JOHNSON, 1988).

As temperaturas de ebulição e fusão aumentam uniformemente com o comprimento da cadeia carbônica e ambos são significativamente mais altos do que os dos hidrocarbonetos com o mesmo número de átomos de carbono (NOWECK e GRAFAHREND, 2000). A influência do grupo hidroxila sobre a polarização da molécula diminui com o aumento do comprimento da cadeia. O hexanol e octanol têm certa solubilidade em água, mas decanol e álcoois graxos de cadeia carbônica superior podem ser considerados como imiscíveis em água. No entanto, o octadecanol e outros álcoois graxos de maior tamanho são ligeiramente higroscópicos e podem absorver umidade do ar durante o armazenamento. Solventes orgânicos, tais como éter de petróleo, álcoois inferiores e éter dietílico são bons solventes para os álcoois graxos (FISK et al., 2009).

O elevado ponto de fusão torna os álcoois graxos, assim como ácidos graxos, compostos que podem potencialmente ser utilizados como materiais de mudança de fase (PCMs – da sigla em inglês – *Phase Change Materials*). Tradicionalmente, energia é armazenada sob a forma de calor sensível, que requer grande volume de material de armazenamento. Este volume de armazenamento pode ser significativamente reduzido se a energia for armazenada sob a forma de calor latente. PCMs são materiais que podem mudar de fase com uma pequena variação de temperatura e assim armazenar ou liberar energia térmica, o que os torna muito atraentes em campos de aplicação, como proteção térmica, controle de temperatura de interiores e na construção de edifícios inteligentes (NKWETTA e HAGHIGHAT, 2014). Mistura de diferentes álcoois graxos mostraram ser eficientes no uso como PCMs, já que apresentam maiores entalpias de fusão em relação aos compostos puros com pequenas faixas de ESL (2 a 4 °C), além de que com a variação da composição a temperatura de fusão pode ser otimizada para casos específicos (VENTOLA et al., 2004b; YUAN et al., 2014). Para se avaliar o uso de mistura de álcoois graxos como PCMs é necessário entender o comportamento das fases sólida e líquida e, assim é possível encontrar na literatura alguns trabalhos sobre o ESL de misturas de álcoois graxos visando esta aplicação (VENTOLA et al., 2002; VENTOLA et al., 2004a,b).

2.1.3. Ésteres graxos

O biodiesel é definido pela norma ASTM International como um combustível composto de monoalquil ésteres de ácidos graxos de cadeia longa, derivados de óleos vegetais ou gorduras animais, que cumprem os requisitos da norma ASTM D6751 (ASTM, 2012). O biodiesel é produzido via reação de transesterificação envolvendo moléculas de TAG com moléculas de um álcool de cadeia curta, normalmente metanol ou etanol, na presença de um catalisador para formar ésteres (metílicos ou etílicos, em função do álcool usado na reação) de ácidos graxos e glicerol (KNOTHE, 2008).

O metanol é o álcool mais utilizado na produção comercial de biodiesel, uma vez que é, em geral, mais barato do que outros álcoois, mas o uso de etanol tem um grande potencial no Brasil, aja que a produção de etanol é muito bem desenvolvida no país e a um custo relativamente baixo. Outros álcoois, além de metanol e etanol, também são interessantes para a produção de biodiesel, pois os ésteres produzidos a partir de álcoois superiores têm diferentes propriedades em comparação aos ésteres metílicos ou etílicos (KNOTHE, 2005).

Como produto da reação de óleos vegetais e gorduras animais, o biodiesel é uma fonte de energia renovável, biodegradável, de baixa toxidade, e diferentemente de combustíveis derivados de petróleo, é livre de enxofre e compostos aromáticos, possuindo maior ponto de fulgor. Por ser um combustível oxigenado, tem uma queima mais completa, reduzindo as emissões de diversos gases poluentes, tais como SO_2, monóxido de carbono, hidrocarbonetos e material particulado (KNOTHE, 2008). Porém, algumas desvantagens importantes do biodiesel incluem o elevado custo da matéria-prima e de armazenamento, a menor estabilidade oxidativa, os problemas de operacionalidade a baixas temperaturas, e, em alguns casos, as maiores emissões de NO_x (MOSER, 2009).

A composição química do biodiesel depende da matéria-prima a partir da qual ele é produzido. Como óleos vegetais e gorduras animais de diferentes origens têm composições em ácidos graxos variáveis, a composição de ésteres graxos do biodiesel é essencialmente igual ao do óleo ou gordura a partir do qual foi produzido. A composição em ésteres de ácidos graxos, juntamente com a presença de contaminantes e os componentes minoritários,

determinam as propriedades do biodiesel. Entre as propriedades do biodiesel, aquelas que são diretamente influenciadas pela sua composição são a operacionalidade a baixa temperatura, a estabilidade oxidativa e de armazenamento, viscosidade, densidade, o número de cetano, ponto de fulgor e conteúdo de energia (LIN et al., 2011). Em suma, são as propriedades do biocombustível que dizem se ele pode ou não ser usado como substituto do diesel convencional e em quais condições isso é possível. Por este motivo, o desenvolvimento de métodos capazes de calcular estas propriedades está sendo amplamente estudado na literatura (KNOTHE, 2005; BAJPAI e TYAGI, 2006; IMAHARA et al., 2006; KNOTHE, 2008; LOPES et al., 2008; CERIANI et al., 2009; COUTINHO et al., 2010; BOOG et al., 2011; COSTA et al., 2011; CARARETO et al., 2012).

2.2. Equilíbrio sólido-líquido

Enquanto existe uma grande quantidade de técnicas experimentais e de trabalhos na literatura sobre o equilíbrio líquido-vapor de misturas orgânicas, a quantidade de investigações sobre termodinâmica do ESL é bem menor. Determinar e compreender a solubilidade de sólidos em solventes puros ou em misturas líquidas é de interesse no projeto de processos químicos, especialmente quando as condições do processo devem ser especificadas para evitar a precipitação de um sólido, ou mesmo quando se deseja a sua precipitação (que é o caso dos equipamentos de cristalização).

Devido à vasta gama de aplicações industriais de óleos vegetais e seus subprodutos, o conhecimento de suas propriedades, assim como de seu comportamento de fases, é de grande importância. Misturas de triacilgliceróis, os principais constituintes de óleos vegetais, muitas vezes são fracionadas por cristalização, de modo que os diagramas de ESL correspondentes são significativos para a concepção de processos de purificação. Além disso, para melhor compreender como misturas de substâncias graxas se comportam na fase sólida e desenvolver novos modelos preditivos, é essencial dispor de dados experimentais precisos e confiáveis.

Existem estudos sistemáticos sobre o ESL de misturas de ácidos graxos na literatura (INOUE et al., 2004a,b,c; COSTA et al., 2007b; COSTA et al., 2009a,b,c; GBABODE et al., 2009). Na grande maioria dos casos estes trabalhos apresentam um comportamento do ESL complexo, seja em função da formação de diversos tipos de arranjos cristalinos, seja devido à miscibilidade dos componentes no estado sólido ou às reações eutética, peritética ou metatética.

Alguns trabalhos publicados (GANDOLFO et al., 2003; GANDOLFO et al., 2004; SCHAINK et al., 2007) avaliaram a capacidade de estruturação de misturas de óleo, formando-se emulsões conhecidas como óleo-gel (em inglês *oleogels*), utilizando álcoois e ácidos graxos como estruturantes daquelas misturas. *Oleogels* são definidos como misturas de líquidos e sólidos lipofílicos, em que os gelificantes lipídicos (em inglês *oleogelators*) estão presentes em concentrações mais baixas (abaixo de 10%). Os *oleogelators*, que tem a capacidade estruturante, podem reter grandes quantidades de óleo líquido por meios de formação de rede de *oleogelators* no óleo. Os trabalhos anteriormente citados mostraram que combinações de ácidos e álcoois graxos com cadeia de comprimento correspondentes têm capacidade estruturante no caso de vários óleos testados. O tipo de óleo vegetal não teve grande efeito sobre a estrutura, mas a proporção entre ácido e álcool tem grande influência sobre a dureza da estrutura obtida, sendo que este efeito foi mais pronunciado para a mistura de ácido esteárico e 1-octadecanol. O cristal formado nesse sistema contribuiu para as propriedades viscoelásticas de emulsões óleo em água ou água em óleo (GANDOLFO et al., 2004).

2.2.1. Termodinâmica do equilíbrio sólido-líquido

O equilíbrio de fases sólidas e líquidas pode ser representado pela equação que relaciona a fugacidade (f) de cada composto i presente nas fases líquida (l) e sólida (s) do sistema. Um ciclo termodinâmico que passa pelo ponto triplo é utilizado para se obter uma expressão que relaciona os coeficientes de atividade (γ) dos componentes na temperatura T, relacionando esta razão à variação da energia de Gibbs, o que resulta em (PRAUSNITZ et al., 1986):

$$\ln\left(\frac{x_i^s\gamma_i^s}{x_i^l\gamma_i^l}\right)=\frac{\Delta H_i^{fus}}{RT_i^{fus}}\left(\frac{T_i^{trip}}{T}-1\right)-\frac{\Delta Cp_i}{R}\left(\frac{T_i^{trip}}{T}-1\right)+\frac{\Delta Cp_i}{R}\ln\frac{T_i^{trip}}{T}$$

Eq.2.1

sendo ΔH_i^{fus} e ΔCp_i a entalpia de fusão e a diferença entre a capacidade calorífica nas fases líquida e sólida do composto *i*, respectivamente. T_i^{trip} a temperatura do ponto triplo do composto *i* com fração molar x_i, e *R* representa a constante universal dos gases. Na Eq.2.1 não são consideradas as transições ou polimorfismos que podem facilmente ocorrer na fase sólida.

Em geral, algumas simplificações da Eq.2.1 são adotadas ao se realizar a modelagem termodinâmica. Supõe-se que a temperatura do ponto triplo se aproxima bastante da temperatura normal de fusão do composto *i* e que a diferença entre as entalpias de fusão de cada composto a estas duas temperaturas é praticamente desprezível. Desta forma, pode-se substituir a temperatura do ponto triplo pela temperatura normal de fusão do componente e utilizar a entalpia de fusão a esta mesma temperatura para se descrever o ESL. Suposições adicionais, normalmente consideradas, são que as capacidades caloríficas das fases líquida e sólida não diferem significativamente e que a contribuição do termo da entalpia é bastante superior aos termos das capacidades caloríficas, desconsiderando-se então este último termo (PRAUSNITZ et al., 1986):

$$\ln\left(\frac{x_i^s\gamma_i^s}{x_i^l\gamma_i^l}\right)=\frac{\Delta H_i^{fus}}{RT_i^{fus}}\left(\frac{T_i^{fus}}{T}-1\right)$$

Eq.2. 2

Além disso, considera-se em muitos casos que não exista formação de uma solução na fase sólida em toda a faixa de composição dos diagramas, isto é, há uma completa imiscibilidade dos componentes em estado sólido e cada composto cristaliza como um sólido puro. Com esta última consideração, a atividade do componente i na fase sólida no equilíbrio, representada por $x_i^s\gamma_i^s$, pode ser substituída pela atividade do sólido puro. i.e., ($x_i^s\gamma_i^s=1$). Assim, a equação do equilíbrio se reduz à:

$$\ln\left(\frac{1}{x_i^l \gamma_i^l}\right) = \frac{\Delta H_i^{fus}}{RT_i^{fus}}\left(\frac{T_i^{fus}}{T} - 1\right)$$

Eq.2. 3

Os coeficientes de atividade refletem o comportamento de misturas em ambas fases, líquida e sólida. Os coeficientes de atividade podem ser descritos por diversos modelos termodinâmicos, como os baseados no conceito de contribuição de grupos ou os modelos moleculares.

2.2.2. Modelos para coeficiente de atividade

Em geral, o ESL de misturas não é representado empregando-se equações cúbicas de estado, mas sim, como representado na Eq.2. 3, em função do coeficiente de atividade. Vários modelos de coeficientes de atividade são utilizados nos cálculos de equilíbrio de fases, os quais podem ser classificados da seguinte forma:

- Modelos para misturas completamente randômicas: A energia molar de excesso de Gibbs é expressa como função da composição média do sistema, a qual representa adequadamente a composição local na vizinhança de qualquer molécula (SANDLER, 1999). Os parâmetros das equações são ajustados em função de dados experimentais. Alguns exemplos são os modelos de Margules-2 ou 3 sufixos e a equação de van Laar .
- Modelos de composição local: Estes modelos assumem que a concentração média da espécie em solução é diferente da sua concentração local. Assim, as concentrações locais são dependentes das interações entre as moléculas e uma função de distribuição radial. Alguns exemplos são os modelos de Wilson (WILSON, 1964), NRTL – NonRandom Two Liquids (RENON e PRAUSNITZ, 1968), e UNIQUAC - **UNI**versal **QUA**si-**C**hemical (ABRAMS e PRAUSNITZ, 1975).
- Modelos de contribuição de grupos: Estes modelos baseiam-se na estrutura molecular de cada componente da mistura. Os coeficientes de atividade são estimados pelas contribuições aditivas dos grupos funcionais, compreendidos nas moléculas. Alguns exemplos são – UNIFAC – UNIquac Functional-group Activity coefficient (FREDENSLUND et al., 1975) e a sua modificação, UNIFAC Dortmund (WEIDLICH e GMEHLING, 1987).

Existem, claramente, outros modelos para o cálculo/predição de coeficientes de atividade disponíveis na literatura além daqueles citados acima. Na sequência discute-se com mais profundidade o conceito de coeficiente de atividade e são descritos os modelos para este coeficiente utilizados no presente trabalho.

a) Coeficiente de atividade

Em uma mistura a atividade do componente *i*, a_i, é definida como:

$$a_i(T,P,x_i)=\frac{f_i(T,P,x_i)}{f_i^0(T^0,P^0,x_i^0)}$$

Eq.2. 4

em que o sobrescrito ^{0} representa o estado padrão e *P* representa a pressão do sistema. Assim como a fugacidade, a atividade é uma medida da tendência de uma substância de "escapar" da fase. Entre os vários estados normais utilizados na literatura, o estado padrão mais amplamente aplicado é o componente puro, ou seja, $x_i^0=1$, na mesma temperatura, pressão, e fase da mistura (TOSUN, 2013). Sob estas condições, a Eq.2. 4 torna-se:

$$a_i(T,P,x_i)=\frac{f_i(T,P,x_i)}{f_i\ (T,P)}$$

Eq.2. 5

Assim, $f_i(T,P)$ representa a fugacidade do composto *i* puro ($f_{i,puro}$). O coeficiente de atividade, γ_i, definido pela Eq.2. 6 abaixo, representa os desvios do comportamento ideal da mistura associados ao composto *i*:

$$a_i = x_i\gamma_i$$

Eq.2. 6

Comparando-se as Eq.2. 5 e Eq.2. 6 obtém-se:

$$\gamma_i(T,P,x_i)=\frac{f_i(T,P,x_i)}{x_i f_i(T,P)}$$

Eq.2. 7

O termo $x_i f_i(T,P)$ representa a fugacidade do composto *i* em uma mistura ideal. A partir da Eq.2. 7 é fácil concluir que $\gamma_i \to 1$ quando $x_i \to 1$. Para uma mistura binária líquida hipotética, o comportamento da fugacidade do componente 1 em função da composição do sistema está representado esquematicamente na Fig.2.1. Quando se trata de uma mistura ideal, a fugacidade do componente 1 varia linearmente com a fração molar na forma representada pela linha reta tracejada na Fig. 2.1.

Quando $f_1(T,P,x_1) > x_1 f_1(T,P)$ como representado na Fig.2.1a, o coeficiente de atividade do componente 1 é maior do que a unidade. Quanto maior for o coeficiente de atividade maior será a tendência de "escape" de um componente na fase líquida. Assim, $\gamma_1 > 1$ pode ser considerada como uma forma de repulsão entre as moléculas dos dois compostos presentes na mistura líquida. Em outras palavras, as interações entre as moléculas do composto 1 são mais fortes do que as interações entre as moléculas do composto 1 com as moléculas do composto 2. Na Fig.2.1b, ao contrário, quando $f_1(T,P,x_1) < x_1 f_1(T,P)$, o coeficiente de atividade é menor que a unidade. Neste caso, um componente prefere ficar na fase líquida porque as interações entre as moléculas do composto 1 com as moléculas do composto 2 são mais fortes do que as interações entre as moléculas do composto 1. Em ambos os casos, quando $x_1 \to 1$, a curva sólida coincide com a linha reta tracejada (TOSUN, 2013).

b) Equação de Margules 2-sufixos e 3-sufixos

A equação Margules 2-sufixos é o modelo empírico mais simples para expressar os coeficientes de atividade dos compostos em uma mistura binária (SANDLER, 1999):

$$\ln \gamma_1 = A.x_2^2$$

$$\ln \gamma_2 = A.x_1^2$$

Eq.2. 8

Uma vez que a função é simétrica em relação à composição, os coeficientes de atividade são imagens especulares um do outro tendo a fração molar 0,5 como referência.

Em geral, o parâmetro *A* é dependente da temperatura e da pressão, e relacionado com o logaritmo dos coeficientes de atividade à diluição infinita (PRAUSNITZ et al., 1986):

$$A = \ln \gamma_1^{\infty} = \ln \gamma_2^{\infty}$$

Eq.2. 9

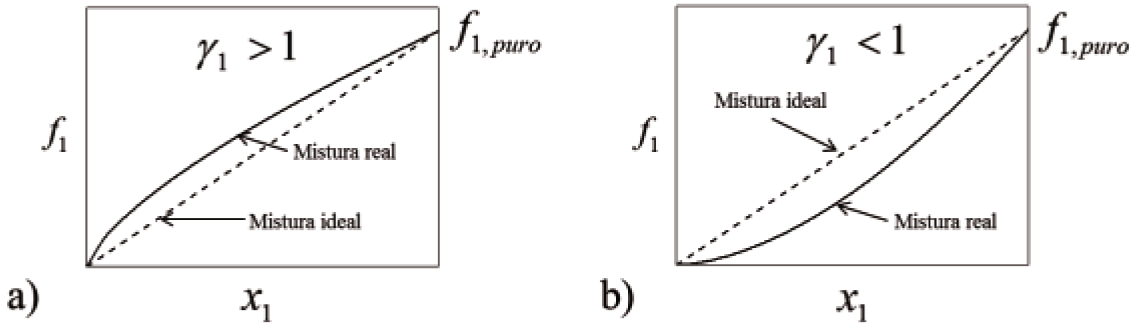

Fig.2. 1. Variação de fugacidade da componente 1 em uma mistura líquida com a composição (f_1 representa $f_1(T,P,x_1)$). a) Caso em que $f_1(T,P,x_1) > x_1 f_1(T,P)$ e; b) Caso em que $f_1(T,P,x_1) < x_1 f_1(T,P)$. Adaptado de (TOSUN, 2013).

Quando A tem um valor positivo, os coeficientes de atividade são maiores do que a unidade, e as interações entre as moléculas do composto 1 são maiores do que as interações entre as moléculas do composto 1 e as moléculas do composto 2. Ao contrário, quando A é negativo, os coeficientes de atividade são menores do que a unidade, e as interações entre as moléculas diferentes são mais fortes do que as interações entre moléculas iguais. A equação Margules 2-sufixos se aplica melhor às misturas de moléculas simples, de tamanho similar, mesma forma e natureza química (SANDLER, 1999).

Para a equação Margules 3-sufixos, os coeficientes de atividade dos compostos em uma mistura binária são expressos sob a forma:

$$\ln \gamma_1 = x_2^2 \left(A + 3B - 4Bx_2\right)$$

$$\ln \gamma_2 = x_1^2 \left(A - 3B + 4Bx_1\right)$$

Eq.2. 10

Os parâmetros A e B podem ser expressos em função dos coeficientes à diluição infinita como (TOSUN, 2013):

$$A = \ln\sqrt{\gamma_1^{\infty}\gamma_2^{\infty}} \qquad \text{e} \qquad B = \ln\sqrt{\frac{\gamma_2^{\infty}}{\gamma_1^{\infty}}}$$

A equação Margules 3-sufixos apresenta bons resultados quando aplicada para modelar misturas moderadamente não ideais (TOSUN, 2013).

c) Equação NRTL

Como citado anteriormente, a equação NRTL é baseada em um modelo de composição local e o coeficiente de atividade em uma mistura binária é definido como (RENON e PRAUSNITZ, 1968):

$$\gamma_1 = \exp\left\{x_2^2.\left[\tau_{12}.\left(\frac{G_{21}}{x_1 + x_2.G_{21}}\right)^2 + \frac{\tau_{12}.G_{12}}{(x_2 + x_1.G_{12})^2}\right]\right\}$$

$$\gamma_2 = \exp\left\{x_1^2.\left[\tau_{21}.\left(\frac{G_{12}}{x_2 + x_1.G_{12}}\right)^2 + \frac{\tau_{21}.G_{21}}{(x_1 + x_2.G_{21})^2}\right]\right\}$$

$$\tau_{12} = \frac{\Delta g_{12}}{RT} \qquad \text{e} \qquad \tau_{21} = \frac{\Delta g_{21}}{RT}$$

$$G_{12} = \exp(-\alpha\tau_{12}) \qquad \text{e} \qquad G_{21} = \exp(-\alpha\tau_{21})$$

Eq.2. 11

A equação NTRL requer dois parâmetros dependentes da temperatura, τ_{12} e τ_{21}, além de um parâmetro adicional, α. O parâmetro Δg_{12} é a energia característica para a interação $1-2$. Uma comparação com os dados experimentais indicam que para equilíbrio líquido-vapor, os valores de α variam entre 0,2 e 0,47. Assim, na ausência de informações, é geralmente recomendado α = 0,3 para realização de cálculos. O parâmetro α está relacionado a não aleatoriedade da mistura, sendo que, para o caso em que este valor é igual a zero, o sistema é totalmente aleatório e o modelo se reduz ao de Margules 2-sufixos

(PRAUSNITZ et al., 1986). A equação NTRL pode ser usada para sistemas altamente não ideais, bem como para sistemas parcialmente miscíveis (TOSUN, 2013).

d) Equação UNIQUAC

O modelo UNIQUAC é dividido em duas partes, uma primeira conhecida como termo combinatorial e a segunda, conhecida como termo residual. Para qualquer componente *i* da mistura, o coeficiente de atividade é dado por (PRAUSNITZ et al., 1986):

$$\ln\gamma_i = \ln\left(\frac{\Phi_i}{x_i}\right) + \frac{z}{2}q_i\ln\frac{\theta_i}{\Phi_i} + l_i - \frac{\Phi_i}{x_i}\sum_{j=1}^{n} l_j x_j - q_i\ln\left[\sum_{j=1}^{n}\theta_j\exp\left(-\frac{\lambda_{ij}-\lambda_{ii}}{q_i RT}\right)\right] + q_i - q_i\sum_{j=1}^{n}\frac{\theta_j\exp\left(-\frac{\lambda_{ij}-\lambda_{ii}}{q_i RT}\right)}{\sum_{k=1}^{n}\theta_k\exp\left(-\frac{\lambda_{jk}-\lambda_{jj}}{q_j RT}\right)}$$

Eq.2. 12

Dado $l_i = (r_i - q_i)z/2 - (r_i - 1)$

$$\Phi_i = \frac{x_i r_i}{\sum_j x_j r_j} \quad \text{e} \quad \theta_i = \frac{x_i q_i}{\sum_j x_j q_j}$$

r_i representa o parâmetro de volume para a espécie i, q_i representa o parâmetro de área superficial para a espécie i e *z* é o número de coordenação e usualmente é definido como 10 para o modelo UNIQUAC.

Coutinho et al. (2006) propuseram uma modificação na utilização do modelo UNIQUAC original para o cálculo da não idealidade de fases sólidas, ampliando a possibilidade de utilizá-lo como uma equação preditiva. A diferença encontra-se na estimativa das energias de interação (λ_{ij}) sem necessariamente ter de recorrer a dados experimentais de equilíbrio. A energia de interação entre duas moléculas idênticas pode ser estimada a partir da entalpia de sublimação de um cristal do componente puro (COUTINHO et al., 1996):

$$\lambda_{ii} = -\frac{2}{z}\left(\Delta H_i^{sub} - RT\right)$$

Eq.2. 13

A entalpia de sublimação, $\Delta H_i^{sub} = \Delta H_i^{vap} + \Delta H_i^{fus}$, é calculada na temperatura de fusão do componente puro (ΔH_i^{vap} é a entalpia de vaporização do composto *i* puro).

Já o par de interações entre moléculas não idênticas (λ_{ij}) é calculado a partir da seguinte relação:

$$\lambda_{ij} = \lambda_{ji} = \lambda_{jj}\left(1 - \alpha_{ij}\right)$$

Eq.2. 14

cujo subíndice *j* faz referência ao componente com a menor cadeia de carbono. O parâmetro α_{ij} tem uma grande importância para descrever a formação de solução sólida, mas mostrou ter pouco impacto sobre a linha liquidus. Para a maior parte de sistemas formados por alcanos e ácidos graxos o valor de α_{ij} varia entre 0,03 a 0,05 (MILHET et al., 2005; COSTA et al., 2007a).

2.2.3. Equilíbrio sólido-líquido a altas pressões

No caso de pressões elevadas a representação do equilíbrio sólido-líquido deve recorrer a equações de estado. Um método preditivo baseado em equações de estado foi proposto por Coutinho et al. (2006) e vem sendo utilizado com êxito para descrever o comportamento do ESL de sistemas multicomponentes em função da pressão (MILHET et al., 2005; COSTA et al., 2007a; KOUAKOU et al., 2013).

O estado de equilíbrio entre duas fases, uma sólida e outra líquida, de um sistema pode ser representado ao se expressar a igualdade de potenciais químicos de cada componente nas fases em equilíbrio (SANDLER, 1999):

$$\mu_i^L\left(T, P, x_i^L\right) = \mu_i^S\left(T, P, x_i^S\right)$$

Eq.2. 15

Esta equação é geralmente apresentada em termos de fugacidade (*f*), grandeza que pode ser definida através da seguinte relação:

$$\left[RTd\left(\ln f_i\right) = d\mu_i\right]_T$$

Eq.2. 16

Esta mudança de variável permite traduzir o ESL pela igualdade de fugacidade de cada componente nas duas fases (SANDLER, 1999):

$$f_i^L\left(T,P,x_i^L\right) = f_i^S\left(T,P,x_i^S\right)$$

Eq.2. 17

Faz-se necessário explicitar as expressões das duas fugacidades (da fase sólida e da fase líquida), pois ao contrário da modelagem do equilíbrio líquido-vapor, neste caso, as variáveis não podem ser calculadas por uma mesma equação já que existe uma diferença significativa de estrutura entre a fase líquida e a fase sólida.

a) Fugacidade da fase líquida

A fugacidade do composto *i* na fase líquida pode ser expressa como (COUTINHO et al., 2006):

$$f_i^L\left(T,P,x_i^L\right) = Px_i^L\phi_i^L$$

Eq.2. 18

em que *P* é a pressão absoluta do sistema, *T* a temperatura do sistema, x_i^L corresponde à fração molar do componente *i* na fase líquida e ϕ_i^L representa o coeficiente de fugacidade do composto na fase líquida. Este coeficiente é calculado a partir da energia livre residual em função da seguinte integral:

$$\ln\phi_i^L = \frac{1}{RT}\frac{\partial}{\partial n_i}\left[n\int_v^\infty\left(P-\frac{RT}{v}\right)dv\right]_{T,v,n_{j\neq i}} + Z - 1 - \ln Z$$

Eq.2. 19

onde *v* é o volume molar da mistura e Z é o fator de compressibilidade definido por:

$$Z = \frac{Pv}{RT}$$

Eq.2. 20

A pressão *P* pode ser calculada por meio de uma equação de estado que descreva a fase líquida. Neste trabalho, aplicou-se a equação de Peng-Robinson (PENG e ROBINSON, 1976) que é usualmente utilizada para sistemas orgânicos. A pressão absoluta é dada pela expressão:

$$P = \frac{RT}{v-b} - \frac{a(T)}{v(v+b)+b(v-b)}$$

Eq.2. 21

Os coeficientes $a(T)$ e b são definidos em função dos coeficientes $a_i(T)$ e b_i dos compostos puros, em função das regras de misturas clássicas:

$$a(T) = \sum_i \sum_j x_i x_j \sqrt{a_i(T) a_j(T)} (1 - k_{ij})$$

Eq.2. 22

$$b = \sum_i x_i b_i$$

Eq.2. 23

Os coeficientes de interação k_{ij} podem ser considerados iguais à zero quando os sistemas estudados não contêm compostos tão assimétricos para justificar o uso de tal fator de correção (COSTA et al., 2007a). Os coeficientes $a_i(T)$ e b_i são expressos em função dos parâmetros críticos e do fator acêntrico de cada composto:

$$a_i(T) = 0{,}45724 \frac{R^2 T_{C_i}^2}{P_{C_i}} \left[1 + m_i \left(1 - \sqrt{\frac{T}{T_{C_i}}} \right) \right]^2$$

Eq.2. 24

$$b_i = 0{,}0778 \frac{R T_{C_i}}{P_{C_i}}$$

Eq.2. 25

O parâmetro m_i é obtido a partir da seguinte correlação que assume duas formas diferentes em função da temperatura crítica T_{C_i} do composto (PENG e ROBINSON, 1976):

$$m_i = 0{,}37464 + 1{,}54226\omega_i - 0{,}26992\omega_i^2 \qquad \text{se} \qquad T_{C_i} < 620K$$

Eq.2. 26

$$m_i = 0{,}379642 + 1{,}48503\omega_i - 0{,}164423\omega_i^2 + 0{,}016666\omega_i^3 \qquad \text{se} \qquad T_{C_i} > 620K$$

Eq.2. 27

A equação de Peng-Robinson é usada para descrever corretamente o equilíbrio líquido-vapor, mas falha no cálculo da densidade da fase líquida. Porém, o conhecimento correto da mesma é essencial para uma boa modelagem do ESL. Para contornar esta situação, foi utilizada uma relação de volume originalmente proposto por Peneloux et al. (1982):

$$v = v' + C_i$$

Eq.2. 28

em que v' é o volume calculado pela equação de Peng-Robinson e C_i a correção do volume. Este termo é obtido a partir da diferença entre o volume molar do composto *i*, calculado pelo método de contribuição de grupo "CG-VOL" (ELBRO et al., 1991), e o volume molar v_i^{EOS} dado pela equação de estado à pressão atmosférica:

$$C_i = \sum_j n_{i,j} \Delta v_{i,j} - v_i^{EOS}(P_{atm})$$

Eq.2. 29

sendo $n_{i,j}$ a quantidade de cada um dos grupos presentes na molécula *i*, e $\Delta v_{i,j}$ o volume molar de cada grupo na temperatura *T*.

b) Fugacidade da fase sólida

A expressão da fugacidade do composto *i* na fase sólida pode ser obtida a partir da seguinte relação de Maxwell:

$$\left(\frac{\partial \mu_i}{\partial P}\right)_T = \left(\frac{\partial v}{\partial n_i}\right)_{T,P,n_{j\neq i}}$$

Eq.2. 30

em que μ_i representa o potencial químico e n_i o número de moles do componente *i*.

A expressão anterior pode ser reescrita em termos da fugacidade como:

$$\left(\frac{\partial \ln f_i^S}{\partial P}\right)_T = \frac{\overline{v_i^S}}{RT}$$

Eq.2. 31

em que v_i^S representa o volume parcial molar da fase sólida.

Integrando-se a Eq.2. 31, chega-se à expressão:

$$\ln f_i^S(P) = \ln f_i^S(P_0) + \frac{1}{RT}\int_{P_0}^{P} \overline{v_i^S} dP$$

Eq.2. 32

O termo $\ln f_i^S(P_0)$ representa a fugacidade da fase sólida do composto *i* à pressão de referência P_0, que é, por conveniência, geralmente igual à pressão atmosférica. Observado que $f_i^{S_0}(P_0)$ é a fugacidade do composto *i* em fase sólida pura na mesma pressão de referência, o termo $\ln f_i^S(P_0)$ é igual a (COSTA et al., 2007a):

$$f_i^S(P_0) = x_i^S \gamma_i^S(P_0) f_i^{S_0}(P_0)$$

Eq.2. 33

O coeficiente de atividade $\gamma_i^S(P_0)$, que traduz os desvios da idealidade da solução sólida à pressão de referência, é calculado a partir de um modelo de energia livre de excesso. De acordo com a Eq.2.2, os coeficientes de atividade das fases sólida e líquida podem ser relacionados em função da entalpia de fusão dos componentes puros. Os estados de referência (*T* e *P*) podem escolhidos de forma que nenhuma transição sólido-sólido necessite ser considerada. A Eq. 2.2 pode ser reescrita em função das fugacidades das fases sólidas e líquida, que no estado de referência fica igual a:

$$\ln \frac{f_i^{S_0}(P_0)}{f_i^{L_0}(P_0)} = -\frac{\Delta H_i^{fus}}{RT}\left(1 - \frac{T}{T_i^{fus}}\right)$$

Eq.2. 34

Combinando-se a Eq.2. 33 e a Eq.2. 34 pode-se expressar a fugacidade do componente *i* na fase sólida à pressão P_0:

$$f_i^S(P_0) = x_i^S \gamma_i^S(P_0) f_i^{L_0}(P_0) \exp\left[-\frac{\Delta H_i^{fus}}{RT}\left(1 - \frac{T}{T_i^{fus}}\right)\right]$$

Eq.2. 35

O segundo termo $\frac{1}{RT}\int_{P_0}^{P} \overline{v_i^S} dP$ da Eq.2. 32 é conhecido como fator de Poynting que reflete o efeito da pressão sobre a fugacidade do composto *i* na fase sólida. Os volumes parciais molares $\overline{v_i^S}$ são grandezas particularmente delicadas de serem medidas no caso de soluções sólidas. Para contornar este problema, Pauly e colaboradores (2000) supuseram que estes volumes parciais molares em fase sólida fossem proporcionais aos volumes molares da fase líquida com a seguinte relação:

$$\overline{v_i^S} = \beta \overline{v_i^{L_0}}$$

Eq.2. 36

Esta relação proporcional foi verificada para os compostos puros de parafinas a partir de dados publicados por Shaerer et al. (1955). No entanto, é essencial contabilizar o

volume de excesso, como por exemplo, indicado no trabalho de Pauly (PAULY et al., 2000) o qual se baseia nos trabalhos de cristalografia de Chevallier e coladoradores (CHEVALLIER et al., 1999a; CHEVALLIER et al., 1999b; CHEVALLIER et al., 1999c) e Dirand et al. (1998), para estimar um novo valor do coeficiente β, ajustado em 0,90 no caso de uma fase cristalina ortorrômbica.

Para álcoois graxos, a estrutura cristalina da fase sólida geralmente encontrada é ortorrômbica (KOLP e LUTTON, 1951; YAMAMOTO et al., 1990; VENTOLA et al., 2002; VENTOLA et al., 2004b). Já no caso dos ésteres etílicos ainda existem poucos estudos na literatura de suas propriedades físicas e nenhum trabalho sobre a estrutura cristalina dos mesmos foi encontrada. Assim foram testados alguns valores de β para verificar qual o valor que melhor se enquadrava na modelagem.

No caso de alcanos, como mostrado no trabalho de Milhet et al. (2005), mais de um tipo de estrutura cristalina pode ser encontrada para as substâncias puras, para alguns alcanos ortorrômbica, para outros rotatória, assim o valor de β variou na modelação conforme a mistura trabalhada e não foi fixada como feito no trabalho original de Pauly et al. (PAULY et al., 2000). Em todos os casos, este coeficiente é assumido como sendo independente da pressão, de modo que o fator de Poynting pode ser facilmente integrado (PAULY et al., 2000):

$$\frac{1}{RT}\int_{P_0}^{P}\overline{v_i^S}\,dP = \frac{\beta}{RT}\int_{P_0}^{P}\overline{v_i^{L_0}}\,dP = \beta\ln\frac{f_i^{L_0}(P)}{f_i^{L_0}(P_0)}$$

Eq.2. 37

Ao combinar as diferentes equações discutidas acima, a expressão final da fugacidade do componente *i* na fase sólida à temperatura *T* e pressão *P* é escrita como:

$$f_i^S(P) = x_i^S\gamma_i^S(P_0)\left[f_i^{L_0}(P_0)\right]^{1-\beta}\left[f_i^{L_0}(P)\right]^{\beta}\exp\left[-\frac{\Delta H_i^{fus}}{RT}\left(1-\frac{T}{T_i^{fus}}\right)\right]$$

Eq.2. 38

O coeficiente de atividade γ_i^S pode ser descrito pelo modelo UNIQUAC preditivo proposto por Coutinho et al. (COUTINHO et al., 2006). O modelo para o ESL sob altas

pressões pode ser considerado então como um método preditivo que usa no cálculo do comportamento das fases apenas as propriedades dos compostos puros, com a possibilidade de um ajuste com os dados experimentais. Uma discussão adicional deste modelo UNIQUAC encontra-se no item *2.2.2. Modelos para coeficiente de atividade*.

2.2.4. Desvios de idealidade da fase sólida

Quando se trata de modelagem termodinâmica, são poucos os trabalhos que representam os desvios de idealidade da fase sólida. O que geralmente se assume, e em alguns casos é aplicável, é que na fase sólida os compostos são imiscíveis. Mas pela experiência e pelas análises já realizadas, para ácidos graxos, álcoois graxos e outras substâncias graxas esta regra não se aplica na maior parte dos casos.

A modelagem termodinâmica do ESL de misturas binárias que possuem solução sólida tem sido aplicada em diferentes áreas. Como exemplo pode-se mencionar os hidrocarbonetos de cadeia longa (ceras) que exibem misturas não ideais tanto na fase líquida, como na fase sólida ($\gamma_i^L \neq 1$ e $\gamma_i^S \neq 1$) (HIMAWAN et al., 2006). Existem na literatura, trabalhos focados em encontrar um modelo apropriado para descrever os coeficientes de atividade da fase sólida e assim, avaliar a capacidade dos parâmetros em descrever misturas multicomponentes (WON, 1986; HANSEN et al., 1988; PEDERSEN et al., 1991; COUTINHO et al., 1996; LIRAGALEANA et al., 1996; COUTINHO, 1999). Equações de estado também têm sido aplicadas (JI et al., 2004).

Slaughter e Doherty (1995) propuseram uma metodologia para o cálculo dos diagramas de fases que apresentam ponto peritético e assim representar os desvios de idealidade da fase sólida. Para os autores, o ponto peritético pode ser descrito como sendo um novo produto gerado por uma reação química (aA + bB ↔ cC), ou associação física, entre os compostos puros em proporção estequiométrica. Este novo composto pode ter uma nova estrutura cristalina ou a mesma estrutura de um dos compostos puros. No método o composto peritético formado é o produto de uma reação química com uma constante de equilíbrio (*K*) dada por:

$$K = \prod_{i=1}^{d} \left(x_i^s \gamma_i^s \right)^{v_i}$$

onde v_i é o coeficiente estequiométrico do componente *i* e *d* é o número de componentes na fase sólida. A constante de equilíbrio é relacionada com a variação da energia livre de Gibbs da reação (ΔG_{ij}°):

$$K = \exp\left(-\frac{\Delta G_{ij}^{\circ}}{RT} \right)$$

A hipótese que na fase sólida os componentes são imiscíveis ($x_i^s \gamma_i^s = 1$), tornaria a constante da reação (*K*) igual a 1 e assim, $\Delta G_{ij}^{\circ} = 0$. Para evitar esta inconsistência, Slaughter and Doherty (1995) propuseram um modelo simples para calcular o coeficiente de atividade da fase sólida:

$$\gamma_i^s = \frac{1}{x_i^s + \varepsilon}$$

Eq.2. 39

em que ε é um número positivo (geralmente proposto como $\varepsilon = 10^{-4}$). Note que este modelo gera uma situação muito próxima da completa imiscibilidade dos compostos na fase sólida. Deve-se ainda ter em mente que, durante a fusão, o novo composto sólido formado se dissocia completamente, o que acarreta o desaparecimento dos seus termos da equação de equilíbrio na fase líquida.

2.2.5. Diagramas de equilíbrio sólido–líquido

Este item discute os diagramas de fases de sistemas binários, alguns dos tipos de diagramas mais comumente encontrados nos sistemas orgânicos. Além disso, discute-se como usar dados termodinâmicos para construir os diagramas de fases.

Para misturas graxas muitos autores indicaram que vários sistemas apresentam dois tipos de comportamento: aqueles que possuem apenas o ponto eutético e sistemas que apresentam os pontos eutético e peritético. Este último surge normalmente devido à

formação de um composto na fase sólida com ponto de fusão incongruente (COSTA, 2004; HIMAWAN et al., 2006). Um terceiro tipo de diagramas de fases, que segundo a literatura também pode ser encontrado nos sistemas graxos, é aquele com formação de solução sólida nas extremidades do diagrama de fases no caso de substâncias solidificarem com diferentes estruturas cristalinas (ARONS e LOOS, 1994; SATO, 2001).

Sistemas binários de álcoois graxos apresentaram três comportamentos distintos assim como apresentado em trabalho anterior (CARARETO, 2010): sistemas com ponto eutético simples, sistemas com ponto eutético e peritético e também sistemas sem reação eutética e/ou peritética. Nestes últimos sistemas há, provavelmente, a formação de solução sólida ao longo de toda a faixa de composição do diagrama de fases, seguindo o comportamento descrito por Bailey (1950) para o sistema composto por ácido palmítico e ácido margárico assim, como para sistemas formados por parafinas (COUTINHO et al., 1996).

Antes de apresentar alguns dos possíveis tipos de diagrama de fases binário, é importante discutir a regra de fases de Gibbs que relaciona o número de variáveis intensivas (graus de liberdade *F*) que podem ser fixadas de forma arbitrária, quando um sistema de *N* fases e *C* componentes está em equilíbrio. A regra das fases de Gibbs é dada pela seguinte relação (FEGLEY, 2012):

$$F = C - N + 2$$

Eq.2. 40

O número de componentes de um sistema, *C*, é o número de variáveis independentes necessárias para se estabelecer a composição de todas as fases. O número de graus de liberdade, *F*, faz referência ao número de variáveis intensivas independentes (*T*, *P*, concentração) que devem ser especificadas para que se determine o estado de um sistema (RICCI, 1966). No caso de um sistema binário, $C = 2$, assim $F = 2 - N + 2$. Se considerarmos um ponto invariante do sistema, ou seja, em que $F = 0$, tem-se que $0 = 2 - N + 2$, portanto, $N = 4$. Para um sistema que a pressão seja mantida constante, o número de fases que podem coexistir em equilíbrio torna-se $N = 3$, de forma que nenhuma das outras variáveis (temperatura ou composição) possa ser alterada sem que ocorra uma

modificação no número de fases presentes. Isso significa dizer que para um sistema binário à pressão constante, o número máximo de fases que pode coexistir é igual a três.

a) Diagrama de fases com ponto eutético simples

Para este tipo de diagrama, os dois componentes da mistura são completamente imiscíveis na fase sólida, e são completamente solúveis um no outro no estado líquido (FEGLEY, 2012). A palavra eutética é derivada da palavra grega *eutektos*, o que significa "fácil para derreter". A reação eutética é definida como uma reação reversível isotérmica de uma fase líquida (l) que se transforma em duas fases sólidas diferentes, α e β, durante o resfriamento da mistura (GAMSJAGER et al., 2008). Em um sistema binário,

$$l \leftrightarrow \alpha + \beta$$

A reação de equilíbrio ocorre ao longo da linha eutética, na temperatura eutética (T_{eut}) representada na Fig.2. 2a. Na composição eutética (x_{eut}) as concentrações das fases líquida e sólida são iguais. As fases sólidas podem ser os componentes puros (no caso da total imiscibilidade dos componentes no estado sólido) ou misturas de fases sólidas (quando há a formação de solução sólida) (GAMSJAGER et al., 2008). A linha eutética (com temperatura T_{eut}) e o ponto eutético (com composição x_{eut}) são invariantes isobáricas do sistema, e representam a composição e a temperatura mínima de fusão do sistema em questão. No diagrama da Fig.2. 2a, a T_{eut} representa a linha solidus (----) do sistema, ou seja, abaixo desta temperatura a mistura está completamente sólida.

No diagrama também estão representadas as temperaturas de fusão dos compostos hipotéticos ($T_{fus,\alpha}$ e $T_{fus,\beta}$). Diferentemente de um composto puro, uma mistura apresenta uma região, após a temperatura eutética, em que a fase líquida coexiste com a fase sólida, como pode ser observado na Fig.2. 2a. A linha liquidus (—) é a curva que delimita as ESL na parte superior do diagrama. Acima desta curva apenas líquido pode existir. Se observarmos o cruzamento da linha liquidus e da linha solidus, elas se encontram no ponto eutético E. De acordo com a regra das fases de Gibbs (Eq.2. 40), em um sistema binário à pressão constante, somente 3 fases podem coexistir, assim, o ponto eutético E atende à regra das fases já que neste ponto as fases α, β e l estão em equilíbrio.

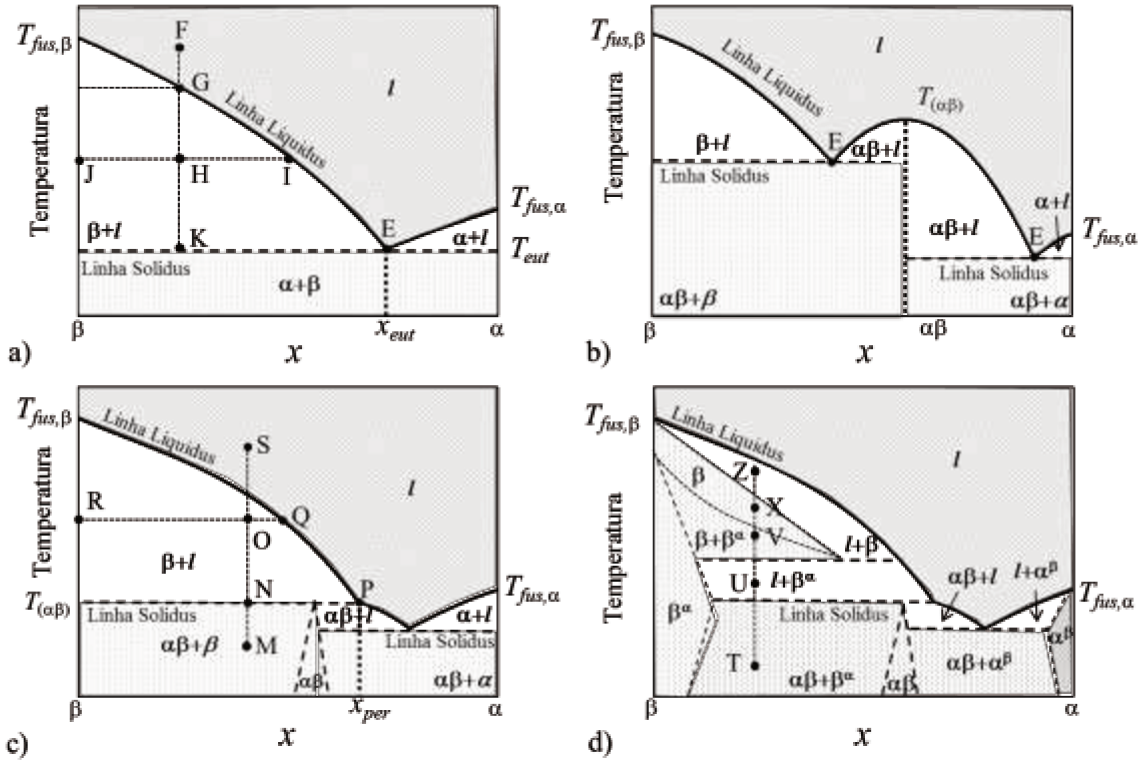

Fig.2. 2. Diagrama de fases do sistema binário formado pelos compostos α e β. A) sistema com ponto eutético simples; b) sistema com formação de composto com ponto de fusão congruente; c) sistema com formação de composto com ponto de fusão incongruente e; d) sistema com formação de solução sólida nos extremos do diagrama e reação metatética. *l* representa a fase líquida; αβ representa o composto peritético formado, β^{α} representa a solução sólida rica no composto β e; α^{β} representa a solução sólida rica no composto α.

Se uma solução, representada pelo ponto F, é resfriada até atingir o ponto G na linha liquidus, nesta temperatura cristais do composto β são formados e o resfriamento posterior da mistura faz com que a composição da fase líquida varie ao longo da curva liquidus. Por exemplo, se a temperatura for abaixada até H, neste ponto pode-se encontrar uma mistura formada pelos cristais puros de β e uma solução líquida de composição correspondente ao ponto I e a proporção de cada uma das fases em equilíbrio é determinada pela relação entre os segmentos de reta $\overline{HI} : \overline{HJ}$, conhecida como a regra da alavanca (NÝVLT, 1977). Continuando o resfriamento da mistura quando a temperatura é igual à temperatura

eutética, no ponto K, os cristais do composto β estão em equilíbrio com uma solução líquida de composição x_{eut}.

b) Diagramas de fases com ponto peritético

Muitos diagramas de fase (incluindo aqueles para os metais, compostos orgânicos, sais, óxidos, e silicatos) incluem a formação de compostos intermediários além da reação eutética. Os compostos intermediários podem decompor-se em uma temperatura abaixo da temperatura eutética, acima da temperatura eutética ou fundir de forma congruente (FEGLEY, 2012).

O comportamento de fusão do composto formado pode ser categorizado em termos de congruência ou incongruência. Os diagramas esquemáticos para sistemas binários com ponto de fusão congruente e incongruente são apresentados na Fig.2. 2b e Fig.2. 2c, respectivamente. No primeiro caso, a fusão do composto formado leva diretamente a uma região de líquido, com a coexistência de sólido e líquido em uma única temperatura (o ponto de fusão do composto - $T_{(\alpha\beta)}$) e, assim, o líquido tem a mesma composição que o sólido que o originou (representado pela linha αβ na Fig.2. 2b). O diagrama de fase de um sistema com o composto que funde de modo congruente exibe um ponto máximo na linha liquidus que corresponde à $T_{(\alpha\beta)}$. Como regra geral, esta temperatura máxima de fusão divide o diagrama de fases em duas regiões que contêm cada uma, um ponto eutético (observe na Fig.2. 2b que existem dois pontos de inflexão na curva, relativos a cada um dos pontos eutéticos). Exemplos de misturas que formam um composto de fusão congruente são: o sistema água + ácido sulfúrico (NÝVLT, 1977) e o sistema magnésio + silício que forma silicato de magnésio (Mg_2Si) (NAYEB-HASHEMI e CLARK, 1984). Observe na Fig. 2.2b que o ponto E, assim como no caso do sistema com ponto eutético simples, está de acordo com a regra das fases de Gibbs já que existem três fases em equilíbrio: β, αβ e *l*.

Já a fusão incongruente acontece quando o composto formado funde a uma temperatura inferior ao ponto de fusão de um (ou ambos) os componentes da mistura, o composto fundem gerando um líquido (contendo um ou ambos os componentes), e um

sólido geralmente um dos componentes puros (na Fig.2. 2c representado pela região β+*l*). Durante o aquecimento do composto com fusão incongruente, existe um intervalo de temperatura de coexistência líquido-sólido antes da sua fusão completa (região αβ+*l* na Fig.2. 2c). Ele é denominado incongruente porque, a sua fusão resulta em um sólido e um líquido, ambos tendo composições diferentes da composição do sólido que os originou. Na Fig.2. 2c, se uma mistura sólida formada pelo composto puro β e pelo composto αβ, representada pelo ponto M, é aquecida até atingir o ponto N na linha solidus, nesta temperatura os dois componentes da mistura (αβ e β) estão em equilíbrio com uma solução líquida de concentração expressa pelo ponto P. Acima desta temperatura o composto αβ deixa de existir e uma região de ESL formada por β+*l* é obtida. No ponto O, por exemplo, uma solução líquida de composição Q está em equilíbrio com cristais de β, em uma razão que também pode ser obtida pela regra da alavanca, em que a fração de cristais β é calculada pela relação entre os segmentos de reta $\overline{OQ}:\overline{RQ}$. Com posterior aquecimento da mistura até o ponto S, somente uma fase líquida de composição M estará então presente no sistema.

O ponto P na Fig.2. 2c é chamado de ponto peritético, que é também um ponto invariável, e em geral, assim como o ponto eutético, é a intersecção de duas curvas liquidus (FEGLEY, 2012). Observe na Fig.2. 2c que o ponto P está separando duas regiões diferentes de ESL, (l + β) e (l + αβ). A reação peritética é definida como uma reação isotérmica e reversível entre duas fases, uma líquida e uma sólida, que durante o resfriamento resulta em uma nova fase sólida (também chamado de composto peritético) (GAMSJAGER et al., 2008). Por exemplo, num sistema binário:

$$l + \beta \leftrightarrow \alpha\beta$$

O estado de equilíbrio ocorre ao longo da linha peritética, caracterizado pela temperatura peritética (T_{per}). A composição peritética (x_{per}) e a temperatura peritética, invariantes isobáricas do sistema, definem o ponto peritético P.

c) Reação metatética e solução sólida

As misturas orgânicas, principalmente quando os componentes possuem formas e tamanhos moleculares muito similares ou iguais, podem apresentar uma solubilidade parcial no estado sólido, normalmente formando uma solução sólida nos extremos dos diagramas de fases. Essas soluções têm pequenas quantidades de um dos componentes da mistura dissolvido no outro, gerando regiões de solubilidade semelhante àquelas mostradas na Fig.2. 2d (em que as soluções sólidas formadas são representadas por β^{α} e α^{β}, solução sólida rica no composto β e solução sólida rica no composto α, respectivamente). Para a maior parte dos sistemas graxos, que são formados por moléculas parecidas, este comportamento é comumente encontrado (VENTOLA et al., 2002; VENTOLA et al., 2004a,b; COSTA et al., 2009a,b,c; CARARETO et al., 2011; COSTA et al., 2011).

Para alguns sistemas binários de ácidos graxos saturados os diagramas de fases se mostraram ainda mais complexos, apresentando além dos pontos eutético e peritético, outra transição que é associada à reação metatética (COSTA et al., 2007b; COSTA et al., 2009a,b,c).

A reação metatética é uma reação isotérmica reversível de uma fase sólida, β, que se transforma em uma fase sólida diferente, β^{α}, mais uma fase líquida, *l*, durante o resfriamento de um sistema (GAMSJAGER et al., 2008). Durante o aquecimento, o líquido e o sólido β^{α}, que são gerados pela reação peritética se recristalizam em uma nova fase sólida β, que, com o aumento da temperatura, começa a se fundir dando origem à região de ESL, em que a fase sólida β está em equilíbrio com o líquido gerado pela fusão:

$$\beta \leftrightarrow \beta^{\alpha} + l$$

A reação metatética também está representada na Fig.2. 2d. Para compreender o diagrama de fases, pode-se, por exemplo, avaliar o comportamento da mistura no ponto T. Neste ponto, a dadas temperatura e concentração, se encontram em equilíbrio duas fases sólidas, $\alpha\beta + \beta^{\alpha}$, a primeira referente ao composto peritético formado (com ponto de fusão incongruente) e a segunda referente à solução sólida formada. Aquecendo-se a mistura até o ponto U, como anteriormente explicado, o composto peritético deixa de existir (na sua temperatura de fusão caracterizada pela linha solidus) e uma solução líquida é formada,

portanto neste ponto o que se tem é uma região de ESL. Aumentando-se a temperatura do sistema até o ponto V, a solução líquida é recristalizada e uma nova fase sólida é formada, devido à reação metatética, e assim, no ponto V, existe uma região em que duas fases sólidas estão coexistindo ($\beta+\beta^{\alpha}$). Com um novo aumento da temperatura (ponto X) a solução sólida β^{α} deixa de existir e, neste ponto X, encontra-se uma região monofásica em que somente β existe. Já no ponto Z é possível encontrar líquido originado da fusão parcial de β, estando este ponto em uma região de ESL.

No tipo de diagrama representado na Fig. 2.2d é possível verificar que a regra de fases de Gibbs também está sendo respeitada em termos dos números de fases presentes em equilíbrio. Em nenhum dos pontos invariantes do sistema (cruzamento das linhas liquidus e solidus) existem mais do que 3 fases em equilíbrio, assim como foi discutido para os outros diagramas apresentados na Fig.2.2.

2.2.6. Caracterização das fases do equilíbrio sólido-líquido

As características das diferentes fases sólidas que podem coexistir no equilíbrio já foram e vem sendo amplamente estudadas empregando diferentes técnicas e procedimentos. Algumas destas técnicas são discutidas na sequência.

a) Difração de raios-X

Uma ferramenta eficiente para caracterização das diferentes fases sólidas é a difração de raios-X. Esta técnica pode ser utilizada de diversas formas para a caracterização de aspectos específicos destes diagramas. O difratograma pode ser utilizado para a identificação das fases, além de estabelecer fronteiras para um sistema. Por exemplo, em um sistema de dois componentes, parâmetros de rede podem variar com a composição dentro de uma região de uma única fase, mas também podem ser invariantes em uma região de duas fases (SMITH, 2008).

A difração de raios-X é usada para se obter características importantes sobre a estrutura cristalina de um material. O resultado se dá pelo fenômeno físico da difração, ou seja, quando os raios-X incidem sobre a estrutura cristalina eles podem penetrar na rede

cristalina ou ser difratados se colidirem com as moléculas que formam o cristal. Com a detecção dos raios difratados é possível traçar o desenho da rede cristalina do material em estudo.

Ventolà e colaboradores (VENTOLA et al., 2002; VENTOLA et al., 2004a,b) utilizaram a difração de raios-X para avaliar o ESL de misturas binárias de álcoois graxos e identificaram diferentes estruturas cristalinas (ou fases polimórficas) para estas misturas. Os autores mostraram que as estruturas que são formadas podem ser monoclínica ou hexagonal e também observaram miscibilidade total ou parcial na fase sólida em função do tipo de mistura binária

b) Espectroscopia de FT-Raman

As espectroscopias Raman e no Infravermelho (FT-IR) são geralmente usadas para obter informações sobre a estrutura e propriedades das moléculas a partir de suas transições vibracionais (LEWIS e MCELHANEY, 2002). A alteração dos movimentos vibracionais das moléculas ocorre com maior intensidade nos sólidos e nos líquidos e são classificados principalmente em estiramento e dobramento. Se a molécula é constituída por mais átomos é fácil imaginar que esses movimentos podem ocorrer ao mesmo tempo, aumentando a complexidade do trabalho.

A combinação de outros métodos espectrométricos com a espectroscopia Raman está sempre presente na literatura como forma de confirmar ou aprimorar resultados. Infelizmente, quando se trata do estudo de sistemas graxos, a quantidade encontrada de trabalhos deixa muito a desejar.

Há quase duas décadas atrás, a difração de raios-X associada à espectroscopia Raman resultou em um trabalho sobre a estrutura cristalina do ácido esteárico (KOBAYASHI et al., 1984). Os autores estudaram apenas a forma β desse ácido através da difração de raios-X e através da espectroscopia Raman foi realizado um estudo minucioso das interações interlamelares da cadeia graxa.

c) Espectroscopia no Infravermelho com transformada de Fourier (FT-IR)

A FT-IR classifica-se como uma análise de infravermelho com comprimento de onda médio (IR-médio) na região entre 2500 a 50000 nm. Até o início da década de 1980, a maioria dos instrumentos para a região do IR-médio era do tipo dispersivo e empregava redes de difração. Entretanto, desde aquele tempo, a instrumentação para o IR-médio modificou-se drasticamente, de tal forma que atualmente a maioria dos instrumentos é baseada em transformada de Fourier. Após este aprimoramento da técnica ela começou a ser utilizada em estudos de microscopia de superfícies, análises de sólidos por refletância total atenuada e por refletância difusa, entre outras (HOLLER et al., 2009).

Inoue e colaboradores (2004c) utilizaram o FT-IR para caracterizar cada uma das fases de misturas binárias de ácido oléico + ácido esteárico e ácido oléico + ácido behênico e também para monitorar eventos moleculares associados à mudança de temperatura das misturas. A partir dos espectros de FT-IR foi possível identificarem a imiscibilidade dos componentes da mistura na fase sólida. Zeng et al. (2009), também utilizaram análises de DSC e FT-IR associadas para caracterizar o ESL de mistura binária de 1-tetradecanol + ácido palmítico e observando os resultados para diferentes frações molares de mistura concluíram que o ácido e o álcool não apresentam miscibilidade na fase sólida, ou seja, cristalizam como sólidos puros. A associação de diferentes técnicas experimentais também foi utilizada no trabalho de Gbabode et al. (2009). Para a mistura de ácido pentadecanóico e ácido hexadecanóico foram utilizados DSC, difração de raios-X e FT-IR. As análises de FT-IR foram essenciais para identificar algumas formas polimórficas que somente com as análises de raios-X não puderam ser caracterizadas.

d) Calorimetria exploratória diferencial (DSC)

A calorimetria exploratória diferencial é uma técnica calorimétrica relativamente recente e derivada da análise térmica diferencial (DTA) (COUTINHO e RUFFIER-MERAY, 1998). Nesta técnica, uma referência e a amostra são aquecidas a uma taxa constante e quando algum evento térmico ocorre, o equipamento detecta a diferença de temperatura entre elas e calcula a quantidade de calor absorvida ou liberada pela amostra. A

técnica de DSC apresenta uma grande vantagem com relação às técnicas visuais de determinação de ELS, pois é capaz de medir transições de fases sólido-sólido que normalmente não podem ser observadas através de técnicas visuais. Muitos dos trabalhos aqui citados utilizaram a técnica de DSC para a determinação dos diagramas de fase de sistemas formados por substâncias graxas (COUTINHO e RUFFIER-MERAY, 1998; GANDOLFO et al., 2003; GANDOLFO et al., 2004; INOUE et al., 2004a,b,c; COSTA et al., 2007b; COSTA et al., 2009a,b,c; CARARETO et al., 2011; COSTA et al., 2011; KOUAKOU et al., 2013).

2.2.7. Calorimetria exploratória diferencial com modulação de temperatura

Esta secção se dedica a uma revisão mais aprofundada da Calorimetria exploratória diferencial com modulação de temperatura (TMDSC - do inglês *Temperature Modulated Differential Scanning Calorimetry*), uma técnica que é pouco utilizada na caracterização do ESL. Nas duas últimas décadas, várias técnicas de TMDSC foram propostas para se obter informações adicionais àquelas disponíveis a partir de DSC convencional (HOLUBOVÁ et al., 2013).

De acordo com as leis de equilíbrio termodinâmico, a temperatura de uma substância pura se mantém constante até que a sua cristalização ou fusão seja completada, isto é, enquanto duas fases coexistirem (Regra das fases de Gibbs) (WUNDERLICH et al., 1997). O fluxo de calor medido durante estes processos, fusão ou cristalização, é governado pelas propriedades da amostra e também depende do instrumento de medida. Ou seja, o fluxo de calor medido depende do calor latente total, da resistência térmica da amostra, de parâmetros experimentais como taxa de aquecimento ou amplitude de modulação e dos perfis de temperatura (HEMMINGER e HÖHNE, 1984; HEMMINGER e CAMMENGA., 1989). Este último fator também é função da condutividade térmica dos materiais que formam a célula, o cadinho e a própria amostra. Por isso os dados de DSC obtidos durante uma transição de primeira ordem nunca representam um pico infinitamente acentuado, como um pulso de Dirac, como exigido pela regra das fases, mas variam de acordo com os diferentes tipos de calorímetro e parâmetros experimentais. Por exemplo, um menor

gradiente de calor devido a uma baixa resistência térmica entre o forno e a amostra, reduz a constante de tempo do instrumento, encurtando o tempo necessário para a amostra completar a transição. Além disso, o DSC pode ser controlado por sensores perto do aquecedor ou da amostra. Neste último caso, o retardo no tempo de leitura da temperatura é aumentado ou diminuído substancialmente durante as análises.

A calorimetria exploratória diferencial e algumas recentes extensões do modo modulado, como a TMDSC, são métodos frequentemente usados no estudo de cinética de reações e de reações reversíveis de primeira ordem. A TMDSC é uma ferramenta de análise térmica útil para distinguir as transições termodinâmicas das transições que ocorrem única e exclusivamente pelas taxas de aquecimento empregadas. Estas últimas, não necessariamente são de interesse no estudo do ESL. A distinção destas transições é feita expondo a amostra simultaneamente a diferentes taxas de aquecimento: uma taxa de aquecimento básica, ou linear, e uma taxa de aquecimento que varia periodicamente, correspondendo a uma modulação de amplitude (GILL et al., 1993; READING et al., 1993). A taxa de fluxo de calor resultante, normalmente é separada por uma transformada de Fourier discreta.

A TMDSC foi uma proposta da empresa TA Instruments e, alguns anos após a sua inserção no mercado, a norte-americana Perkin-Elmer apresentou uma nova ferramenta para o DSC que ficou conhecida como *Stepscan* DSC. A técnica *stepscan* DSC só pode ser utilizada em equipamentos de compensação de potência com tempo de resposta rápido e com amostras de massa muito pequena (na ordem de 5 mg) (PIELICHOWSKI et al., 2004).

O *stepscan* DSC consiste na aplicação de ciclos que intercalam uma etapa de aquecimento (ou resfriamento) em uma taxa linear em um pequeno intervalo de temperatura seguido de uma etapa em que a amostra é mantida isotérmica até que o fluxo de calor estabilize abaixo de um critério pré-determinado. Segundo o fabricante, o *stepscan* DSC consegue separar transições reversíveis de transições de efeito cinético assim como o TMDSC, porém o algoritmo de cálculo não está disponível na literatura, por ser ainda uma patente ativa (BAICHOO et al., 2006). A principal vantagem da técnica *stepscan* é o fato de que a mesma não utiliza fluxo de calor com taxas de aquecimento variáveis como é requerido no caso da técnica TMDSC, o que torna mais fácil a calibração do equipamento.

Apesar destas diferenças ambas as técnicas têm as mesmas aplicações, embora ainda seja difícil encontrar trabalhos que utilizem a técnica *stepscan* na literatura.

Em ambos os casos, TMDSC e *stepscan* DSC, o mesmo conceito é aplicado e com o objetivo de separar mudanças no calor específico do fluxo de calor devido a processos cinéticos deve-se representar o fluxo de calor em função do tempo $\left(\frac{dq}{dt}\right)$ em dois componentes distintos:

$$\left(\frac{dq}{dt}\right) = Cp(T).\beta + \frac{dq}{dt}(T,t)$$

Eq.2. 41

em que $\beta = \frac{dT}{dt}$ é a taxa linear de aquecimento/resfriamento e $\frac{dq}{dt}(T,t)$ representa o fluxo de calor em um determinando instante de tempo devido a processos cinéticos relativos ao comportamento da amostra.

Existem quatro parâmetros que devem ser controlados em uma análise de *stepscan* DSC (Fig.2. 3): o intervalo de temperatura entre dois segmentos isotérmicos subsequentes (ΔT), a taxa de aquecimento linear (β), o período em que a amostra fica em estado isotérmico Δt e o critério de estabilidade do fluxo de calor (em mW) durante o estado isotérmico. Este último parâmetro é usado para encurtar a etapa isotérmica, ou seja, se o fluxo de calor que deve ser fornecido para a amostra, de forma que ela permaneça a uma certa temperatura, for menor do que o critério de estabilidade a etapa isotérmica é interrompida antes mesmo que o tempo total pré-determinado seja cumprido e um novo ciclo de aquecimento é iniciado. Um critério de estabilidade menor requer um tempo maior na etapa isotérmica, mas permite uma maior precisão na medição (SANDOR et al., 2002). Para a calibração do equipamento uma taxa de aquecimento relativamente lenta (por exemplo, de 2 °C min^{-1}) é recomendada, porque a taxa de aquecimento global é geralmente lenta nas análises de *stepscan*.

Após ser atingido o critério de equilíbrio da amostra em uma dada temperatura, a temperatura é aumentada ou diminuída em um intervalo (em função da taxa de aquecimento/resfriamento β) e, novamente, a etapa isotérmica é iniciada no novo valor de

temperatura que fora estabelecido, até que o Δt ou o critério de estabilidade sejam atingidos novamente. O componente reversível do fluxo de calor é calculado na parte do ciclo de aquecimento e o componente irreversível apenas na etapa isotérmica. O tempo em que a amostra permanece na etapa isotérmica varia e pode ser controlado pelo software do equipamento, que permite que a amostra atinja um estado próximo do equilíbrio térmico na temperatura determinada (BAICHOO et al., 2006).

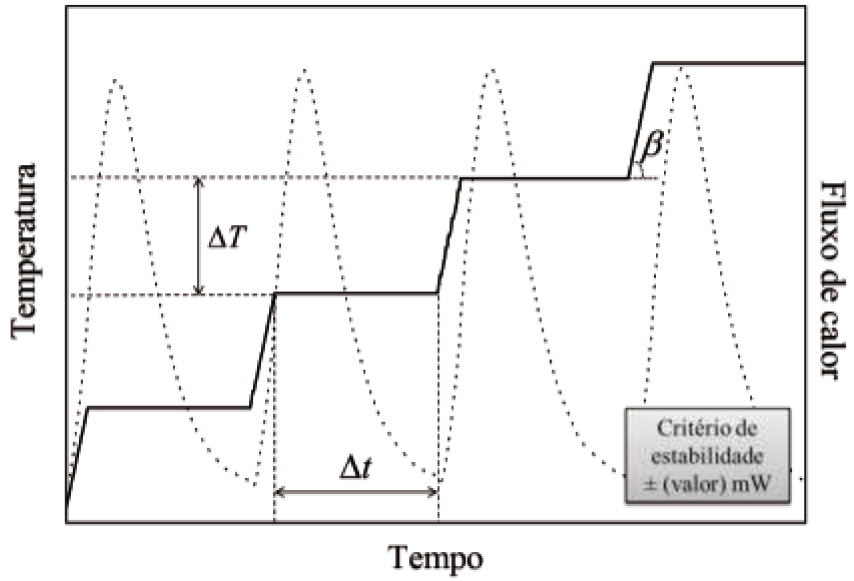

Fig.2. 3. Esquema de temperatura e fluxo de calor em uma análise de *stepscan* DSC em função do tempo de análise.

Depois de realizada a coleta de dados utilizando a análise de *stepscan*, em uma série de intervalos de temperaturas igualmente espaçados, é possível gerar uma curva térmica que tem o perfil como o apresentado na Fig.2. 4 para o 1-octanol. Os pequenos picos (linha em azul na Fig.2. 4) representam cada um dos intercâmbios entre uma etapa de aquecimento e uma etapa isotérmica da resposta de *stepscan*. A interpretação dos resultados pode ser feita com a ajuda do software do equipamento. A resposta final é então separada em duas respostas diferentes: $Cp(T)$ e $\frac{dq}{dt}(T,t)$, este último representa o fluxo de calor devido a um processo cineticamente controlado.

A resposta de $Cp(T) = \left(\frac{dq}{dt}\right) \Big/ \left(\frac{dT}{dt}\right)$ reflete os eventos reversíveis (ou termodinâmicos) da amostra, como por exemplo, uma transição de fase como a fusão ou de transição vítrea (na Fig.2. 4 representado pela linha preta em destaque). A resposta cinética, ou $\frac{dq}{dt}(T,t)$, reflete processos irreversíveis que ocorrem durante o experimento, como relaxação ou cristalização de uma fase metaestável (na Fig.2. 4 representado pela fina linha preta). Perceba que as curvas cinética e termodinâmica apresentam picos muito próximos e cada um destes picos representa uma resposta. No caso da curva termodinâmica o pico equivale à transição de fases sólida para líquida e para a curva cinética, o pico é, muito provavelmente, associado à presença de uma transição polimórfica metaestável. O fluxo de calor da resposta termodinâmica (linha preta em destaque na Fig.2. 4) pode ser obtido por integração da curva de calor específico.

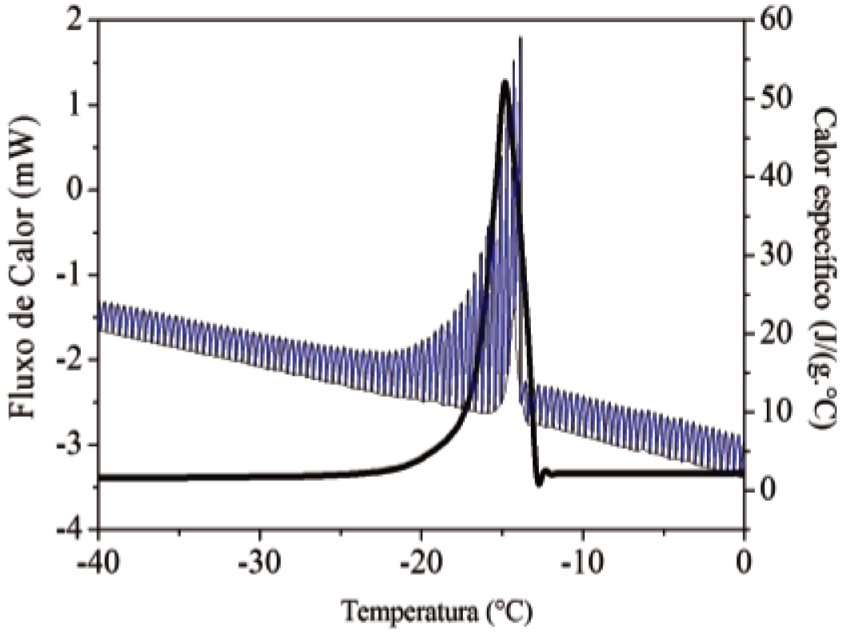

Fig.2. 4. Resposta do *stepscan* DSC para 1-octanol. Parâmetros de análises: $\Delta T = 2°C$, $\beta = 2°C/\min$, $\Delta t = 2$ min e critério de estabilidade = ± 0.002 mW. Linha azul representa o fluxo de calor (mW) para a análise de *stepscan*; linha preta fina representa o sinal de *stepscan* para o componente cinético (em mW) e; linha preta em destaque representa o sinal de *stepscan* para o componente termodinâmico (em J/(g.°C)).

É importante salientar que a técnica *stepscan* DSC, ainda que promissora, é pouco usada como ferramenta de estudos do equilíbrio de fases, embora a mesma técnica já seja bem difundida para o estudo de transição vítrea e outras transições (SANDOR et al., 2002; ČERNOŠEK et al., 2003; HOLUBOVÁ et al., 2009; HOLUBOVÁ et al., 2013) ou ainda na determinação do calor específico (MERZLYAKOV e SCHICK, 2001; PIELICHOWSKI et al., 2004). Desta forma, os trabalhos apresentados nesta tese são pioneiros no que diz respeito ao uso da técnica para se determinar o ESL em sistemas graxos.

2.3. Ponto de fulgor

A pressão de vapor de um composto inflamável é uma propriedade termodinâmica importante por permitir avaliar sua volatilidade, estabilidade e segurança. O ponto de fulgor está associado à combustão de um composto volátil e assim define os parâmetros de segurança de armazenamento de um material combustível. Uma baixa volatilidade é indicada como responsável pela demora na ignição e pobre atomização de biodieseis (GUO et al., 2009).

O ponto de fulgor (FP) de um líquido inflamável é definido como a temperatura na qual a pressão de vapor desse líquido é suficiente para produzir uma concentração de vapor do composto inflamável no ar que corresponde ao menor limite de flamabilidade do mesmo (*LFL*) (LIAW et al., 2002; LIAW et al., 2004). Este parâmetro fornece o conhecimento necessário para a compreensão dos mecanismos de combustão de substâncias puras ou misturas. Além disso, é de importância prática, por considerações de segurança no armazenamento e transporte, processamento e manuseio de um dado composto. Enfim, é uma das principais propriedades utilizadas para avaliar os riscos de explosão e incêndio em locais de armazenamento e transporte de compostos químicos.

Alguns trabalhos que abordaram a predição do FP de compostos puros se basearam no conceito de contribuição de grupos funcionais das moléculas (PAN et al., 2007; GHARAGHEIZI e ALAMDARI, 2008; VALENZUELA et al., 2011; BAGHERI et al., 2012a; BAGHERI et al., 2012b; GHARAGHEIZI et al., 2012; HUKKERIKAR et al., 2012), gerando um conjunto de parâmetros específicos que permite estimar esta propriedade para substâncias em que os valores de ponto de fulgor inexistem ou são muito caros para ser obtidos.

Valores confiáveis de pontos de fulgor são sempre desejáveis, e podem ser medidos por dois métodos experimentais atualmente aceitos, os teste em uma câmara fechada ou aberta de ensaio (LIAW et al., 2008b). O valor do ponto de fulgor medido em câmara aberta é normalmente maior do que o valor obtido por meio da utilização do teste em câmara fechada (LIAW et al., 2003a). Ambos são métodos de ensaio dinâmico que dependem da taxa de aquecimento que é específica para cada material. Existem métodos de

análise com taxas de aquecimento lentas disponíveis, tais como o Método de Ensaio ASTM D3941 (para tintas, resinas e produtos afins e produtos de elevada viscosidade na faixa de temperaturas de 0 °C a 110 °C), no qual as condições de ensaio estão próximas à situação de equilíbrio. É importante ressaltar que o ponto de fulgor deve, portanto, ser definido em termos de um método de ensaio padrão, e nenhuma correlação válida em geral pode ser garantida entre os resultados obtidos por diferentes métodos de teste, ou em aparelhos de teste diferentes do especificado (ASTM, 2011).

Para produtos provenientes do petróleo e biodiesel, existem normas específicas como a ASTM D93 (ASTM, 2011) para equipamentos de ponto de fulgor de câmara fechada, com uma taxa de aquecimento, velocidade de rotação do agitador da mistura e intervalos de temperatura do teste de chama específicos. No caso do biodiesel, em que a norma ASTM D93 é aplicada no procedimento C, deve-se operar o equipamento aplicando-se uma taxa de aquecimento de 3 °C min^{-1}, na qual o sistema de agitação da amostra deve ter uma velocidade de rotação de 90 a 120 rpm. Nestas condições os testes de ignição devem ser iniciados a uma temperatura de 24 °C abaixo daquela que se estima ser o ponto de fulgor e os testes de ignição subsequentes devem ser realizados a cada 2 °C.

A qualidade do biodiesel, como já mencionado, depende de vários fatores e é um reflexo de suas características químicas e físicas. O FP do biodiesel é uma propriedade importante, pois está relacionada com a segurança durante toda a produção, armazenamento e transporte do mesmo. O biodiesel apresenta alto ponto de fulgor (geralmente entre 160-170 °C) se comparado com combustíveis de origem mineral cujo ponto de fulgor mínimo pode ser próximo de 38 °C (ANP, 2009). Com relação ao FP mínimo regulamentado para biodiesel (ASTM, 2012) a temperatura mínima fixada é de 130 ºC. Mesmo quantidades muito pequenas de álcool presente podem provocar uma diminuição significativa no ponto de fulgor e, portanto, de acordo com os regulamentos, tanto o teor de álcool e o ponto de fulgor devem ser determinados para cada lote de biodiesel produzido. Vários métodos de análise foram concebidos para a determinação do álcool residual no biodiesel. A maioria usa cromatografia gasosa e, mais recentemente, análises de espectrofotometria NIR, que faz uso de ferramentas quimiométricas (FELIZARDO et al., 2007). Um novo método mais simples, de baixo custo, foi proposto para a análise quantitativa de álcool residual no

biodiesel por meio de determinação do ponto de fulgor e mostrou resultados válidos para biodieseis metílicos e etílicos de óleo de soja e milho e de gordura bovina (BOOG et al., 2011).

2.3.1. Termodinâmica do equilíbrio líquido-vapor associada ao ponto de fulgor de misturas

Para o caso de uma mistura formada por dois componentes inflamáveis, com vapores dos componentes 1 e 2 dissolvidos no ar, a relação entre a composição da fase vapor e o limite de flamabilidade de cada um dos compostos, LFL_1 e LFL_2, pode ser descrita pela regra de Le Chatelier (1891), conforme Eq.2. 42. O ponto de fulgor de um composto inflamável está relacionado com a sua volatilidade a pressão ambiente. Quando em mistura o FP de um composto também depende das forças de interação com os outros componentes da mistura.

$$1 = \sum \frac{y_i}{LFL_i} = \frac{y_1}{LFL_1} + \frac{y_2}{LFL_2}$$

Eq.2. 42

em que y_i representa a fração molar do composto *i* na fase vapor.

A partir da definição de FP para um composto puro, o menor limite de flamabilidade do componente *i*, LFL_i, é expresso em função da pressão de vapor desse componente no FP, $P_{i,fp}^{sat}$, como mostra a Eq.2. 43, onde P é a pressão ambiente (LIAW et al., 2002).

$$LFL_i = \frac{P_{i,fp}^{sat}}{P}$$

Eq.2. 43

A composição da substância inflamável *i* na fase vapor pode se obtida a partir do equilíbrio líquido-vapor (ELV). Para cada componente *i* da mistura, a condição de equilíbrio entre a fase líquida e a fase vapor a baixas pressões é dada pela Eq.2. 44.

$$y_i \phi_i P = x_i \gamma_i f_i$$

Eq.2. 44

Considerando baixos valores de P, é possível admitir que a fase vapor tenha o comportamento de um gás ideal, assim o ϕ_i para o componente *i* assume o valor igual a 1. Considera-se que a fugacidade do líquido puro *i*, f_i, a *T* e *P* do sistema, pode ser aproximada por sua pressão de vapor, assim como mostra a Eq.2. 45. Então, a relação de ELV se reduz a Eq.2. 46 e, substituindo as Eq.2. 45 e Eq.2. 46 na Eq.2. 42, temos a Eq.2. 47 (LIAW et al., 2002).

$$f_i \cong P_i^{sat}$$

Eq.2. 45

$$y_i = \frac{x_i \gamma_i P_i^{sat}}{P}$$

Eq.2. 46

$$1 = \sum \frac{x_i \gamma_i P_i^{sat}}{P_{i,fp}^{sat}} = \frac{x_1 \gamma_1 P_1^{sat}}{P_{1,fp}^{sat}} + \frac{x_2 \gamma_2 P_2^{sat}}{P_{2,fp}^{sat}}$$

Eq.2. 47

A pressão de vapor varia com a temperatura para uma substância pura *i*, e pode ser estimada pela Eq.2. 48, conhecida como equação de Antoine. A pressão de vapor de uma substância pura *i* no seu FP como apresentado na Eq.2. 47 pode ser estimada substituindo-se $T_{i,fp}$ na Eq.2. 48.

$$\log P_i^{sat} = A_i - \frac{B_i}{T + C_i}$$

Eq.2. 48

Embora as constantes para a equação de Antoine sejam bem definidas para uma vasta gama de compostos, como o etanol, por exemplo, no caso dos ésteres etílicos não existem valores para as constantes de Antoine com validade para uma ampla faixa de temperatura, incluindo a temperatura ambiente que é de interesse para armazenamento destes compostos. Por isso, quando se trata de ésteres é necessário o uso de um modelo

preditivo do tipo contribuição de grupos. Nesta tese utilizou-se o método desenvolvido especialmente para substâncias graxas proposto por Ceriani e Meirelles (2004).

Em uma mistura ideal o coeficiente de atividade é igual à unidade ($\gamma_i\big|_{\forall i} = 1$), assim a Eq.2. 42 pode ser reduzida para uma forma simples. Esta suposição é razoável para misturas cujos componentes possuem muita similaridade, como, por exemplo, vários ésteres etílicos presentes nos diferentes tipos de biodiesel. No caso de misturas contendo etanol e os componentes do biodiesel a não-idealidade da mistura deve ser considerada e o coeficiente de atividade pode ser estimado usando modelos termodinâmicos como Margules, NRTL, Wilson ou UNIQUAC (LIAW et al., 2002; LIAW e CHIU, 2003; LIAW et al., 2004; LIAW e CHIU, 2006; LIAW e LIN, 2007; LIAW et al., 2008a; OLIVEIRA et al., 2011) ou a partir de um método de contribuição de grupos como UNIFAC (LIAW et al., 2011).

Os parâmetros de interação binários dos modelos termodinâmicos são tipicamente obtidos a partir de dados de equilíbrio líquido-vapor (ELV) ou líquido-líquido (ELL). Vários trabalhos da literatura mostraram que estes parâmetros de ELV ou ELL podem predizer o FP de misturas miscíveis ou parcialmente miscíveis com uma boa correlação (LIAW et al., 2002; LIAW e CHIU, 2003; LIAW et al., 2003a; LIAW et al., 2003b; LIAW et al., 2004; LIAW e CHIU, 2006; LIAW e LIN, 2007; LIAW et al., 2008a; LIAW et al., 2008b). Infelizmente, no caso de misturas de ésteres etílicos ou biodiesel e etanol, são poucos ou não existem dados de ELV ou ELL, e por consequência, nenhum parâmetro de interação está disponível na literatura para as condições de temperatura e pressão de interesse deste trabalho, dificultando a predição do ponto de fulgor de misturas de biodiesel e etanol.

Existem diferentes métodos para o cálculo de parâmetros de interação binários usando dados de ELL e ELV, cada um deles tem suas próprias características, dificuldades e incertezas associadas. Noorollahy e colaboradores (2010) propuseram o uso de medidas de ponto de fulgor para determinar os parâmetros de interação binária de ELV em função das equações descritas anteriormente. Dados de ELV ou ELL fornecidos na literatura para algumas misturas binárias de etanol, 1-propanol, 1-butanol, 2-butanol, 1-octanol, n-octano, água e ácido propiônico foram comparados e se mostraram compatíveis com aqueles

calculados à partir das análises de ponto de fulgor das misturas correspondentes. A rapidez e facilidade de aquisição das análises são umas das grandes vantagens do método de determinação dos parâmetros dos modelos de coeficiente de atividade a partir de dados experimentais de ponto de fulgor.

Algumas misturas podem gerar temperaturas mínima (LIAW et al., 2003a) ou máxima (LIAW e LIN, 2007) do FP, no caso de desvio positivo ou negativo da idealidade, respectivamente. Exemplos de misturas que apresentam mínimo de fulgor são octano + 1-butanol e metil acrilato + metanol (LIAW et al., 2003a). E misturas que apresentam desvios negativos de idealidade, e com isso, ponto de máximo de fulgor são acetofenona + fenol e ciclohexilamina + ciclohexano (LIAW e LIN, 2007). Um modo simples de se compreender este efeito sobre o comportamento do FP é que desvios negativos da idealidade significam que as interações entre as moléculas da mistura na fase líquida, em uma dada concentração, são mais atrativas/fortes em relação às interações das substâncias puras, assim, as moléculas tem preferência por permanecer na fase líquida, o que acarreta no aumento da temperatura na qual o LFL dos compostos será atingido. A conclusão inversa é feita quando os desvios da idealidade da fase líquida são positivos, assim a "preferência" das moléculas em permanecer na fase vapor, abaixando a temperatura na qual os LFLs são atingidos.

Dos exemplos anteriores, todos os componentes das misturas eram substâncias inflamáveis, porém as mesmas em misturas com água podem ter uma flamabilidade característica, maior, menor ou igual ao valor das substâncias puras. Deste modo, existem modelos na literatura para se predizer o FP de soluções aquosas com compostos orgânicos (LIAW e CHIU, 2003). Para ressaltar a importância da compreensão do comportamento do FP de soluções aquosas, vale a pena descrever a experiência de uma empresa de descarte de resíduos químicos de Taiwan para a qual foi proposto diluir com água resíduos altamente inflamáveis de forma a aumentar o FP destas misturas e diminuir os riscos de estocagem. No entanto, o resultado da diluição das soluções de resíduos com água revelou que o FP das soluções de resíduos não aumentou como se esperava, mas a quantidade de soluções de resíduos a ser tratada aumentara substancialmente, elevando o custo global e o risco de estocagem dos resíduos (LIAW e CHIU, 2003).

Referências

ABRAMS, D. S.; PRAUSNITZ, J. M. Statistical thermodynamics of liquid mixtures: A new expression for the excess Gibbs energy of partly or completely miscible systems. **AICHE Journal,** v. 21, n. 1, p. 116-128, 1975.

ANP, A. N. D. P. **RESOLUÇÃO ANP Nº 42 Gás Natural e Biocombustíveis**. Brasil 2009.

ARONS, J. D. S.; LOOS, T. W. D. Phase Behavior: Phenomena, Significance, and Models. In: SANDLER, S. I. (Ed.). **Models for thermodynamic and phase equilibria calculations**. New York: arcel Dekker, Inc, 1994. p.363-505.

ASTM. **D93 34/99 Standard Test Methods for Flash Point by Pensky-Martens Closed Cup Tester** 2011.

ASTM, S. **D6751-12 Standard Specification for Biodiesel Fuel Blend Stock (B100) for Middle Distillate Fuels**. West Conshohocken, PA: ASTM International 2012.

BAGHERI, M.; BAGHERI, M.; HEIDARI, F.; FAZELI, A. Nonlinear molecular based modeling of the flash point for application in inherently safer design. **Journal of Loss Prevention in the Process Industries,** v. 25, n. 1, p. 40-51, 2012a.

BAGHERI, M.; BORHANI, T. N. G.; ZAHEDI, G. Estimation of flash point and autoignition temperature of organic sulfur chemicals. **Energy Conversion and Management,** v. 58, n. 0, p. 185-196, 2012b.

BAICHOO, N.; MACNAUGHTAN, W.; MITCHELL, J.; FARHAT, I. A STEPSCAN Differential Scanning Calorimetry Study of the Thermal Behavior of Chocolate. **Food Biophysics,** v. 1, n. 4, p. 169-177, 2006.

BAILEY, A. E. **Melting and solidification of fats**. New York: Interscience publishers, 1950.

BAJPAI, D.; TYAGI, V. K. Biodiesel: source, production, composition, properties and its benefits. **J. Oleo Sci.,** v. 55, n. 10, p. 87 - 502, 2006.

BLOOM, M.; EVANS, E.; MOURITSEN, O. G. Physical properties of the fluid lipid-bilayer component of cell membranes: a perspective. **Quarterly Reviews of Biophysics,** v. 24, n. 03, p. 293-397, 1991.

BOOG, J. H. F.; SILVEIRA, E. L. C.; CALAND, L. B.; TUBINO, M. Determining the residual alcohol in biodiesel through its flash point. **Fuel,** v. 90, p. 905-907, 2011.

CANOIRA, L.; ALCÁNTARA, R.; GARCIA-MARTÍNEZ, M. J.; CARRASCO, J. Biodiesel from Jojoba oil-wax: Transesterification with methanol and properties as a fuel. **Biomass and Bioenergy,** v. 30, n. 1, p. 76-81, 2006.

CARARETO, N. D. D. **Estudo do equilíbrio sólido-líquido em sistemas binários de álcoois graxos através da Calorimetria Exploratória Diferencial**. 2010. Dissertação (Mestre em Engenharia de Alimentos). Departamento de Engenharia de Alimentos, UNICAMP, Campinas.

CARARETO, N. D. D.; COSTA, M. C.; ROLEMBERG, M. P.; KRÄHENBÜHL, M. A.; MEIRELLES, A. J. A. The solid–liquid phase diagrams of binary mixtures of even saturated fatty alcohols. **Fluid Phase Equilibria,** v. 303, n. 2, p. 191.e1-191.e8, 2011.

CARARETO, N. D. D.; KIMURA, C. Y. C. S.; OLIVEIRA, E. C.; COSTA, M. C.; MEIRELLES, A. J. A. Flash points of mixtures containing ethyl esters or ethylic biodiesel and ethanol. **Fuel,** v. 96, n. 0, p. 319-326, 2012.

CERIANI, R.; GANI, R.; MEIRELLES, A. J. A. Prediction of heat capacities and heats of vaporization of organic liquids by group contribution methods. **Fluid Phase Equilibria,** v. 283, n. 1-2, p. 49-55, 2009.

ČERNOŠEK, Z.; HOLUBOVÁ, J.; ČERNOŠKOVÁ, E. Non-isothermal structural relaxation and the glass transition temperature. **Solid State Sciences,** v. 5, n. 8, p. 1087-1093, 2003.

CHEVALLIER, V.; PETITJEAN, D.; BOUROUKBA, M.; DIRAND, M. Mixtures of numerous different n-alkanes: 2. Studies by X-ray diffraction and differential thermal analyses with increasing temperature. **Polymer,** v. 40, n. 8, p. 2129-2137, 1999a.

CHEVALLIER, V.; PETITJEAN, D.; RUFFIER-MERAY, V.; DIRAND, M. Correlations between the crystalline long c-parameter and the number of carbon atoms of pure n-alkanes. **Polymer,** v. 40, n. 21, p. 5953-5956, 1999b.

CHEVALLIER, V.; PROVOST, E.; BOURDET, J. B.; BOUROUKBA, M.; PETITJEAN, D.; DIRAND, M. Mixtures of numerous different n-alkanes: 1. Structural studies by X-ray diffraction at room temperature—Correlation between the crystallographic long c parameter and the average composition of multi-alkane phases. **Polymer,** v. 40, n. 8, p. 2121-2128, 1999c.

COSTA, M. C. **Determinação Experimental e Modelagem Termodinâmica do Equilíbrio Sólido-Líquido de Misturas Binárias de Ácidos Graxos Saturados usando a Calorimetria Exploratória Diferencial**. 2004. Dissertação (Mestre em Engenharia Química). Faculdade de Engenharia Química, Universidade Estadual de Campinas, Campinas.

COSTA, M. C.; BOROS, L. A. D.; BATISTA, M. L. S.; COUTINHO, J. A. P.; KRÄHENBÜHL, M. A.; MEIRELLES, A. J. A. Phase diagrams of mixtures of ethyl palmitate with fatty acid ethyl esters. **Fuel,** v. 91, n. 1, p. 177-181, 2012.

COSTA, M. C.; BOROS, L. A. D.; COUTINHO, J. O. A. P.; KRAHENBUHL, M. A.; MEIRELLES, A. J. A. Low-Temperature Behavior of Biodiesel: Solid–Liquid Phase Diagrams of Binary Mixtures Composed of Fatty Acid Methyl Esters. **Energy & Fuels,** v. 25, n. 7, p. 3244-3250, 2011.

COSTA, M. C.; KRAHENBUHL, M. A.; MEIRELLES, A. J. A.; DARIDON, J. L.; PAULY, J.; COUTINHO, J. A. P. High pressure solid-liquid equilibria of fatty acids. **Fluid Phase Equilibria,** v. 253, n. 2, p. 118-123, 2007a.

COSTA, M. C.; ROLEMBERG, M. P.; BOROS, L. A. D.; KRAHENBUHL, M. A.; DE OLIVEIRA, M. G.; MEIRELLES, A. J. A. Solid-liquid equilibrium of binary fatty acid mixtures. **Journal of Chemical and Engineering Data,** v. 52, n. 1, p. 30-36, 2007b.

COSTA, M. C.; ROLEMBERG, M. P.; MEIRELLES, A. J. A.; COUTINHO, J. A. P.; KRÄHENBÜHL, M. A. The solid-liquid phase diagrams of binary mixtures of even saturated fatty acids differing by six carbon atoms. **Thermochimica Acta,** v. 496, n. 1-2, p. 30-37, 2009a.

COSTA, M. C.; SARDO, M.; ROLEMBERG, M. P.; COUTINHO, J. A. P.; MEIRELLES, A. J. A.; RIBEIRO-CLARO, P.; KRAHENBUHL, M. A. The solid-liquid phase diagrams of binary mixtures of consecutive, even saturated fatty acids. **Chemistry and Physics of Lipids,** v. 160, n. 2, p. 85-97, 2009b.

COSTA, M. C.; SARDO, M.; ROLEMBERG, M. P.; RIBEIRO-CLARO, P.; MEIRELLES, A. J. A.; COUTINHO, J. A. P.; KRAHENBUHL, M. A. The solid-liquid phase diagrams of binary mixtures of consecutive, even saturated fatty acids: differing by four carbon atoms. **Chemistry and Physics of Lipids,** v. 157, n. 1, p. 40-50, 2009c.

COUTINHO, J. A. P. Predictive local composition models: NRTL And UNIQUAC and their application to model solid–liquid equilibrium of n-alkanes. **Fluid Phase Equilibria,** v. 158–160, p. 447–457, 1999.

COUTINHO, J. A. P.; GONÇALVES, M.; PRATAS, M. J.; BATISTA, M. L. S.; FERNANDES, V. F. S.; PAULY, J.; DARIDON, J. L. Measurement and modeling of biodiesel cold-flow properties. **Energy & Fuels,** v. 24, n. 4, p. 2667-2674, 2010.

COUTINHO, J. A. P.; KNUDSEN, K.; ANDERSEN, S. I.; STENBY, E. H. A Local Composition Model For Paraffinic Solid Solutions. **Chemical Engineering Science,** v. 51, p. 3273, 1996.

COUTINHO, J. A. P.; MIRANTE, F.; PAULY, J. A new predictive UNIQUAC for modeling of wax formation in hydrocarbon fluids. **Fluid Phase Equilibria,** v. 247, n. 1–2, p. 8-17, 2006.

COUTINHO, J. A. P.; RUFFIER-MERAY, V. A new method for measuring solid-liquid equilibrium phase diagrams using calorimetry. **Fluid Phase Equilibria,** v. 148, p. 147-160, 1998.

DIJKSTRA, A. J.; SEGERS, J. C. Production and Refining of Oils and Fats. In: (Ed.). **The Lipid Handbook with CD-ROM, Third Edition**: CRC Press, 2007. p.143-262.

DIRAND, M.; CHEVALLIER, V.; PROVOST, E.; BOUROUKBA, M.; PETITJEAN, D. Multicomponent paraffin waxes and petroleum solid deposits: structural and thermodynamic state. **Fuel,** v. 77, n. 12, p. 1253-1260, 1998.

ELBRO, H. S.; FREDENSLUND, A.; RASMUSSEN, P. Group contribution method for the prediction of liquid densities as a function of temperature for solvents, oligomers, and polymers. **Industrial & Engineering Chemistry Research,** v. 30, n. 12, p. 2576-2582, 1991/12/01 1991.

FEGLEY, B. **Practical Chemical Thermodynamics for Geoscientists**. St. Louis: Academic Press, 2012.

FELIZARDO, P.; BAPTISTA, P.; MENEZES, J. C.; CORREIA, M. J. N. Multivariate near infrared spectroscopy models for predicting methanol and water content in biodiesel. **Analytica Chimica Acta,** v. 595, n. 1–2, p. 107-113, 2007.

FISK, P. R.; WILDEY, R. J.; GIRLING, A. E.; SANDERSON, H.; BELANGER, S. E.; VEENSTRA, G.; NIELSEN, A.; KASAI, Y.; WILLING, A.; DYER, S. D.; STANTON, K. Environmental properties of long chain alcohols. Part 1: Physicochemical, environmental fate and acute aquatic toxicity properties. **Ecotoxicology and Environmental Safety,** v. 72, n. 4, p. 980-995, 2009.

FREDENSLUND, A.; JONES, R. L.; PRAUSNITZ, J. M. Group contribution estimation of activity coefficients in non ideal liquid mixtures. **AIChE Journal,** v. 21, p. 1086-1099, 1975.

GAMSJAGER, H.; LORIMER, J. W.; SCHARLIN, P.; SHAW, D. G. Glossary of terms related to solubility. **Pure and Applied Chemistry,** v. 80, n. 2, p. 233-276, 2008.

GANDOLFO, F.; BOT, A.; FLÖTER, E. Structuring of edible oils by long-chain FA, fatty alcohols, and their mixtures. **Journal of the American Oil Chemists' Society,** v. 81, n. 1, p. 1-6, 2004.

GANDOLFO, F. G.; BOT, A.; FLOTER, E. Phase diagram of mixtures of stearic acid and stearyl alcohol. **Thermochimica Acta,** v. 404, n. 1-2, p. 9-17, 2003.

GBABODE, G.; NEGRIER, P.; MONDIEIG, D.; MORENO, E.; CALVET, T.; CUEVAS-DIARTE, M. À. Fatty acids polymorphism and solid-state miscibility: Pentadecanoic acid–hexadecanoic acid binary system. **Journal of Alloys and Compounds,** v. 469, n. 1–2, p. 539-551, 2009.

GHARAGHEIZI, F.; ALAMDARI, R. F. Prediction of Flash Point Temperature of Pure Components Using a Quantitative Structure–Property Relationship Model. **QSAR & Combinatorial Science,** v. 27, n. 6, p. 679-683, 2008.

GHARAGHEIZI, F.; ILANI-KASHKOULI, P.; FARAHANI, N.; MOHAMMADI, A. H. Gene expression programming strategy for estimation of flash point temperature of non-electrolyte organic compounds. **Fluid Phase Equilibria,** v. 329, n. 0, p. 71-77, 2012.

GILL, P.; SAUERBRUNN, S.; READING, M. Modulated differential scanning calorimetry. **Journal of Thermal Analysis and Calorimetry,** v. 40, n. 3, p. 931-939, 1993.

GUNSTONE, F. D.; **PADLEY, F. B. Lipid Technologies and Applications**. Marcel Dekker, 1997. ISBN 9780824798383.

GUO, Y.; YANG, F.; XING, Y.; LI, D.; FANG, W.; LIN, R. Study on volatility and flash point of the pseudo binary mixtures of sunflower-based biodiesel + methylcyclohexane. **Fluid Phase Equilibria,** v. 276, n. 2, p. 127-132, 2009.

GURR, M. I.; JAMES, A. T. **Lipid Biochemistry: an Introduction**. Cornell University Press, 1971. ISBN 9780801406522.

HANSEN, J. H.; FREDENSLUND, A.; PEDERSEN, K. S.; RONNINGSEN, H. P. Thermodynamic Model for Predicting Wax Formation in Crude Oils. **AICHE Journal,** v. 34, p. 1937, 1988.

HARWOOD, J. L.; SCRIMGEOUR, C. M. Fatty Acid and Lipid Structure. In: (Ed.). **The Lipid Handbook with CD-ROM, Third Edition**: CRC Press, 2007. p.1-36.

HEMMINGER, W. F.; CAMMENGA., H. K. Methoden der thermischen Analyse. **Crystal Research and Technology,** v. 24, n. 11, p. 1187-1187, 1989.

HEMMINGER, W. F.; HÖHNE, G. **Calorimetry**. Weinheim: VCH, 1984.

HIMAWAN, C.; STAROV, V. M.; STAPLEY, A. G. F. Thermodynamic and kinetic aspects of fat crystallization. **Advances in Colloid and Interface Science,** v. 122, n. 1-3, p. 3-33, 2006.

HOLLER, F. J.; SKOOG, D. A.; SATNLEY, R. C. **Princípios de Análise Instrumental**. 6. Porto Alegre: Bookman, 2009.

HOLUBOVÁ, J.; ČERNOŠEK, Z.; ČERNOŠKOVÁ, E. The selenium based chalcogenide glasses with low content of As and Sb: DSC, StepScan DSC and Raman spectroscopy study. **Journal of Non-Crystalline Solids,** v. 355, n. 37–42, p. 2050-2053, 2009.

HOLUBOVÁ, J.; ČERNOŠKOVÁ, E.; ČERNOŠEK, Z. StepScan DSC. **Journal of Thermal Analysis and Calorimetry,** v. 111, n. 2, p. 1633-1638, 2013/02/01 2013.

HUKKERIKAR, A. S.; SARUP, B.; TEN KATE, A.; ABILDSKOV, J.; SIN, G.; GANI, R. Group-contribution+ (GC+) based estimation of properties of pure components: Improved property estimation and uncertainty analysis. **Fluid Phase Equilibria,** v. 321, n. 0, p. 25-43, 2012.

IMAHARA, H.; MINAMI, E.; SAKA, S. Thermodynamic study on cloud point of biodiesel with its fatty acid composition. **Fuel,** v. 85, n. 12-13, p. 1666-1670, 2006.

INOUE, T.; HISATSUGU, Y.; YAMAMOTO, R.; SUZUKI, M. Solid-liquid phase behavior of binary fatty acid mixtures 1. Oleic acid/stearic acid and oleic acid/behenic acid mixtures. **Chemistry and Physics of Lipids,** v. 127, n. 2, p. 143-152, 2004a.

INOUE, T.; HISATSUGU, Y.; SUZUKI, M.; WANG, Z. N.; ZHENG, L. Q. Solid-liquid phase behavior of binary fatty acid mixtures 3. Mixtures of oleic acid with capric acid (decanoic acid) and caprylic acid (octanoic acid). **Chemistry and Physics of Lipids,** v. 132, n. 2, p. 225-234, 2004b.

INOUE, T.; HISATSUGU, Y.; ISHIKAWA, R.; SUZUKI, M. Solid-liquid phase behavior of binary fatty acid mixtures 2. Mixtures of oleic acid with lauric acid, myristic acid, and palmitic acid. **Chemistry and Physics of Lipids,** v. 127, n. 2, p. 161-173, 2004c.

JI, H.-Y.; TOHIDI, B.; DANESH, A.; TODD, A. C. Wax phase equilibria: developing a thermodynamic model using a systematic approach. **Fluid Phase Equilibria,** v. 216, n. 2, p. 201-217, 2004.

JOHNSON, R. W. Fatty alcohols. In: JOHNSON, R. W. e FRITZ, E. (Ed.). **Fatty acids in industry**. New York: Marcel Dekker, 1988. p.217-231.

KNOTHE, G. Dependence of biodiesel fuel properties on the structure of fatty acid alkyl esters. **Fuel Processing Technology,** v. 86, n. 10, p. 1059-1070, 2005.

KNOTHE, G. “Designer” Biodiesel: Optimizing Fatty Ester Composition to Improve Fuel Properties. **Energy & Fuels,** v. 22, n. 2, p. 1358-1364, 2008/03/01 2008.

KOBAYASHI, M.; KOBAYASHI, T.; ITOH, Y.; SATO, K. Polytypism in Normal-Fatty Acids and Low-Frequency Raman-Spectra - Stearic-Acid β-Form. **Journal of Chemical Physics,** v. 80, n. 6, p. 2897-2903, 1984.

KOGAN, A.; GARTI, N. Microemulsion as transdermal drug delivery vehicles. **Adv. Colloid Interface Science,** v. 123-126, p. 369-385, 2006.

KOLP, D. G.; LUTTON, E. S. The polymorphism of n-hexadecanol and n-octadecanol. **Journal of American Chemical Society,** v. 73, p. 5593-5595, 1951.

KOUAKOU, A. C.; MAPIHAN, K. L.; PAULY, J. Solid-liquid equilibria under high pressure of pure fatty acid methyl esters. **Fuel,** v. 109, p. 297-302, 2013.

LE CHATELIER, H. Estimation of firedamp by flammability limits. **Annual Mines,** v. 19, n. 8, p. 388-395, 1891.

LEWIS, R.; MCELHANEY, R. N. Vibrational Spectroscopy of Lipids. In: CHALMERS, J. M. e GRIFFITHS, P. R. (Ed.). **Handbook of Vibrational Spectroscopy**. London: Wiley, v.5, 2002. p.3447 - 3464.

LIAW, H.-J.; CHEN, C.-T.; GERBAUD, V. Flash-point prediction for binary partially miscible aqueous-organic mixtures. **Chemical Engineering Science,** v. 63, n. 18, p. 4543-4554, 2008a.

LIAW, H.-J.; CHIU, Y.-Y. The prediction of the flash point for binary aqueous-organic solutions. **Journal of Hazardous Materials,** v. A101, p. 83-106, 2003.

LIAW, H.-J.; CHIU, Y.-Y. A general model for predicting the flash point of miscible mixtures. **Journal of Hazardous Materials,** v. 137, n. 1, p. 38-46, 2006.

LIAW, H.-J.; GERBAUD, V.; LI, Y.-H. Prediction of miscible mixtures flash-point from UNIFAC group contribution methods. **Fluid Phase Equilibria,** v. 300, n. 1-2, p. 70-82, 2011.

LIAW, H.-J.; LEE, T.-P.; TSAI, J.-S.; HSIAO, W.-H.; CEHN, M.-H.; HSU, T.-T. Binary liquid solutions exhibiting minimum flash-point behavior. **Journal of Loss Prevention in the Process Industries,** v. 16, p. 173-186, 2003a.

LIAW, H.-J.; LEE, Y.-H.; TANG, C.-L.; HSU, H.-H.; LIU, J.-H. A mathematical model for predicting the flash point of binary solutions. **Journal of Loss Prevention in the Process Industries,** v. 15, p. 429-438, 2002.

LIAW, H.-J.; LIN, S.-C. Binary mixtures exhibiting maximum flash-point behavior. **Journal of Hazardous Materials,** v. 140, n. 1-2, p. 155-164, 2007.

LIAW, H.-J.; LU, W.-H.; GERBAUD, V.; CHEN, C.-C. Flash-point prediction for binary partially miscible mixtures of flammable solvents. **Journal of Hazardous Materials,** v. 153, n. 3, p. 1165-1175, 2008b.

LIAW, H.-J.; TANG, C.-L.; LAI, J.-S. A model for predicting the flash point of ternary flammable solutions of liquid. **Combustion and Flame,** v. 138, n. 4, p. 308-319, 2004.

LIAW, H. J.; LEE, T. P.; TSAI, J. S.; HSIAO, W. H.; CHEN, M. H.; HSU, T. T. Binary liquid solutions exhibiting minimum flash-point behavior. **Journal of Loss Prevention in the Process Industries,** v. 16, n. 3, p. 173-186, 2003b.

LIN, L.; CUNSHAN, Z.; VITTAYAPADUNG, S.; XIANGQIAN, S.; MINGDONG, D. Opportunities and challenges for biodiesel fuel. **Applied Energy,** v. 88, n. 4, p. 1020-1031, 2011.

LIRAGALEANA, C.; FIROOZABADI, A.; PRAUSNITZ, J. M. Thermodynamics of wax precipitation in petroleum mixtures. **AICHE Journal,** v. 42, p. 239, 1996.

LOPES, J. C. A.; BOROS, L.; KRAHENBUHL, M. A.; MEIRELLES, A. J. A.; DARIDON, J. L.; PAULY, J.; MARRUCHO, I. M.; COUTINHO, J. A. P. Prediction of cloud points of biodiesel. **Energy & Fuels,** v. 22, n. 2, p. 747-752, Mar-Apr 2008.

MERZLYAKOV, M.; SCHICK, C. Step response analysis in DSC -- a fast way to generate heat capacity spectra. **Thermochimica Acta,** v. 380, n. 1, p. 5-12, 2001.

MILHET, M.; PAULY, J.; COUTINHO, J. A. P.; DIRAND, M.; DARIDON, J. L. Liquid–solid equilibria under high pressure of tetradecane + pentadecane and tetradecane + hexadecane binary systems. **Fluid Phase Equilibria,** v. 235, n. 2, p. 173-181, 2005.

MOSER, B. Biodiesel production, properties, and feedstocks. **In Vitro Cellular & Developmental Biology - Plant,** v. 45, n. 3, p. 229-266, 2009/06/01 2009.

MOSSELMAN, C. On the polymorphism and the enthalpies of phase-transition of 1-decanol, 1-dodecanol, 1-tetradecanol, 1-hexadecanol and 1-octadecanol. **Archiv Der Pharmazie,** v. 314, n. 3, p. 279-281, 1981.

NAYEB-HASHEMI, A. A.; CLARK, J. B. The Mg−Si (Magnesium-Silicon) system. **Bulletin of Alloy Phase Diagrams,** v. 5, n. 6, p. 584-592, 1984/12/01 1984.

NKWETTA, D. N.; HAGHIGHAT, F. Thermal energy storage with phase change material—A state-of-the art review. **Sustainable Cities and Society,** v. 10, n. 0, p. 87-100, 2014.

NOOROLLAHY, M.; MOGHADAM, A. Z.; GHASRODASHTI, A. A. Calculation of mixture equilibrium binary interaction parameters using closed cup flash point measurements. **Chemical Engineering Research and Design,** v. 88, n. 1, p. 81-86, 2010.

NOWECK, K.; GRAFAHREND, W. Fatty Alcohols. In: (Ed.). **Ullmann's Encyclopedia of Industrial Chemistry**: Wiley-VCH Verlag GmbH & Co. KGaA, 2000.

NÝVLT, J. **Solid-liquid phase-equilibria**. Amsterdam: Elsevier, 1977.

O'BRIEN, R. D. **Fats and Oils: Formulating and Processing for Applications**. CRC Press, 2008. ISBN 978-1-4200-6166-6.

OLIVEIRA, M. B.; BARBEDO, S.; SOLETTI, J. I.; CARVALHO, S. H. V.; QUEIMADA, A. J.; COUTINHO, J. A. P. Liquid-liquid equilibria for the canola oil biodiesel + ethanol + glycerol system. **Fuel,** v. 90, n. 8, p. 2738-2745, 2011.

PALMQUIST, D. L. Omega-3 fatty acids in metabolism, health, and nutrition and for modified animal product foods. **Professional Animal Scientist,** v. 25, n. 3, p. 207-249, 2009.

PAN, Y.; JIANG, J.; WANG, Z. Quantitative structure-property relationship studies for predicting flash points of alkanes using group bond contribution method with back-propagation neural network. **Journal of Hazardous Materials,** v. 147, n. 1-2, p. 424-430, 2007.

PAULY, J.; DARIDON, J.-L.; COUTINHO, J. A. P.; LINDELOFF, N.; ANDERSEN, S. I. Prediction of solid–fluid phase diagrams of light gases–heavy paraffin systems up to 200 MPa using an equation of state–GE model. **Fluid Phase Equilibria,** v. 167, n. 2, p. 145-159, 2000.

PEDERSEN, K. S.; SKOVBORG, P.; RONNINGSEN, H. P. Wax Precipitation From North Sea Crude Oils & Temperature Modeling. **Energy & Fuels,** v. 5, p. 924, 1991.

PÉNELOUX, A.; RAUZY, E.; FRÉZE, R. A consistent correction for Redlich-Kwong-Soave volumes. **Fluid Phase Equilibria,** v. 8, n. 1, p. 7-23, 1982.

PENG, D.-Y.; ROBINSON, D. B. A New Two-Constant Equation of State. **Industrial & Engineering Chemistry Fundamentals,** v. 15, n. 1, p. 59-64, 1976/02/01 1976.

PERNETTI, M.; MALSSEN, K. F. V.; FLÖTER, E.; BOT, A. Structuring of edible oils by alternatives to crystalline fat. **Current Opinion in Colloid & Interface Science,** v. 12, p. 221–231, 2007.

PIELICHOWSKI, K.; FLEJTUCH, K.; PIELICHOWSKI, J. Step-scan alternating DSC study of melting and crystallisation in poly(ethylene oxide). **Polymer,** v. 45, n. 4, p. 1235-1242, 2004.

PRAUSNITZ, J. M.; LICHTENTHALER, R. N.; AZEVEDO, E. G. A. **Molecular thermodynamics of fluid-phase equilibria**. 2. New Jersey: Prentice-Hall, 1986.

READING, M.; ELLIOTT, D.; HILL, V. A new approach to the calorimetric investigation of physical and chemical transitions. **Journal of Thermal Analysis and Calorimetry,** v. 40, n. 3, p. 949-955, 1993.

RENON, H.; PRAUSNITZ, J. M. Local compositions in thermodynamic excess functions for liquid mixtures. **AICHE Journal,** v. 14, n. 1, p. 135-144, 1968.

RICCI, J. E. **The Phase Rule and Heterogeneous equilibrium**. New York: Dover, 1966.

SANDLER, S. I. **Chemical and engineering thermodynamics**. 3. New York: John Wiley & Sons, Inc., 1999.

SANDOR, M.; BAILEY, N. A.; MATHIOWITZ, E. Characterization of polyanhydride microsphere degradation by DSC. **Polymer,** v. 43, n. 2, p. 279-288, 2002.

SATO, K. Crystallization behavior of fats and lipids - a review. **Chemical Engineering Science,** v. 56, p. 2255-2265, 2001.

SCHAERER, A. A.; BUSSO, C. J.; SMITH, A. E.; SKINNER, L. B. Properties of Pure Normal Alkanes in the C17 to C36 Range. **Journal of the American Chemical Society,** v. 77, n. 7, p. 2017-2019, 1955/04/01 1955.

SCHAINK, H. M.; VAN MALSSEN, K. F.; MORGADO-ALVES, S.; KALNIN, D.; VAN DER LINDEN, E. Crystal network for edible oil organogels: Possibilities and limitations of the fatty acid and fatty alcohol systems. **Food Research International,** v. 40, n. 9, p. 1185-1193, 2007.

SLAUGHTER, D. W.; DOHERTY, M. F. Calculation of Solid-Liquid Equilibrium and Crystallization Paths for Melt Crystallization Processes. **Chemical Engineering Science,** v. 50, n. 11, p. 1679-1694, 1995.

SMITH, A. L. Chapter 5 The quartz crystal microbalance. In: MICHAEL, E. B. e PATRICK, K. G. (Ed.). **Handbook of Thermal Analysis and Calorimetry**: Elsevier Science B.V., v.5, 2008. p.133-169.

TAN, J.; MCKENZIE, C.; POTAMITIS, M.; THORBURN, A. N.; MACKAY, C. R.; MACIA, L. Chapter Three - The Role of Short-Chain Fatty Acids in Health and Disease.

In: FREDERICK, W. A. (Ed.). **Advances in Immunology**: Academic Press, v.Volume 121, 2014. p.91-119.

TOSUN, I. Chapter 8 - Excess Mixture Properties and Activity Coefficients. In: (Ed.). **The Thermodynamics of Phase and Reaction Equilibria**. Amsterdam: Elsevier, 2013. p.271-349.

VALENZUELA, E. M.; VÁZQUEZ-ROMÁN, R.; PATEL, S.; MANNAN, M. S. Prediction models for the flash point of pure components. **Journal of Loss Prevention in the Process Industries,** v. 24, n. 6, p. 753-757, 2011.

VENTOLA, L.; CALVET, T.; CUEVAS-DIARTE, M. A.; MONDIEIG, D.; OONK, H. A. J. The C19H39OH-C20H41OH system: Experimental phase diagram and thermodynamic modelling. **Physical Chemistry Chemical Physics,** v. 4, n. 10, p. 1953-1956, 2002.

VENTOLA, L.; CALVET, T.; CUEVAS-DIARTE, M. A.; OONK, H. A. J.; MONDIEIG, D. Solid-solid and solid-liquid equilibria in the n-alkanols family: C18H37OH-C20H41OH system. **Physical Chemistry Chemical Physics,** v. 6, n. 13, p. 3726-3731, Jul 7 2004a.

VENTOLA, L.; CALVET, T.; CUEVAS-DIARTE, M. A.; RAMIREZ, M.; OONK, H. A. J.; MONDIEIG, D.; NEGRIER, P. Melting behaviour in the n-alkanol family. Enthalpy-entropy compensation. **Physical Chemistry Chemical Physics,** v. 6, n. 8, p. 1786-1791, 2004b.

WEIDLICH, U. E.; GMEHLING, J. A modified UNIFAC (Dortmund) model. 1. **Industrial & Engineering Chemistry Research,** v. 26, p. 1372-1381, 1987.

WILSON, G. M. Vapor-Liquid Equilibrium. XI. A New Expression for the Excess Free Energy of Mixing. **Journal of the American Chemical Society,** v. 86, n. 2, p. 127-130, 1964/01/01 1964.

WON, K. W. Thermodynamics for solid solution-liquid-vapor equilibria: wax phase formation from heavy hydrocarbon mixtures. **Fluid Phase Equilibria,** v. 30, p. 265-279, 1986.

WUNDERLICH, B.; BOLLER, A.; OKAZAKI, I.; ISHIKIRIYAMA, K. Heat-capacity determination by temperature-modulated DSC and its separation from transition effects. **Thermochimica Acta,** v. 304-305, n. 0, p. 125-136, 1997.

YAMAMOTO, T.; NOZAKI, K.; HARA, T. X-ray and thermal studies on the rotator phases of normal higher alcohols C17H35OH, C18H37OH, and their mixtures. **Journal of Chemical Physics,** v. 92, n. 1, p. 631-641, 1990.

YUAN, Y.; ZHANG, N.; TAO, W.; CAO, X.; HE, Y. Fatty acids as phase change materials: A review. **Renewable and Sustainable Energy Reviews,** v. 29, n. 0, p. 482-498, 2014.

ZENG, J. L.; CAO, Z.; YANG, D. W.; XU, F.; SUN, L. X.; ZHANG, L.; ZHANG, X. F. Phase diagram of palmitic acid-tetradecanol mixtures obtained by DSC experiments. **Journal of Thermal Analysis and Calorimetry,** v. 95, n. 2, p. 501-505, 2009.

Capítulo 3. Flash points of mixtures containing ethyl esters or ethylic biodiesel and ethanol

*Natália D. D. Carareto, Cecília Y. C. S. Kimura; Elis C. Oliveira; Mariana C. Costa; Antonio J. A. Meirelles**

EXTRAE, Department of Food Engineering, Faculty of Food Engineering, University of Campinas, UNICAMP, Campinas, Brazil.

Trabalho publicado na revista **Fuel** (2012), Doi:10.1016/j.fuel.2012.01.025.

Abstract

The flash points (FPs) of some pure fatty acid ethyl esters (FAEEs) and their mixtures with ethanol were measured in the present study. An empirical model to predict the FPs of pure FAEEs as a function of the number of carbon atoms and double bonds of the fatty acid residue chain was adjusted and the predictive equation agrees well with the experimental data (R^2 = 0.9753). NRTL parameters for the binary interaction between the components of the ethanol + FAEE systems were also adjusted assuming that they can be expressed as a function of the number of carbon atoms and double bonds of the fatty acid residue. Assuming that the interactions between FAEEs are ideal, the prior approach was tested for predicting the FPs of FAEE + ethanol multicomponent mixtures, i.e. mixtures similar to those found in all the stages of the ethylic biodiesel production process. The model was able to predict the experimental FP for different compositions of the palm oil biodiesel + ethanol system with minimal deviations.

Keywords

- Flash point
- Fatty acid ethyl esters (FAEEs)
- Ethylic biodiesel
- Ethanol

3.1. Introduction

Currently, biodiesel is an important alternative to conventional fossil-based diesel fuel. This biofuel is considered an environmentally friendly fuel, since it is nontoxic, and has low emission profiles compared to petroleum diesel and negligible sulfur content, and furthermore, offers many important technical advantages over petrodiesel, such as its inherent lubricity, higher flash point and biodegradability [1–3].

Biodiesel is obtained by transesterification of fatty feedstock with short-chain alcohols, usually methanol or ethanol, resulting in the conversion of triacylglycerol into mono-alkyl esters of long-chain fatty acids [1]. Therefore, properties of the biodiesel produced are dependent on the characteristics of the raw material and also the alcohol used in the reaction. In contrast to methanol, usually obtained from fossil sources, bioethanol is a renewable alcohol [4]. However, the production of ethyl biodiesel has not yet been sufficiently developed for efficient use on an industrial scale. As well, information on the physicochemical properties required to improve this process is still scarce in the open literature. For instance, data on the liquid–liquid and vapor–liquid equilibria of mixtures in the purification and reaction steps of ethyl biodiesel production have only recently been published [5–7].

One of the most important physicochemical properties for establishing the potential for fire and explosion of a hazardous material such as a fuel is its flash point (FP). The FP is related to the vapor pressure of a flammable liquid and is defined as the lowest temperature at which it can form a combustible mixture with air [8]. As temperature increases, the vapor pressure increases and the amount of evaporated flammable liquid in equilibrium with the air also increases. When the FP is reached, a simple ignition source is able to combust the mixture [9]. Experimental FP data have clearly become important in ensuring safe storage of flammable materials, and for this reason a series of studies for predicting the FP of pure substances and their mixtures can be encountered in the literature [9–16]. Flash point data on different biodiesels reported in the literature [3,17–20] show values significantly higher than those obtained for conventional diesel. Flash point does not directly affect biofuel combustion, but a higher FP makes biodiesel safer for storage,

handling and transportation [21]. On the other hand, the low vapor pressure of biodiesel components can cause ignition delay and some combustion problems [19].

Biodiesel production around the world is based on the methanolic route, and thus is dependent on a nonrenewable alcohol source. The use of ethanol, a renewable alcohol, results in a biofuel with more attractive properties, such as a higher specific energy, a higher cetane index, better lubricity and enhanced cold flow behavior [22,23]. Mixtures of biodiesel and ethanol are encountered along the biodiesel production process and information on their FPs is important for safety purposes in industrial plants.

The aim of this work was to measure the FPs of binary mixtures of FAEEs with ethanol, to correlate this data using a thermodynamic approach and to test this approach to predicting FP values of multicomponent mixtures containing ethylic biodiesel and ethanol.

3.2. Mathematical model for predicting the flash points of miscible mixtures

Le Chatelier's rule [24] for a flammable mixture of vapor + air can be expressed as

$$1 = \sum_i \frac{y_i}{LFL_i}$$

Eq.3. 1

where y_i is the vapor phase composition of a flammable substance i, and LFL_i is the lower flammable limit of the pure component i. The LFL_i is expressed in relation to the pure component *i* vapor pressure at its flash point, $P_{i,FP}^{sat}$, as:

$$LFL_i = \frac{P_{i,FP}^{sat}}{P}$$

Eq.3. 2

where *P* in the equation above represents the ambient pressure.

The FP of a pure substance is measured at atmospheric pressure. Under this condition the vapor phase usually exhibits an ideal behavior. In the case of a liquid mixture containing flammable substances in the presence of the non-condensable components of air, the vapor–liquid equilibrium of component *i* is given by:

$$y_i P = x_i \gamma_i P_i^{sat}$$

Eq.3. 3

where γ_i is liquid phase activity coefficient.

As proposed by Liaw et al. [12], the substitution of Eq.3. 2 and Eq.3. 3 into Eq.3. 1 results in Eq.3. 4, which allows evaluation of FPs for a flammable liquid mixture:

$$1 = \sum_{\mathrm{i}} \frac{\mathrm{x_i} \gamma_i P_i^{sat}}{P_{i,FP}^{sat}}$$

Eq.3. 4

The vapor pressure for a pure substance is a function of temperature and can be estimated by the Antoine equation:

$$log_{10} P_i^{sat} = A_i - \frac{B_i}{T + C_i}$$

Eq.3. 5

Although the Antoine constants (A_i, B_i and C_i) are well-defined for ethanol, there is no information in the literature regarding these constants for FAEEs within the temperature range of interest. For this reason a predictive model, based on a group contribution method [25] specially developed for fatty components, was employed for estimating the FAEE vapor pressures.

For an ideal liquid mixture the activity coefficients of all components are equal to one, so Eq.3. 4 can be reduced to a simpler form. This assumption may be reasonable for mixtures whose components have the same functional group and similar molecular sizes, for instance biodiesel mixtures of methyl or ethyl esters. In the case of mixtures containing ethanol and biodiesel components the non-idealities of the liquid phase must be considered and the activity coefficients estimated using molecular models, such as the Margules, NRTL, Wilson or UNIQUAC equations [9–16,26] or a group contribution approach, such

as the UNIFAC [27] method. Binary interaction parameters of these models are typically obtained from vapor–liquid (VLE) or liquid–liquid (LLE) equilibrium data. Results reported in the literature show that these parameters from LLE and VLE data can predict the FPs of miscible or partially miscible mixtures with good accuracy [9–16,26].

Unfortunately, in the case of FAEE + ethanol mixtures no VLE or LLE data and consequently no interaction parameters were available in the literature for the temperature and pressure conditions used in the present work. To make up for this lack of data, the FP data measured in the present work was used for adjusting the binary interaction parameters of the NRTL model (see Table 3. 1), as already proposed by Noorollahy et al. [28] for different binary mixtures. The algorithm for obtaining the binary interaction parameters for NRTL equation from FP experimental data is depicted in Fig. 3. 1. The NRTL model allows the extension of equilibrium calculations from binary to multicomponent systems, so the interaction parameters obtained can be used for predicting the FPs of multicomponent mixtures, such as those containing biodiesel and ethanol. In the present study, this type of prediction was tested using FP data for ethylic solutions of palm oil biodiesel.

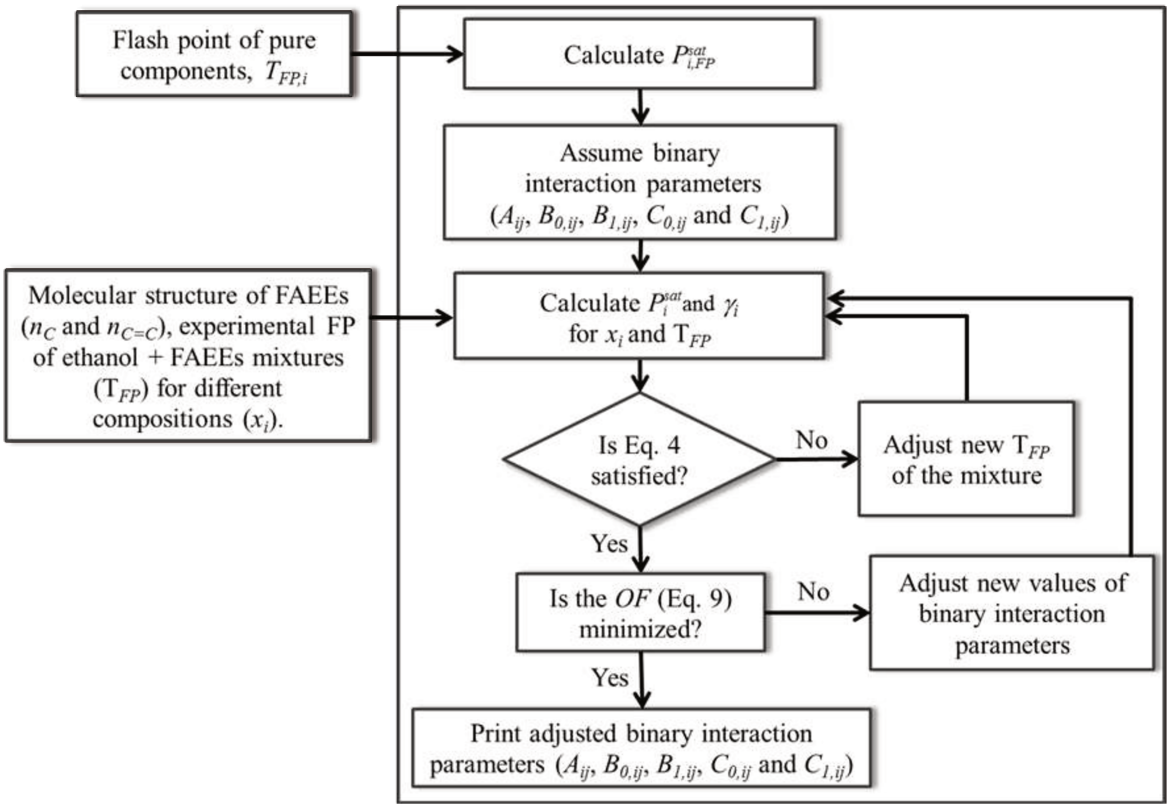

Fig. 3. 1. Procedure for adjustment of NRTL binary interaction parameters of a flammable mixture using FP experimental data.

Table 3. 1. NRTL model for activity coefficients of multicomponent mixtures.

Name	$ln\,\gamma_i$
NRTL	$$ln\,\gamma_i = \frac{\sum_j^N \tau_{ji} G_{ji} x_j}{\sum_j^N G_{ji} x_j} + \sum_j^N \frac{x_j G_{ij}}{\sum_k^N G_{kj} x_k}\left(\tau_{ij} - \frac{\sum_k^N x_k \tau_{kj} G_{kj}}{\sum_k^N x_k G_{kj}}\right)$$ where $\Delta G_{ij} = exp\left(-\alpha_{ij}\tau_{ij}\right)$ and $\tau_{ij} = \frac{\Delta g_{ij}}{RT}$

3.3. Materials and methods

3.3.1. Materials

The FAEEs were purchased from Tecnosyn (Brazil) or Sigma-Aldrich (Germany) and the ethanol was supplied by Synth (Brazil). All reagents were used without further purification. Purity of the FAEEs was determined by gas chromatographic analysis (Table 3. 2). The ethyl oleate and ethyl linoleate used are technical grade reactants and their compositions are given in Table 3. 3. Palm oil was kindly supplied by Agropalma (Companhia Refinadora da Amazônia, Brazil). Sodium hydroxide was purchased from Carlo Erba Reagents (Italy). Acetic acid and sodium sulfate were purchased from Ecibra (Brazil).

Table 3. 2. Flash points of pure ethanol and FAEEs measured in this study.

Component (CAS number)	Fatty chain (C*x*:*y*[a])	Molar mass	FP (K)	Purity (*w*/*w*)	Supplier
ethanol (64-17-5)	-	46.0684	287 ± 1	0.995[b]	Synth
ethyl caproate (123-66-0)	C6:0	144.2114	330.7 ± 0.5	0.980[c]	Tecnosyn
ethyl caprylate (106-32-1)	C8:0	172.2646	361.0 ± 1	0.998 [b]	Sigma-Aldrich
ethyl caprate (110-38-3)	C10:0	200.3178	387.6 ± 0.6	0.998[b]	Sigma-Aldrich
ethyl laurate (106-33-2)	C12:0	228.3709	400.0 ± 1	0.992[c]	Tecnosyn
ethyl myristate (124-06-1)	C14:0	256.4241	424.0 ± 2	0.995[c]	Tecnosyn
ethyl palmitate (628-97-7)	C16:0	284.4772	434.0 ± 2	0.984[c]	Tecnosyn
ethyl stearate (111-61-5)	C18:0	312.5304	464.0 ± 2	0.979 [b]	Sigma-Aldrich
ethyl oleate (111-62-6)	C18:1	*technical grade*	427.0 ± 3	0.782[c]	Tecnosyn
		310.5145	432[d] ± 6[e]	-	-
ethyl linoleate (544-35-4)	C18:2	*technical grade*	429.0 ± 3	0.727[c]	Sigma-Aldrich
		308.4986	428[d] ± 6[e]	-	-

[a] in C*x*:*y*, *x* = number of carbons in the fatty chain and *y* = number of double bonds;
[b] according to the supplier;
[c] measured by gas chromatography analysis;
[d] calculated as an ideal mixtures;
[e] estimated by error propagation.

Table 3. 3. Composition of technical grade ethyl oleate and ethyl linoleate.

		Percentage (% *w*/*w*)	
FAEE	Fatty chain (C*x*:*y*)	Ethyl oleate	Ethyl linoleate
ethyl caprylate	C8:00	0.04	-
ethyl caprate	C10:0	1.23	-
ethyl laurate	C12:0	2.80	-
ethyl myristate	C14:0	0.08	0.09
ethyl pentadecanoate	C15:0	-	0.04
ethyl palmitate	C16:0	4.45	7.20
ethyl palmitoleate	C16:1	0.03	0.10
ethyl n-heptadecanoate	C17:0	0.13	0.09
ethyl stearate	C18:0	2.10	2.59
ethyl elaidate	C18:1	0.80	-
ethyl oleate	C18:1	78.16	14.08
trans ethyl linoleate	C18:2	0.55	2.03
ethyl linoleate	C18:2	8.70	72.67
ethyl linolenate	C18:3	0.32	0.42
ethyl arachidate	C20:0	0.21	0.34
ethyl eicosenoate	C20:1	0.40	0.16
ethyl behenate	C22:0	-	0.11
ethyl lignocerate	C24:0	-	0.08

3.3.2. Biodiesel synthesis

The transesterification reaction was performed using one part vegetable oil and six parts ethanol, both in moles, and an amount of catalyst (sodium hydroxide) corresponding to 1% of the oil mass. This mixture was stirred for 3 h at a temperature near 60 °C. After the reaction, acetic acid was added to neutralize the sodium hydroxide and then the mixture was transferred to a separation funnel in order to separate the ester phase (less dense) from

the glycerol phase. The upper fraction was washed five times with aqueous ethanol solutions, increasing the water content of these solutions in each step. The final wash was performed using pure water. This sequence of washing procedures allowed for elimination of glycerol and catalyst residues. The ester phase was dehydrated by percolation through a bed of sodium sulfate crystals. Afterwards, the biodiesel was heated to 80 °C in a rotaevaporator under vacuum in order to complete the drying process and eliminate the residual alcohol.

3.3.3. Flash points measurements

In this study, a closed-cup analyzer (ISL, model FP93 5G2, France) was used to measure the FPs of pure FAEEs and their binary mixtures with different ethanol compositions. The equipment was operated according to the standard test method ASTM D93 A, by which the equipment heated the liquid sample under constant stirring at a steady rate of 5–6 °C/min and the FP was determined using an igniter at specified temperature intervals.

3.4. Results and discussion

3.4.1. Flash points of pure substances

The measured FPs of the pure FAEEs and ethanol are listed in Table 3. 2. Measurements were performed at least in triplicate for all reactants and show standard deviations within the range of 0.5–3.0 K. Note that in the case of the technical grade reactants (ethyl oleate and ethyl linoleate) the FP standard deviations are larger than the FP standard deviations of the pure substances. This can be attributed to the presence of significant amounts of minor components, which contributes to the dispersion of the experimental values. The coefficients of variation for these measurements are within the

range of 0.7–0.15%, a range of values similar to those observed for FP data already reported in the literature [14,15]. No FP data for pure FAEEs were found in the literature, so a comparison between experimental values from different sources was not possible. Taking experimental uncertainties into account, the ethanol FP measured in the present work is in very good agreement with values published in the literature, where reported values are either 286 or 287 K [14,29].

In the case of the ethyl oleate and ethyl linoleate, which are technical grade reactants, the measured data represent FP values of two mixtures of FAEEs and not the values of the pure reactants. Since the compositions of the technical reactants are known, the FP values of pure ethyl oleate and linoleate can be estimated using Eq.3. 4. For this purpose, both compositions were normalized in terms of the FAEEs listed in Table 3. 2, indicating that for this estimation the presence of some minor components, for instance ethyl elaidate in the case of the commercial ethyl oleate or ethyl pentadecanoate in the case of the commercial ethyl linoleate, were not considered. Furthermore, the mixture was considerated ideal ($\gamma_i = 1$). The assumption of ideal behavior has proved to be a good basis for predicting the melting points of binary FAEE mixtures [30]. A similar behavior can also be observed in the case of vapor–liquid equilibrium of FAEE mixtures, however only as an approximation [31]. Silva et al. [31] measured VLE data for binary systems containing ethyl palmitate, ethyl oleate and ethyl linoleate within the temperature range of 502–538 K. Predictions of the boiling temperatures based on the ideal solution hypothesis resulted in standard deviations between experimental and calculated values within the range of 0.5–1.1 K, values slightly higher than those reported by the authors when the activity coefficients were calculated using the NRTL model (0.35–0.82 K).

Based on the experimental data for saturated esters and estimated values for pure unsaturated esters (Table 3. 2), the FPs of FAEEs were expressed as a function of the carbon chain length and the number of double bonds, as indicated in Fig. 3. 2. In order to express the dependence of the FPs on the number of carbon atoms, different mathematical functions such as exponential and logarithmic functions were tested, but the best results were obtained using a quadratic function. In the case of the double bonds the limited set of experimental data prevented the use of any function other than linear. Thus, the dependence

was well described by the relationship presented in Eq.3. 6 below (R^2 = 0.9753). With this empirical model, the FPs of other ethyl esters, for instance ethyl pentadecanoate, which is an expensive reagent, can be accurately estimated.

$$T_{FP,i}(K) = 251.2 + 13.97 \cdot n_C - 0.1198 \cdot n_C^2 - 19.9 \cdot n_{C=C}$$

Eq.3. 6

where $T_{FP,i}$ refers to FP of component *i*, n_C stands for the number of carbons atoms in the fatty acid residue chain and $n_{C=C}$ represents the number of double bonds. The influence of the number of carbon atoms was well represented as a quadratic function, while the influence of the double bonds was assumed to be linear due to the scarcity of data available.

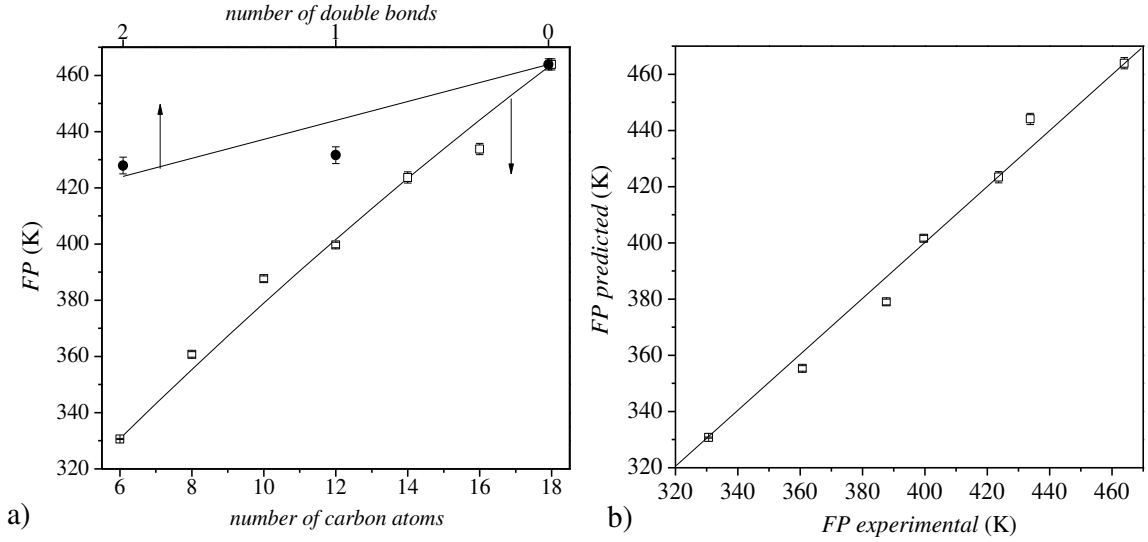

Fig. 3. 2. Flash points of FAEE. a) (□) experimental data as a function of the number of carbons in the fatty chain; (●) experimental data as a function of the number of double bonds for C18:0, C18:1 and C18:2 ethyl esters; (—) represents the empirical model; b) FP predicted values versus experimental values for saturated ethyl esters.

As indicated in Fig. 3. 2a and Eq.3. 6, the FPs of ethyl fatty esters increase with the carbon chain length and decrease with the number of unsaturation. This behavior reflects the fact that volatilities of fatty compounds decrease with the carbon chain length and increase with the number of double bonds, as indicated by known group contribution

approaches to estimating their vapor pressures [25,32,33]. The root mean square deviation (RMSD) between experimental data and the empirical model was estimated according to Eq.3. 7 below and is 6.5 K. As can be seen in Fig. 3. 2b, there is good agreement between experimental and calculated values. Note that the FP values vary from 330 to 464 K (see Table 3. 2), so a deviation of 6.5 K is not greater than 2%. If one analyzes only the case of saturated ethyl esters ($n_{C=C}$ = 0), the proposed equation (Eq.3. 6) exhibits a better correlation with the experimental data (R^2 = 0.9853) with a *RMSD* of 5.1 K.

$$RMSD = \sqrt{\sum_{k=1}^{m}\left(\frac{\left(T_{FP,k}^{\exp} - T_{FP,k}^{\mathrm{mod}}\right)^2}{m}\right)}$$

Eq.3. 7

where m is the total number of experimental measurements and the superscripts exp and mod stand for experimental and calculated values, respectively.

3.4.2. Flash points of mixtures containing fatty acid ethyl esters and ethanol

Flash points for the mixtures of ethanol (1) + FAEEs (2) (ethyl caproate, ethyl laurate, ethyl myristate, ethyl palmitate, ethyl oleate or ethyl linoleate) are presented in Table 3. 4, Fig. 3. 3 and Fig. 3. 4. These data show standard deviations within the range of 0.5– 1.2 K, with the lesser values occurring for the lower FPs, so the coefficients of variation are within the range of 0.2–0.4%, also similar to those observed for FP data on the pure reactants.

Except for ethyl palmitate, all ethyl esters used in the mixtures investigated in this work have melting points below the FP of pure ethanol, so FP measurements could be performed for the entire range of compositions. In the case of ethyl palmitate, the composition interval studied comprises only the region rich in ethyl palmitate, as shown in Fig. 3. 3d.

The differences between the FPs of pure ethyl esters and pure ethanol are large, ranging from 43.5 to 146.6 K. This behavior is a consequence of the also large differences in volatilities between these components. In fact, vapor–liquid equilibrium data for ethanol

+ ethyl ester mixtures, measured at temperatures and pressures close to the critical properties of ethanol (T_c = 513.9 K, P_c = 6.15 MPa), show that the molar fractions of ethanol in the vapor phase are very close to one for pressures lower than 6.0 MPa, indicating that even at temperatures higher than most values used in the present work the amount of ethyl ester in the vapor phase remains low [34]. The boiling point of mixtures containing components with such a large difference in volatilities usually shows the reason the FP temperature shows a steep decrease with the ethanol concentration in the region close to the pure heavy component. On the other hand, in the entire ethanol-rich region the FP temperatures change only slightly.

Table 3. 4. Flash points of binary mixtures of ethanol (1) + selected FAEE (2) for different compositions.

ethyl caprate		ethyl laurate		ethyl myristate	
x_1	T (K)	x_1	T (K)	x_1	T (K)
1.000	287.0	1.000	287.0	1.000	287.0
0.801	289.8	0.804	289.1	0.800	289.3
0.600	293.2	0.622	290.1	0.600	289.3
0.401	295.9	0.428	292.5	0.400	292.1
0.300	298.5	0.300	294.1	0.300	294.3
0.200	301.8	0.224	297.8	0.200	298.4
0.150	304.8	0.151	301.9	0.150	301.7
0.100	309.8	0.115	304.8	0.100	309.3
0.050	316.8	0.050	320.2	0.050	323.7
0.000	330.7	0.000	400.0	0.000	424.0
ethyl palmitate		ethyl oleate[a]		ethyl linoleate[a]	
x_1	T (K)	x_1	T (K)	x_1	T (K)
1.000	287.0	1.000	287.0	1.000	287.0
0.150	302.5	0.800	288.2	0.600	288.8
0.125	304.2	0.600	288.9	0.345	291.9
0.100	309.1	0.400	291.3	0.200	297.9
0.075	316.2	0.300	294.9	0.111	307.4
0.050	331.8	0.200	299.5	0.060	313.9
0.025	349.9	0.150	304.5	0.000	429.0
0.000	434.0	0.100	311.3		
		0.050	323.9		
		0.000	427.0		

[a] technical grade reagent

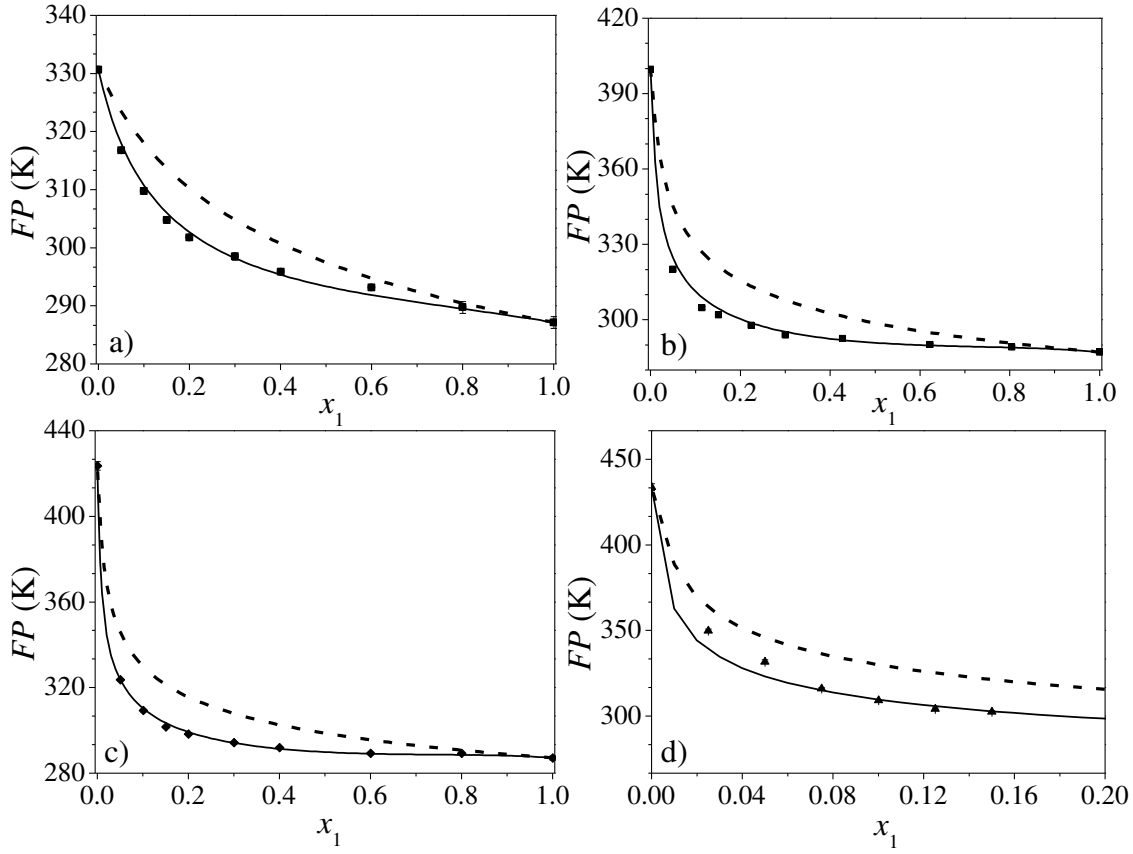

Fig. 3. 3. Comparison of the flash point prediction curves with experimental data on the ethanol (1) + FAEE binary mixtures (2). (—) NRTL model; (- - -) ideal curve. a) ethanol + ethyl caproate (●); b) ethanol + ethyl laurate (■); c) ethanol + ethyl myristate (♦); d) ethanol + ethyl palmitate (▲).

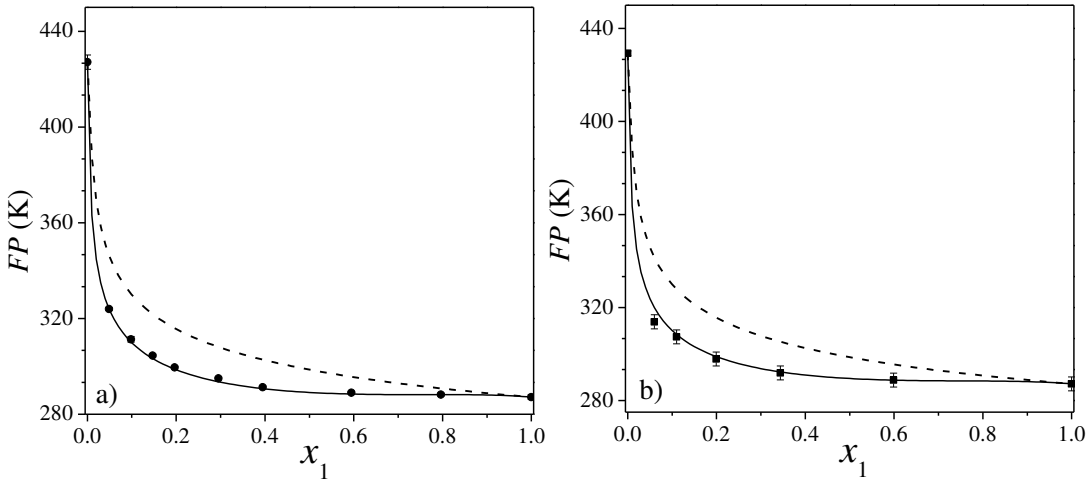

Fig. 3. 4. Comparison of the flash point prediction curves with experimental data on the ethanol (1) + unsaturated FAEE mixtures (2). (—) NRTL model; (- - -) ideal curve. a) ethanol + ethyl oleate (●); b) ethanol (1) + ethyl linoleate (■).

As indicated in Fig.3.3 and Fig.3.4, the values in the complete set of FP experimental data for the binary mixtures are lower than those calculated for the corresponding ideal mixtures. This indicates the positive deviations of these mixtures from ideal behavior. In other words, the volatilities of these mixtures are higher and their boiling points lower than the corresponding values estimated for an ideal mixture of the same components, which indicates that the formation of these mixtures is associated with the predominance of repulsive interactions. Nevertheless, this effect is not strong enough to cause FP values to be lower than the value obtained for the pure light component, a behavior that can be observed in the case of some mixtures composed of ethanol and other flammable substances [13,26].

Based on the experimental FP values measured in this work and Eq.3. 4 above, interaction parameters for the NRTL model were adjusted so that the observed deviations from ideal behavior would be taken into account. For this adjustment procedure the vapor pressures of ethanol were calculated using the Antoine equation with constants published in the literature [35] and shown in Table 3. 5. Experimental vapor pressure data or Antoine constants for FAEEs are not available in the literature for the required temperature range.

For this reason the FAEE vapor pressures were estimated using the predictive model developed by Ceriani and Meirelles [25] for fatty components.

Table 3. 5. Antoine equation´s constants for ethanol used in the FP prediction model.

Temperature range (K)	A	B	C	Range used in this study (K)
364.8 - 513.91	4.92531	1432.526	-61.819	T > 365
292.77 - 366.63	5.24677	1598.673	-46.424	340 < T ≤ 365
273. - 351.70	5.37229	1670.409	-40.191	T ≤ 340

The first set of NRTL parameters obtained for the mixtures of saturated FAEEs and ethanol indicated that the parameter values depend on the fatty acid chain length. For this reason an equation to express the value of the binary interaction parameters as a function of the number of carbons atoms in the fatty acid residue chain was fitted to the experimental data (Eq. 3.8). An additional term was included in this equation to take into account the effect of the number of double bonds of unsaturated FAEEs. Since the differences between the FP of ethanol and those of pure FAEEs are large, the dependence of temperature was also explicitly included in the proposed equation. The following equation was then used for adjusting the NRTL interaction parameters

$$\Delta g_{ij} = A_{ij} + B_{ij} \cdot n_C + C_{ij} \cdot n_{C=C}$$

Eq.3. 8

where $B_{ij} = B_{0,ij} + B_{1,ij} \cdot T$ and $C = C_{0,ij} + C_{1,ij} \cdot T$.

The values of these parameters are provided in Table 3.6. In order to adjust this set of parameters, data on the binary mixtures containing saturated FAEEs as well as data on the mixtures containing the technical grade reactants (ethyl oleate and linoleate) were used. As explained above in the case of technical grade reagents, only FAEEs whose FP values are given in Table 3.2 were considered and ideal behavior was assumed for the interaction between FAEEs. To adjust the values of the parameters, the following objective function (OF) was minimized (Eq.3.9) using the entire set of experimental data given in Table 3.4 and the NRTL interaction parameters calculated according to Eq.3.8.

$$OF = \sqrt{\sum_{i=1}^{m}\left(\frac{\left(T_{FP,i}^{\exp} - T_{FP,i}^{\mathrm{mod}}\right)^2}{m}\right)}$$

Eq.3. 9

Table 3. 6. NRTL binary interaction parameters for ethanol (1) + FAEEs (2) systems (Eq.3.8).

	Binary parameters				
	A (J/mol)	B_0 (J/mol)	B_1 (J/mol.K)	C_0 (J/mol)	C_1 (J/mol.K)
Δg_{12}	23.0447	123.61	1.0603	-28.99	-2.6146
Δg_{21}	11.6195	126.98	-0.5179	29.79	0.0896
($\alpha_{12} = 0.2785$)					

The *RMSD* between experimental data for the ethanol + FAEE systems and the values calculated using the NRTL model are lower than 2.8 K, with the exception of the ethyl palmitate + ethanol system in which case the deviation was 5.7 K (Table 3. 7). As mentioned previously, the melting temperature of ethyl palmitate is higher than the ethanol FP temperature, hindering FP determination of FP for the complete range of molar fractions. Therefore, calculation of the *RMSD* is restricted to the composition range within which small changes in concentration cause significant changes in the FP and thus increase the corresponding deviations between experimental and calculated values.

Table 3. 7. *RMSD* between experimental and calculated FP data.

System	*RMSD* (K)
ethanol + ethyl caproate	0.9
ethanol + ethyl laurate	2.4
ethanol + ethyl miristate	0.9
ethanol + ethyl palmitate	5.7
ethanol + ethyl oleate	0.8
ethanol + ethyl linoleate	2.8

3.4.3. Flash points of palm oil ethyl biodiesel and its mixtures with ethanol

In order to evaluate the capacity of the approach described above for predicting the FPs of mixtures containing ethylic biodiesel + ethanol, experimental data were obtained for mixtures containing ethanol + palm oil ethyl biodiesel. The composition of the palm oil ethyl biodiesel produced is given in Table 3. 8. The biodiesel is composed mainly of ethyl palmitate (41.19%) and ethyl oleate (42.10%). It contains considerable amounts of ethyl stearate (4.72%) and ethyl linoleate (9.14%) as well as small amounts of ethyl myristate (0.92%) and other ethyl esters. The FPs of palm oil biodiesel and its mixtures with ethanol were measured and are presented in Table 3. 9 and Fig. 3. 5. FP values of the mixture are similar to those observed for the binary systems measured in the present work and to prior data reported in the literature for different biodiesel mixtures [18–20]. The standard deviations varied from 0.6 to 3.4 K and the corresponding coefficients of variation from 0.2% to 1.1%.

The binary interaction parameters of the NRTL model can be used for predicting activity coefficients in multicomponent systems, but this requires parameter values for all binary subsystems that compose the multicomponent mixture. In the case of ethylic biodiesel as well as for the technical grade ethyl oleate and linoleate, the ester molecules have the same functional groups and similar carbon chain lengths, so in its pure form biodiesel can be considered an ideal solution and the corresponding binary interaction parameters between FAEEs are neglected. Therefore the deviations from an ideal behavior of solutions containing ethanol and biodiesel could be estimated based only on the binary interaction parameters between each FAEE and ethanol (Eq.3.8), neglecting the contribution to non-ideality due to interactions between FAEEs.

Flash point values of the ethylic biodiesel + ethanol mixtures were predicted using the composition given in Table 3. 8 and considering Eq.3.4, where the FP of the minor components were predicted by Eq.3.6 and the activity coefficients for each ethanol–FAEE binary pair were predicted by the NRTL model with interaction parameters given by Eq.3.8. The corresponding curve is shown in Fig. 3. 5 and the RMSD value is equal to 3.4 K. It should be noted that the deviation between experimental and predicted values is larger

due mainly to temperature differences between the experimental and predicted FP values of pure palm oil biodiesel (see Fig. 3. 5).

Table 3. 8. Composition of palm oil ethylic biodiesel by GC analysis.

FAEE	Fatty chain (C*x*:*y*)	Percentage (% *w*/*w*)
Ethyl caproate	C6:0	0.03
ethyl caprylate	C8:0	0.04
ethyl caprate	C10:0	0.06
ethyl laurate	C12:0	0.39
ethyl myristate	C14:0	0.92
ethyl pentadecanoate	C15:0	0.05
ethyl palmitate	C16:0	41.19
ethyl palmitoleate	C16:1	0.14
ethyl heptadecanoate	C17:0	0.10
ethyl stearate	C18:0	4.72
ethyl oleate	C18:1	42.10
trans ethyl linoleate	C18:2	0.18
ethyl linoleate	C18:2	9.14
ethyl linolenate	C18:3	0.22
ethyl arachidate	C20:0	0.38
ethyl eicosenoate	C20:1	0.15
ethyl behenate	C22:0	0.06
ethyl lignocerate	C24:0	0.13

The proposed approach to predicting the FP of biodiesel blends with ethanol proved to be a good alternative with low deviations in almost the entire range of mixture compositions. Further improvement of this approach requires additional FP measurements for pure unsaturated FAEEs as well as a more precise evaluation of the deviations from ideal behavior occasionally found in mixtures containing only pure ethyl esters. Such an

improvement may help to diminish the slightly higher deviations observed for the composition range close to that of pure biodiesel.

Table 3. 9. Flash points of ethanol (1) + palm oil ethylic biodiesel (2) mixtures.

Palm oil ethyl biodiesel	
x_1	*FP* (K)
1.000	287.0
0.800	287.1
0.592	287.8
0.401	293.9
0.199	298.9
0.151	302.5
0.099	307.8
0.050	323.9
0.000	421.8

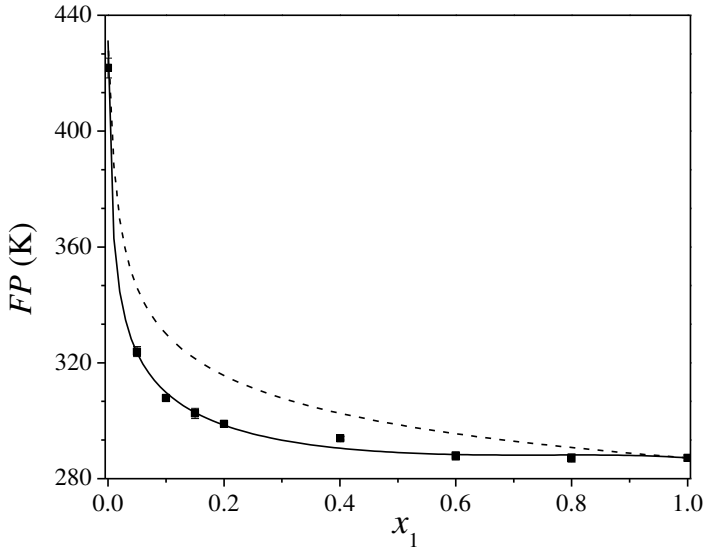

Fig. 3. 5. Comparison of the flash point prediction curves with experimental data on the ethanol (1) + ethyl palm oil biodiesel (2) mixture. (■) experimental data for mixtures containing palm oil biodiesel; (—) NRTL model; (- - -) ideal curve.

3.5. Conclusions

Flash points of ethyl esters were measured and an empirical model was proposed for expressing these values as a function of the number of carbon atoms and double bonds in the fatty acid residue. Flash points were also measured for binary and multicomponent mixtures containing ethyl esters and ethanol. Using Eq.3. 4 for calculating the FPs of mixtures, NRTL parameters were adjusted for the interactions between esters and ethanol and expressed as a function of the number of carbon atoms and double bonds in the fatty acid residue. This complete set of parameters was tested in the prediction of FP values for mixtures containing palm oil biodiesel + ethanol. The *RMSD* between experimental and calculated values was lower than 6.5 K for pure FAEEs, 5.7 K for ester + ethanol mixtures and 3.4 K for biodiesel + ethanol mixtures.

Acknowledgments

The authors are grateful to CNPq (304495/2010-7, 480992/ 2009-6, 552280/2010-0, 142193/2010-0), FAPESP (2008/09502-0, 2008/56258-8, 2009/54137-1), CAPES, PIBIQ and FAEPEX/UNICAMP for their financial support and assistantships.

References

[1] Moser BR. Biodiesel production, properties, and feedstocks. In Vitro Cell Dev Biol—Plant 2009;45:229–66.

[2] Meher LC, Sagar DV, Naik SN. Technical aspects of biodiesel production by transesterification—a review. Renew Sustain Energy Rev 2006;10:248–68.

[3] Bouaid A, Martinez M, Aracil J. A comparative study of the production of ethyl esters from vegetable oils as a biodiesel fuel optimization by factorial design. Chem Eng J 2007;134:93–9.

[4] da Conceição LRV, da Costa CEF, da Rocha Filho GN, Zamian JR. Obtaining and characterization of biodiesel from jupati (Raphia taedigera Mart.) oil. Fuel 2011;90:2945–9.

[5] Oliveira MB, Barbedo S, Soletti JI, Carvalho SHV, Queimada AJ, Coutinho JAP. Liquid–liquid equilibria for the canola oil biodiesel + ethanol + glycerol system. Fuel 2011;90:2738–45.

[6] Follegatti-Romero LA, Lanza M, Batista FRM, Batista EAC, Oliveira MB, Coutinho JAP, et al. Liquid–liquid equilibrium for ternary systems containing ethyl esters, anhydrous ethanol and water at 298.15, 313.15, and 333.15 K. Ind Eng Chem Res 2010;49:12613–9.

[7] Oliveira MB, Queimada AJ, Coutinho JAP. Phase equilibria of ester + alcohol systems and their description with the cubic-plus-association equation of state. Ind Eng Chem Res 2010;49:3452–8.

[8] Crowl DA, Louvar JF. Chemical Process Safety: fundamentals with applications. 2nd ed. Upper Saddle River: Prentice Hall PTR; 2002.

[9] Liaw H-J, Chiu Y-Y. A general model for predicting the flash point of miscible mixtures. J Hazard Mater 2006;137:38–46.

[10] Liaw H-J, Lee Y-H, Tang C-L, Hsu H-H, Liu J-H. A mathematical model for predicting the flash point of binary solutions. J Loss Prevent Process Ind 2002;15:429–38.

[11] Liaw H-J, Chiu Y-Y. The prediction of the flash point for binary aqueous-organic solutions. J Hazard Mater 2003;101:83–106.

[12] Liaw H-J, Tang C-L, Lai J-S. A model for predicting the flash point of ternary flammable solutions of liquid. Combust Flame 2004;138:308–19.

[13] Vidal M, Rogers WJ, Mannan MS. Prediction of minimum flash point behavior for binary mixtures. Process Saf Environ Prot 2006;84:1–9.

[14] Liaw H-J, Chen C-T, Gerbaud V. Flash-point prediction for binary partially miscible aqueous-organic mixtures. Chem Eng Sci 2008;63:4543–54.

[15] Liaw H-J, Lu W-H, Gerbaud V, Chen C-C. Flash-point prediction for binary partially miscible mixtures of flammable solvents. J Hazard Mater 2008;153:1165–75.

[16] Kim SY, Lee B. A prediction model for the flash point of binary liquid mixtures. J Loss Prevent Process Ind 2010;23:166–9.

[17] Cernoch M, Hájek M, Skopal F. Relationships among flash point, carbon residue, viscosity and some impurities in biodiesel after ethanolysis of rapeseed oil. Bioresour Technol 2010;101:7397–401.

[18] Boog JHF, Silveira ELC, de Caland LB, Tubino M. Determining the residual alcohol in biodiesel through its flash point. Fuel 2011;90:905–7.

[19] Guo Y, Wei H, Yang F, Li D, Fang W, Lin R. Study on volatility and flash point of the pseudo-binary mixtures of sunflowerseed-based biodiesel + ethanol. J Hazard Mater 2009;167:625–9.

[20] Guo Y, Yang F, Xing Y, Li D, Fang W, Lin R. Study on volatility and flash point of the pseudo binary mixtures of sunflower-based biodiesel + methylcyclohexane. Fluid Phase Equilib 2009;276:127–32.

[21] Caro PS, Mouloungui Z, Vaitilingom G, Berge JC. Interest of combining an additive with diesel–ethanol blends for use in diesel engines. Fuel 2001;80:565–74.

[22] Lopes JCA, Boros L, Krahenbuhl MA, Meirelles AJA, Daridon JL, Pauly J, et al. Prediction of cloud points of biodiesel. Energy Fuels 2008;22:747–52.

[23] Foglia TA, Nelson LA, Dunn RO, Marmer WN. Low-temperature properties of alkyl esters of tallow and grease. J Am Oil Chem Soc 1997;74:951–5.

[24] Le Chatelier H. Estimation of firedamp by flammability limits. Ann Mines 1891;19:388–95.

[25] Ceriani R, Meirelles AJA. Predicting vapor–liquid equilibria of fatty systems. Fluid Phase Equilib 2004;215:227–36.

[26] Liaw HJ, Lee TP, Tsai JS, Hsiao WH, Chen MH, Hsu TT. Binary liquid solutions exhibiting minimum flash-point behavior. J Loss Prevent Process Ind 2003;16:173–86.

[27] Liaw H-J, Gerbaud V, Li Y-H. Prediction of miscible mixtures flash-point from UNIFAC group contribution methods. Fluid Phase Equilib 2011;300:70–82.

[28] Noorollahy M, Moghadam AZ, Ghasrodashti AA. Calculation of mixture equilibrium binary interaction parameters using closed cup flash point measurements. Chem Eng Res Des 2010;88:81–6.

[29] Li D-g, Zhen H, Xingcai L, Wu-gao Z, Jian-guang Y. Physico-chemical properties of ethanol–diesel blend fuel and its effect on performance and emissions of diesel engines. Renew Energy 2005;30:967–76.

[30] Boros L, Batista MLS, Vaz RV, Figueiredo BR, Fernandes VFS, Costa MC, et al. Crystallization behavior of mixtures of fatty acid ethyl esters with ethyl stearate. Energy Fuels 2009;23:4625–9.

[31] Silva LYA, Falleiro RMM, Meirelles AJA, Krähenbühl MA. Vapor–liquid equilibrium of fatty acid ethyl esters determined using DSC. Thermochim Acta 2011;512:178–82.

[32] Bokis CP, Chen C-C, Orbey H. A segment contribution method for the vapor pressure of tall-oil chemicals. Fluid Phase Equilib 1999;155:193–203.

[33] Tu C-H, Liu C-P. Group-contribution estimation of the enthalpy of vaporization of organic compounds. Fluid Phase Equilib 1996;121:45–65.

[34] Shimoyama Y, Iwai Y, Abeta T, Arai Y. Measurement and correlation of vapor–liquid equilibria for ethanol + ethyl laurate and ethanol + ethyl myristate systems near critical temperature of ethanol. Fluid Phase Equilib 2008;264:228–34.

[35] Burgess DR. Thermochemical data. In: Linstrom PJ, Mallard WG, editors. NIST Chemistry WebBook, NIST Standard Reference Database Number 69, National Institute of Standards and Technology, Gaithersburg MD, 20899.

Capítulo 4. The binary solid-liquid phase diagrams of caprylic or capric acid + 1-octanol or 1-decanol

Natália D. D. Carareto[a], Thamires Castagnaro[a], Mariana C. Costa[b], Antonio J. A. Meirelles[a]*

[a] EXTRAE, Department of Food Engineering, Faculty of Food Engineering, University of Campinas, UNICAMP, Rua Monteiro Lobato, 80 CEP 13083-862 Campinas, São Paulo, Brasil.

[b] School of Applied Science, University of Campinas, UNICAMP, Rua Pedro Zaccaria, 1300 CEP 13484-350 Limeira, São Paulo, Brasil.

Trabalho submetido em 17 de dezembro de 2013 na revista **Journal of Chemical Thermodynamics**

Abstract

In the present study the phase diagrams of four fatty acid + fatty alcohol binary mixtures composed of caprylic (C8O2) or capric acid (C10O2) + 1-octanol (C8OH) or 1-decanol (C10OH) were obtained by differential scanning calorimetry (DSC). The systems presented the occurrence of the eutectic and peritectic reactions. An exothermic transition on a standard DSC for the C8O2 + C10OH and C10O2 + C8OH systems occurs associated to the melting of a metastable phase. A *stepscan* DSC method was used in order to avoid the formation of this metastable phase during the heating of the mixtures. The approach suggested by Slaughter and Doherty (Chem. Eng. Sci. 1995, 50, 1679-1694) was used for modeling the solid phase, and Margules-2-suffix, Margules-3-suffix and NRTL models were applied for calculating the activity coefficients of the liquid phase. The best modeling results were obtained using the Margules 3-suffix with an average deviation between experimental and calculated values ranging from 0.3 to 0.9 K.

Keywords

- Solid-liquid equilibrium;
- Fatty acid;
- Fatty alcohol;
- DSC:
- Stepscan DSC

4.1. Introduction

The solid-liquid equilibrium (SLE) and other properties from mixtures of fatty acids and fatty alcohols are intensely studied because of their potential as structuring agents in food and pharmaceutical products (JOHNSON, 1988; DANIEL e RAJASEKHARAN, 2003; GANDOLFO et al., 2004; SCHAINK et al., 2007), and as phase change materials (VENTOLA et al., 2002; VENTOLA et al., 2004). These compounds are thermo-sensitive and high added value by-products from the vegetable oil industry (CARARETO et al., 2011), consequently they need refining processes under mild temperature conditions. The use of crystallization for the purification of these substances guarantees a range of temperature lower than that required by the usual destillative processes. Besides its importance for the development of purification processes based on crystallization, the knowledge of SLE of fatty mixtures can contribute for a better understanding of the melting behavior from complex fatty mixtures, such as edible oils and natural waxes. The most common type of phase diagram found in fatty systems presents a simple eutectic point with the possible occurrence of a solid solution on the extremes of the composition range (TIMMS, 1984).

In the food industry, fatty acids, fatty alcohols and their mixtures are important due to their potential in structuring edible oils (GANDOLFO et al., 2004). There are some prior studies on the solid-liquid equilibrium of these mixtures: Gandolfo et al. (2003) investigated the phase behavior of stearic acid, stearyl alcohol, and their mixtures, observing an eutectic behavior for the solid–liquid equilibrium line; the melting behavior for the mixture of palmitic acid + 1-tetradecanol has been studied by DSC and an eutectic point near to 0.7 molar fraction of 1-tetradecanol was also observed (ZENG et al., 2009).

DSC is one of the most used techniques to investigate solid-liquid phase diagrams of organic mixtures (COUTINHO e RUFFIER-MERAY, 1998). Usually, a linear heating rate is used to evaluate the thermal transitions since it is a well-established method (VENTOLA et al., 2002; INOUE et al., 2004a,b,c; COSTA et al., 2007; COSTA et al., 2009a,b,c; CARARETO et al., 2011; COSTA et al., 2011). The Temperature-modulated

differential scanning calorimetry (TMDSC) technique was recently proposed to obtain a better understanding of thermal phase transitions, especially in the case of polymer systems (SAUER et al., 2000). The combination of a linear rate superimposed by a sinusoidal heating sign was suggested to permit the deconvolution of reversible and non-reversible transitions (SCHAWE e HÖHNE, 1996; JIANG et al., 2002). The theory and principles of TMDSC can be found in (SCHAWE, 1995; WUNDERLICH et al., 1997). Stepscan DSC is an easy-to-handle version of the TMDSC and it consists in multiple cycles of linear heating rate within a small temperature range followed by an isothermal period until the heat flow becomes stable below a predetermined criterion (BAICHOO et al., 2006). The heat flow response to the heating (or cooling) segment is the thermodynamic component and reflects the reversing changes of the samples, as the eutectic or peritectic reactions (SANDOR et al., 2002).

The present paper is intended to study the solid-liquid phase behavior of binary mixtures of C8O2 or C10O2 + C8OH or C10OH by using two different DSC methods: the first one applying a linear heating rate based on a well-established methodology (BOROS et al., 2009; COSTA et al., 2009a,b,c; CARARETO et al., 2011; COSTA et al., 2011) and a new stepscan DSC method for measuring SLE for systems that present an exothermic transition when applied the linear heating rate. The SLE for the binary systems was modeled using Margules 2-suffix, Margules 3-suffix and NRTL models for calculating the liquid phase activity coefficients and the Slaughter and Doherty approach (SLAUGHTER e DOHERTY, 1995) was applied to the solid domain due to the peritectic compound formation with an incongruent melting point.

4.2. Experimental Section

4.2.1. Materials

The fatty acids and alcohols listed in Table 4. 1 were used to prepare the samples with no further purification. The DSC was calibrated using the following standards: indium

(CAS number 7440-74-6 and purity of 0.9999 molar fraction) supplied by TA instruments or Perkin-Elmer; cyclohexane (CAS number 110-82-7 and purity of 0.999 molar fraction) and naphthalene (CAS number 91-20-3 and purity of 0.999 molar fraction), both purchased from Merck. Commercial nitrogen was used to provide an inert atmosphere while preparing the binary samples (0.999 molar fraction) and high purity nitrogen was used as the purge gas in the calorimeter (0.9999 molar fraction), both were supplied by Air Liquide.

Samples were prepared according to the methodology described elsewhere (CARARETO et al., 2011) for four binary systems: C8O2 + C8OH, C8O2 + C10OH, C10O2 + C8OH and C10O2 + C10OH. The molar fractions were selected to cover the entire range of composition. To perform all the DSC analyses, the samples were weighed in a Perkin-Elmer AD-6 microbalance (±0.02 mg) and placed in hermetic aluminum pans.

Table 4. 1. Fatty acids and alcohols melting temperature, purity and respective suppliers

Reactant (CAS number)	$T_{melting}$ (K)[a]	$\Delta H_{melting}$ (kJ mol^{-1}) [a]	Purity[b] (w/w)	Supplier
C8O2 (124-07-2)	289.7 K	21.363	0.991	Sigma Aldrich
C10O2 (334-48-5)	305.3 K	27.991	0.990	Sigma Aldrich
C8OH (111-87-5)	258.7 K	23.700	0.995	Fluka
C10OH (112-30-1)	280.3 K	28.790	0.994	Sigma Aldrich

[a] measured by standard DSC method; [b] according to the supplier.

4.2.2. Differential scanning calorimetry (DSC)

The DSC analyses were performed using two different methods. The first method was named as standard DSC and performed for the four binary systems according to the methodology described in a previous work (CARARETO et al., 2011). In this case a TA Instrument MDSC 2920 calorimeter was used applying a linear heating rate of 1 K min^{-1}. Analyses of stepscan DSC were also performed for two binary systems using a Perkin-Elmer model DSC 8500 calorimeter coupled to a cooling system (Intracooler III).

As far as we know, there is no prior report in the open literature on the use of stepscan DSC for measuring SLE of organic systems. For this reason, an appropriate methodology had to be developed based on the different parameters that influence the stepscan DSC analysis. Several sets of parameters were tested and the values listed in Table 4. 2 were those selected on the basis of the obtained results. The parameters used in the stepscan DSC that have to be selected are heating rate, second temperature, isothermal step and criteria of stability, as indicated in Fig.4. 1.

Table 4. 2. Stepscan DSC experimental parameters used in this study.

DSC parameter	κ	ΔT	Δt	Criteria of stability
Value	2 K min^{-1}	0.2 K	2 min	0.002 mW

The linear heating rate (in Fig.4. 1 represented by $\kappa = dT/dt$) is related to the sensitivity of the stepscan DSC analysis (JIANG et al., 2002). For stepscan DSC higher heating rates generate higher noises, but rates lower than 20 K min^{-1} allow a stable baseline. A heating rate of 2 K min^{-1} is recommended by the equipment manufacturer and was used in this study.

The second temperature (ΔT in Fig.4. 1) is related to the temperature range used in every cycle of analysis and it affects the equipment sensitivity. A small second temperature enhances sensitivity, and it can difficult the differentiation of transitions and noises. Exactly this occurred in the present case when a second temperature equal to 0.1 K was selected. For a second temperature equal to 0.2 or 0.3 K, this difficulty does not occur and no significant differences were observed in the obtained results. Nevertheless, the lower value was selected (0.2 K) taking into account that fatty systems usually exhibit a large number of transitions within a small temperature interval, as observed in previous works (COSTA et al., 2007; COSTA et al., 2009a,b,c; CARARETO et al., 2011).

The isothermal step (Δt in Fig.4. 1) is a specific feature of the stepscan method that allows the sample to reach thermal equilibrium during the analysis, while the constant heating rate used in the standard DSC method may provide at best a quasi-equilibrium

state. The use of small samples and slow heating rates, usually within the range (0.1 – 2.0) K min^{-1}, minimizes the effect of this quasi-equilibrium state, making the standard DSC methodology reliable with relative low uncertainty values, as shown in prior works (INOUE et al., 2004a,b,c; COSTA et al., 2007; COSTA et al., 2009a,b,c; CARARETO et al., 2011). This is particularly important for materials with low thermal conductivity, such as fatty compounds, in which case the occurrence of temperature gradients within large samples is more probable. In order to avoid this risk, even in the case of the stepscan methodology, samples with a mass within the range (3-5) mg were used and isothermal steps (Δt) of 1, 2 and 3 min were tested.

A step of 1 min gave results difficult to be interpreted, suggesting that the selected Δt was insufficient to reach thermal equilibrium. In case of isothermal periods of 2 and 3 min the thermal curves could be easily interpreted and they gave similar results. The period of 2 min was selected in order to shorten the total time of each analysis.

The effective isothermal period depends on the maximal period discussed above and on a pre-defined stability criterion for the heat flow during the isothermal step. This criterion allows shortening the isothermal period. In fact, if 7 consecutives data points of heat flow fall within the selected range of stability criteria the isothermal step ends before the fixed maximal value of isothermal period. On the other hand, if the stability criterion is fixed at a high value, the isothermal step could be crossed over with the sample not attaining thermal equilibrium. A stability criterion for the heat flow of 0.002 mW was selected in the present study because it allowed thermal equilibrium and gave the best repeatability of results.

Stepscan DSC standard deviations were obtained by performing repeated experimental runs at least three times for selected binary mixtures. The standard deviations of the measurements ranged from 0.2 to 0.4 K. On this basis the uncertainty of the phase equilibrium data measured in present study was estimated to be not larger than 0.4 K. The temperature uncertainty for the standard DSC analysis was already reported in several studies ranging from 0.1 to 0.3 K (VENTOLA et al., 2002; COSTA et al., 2007; COSTA et al., 2009a,b,c; KOLODZIEJ et al., 2009). In effect, the temperature uncertainty from the stepscan DSC method can be slightly higher than the value for standard DSC, nevertheless

this increase in standard deviation arises from the chosen temperature step, as in this case $\Delta T = 0.2K$. Anyway, this loss in data accuracy is offset by the fact that the stepscan method allows deconvolution of the thermal curves, so that kinetic effects are eliminated and only the truly reversible transitions are kept in the thermal curves.

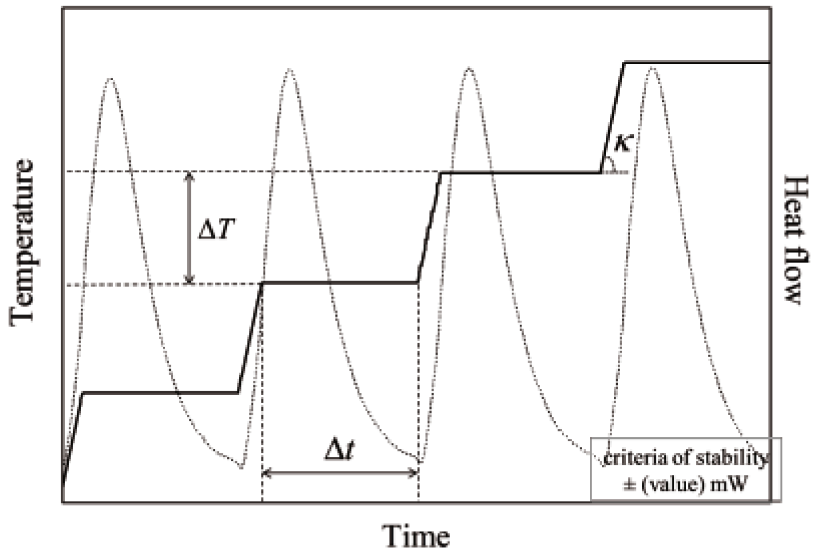

Fig.4. 1. Schematic illustration for programmed temperature (—) or heat flow (···) response versus time in a stepscan DSC analysis.

4.3. Results and discussion

4.3.1. Standard DSC

The standard DSC analysis was perfomed for the four binary systems mentioned above. According to the standard DSC curves, the existence of overlapping peaks can be observed throughout almost the entire range of composition, suggesting complex phase diagrams for all systems. For the C8O2 + C10OH and C10O2 + C8OH systems, the

standard DSC curves showed an exothermic transition for different compositions (see Fig.4. 2a for the C8O2 + C10OH system). On the other hand, the C8O2 + C8OH and C10O2 + C10OH systems do not present exothermic transitions in the analysed temperature range (Fig.4. 2b for the C8O2 + C8OH).

As can be noted in Fig.4. 2a, the exothermic transition occurs around 267 K for the entire range of composition. The intensity (enthalpy) of the mentioned transition increases until reaching a maximum value around a concentration of $x_{C8O2} \cong 0.4$. This type of exothermic transition can be found also for other fatty systems, as triacilglycerols, and it is related to the crystallization of a metastable state as a consequence of the applied heating rate (SINGH et al., 1999). For the pure components, C8O2 and C10OH, this exothermic transition does not occur and its presence on the standard DSC curves for the binary systems is an indicative that a new solid phase is being formed. However, the standard DSC curves make difficult to interpret these results from a quantitative point of view, since the exothermic and endothermic peaks overlapped, masking the real enthalpy of each transition and sometimes precluding a reliable analysis of the behavior of thermodynamic transitions, for instance eutectic and peritectic reactions, as a function of the composition, the so called Tamman plot. A deeper discussion about these two systems, C8O2 + C10OH and C10O2 + C8OH, will be made in the next section on the basis of the stepscan DSC results.

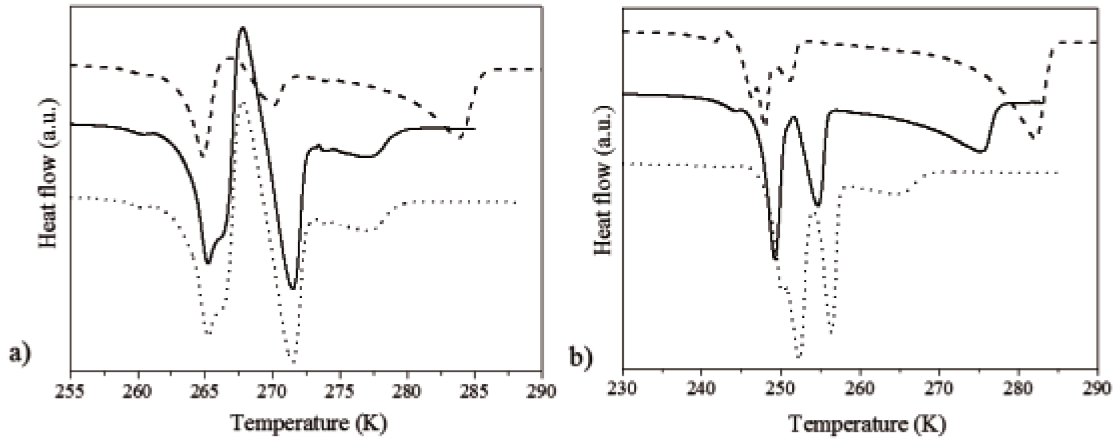

Fig.4. 2. Standard DSC thermal curves for (a) C8O2 + C10OH and (b) C8O2 + C8OH systems. In both set of DSC curves the lines represent: (- -) $x_{C8O2} \cong 0.8$; (—) $x_{C8O2} \cong 0.6$, and (···) $x_{C8O2} \cong 0.4$.

The SLE data of the systems C8O2 + C8OH and C10O2 + C10OH are presented in Tables 4.3-4. Note that these experimental data were measured using only the standard DSC because they do not exhibit exothermic transitions. Figs.4.3 and 4 show the phase diagrams of the C8O2 + C8OH and C10O2 + C10OH systems, respectively.

The liquidus line represents the border between the region of liquid phase and the regions of solid and liquid coexistence. Two inflexions can be observed in the liquidus line: the most pronounced one, close to x_{C8OH} or $x_{C10OH} \cong 0.8$, corresponds to the eutectic point. The second one, close to $x_{C8OH} \cong 0.65$ or $x_{C10OH} \cong 0.6$, is associated with the peritectic reaction.

Table 4. 3. Solid–liquid equilibrium data for C8O2 + C8OH system from standard DSC.

x_{C8OH}	$T_{trans,sol\text{-}sol(2)}$ (K)	$T_{trans,sol\text{-}sol(1)}$ (K)	$T_{eutectic}$ (K)	$T_{peritectic}$ (K)	$T_{melting}$ (K)
1.0000					259.0
0.8974	249.7		251.1		256.2
0.8503	249.5		251.7		253.4
0.7990	250.6				252.9
0.7552	248.5		251.5		253.3
0.6969	250.2		251.9		256.7
0.6511	249.3		251.9		257.0
0.6020	250.4		252.5	256.4	264.3
0.5499	249.6		251.4	256.2	268.8
0.5036	250.3			256.3	270.4
0.4065	249.3			254.7	275.0
0.2987	249.2			255.2	280.1
0.1977	248.1	251.2			282.2
0.1064	247.8	250.2			285.7
0.0000					289.6

Table 4. 4. Solid–liquid equilibrium data for C10O2 + C10OH system from standard DSC.

x_{C10OH}	$T_{trans,sol\text{-}sol(2)}$ (K)	$T_{trans,sol\text{-}sol(1)}$ (K)	$T_{eutectic}$ (K)	$T_{peritectic}$ (K)	$T_{melting}$ (K)
1.0000					280.3
0.9456		272.4	275.8		278.7
0.8988		272.6	275.9		278.1
0.7998	270.6	272.8			275.8
0.7043		272.6	275.5		279.0
0.5971	270.7	272.4	274.9		280.8
0.4989	271.3			279.9	287.9
0.3950	271.0			279.3	291.9
0.3194	273.4			279.3	295.5
0.2077	271.3			278.2	299.0
0.1058	269.5	275.4		278.0	301.9
0.0000					305.3

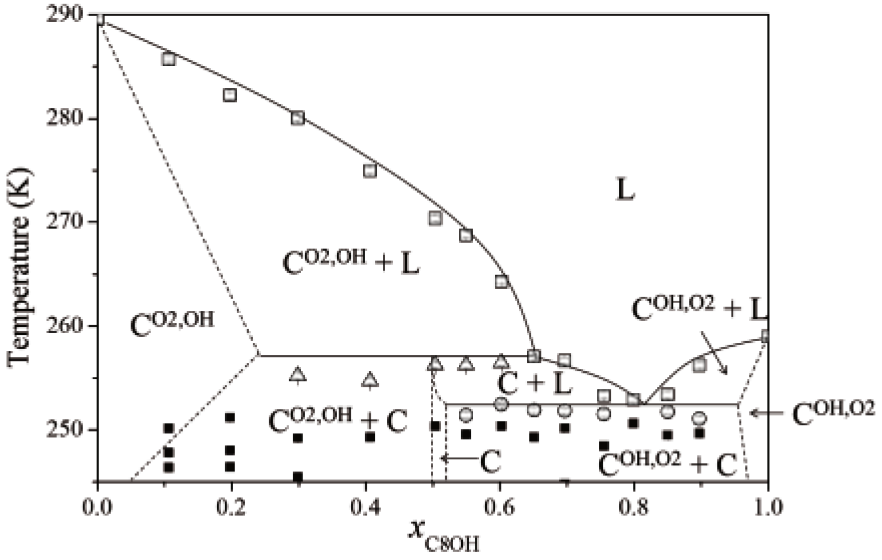

Fig.4. 3. Phase diagram of the C8O2 + C8OH system by standard DSC. (□) melting temperature; (Δ) peritectic reaction; (○) eutectic reaction; (■) temperature of solid-solid transition. (—) and (---) are guides to the eyes. L: liquid phase; $C^{O2,OH}$: solid solution rich in the fatty acid; $C^{OH,O2}$: solid solution rich in the fatty alcohol; C: peritectic compound.

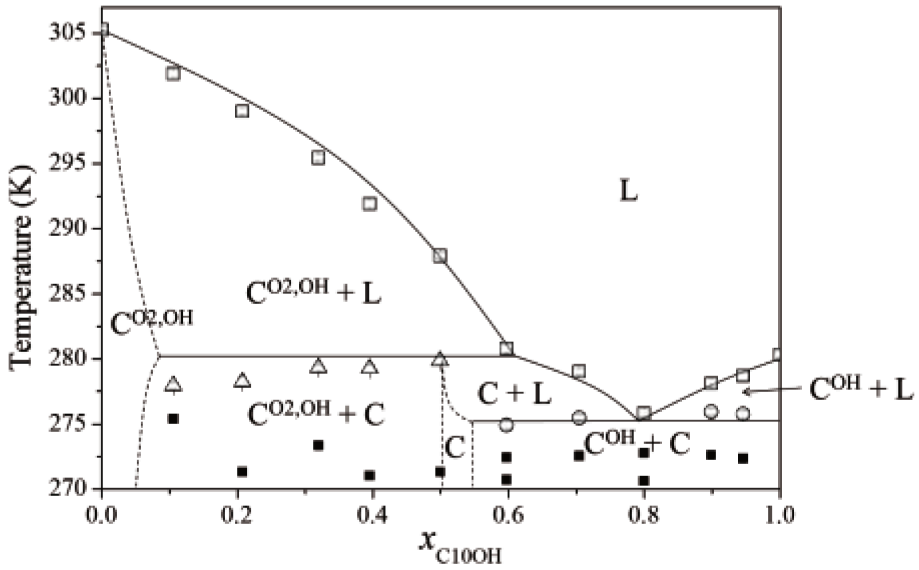

Fig.4. 4. Phase diagram of the C10O2 + C10OH system by standard DSC. (□) melting temperature; (Δ) peritectic reaction; (○) eutectic reaction; (■) solid-solid transition. (—) and (---) are guides to the eyes. L: liquid phase; $C^{O2,OH}$: solid solution rich in the fatty acid; C^{OH}: fatty alcohol in solid state; C: peritectic compound.

The Tamman plot for both systems is represented in Fig.4. 5. The enthalpies of the eutectic and peritectic reactions are represented as a function of the mixture composition, increasing linearly as the mixture concentration comes close to the eutectic or peritectic composition, a behavior well documented in the literature (COSTA et al., 2009a,b,c; CARARETO et al., 2011). The Tamman plot also indicates the formation of a solid solution close to the pure fatty acid region, meaning that the two compounds are partially miscible in the solid state (the solid solution is represented in the phase diagrams by the region $C^{O2,OH}$, as can be noted in Figs.4. 3-4). In the case of C8O2 + C8OH, a second solid solution is also indicated by the Tamman plot (Fig.4. 5a) close to the region rich in the fatty alcohol (region $C^{OH,O2}$), but for the system C10O2 + C10OH, the Tamman (Fig.4. 5b) indicates that in this region the fatty acid and the fatty alcohol are imiscible on the solid state.

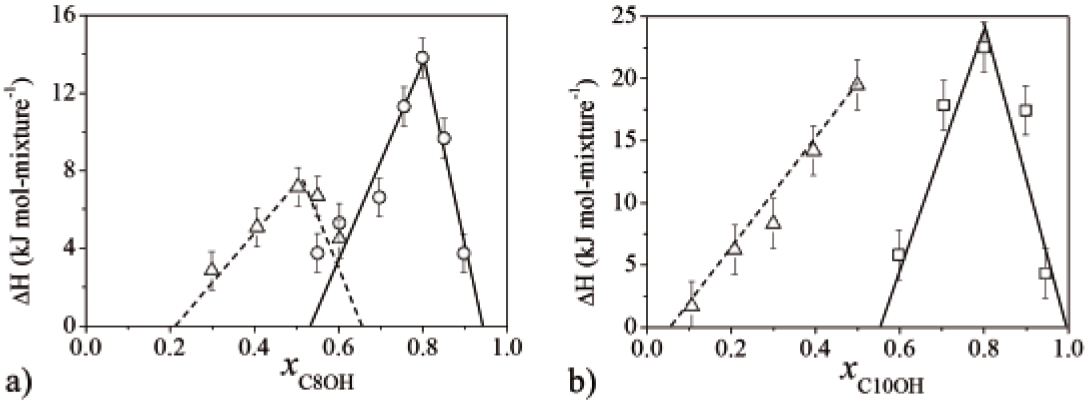

Fig.4. 5. Tamman plot from standard DSC: a) C8O2 + C8OH system and b) C10O2 + C10OH system. Enthalpy for (Δ) peritectic reaction and (○) eutectic reaction. (—) and (---) are guides to the eyes.

The occurrence of peritectic transition and the partial solubility in the solid state make the phase diagrams for the systems C8O2 + C8OH and C10O2 + C10OH more complex than the common diagram with a simple eutectic point, and allows their classification as type 2-IIIa system, according to the suggestion of Nývlt (1977). For the C8O2 + C8OH system, the following domains can be identified in Fig.4. 3: one

homogeneous liquid phase - region (L), 3 monophasic solid domains - regions ($C^{O2,OH}$), ($C^{OH,O2}$) and (C); 3 biphasic solid-liquid domains - region ($C^{O2,OH}$ + L), ($C^{OH,O2}$ + L) and (C + L) and; 2 biphasic solid-solid domains – regions ($C^{O2,OH}$ + C) and ($C^{OH,O2}$ + C).

For the C10O2 + C10OH system, which presents solid phase imiscibility in the region rich in C10OH, the phase diagram is slightly different from the C8O2 + C8OH, and is divided in the following domains (Fig.4. 4): one homogeneous liquid phase - region (L), 2 monophasic solid domains - regions ($C^{O2,OH}$) and (C); 3 biphasic solid-liquid domains - region ($C^{O2,OH}$ + L), (C^{OH} + L) and (C + L) and; 2 biphasic solid-solid domains – regions ($C^{O2,OH}$ + C) and (C^{OH} + C).

4.3.2. Stepscan DSC

The standard DSC thermal curves of the C8O2 + C10OH and C10O2 + C8OH binary systems presented an exothermic transition for almost all the compositions close to the eutectic temperature, as can be noted in Fig.4. 2a. In order to investigate the occurrence of the exothermic transitions the stepscan DSC method was used, since this methodology allows to separate kinetic effects from thermodinamic transitions (JIANG et al., 2002).

The stepscan DSC curve has a non-usual profile, where steps from the method can be identified as the small well-defined peaks in a small temperature range (Fig.4. 1). The sum of all peaks generates the stepscan DSC response, which is splited in two different components: the thermodynamic and the non-reversing ones. The thermodynamic component is associated to the heat flow response during the heating or cooling step (when $\kappa = dT/dt$ is applied) while the non-reversing response is obtained from the heat flow variation during the isothermal step (Δt in Fig.4. 1). In this way, the total heating flow can be easily separated into the two signals because the reversing part is taken during the heating step and the non-reversing from the isothermal one (Sandor et al., 2002). The reversing thermodynamic and non-reversing contribution can be extracted from the data

with a interpretation similar to the TMDSC method and is described in Eq.4. 1 (READING et al., 1994; SANDOR et al., 2002):

$$\frac{dH}{dt} = Cp \cdot \left(dT/dt\right) + f(t,T)$$

Eq.4. 1

where *dH*/*dt* is the overall heat flow, *Cp* is related to the reversible part (heat capacity term), *dT*/*dt* the heating rate, and $f(t,T)$ is a function of time and temperature related to the kinetic response (or non-reversing). By treating the $f(t,T)$ as an effective baseline, this can be removed from the stepscan response and the Cp term can be calculated as the heat flow divided by the heating rate:

$$Cp = \left(\frac{dH}{dt}\right) \Big/ \left(\frac{dT}{dt}\right)$$

Eq.4. 2

An usual thermal curve for a stepscan DSC analysis is presented in Fig.4. 6 for the the system C10O2 + C8OH at $x_{C8OH} = 0.9307$. It is easy to observe that the response is different from a standard DSC thermal curve. The peaks represent the interchange between the heating step and the isothermal one. The interpretation of the results was made with the help of Perkin Elmer software Pyris®. The two different signals are represented in Fig.4. 6: specific heat (J g^{-1} °C^{-1}) – or reversing signal – and heat flow (mW) – or non-reversing signal.

The heat flow for the thermodynamic response is obtained by integrating the specific heat curve (the software Pyris® has the tool which permits this calculation). The thermodynamic heat flow is represented for C10O2 + C8OH system in Fig.4. 7a for the composition $x_{C8OH} = 0.3349$. Observe that, with the exception of the exothermic peak of

the standard DSC analysis, the others peaks, related to thermodynamic events, have the same profile in both curves.

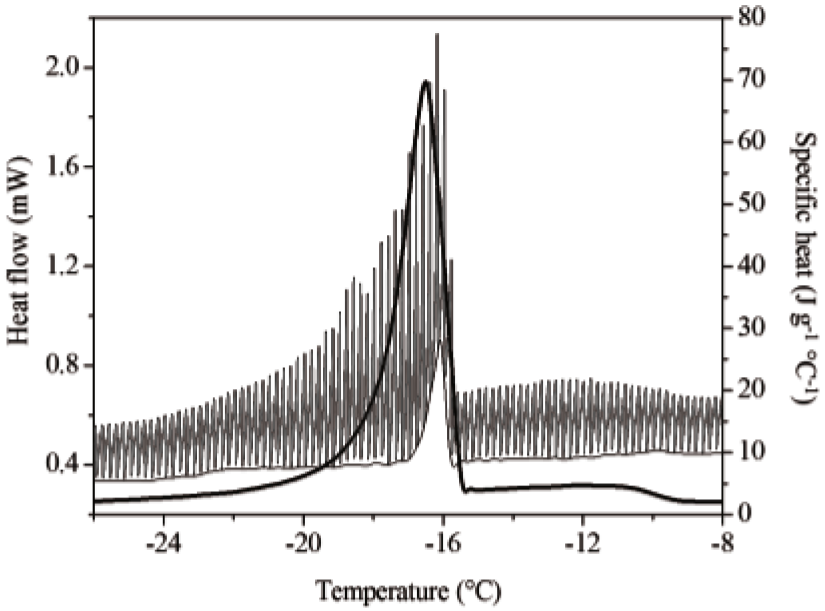

Fig.4. 6. Stepscan DSC response for the system C10O2 + C8OH at $x_{C8OH} = 0.9307$. Gray line represents the stepscan thermal curve (non-treated response); thin black line represents the non-reversing (or kinetic) response and the bold black line represents the specific heat (or thermodynamic) response.

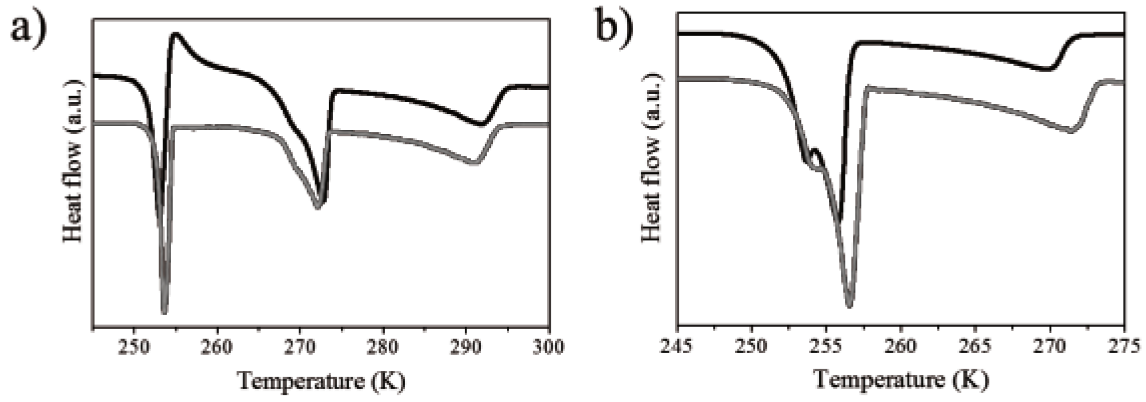

Fig.4. 7. DSC thermal curves of the system C10O2 + C8OH for standard (black line) and stepscan (gray line) DSC. (a) $x_{C8OH} = 0.3349$ and; (b) $x_{C8OH} = 0.8762$.

The root mean square deviation (*RMSD*) between both experimental data (standard DSC and stepscan DSC) for the mixture´s melting temperature (T_m) was estimated according to Eq.4. 3, and is equal to 0.5 K. This value is lower than the sum of the standard deviations from both methods and a major part of it can be attributed to the higher temperature differences close to eutectic point concentration range. Furthermore, when comparing the thermal curves for a composition $x_{C8OH} = 0.8762$ (Fig.4. 7b), one can observe that they have the same shape for both DSC methods, since no non-reversing transition was detected.

$$RMSD = \sqrt{\sum_{i=1}^{m}\left(\frac{\left(T_{\mathrm{m,standard}} - T_{\mathrm{m,stepscan}}\right)^2}{n}\right)}$$

Eq.4. 3

where n is the number of experimental measurements.

From the stepscan DSC, it was possible to evaluate the SLE of the binary systems, as proposed in Figs.4.8-9 with the experimental data found in Tables 4.5-6 for the C10O2 + C8OH and C8O2 + C10OH systems, respectively.

Table 4. 5. Solid–liquid equilibrium data for C10O2 + C8OH system from stepscan DSC.

x_{C8OH}	$T_{trans,sol-sol}$ (K)	$T_{eutectic}$ (K)	$T_{peritectic}$ (K)	$T_{melting}$ (K)
1.0000				259.0
0.9639				256.7
0.9307		256.7		262.2
0.8762	254.4	257.4		265.3
0.7510	254.0	256.6		271.4
0.6381	253.9	255.3	274.4	275.8
0.5312	253.5	254.8	273.7	281.4
0.4300	253.7		273.2	287.2
0.3349	253.6		272.1	291.7
0.2450	253.3		271.4	295.0
0.1616	253.4		269.9	298.5
0.0789	253.2		270.7	302.2
0.0491	252.6		270.1	303.3
0.0000				305.3

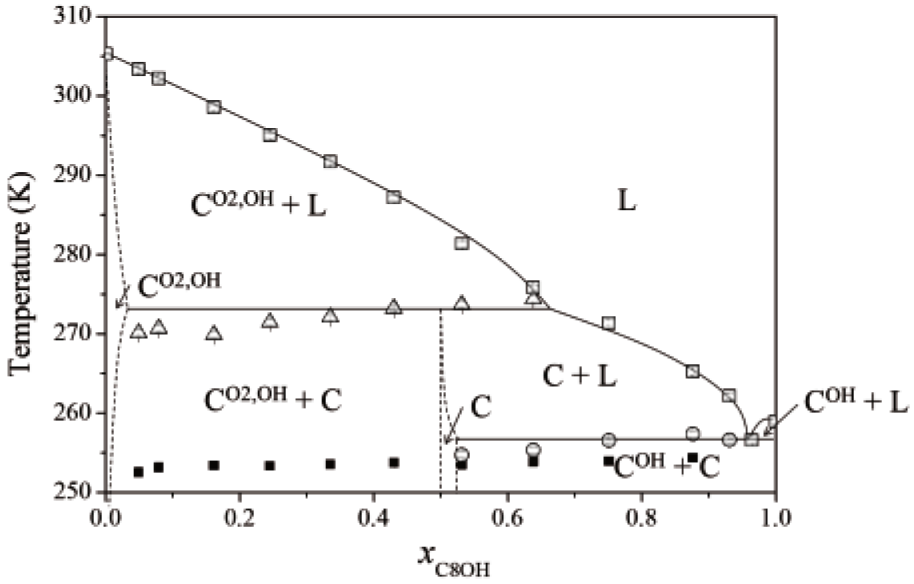

Fig.4. 8. Phase diagram of the C10O2 + C8OH system by stepscan DSC. (□) melting temperature; (Δ) peritectic reaction; (○) eutectic reaction; (■) solid-solid transition. (—) and (---) are guides to the eyes. L: liquid phase; $C^{O2,OH}$: solid solution rich in the fatty acid; C^{OH}: fatty alcohol in solid state; C: peritectic compound.

The Tamman plot of the C10O2 + C8OH systems was calculated using the stepscan DSC data (Fig.4. 10a). The system presented peritectic and eutectic reactions and a region of solid solution close to the concentration area rich in the fatty acid (region $C^{O2,OH}$ in the phase diagrams, Fig.4. 8). The region of SLE with fatty alcohol composition higher than the eutectic point is very small, making difficult the clear identification of the eutectic transition separated from the mixture´s melting and precluding the confirmation of a possible solid solution in this part of the diagram. Taking this difficulty into account we suggest in the present case to interpret that in this regions the components of the mixture are immiscible on the solid state.

Table 4. 6. Solid–liquid equilibrium data for C8O2 + C10OH system from stepscan DSC.

x_{C10OH}	$T_{trans,sol\text{-}sol(3)}$ (K)	$T_{trans,sol\text{-}sol(2)}$ (K)	$T_{trans,sol\text{-}sol(1)}$ (K)	$T_{eutectic}$ (K)	$T_{melting}$ (K)
1.0000					280.3
0.9521	264.1				277.8
0.8991	264.3	266.1		270.1	276.8
0.8524	263.6	265.9		269.9	275.3
0.8021	264.3	265.8		270.4	274.4
0.7500	263.9	265.2		270.2	272.8
0.6986	263.9	266.0		270.8	272.0
0.6498	263.7	265.8			270.9
0.5933	264.3		269.1		270.4
0.5496	263.7	266.7	268.6		271.5
0.5053	263.6	265.3	267.3		271.7
0.4696	263.6	265.0	267.7		271.7
0.4536	263.6		266.1	270.5	272.4
0.4046	264.3			270.4	273.8
0.3517			266.4	270.7	276.2
0.3000			266.7	270.4	278.5
0.1987	263.9		266.7	270.8	282.0
0.1557		265.2	268.0	270.3	283.5
0.0717		265.9			286.3
0.0000					289.3

Moreover, it is possible to observe a transition close to the eutectic temperature for the C10O2 + C8OH system which exists in the entire range of composition (in Fig.4. 8 represented by ■). The enthalpies of this transition were analysed and plotted versus the system composition (Fig.4. 10a). Even with considerable values of measured enthalpies

(ranging from 0.2 to 6 kJ mol-mixture^{-1}) it was not possible to evidence a behavior similar to that observed for peritectic and eutectic reactions. We suppose that this thermal event corresponds to a solid-solid transition of the mixture, unfortunately a better interpretation of these transitions requires the use of other tecniques like X-ray diffraction or microscopy.

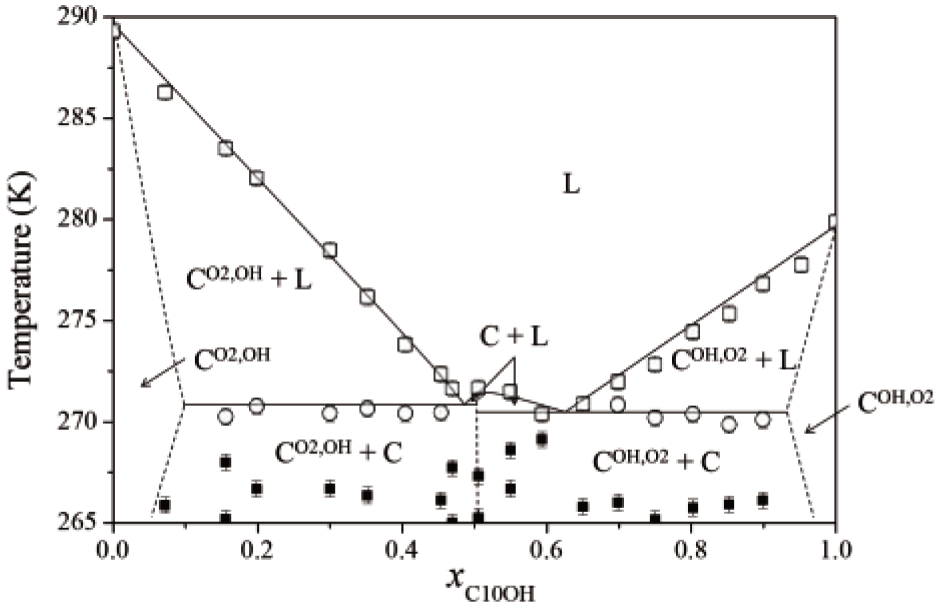

Fig.4. 9. Phase diagram of the C8O2 + C10OH system by stepscan DSC. (□) melting temperature; (○) eutectic reaction; (■) solid-solid transition. (—) and (---) are guides to the eyes. L: liquid phase; $C^{O2,OH}$: solid solution rich in the fatty acid; $C^{OH,O2}$: solid solution rich in the fatty alcohol; C: peritectic compound.

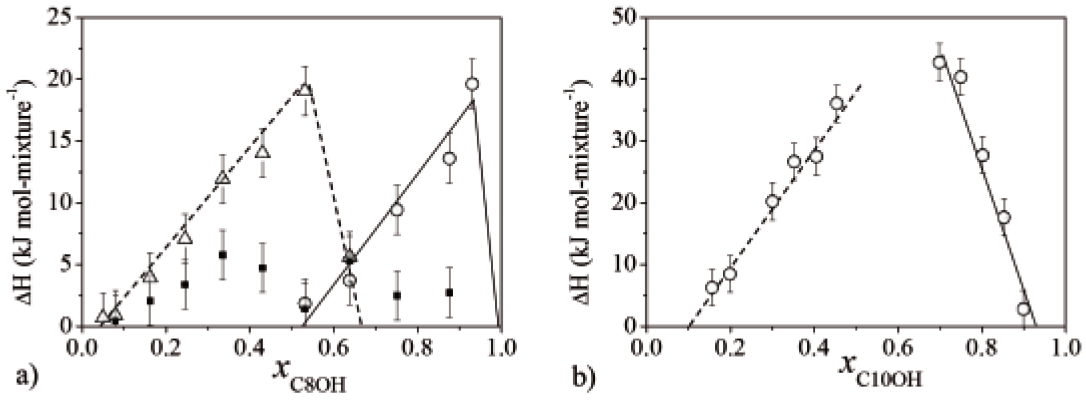

Fig.4. 10. Tamman plot from stepscan DSC. Enthalpy for (Δ) peritectic reaction, (○) eutectic reaction and; (■) solid-solid transition. (a) for C10O2 + C8OH system and (b) for C8O2 + C10OH system. (—) and (---) are guides to the eyes.

The results from the stepscan DSC analyses allow us to divide the phase diagram of the C10O2 + C8OH system (Fig.4. 8) in a way similar to the phase diagram proposed for the C10O2 + C10OH system: one homogeneous liquid phase - region (L), 2 monophasic solid domains - regions ($C^{O2,OH}$) and (C); 3 biphasic solid-liquid domains - regions ($C^{O2,OH}$ + L), (C^{OH} + L) and (C + L); and 2 biphasic solid-solid domains – regions ($C^{O2,OH}$ + C) and (C^{OH} + C).

For the C8O2 + C10OH system, the Tamman plot (Fig.4. 10b) clearly shows the existence of solid solutions at both ends of the phase diagram, i.e. in the regions rich in C10OH or in C8O2. For this system, there are two inflections points in the liquidus line, which can be related to the peritectic and eutectic reactions. Note in Fig.4. 9 that both inflections points occur around 270 K and the stepscan DSC results presented a transition at temperatures around 270 K in almost all range of concentration. Analysing the enthalpy of the transitions, it is easy to verify that there are a relation with the system concentration (Fig.4. 10b). A thorough analysis of the system melting behavior makes us suggest that the mixture of 1-decanol and caprylic acid forms a congruently melting compound, according to the Nývlt classification 2-Ib_1 (NÝVLT, 1977) and not a system with incongruently melting peritectic and eutectic points as are generally suggest for other fatty systems (COSTA et al., 2009a,b,c).

The phase diagram of a system with a compound that melts congruently exhibits a maximum point of melting temperature which corresponds to the compound fusion. As a general rule, this maximum melting temperature divides the phase diagram into two regions containing, each one, an eutectic point. This congruent point corresponds to the compound's stoichiometry (NÝVLT, 1977; WHITE e PERRY, 1994). Examples of mixtures that form a congruently melting compound are the system water + sulphuric acid (NÝVLT, 1977) and the system magnesium + silicon which forms magnesium silicide (Mg_2Si) (NAYEB-HASHEMI e CLARK, 1984). Based on the analysis of the phase diagram, we assume that the formed compound is constituted by a 1 molecule of C8O2 and 1 molecule of C10OH, since the inflection point of the liquidus line is close to 0.5 molar concentration (for the Mg-Si phase diagram this point is close to 0.33 molar concentration of Si) with the eutectic points occuring at $x_{C10OH} \cong 0.47$ and $x_{C10OH} \cong 0.63$ with a corresponding average temperature of (270.7 ± 0.4) K and (270.3 ± 0.3) K. The deviation for the eutectic temperature was estimated from the evaluated $T_{eutectic}$ at the different compositions. Note in Table 4. 6 and Fig.4. 9 that all the two are identified as eutectic transitions.

As a result, the SLE phase diagram for the C8O2 + C10OH can be divided in the following regions: one homogeneous liquid phase - region (L), 2 monophasic solid domains - regions ($C^{O2,OH}$) and ($C^{OH,O2}$); 3 biphasic solid-liquid domains - regions ($C^{O2,OH}$ + L), ($C^{OH,O2}$ + L) and (C + L) and; 2 biphasic solid-solid domains – regions ($C^{O2,OH}$ + C) and ($C^{OH,O2}$ + C).

4.3.3. Modeling Approach

The following simplifications are typically proposed for modeling SLE (PRAUSNITZ et al., 1986): i) the triple point temperature of component *i* is very close to its melting temperature; ii) the difference between the heat capacities of the liquid and solid phases is negligible; iii) the contribution of enthalpy is higher than that of the heat capacity,

and iv) the components are immiscible in the solid domain $\left(x_i^s \gamma_i^s = 1\right)$. Based on these simplifications the SLE can be described by Eq.4. 4 (PRAUSNITZ et al., 1986):

$$\ln\left(\frac{1}{x_i^l \gamma_i^l}\right) = \frac{\Delta H_{i,m}}{RT_{i,m}}\left(\frac{T_{i,m}}{T} - 1\right)$$

Eq.4. 4

where x_i is the mole fraction of component *i*, γ_i^l e γ_i^s are the activity coefficients of the solid and liquid phases, respectively, $\Delta H_{i,m}$ and $T_{i,m}$ are the melting enthalpy and temperature of component *i*, *T* is the equilibrium temperature and *R* is the universal gas constant.

Margules-2-suffix, Margules-3-suffix and NRTL models were used to calculate the liquid phase activity coefficients. The interaction parameters were obtained by adjusting the models to the experimental equilibrium data, using the Simplex Downhill method (Press *et al.*, 1992), as suggested in previous works (COSTA et al., 2007; CARARETO et al., 2011).

Note that the assumption of a pure solid phase does not take into account the partial miscibility observed for the fatty acid + alcohol systems (see Figs. 4. 3-4, 8-9). Nevertheless, the region of solid solution is quite small and its exact boundaries are not well defined. For this reason we opted, in the case of the modeling approach, to disregard the miscibility in the solid state and to emphasize the good description of the liquidus line.

For the description of the peritectic reaction, the solid phase was modeled using an approach suggested by Slaughter and Doherty (1995), according to which the peritectic compound C is the product of a chemical reaction involving components A and B ($aA + bB \rightarrow cC$), with the equilibrium constant of the reaction (*K*) given by:

$$K = \prod_{i=1}^{d}\left(x_i^s \gamma_i^s\right)^{v_i}$$

where v_i is the stoichiometric coefficient for component *i* and *d* is the number of components in the solid phase. From the phase diagrams presented in Figs. 3, 4, 8 and 9 the peritectic reaction stoichiometry could be estimated for each system. Thus the stoichiometric coefficients for all the systems were equal to $1A + 1B \rightarrow 1C$ (where A

represents the fatty acid and B represents the fatty alcohol and C the peritectic compound). The equilibrium constant (*K*) is related to the variation in the Gibbs energy of reaction (ΔG_{ij}°):

$$K = \exp\left(-\frac{\Delta G_{ij}^{\circ}}{RT}\right)$$

The assumption of immiscibility in the solid phase ($x_i^s \gamma_i^s = 1$) makes the reaction constant (*K*) equal to 1, causing that the Gibbs energy of the reaction vanishes ($\Delta G_{ij}^{\circ} = 0$). To prevent this inconsistency, Slaughter and Doherty (1995) proposed a simple model for calculating the activity coefficients in the solid phase:

$$\gamma_i^s = \frac{1}{x_i^s + \varepsilon}$$

Eq.4. 5

where ε is a small positive number ($\varepsilon = 10^{-4}$).

The algorithm used in the modeling fits simultaneously the ΔG_{ij}° value of the peritectic reaction and the interaction parameters of the liquid phase activity coefficient models. The objective function is presented in Eq.4. 6:

$$S = \frac{1}{2}\sum_{i=1}^{N}\left(\frac{T_i^{\text{experimental}} - T_i^{\text{calculated}}}{\sigma_{T_i}}\right)^2$$

Eq.4. 6

where *N* is the number of experimental measurements and σ_{T_i} represents the temperature uncertainty.

Table 4.7 shows the RMSD between the experimental data and the calculated melting temperatures using the modeling approach described above and also the ideal behavior assumption for the liquid phase. The adjusted parameters for Margules-2-suffix, Margules-3-suffix and NRTL are given in Table 4.8. The modeling results for the system C8O2 + C8OH are shown in Fig.4. 11a. The best fit was obtained using Margules-3-suffix model with RMSD ranging from 0.3 to 0.9 K. It is important to emphasize, that in the case

of the C8O2 + C10OH, the modeling was able to describe the presence of the congruently melting compound (peritectic compound) as can be seen in Fig.4. 12a.

Table 4. 7. *RMSD* between experimental data and modeling.

System	RMSD (K)			
	Margules 2-suffix	Margules 3-suffix	NRTL	Ideal curve
C8O2 + C8OH	1.3	0.9	1.1	1.6
C8O2 + C10OH	0.5	0.5	0.5	1.5
C10O2 + C8OH	1.2	0.6	1.0	3.5
C10O2 + C10OH	0.4	0.3	0.3	1.2

Table 4. 8. Adjusted parameters obtained for Margules-2-suffix, Margules-3-suffix and NRTL models.

System	Margules					NRTL[a]		
	2-suffix[a] (J mol^{-1})		3-suffix[a] (J mol^{-1})			($\alpha_{12} = 0.3$) (J mol^{-1})		
	A_{12}	$-\Delta G^{\circ}_{12}$	A_{12}	A_{21}	$-\Delta G^{\circ}_{12}$	Δg_{12}	Δg_{12}	$-\Delta G^{\circ}_{12}$
C8O2 + C8OH	263.0	195.0	647.9	-1703.1	951.2	-2602.8	4501.1	1441.3
C8O2 + C10OH	58.0	960.0	33.32	-455.6	1099.8	-2378.0	3337.4	1064.5
C10O2 + C8OH	-1547.2	3108.4	-1683.5	1682.1	1159.1	-2682.3	1992.2	2943.2
C10O2 + C10OH	-118.0	1139.0	-53.60	-1002.4	1463.6	-2997.0	4476.8	1326.7

[a] component (1) makes reference to the lower $T_{melting}$ on the binary system.

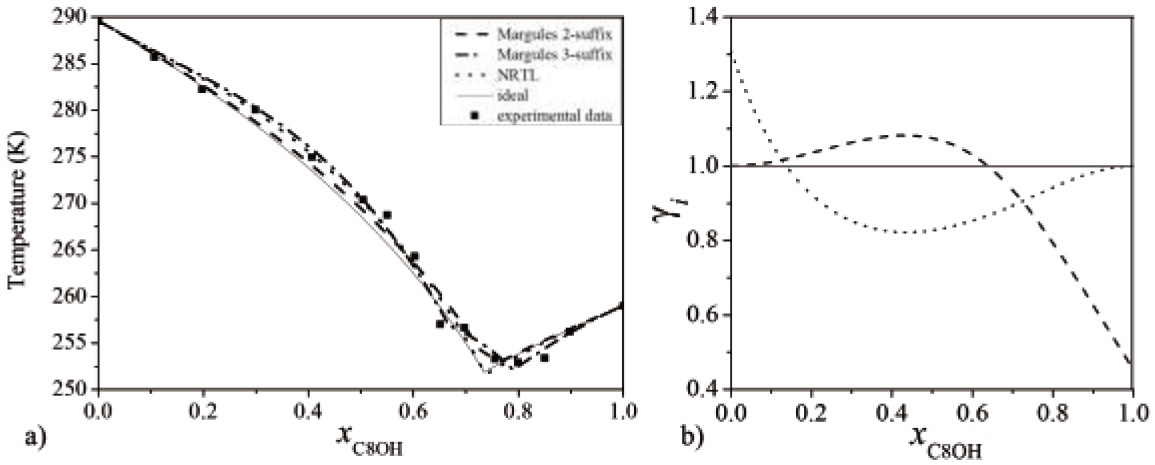

Fig.4. 11. Modeling of the system C8O2 + C8OH. a) liquidus lines for: (■) experimental standard DSC data; (—) Ideal curve; (···) NRTL model; (---) Margules 2-suffix model and (-·-) Margules 3-suffix model; b) liquid activity coefficient for Margules 3-suffix model: (---) C8O2 and (···) C8OH.

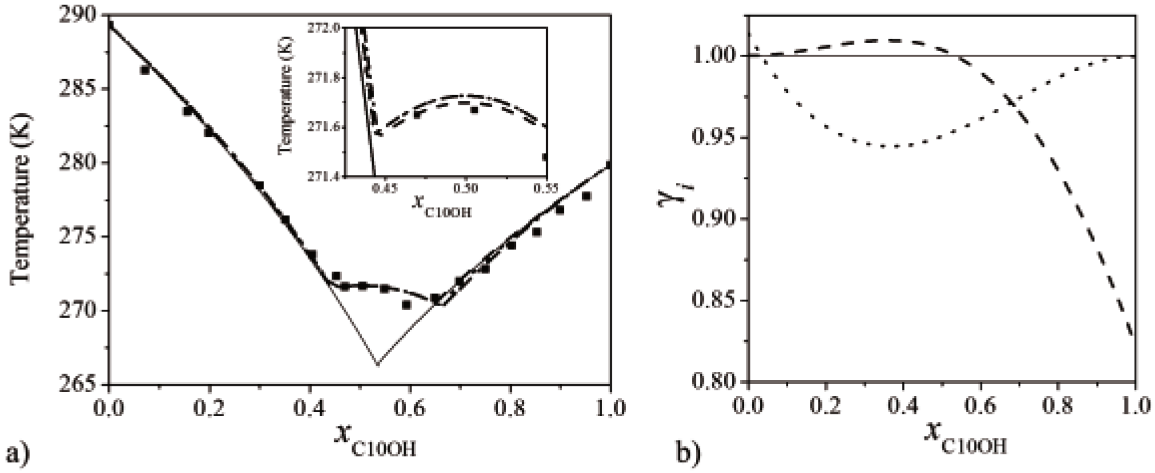

Fig.4. 12. Modeling of the system C8O2 + C10OH. a) liquidus lines for: (■) experimental standard DSC data; (—) Ideal curve; (···) NRTL model; (---) Margules 2-suffix model and (-·-) Margules 3-suffix model; b) liquid activity coefficient for Margules 3-suffix model: (---) C8O2 and (···) C8OH.

The values of the liquid phase activity coefficients indicated that these systems are slightly non-ideal. An ideal curve for the systems C8O2 + C8OH and C8O2 + C10OH is represented in Fig.4. 11a and Fig.4. 12a in order to compare the results. It is worth noting

that the deviations of the ideal liquidus lines were positive at low concentrations of fatty alcohols and negative at high concentrations of this compound. This behavior was already reported in previous work for others fatty acid + fatty alcohols mixtures (MÁXIMO et al., in press).

This phenomenon can be explained by means of changes of the H-bonds between acid and alcohol molecules as a function of the components´ concentration. Since the energy of H-bonding interactions between carboxyl moieties is greater than that observed between the hydroxyl groups belonging to alcohol molecules, when adding molecules of alcohol to the pure organic acid, some of these strong bonds between two carboxylic acids are probably replaced by a relatively weaker hydroxyl and carboxyl H-bonding interactions, explaining the positives deviations. On the other hand, when adding molecules of fatty acid to the pure alcohol, the stronger H-bonding interaction between hydroxyl and carboxyl groups causes the negative deviations of the alcohol activity coefficients. This interchange of H-bonding interactions is, very likely, responsible for the inversion in the trend of alcohol and acid activity coefficients. Moreover, Fig.4.11b and Fig.4.12b show the activity coefficients of the liquid phase calculated from the 3-suffix Margules model for the systems C8O2 + C8OH and C8O2 + C10OH, respectively (Máximo et al., in press).

4.4. Conclusions

In this study the phase diagrams of four specific fatty acid + fatty alcohol binary mixtures were published for the first time. The DSC analyses showed that the systems have eutectic and peritectic reactions. The stepscan DSC analysis was used, for the first time, as a tool to evaluate the SLE with a good repeatability and accuracy. The standard deviations obtained for the stepscan DSC have values similar to those estimated using standard DSC. The stepscan DSC showed to be a good technique to analyse the SLE of complex mixtures, such as fatty systems, since it allows to distinguish kinetic effects from thermodynamics transitions. Taking into account that there are many parameters to be adjusted in the stepscan DSC, possibly other methods than that presented in this work can also achieve

good results. The Slaughter and Doherty approach permitted a good fit of the liquidus line for the investigated systems, with Margules-3-suffix model giving the best modeling results.

Acknowledgments

The authors are grateful to CNPq (304495/2010-7, 483340/2012-0, 552280/2010-0, 142193/2010-0), FAPESP (2008/09502-0, 2008/56258-8, 2012/05027-1), CAPES and FAEPEX/UNICAMP for their financial support and assistantships.

References

BAICHOO, N.; MACNAUGHTAN, W.; MITCHELL, J.; FARHAT, I. A STEPSCAN Differential Scanning Calorimetry Study of the Thermal Behavior of Chocolate. **Food Biophysics**, v. 1, n. 4, p. 169-177, 2006. ISS

BOROS, L.; BATISTA, M. L. S.; VAZ, R. V.; FIGUEIREDO, B. R.; FERNANDES, V. F. S.; COSTA, M. C.; KRÄHENBÜHL, M. A.; MEIRELLES, A. J. A.; COUTINHO, J. A. P. Crystallization Behavior of Mixtures of Fatty Acid Ethyl Esters with Ethyl Stearate. **Energy & Fuels**, v. 23, n. 9, p. 4625-4629, 2009.

CARARETO, N. D. D.; COSTA, M. C.; ROLEMBERG, M. P.; KRÄHENBÜHL, M. A.; MEIRELLES, A. J. A. The solid–liquid phase diagrams of binary mixtures of even saturated fatty alcohols. **Fluid Phase Equilibria**, v. 303, n. 2, p. 191.e1-191.e8, 2011.

COSTA, M. C.; BOROS, L. A. D.; COUTINHO, J. O. A. P.; KRÄHENBÜHL, M. A.; MEIRELLES, A. J. A. Low-Temperature Behavior of Biodiesel: Solid–Liquid Phase Diagrams of Binary Mixtures Composed of Fatty Acid Methyl Esters. **Energy & Fuels**, v. 25, n. 7, p. 3244-3250, 2011.

COSTA, M. C.; ROLEMBERG, M. P.; BOROS, L. A. D.; KRAHENBUHL, M. A.; DE OLIVEIRA, M. G.; MEIRELLES, A. J. A. Solid-liquid equilibrium of binary fatty acid mixtures. **Journal of Chemical and Engineering Data**, v. 52, n. 1, p. 30-36, 2007.

COSTA, M. C.; ROLEMBERG, M. P.; MEIRELLES, A. J. A.; COUTINHO, J. A. P.; KRÄHENBÜHL, M. A. The solid-liquid phase diagrams of binary mixtures of even saturated fatty acids differing by six carbon atoms. **Thermochimica Acta**, v. 496, n. 1-2, p. 30-37, 2009a.

COSTA, M. C.; SARDO, M.; ROLEMBERG, M. P.; COUTINHO, J. A. P.; MEIRELLES, A. J. A.; RIBEIRO-CLARO, P.; KRAHENBUHL, M. A. The solid-liquid phase diagrams of binary mixtures of consecutive, even saturated fatty acids. **Chemistry and Physics of Lipids**, v. 160, n. 2, p. 85-97, 2009b.

COSTA, M. C.; SARDO, M.; ROLEMBERG, M. P.; RIBEIRO-CLARO, P.; MEIRELLES, A. J. A.; COUTINHO, J. A. P.; KRAHENBUHL, M. A. The solid-liquid phase diagrams of binary mixtures of consecutive, even saturated fatty acids: differing by four carbon atoms. **Chemistry and Physics of Lipids**, v. 157, n. 1, p. 40-50, 2009c.

COUTINHO, J. A. P.; RUFFIER-MERAY, V. A new method for measuring solid-liquid equilibrium phase diagrams using calorimetry. **Fluid Phase Equilibria**, v. 148, p. 147-160, 1998.

DANIEL, J.; RAJASEKHARAN, R. Organogelation of plant oils and hydrocarbons by long-chain saturated FA, fatty alcohols, wax esters, and dicarboxylic acids. **Journal of the American Oil Chemists Society**, v. 80, n. 5, p. 417-421, 2003.

GANDOLFO, F.; BOT, A.; FLÖTER, E. Structuring of edible oils by long-chain FA, fatty alcohols, and their mixtures. **Journal of the American Oil Chemists' Society**, v. 81, n. 1, p. 1-6, 2004.

GANDOLFO, F. G.; BOT, A.; FLOTER, E. Phase diagram of mixtures of stearic acid and stearyl alcohol. **Thermochimica Acta**, v. 404, n. 1-2, p. 9-17, 2003.

INOUE, T.; HISATSUGU, Y.; ISHIKAWA, R.; SUZUKI, M. Solid-liquid phase behavior of binary fatty acid mixtures 2. Mixtures of oleic acid with lauric acid, myristic acid, and palmitic acid. **Chemistry and Physics of Lipids**, v. 127, n. 2, p. 161-173, 2004a.

INOUE, T.; HISATSUGU, Y.; SUZUKI, M.; WANG, Z. N.; ZHENG, L. Q. Solid-liquid phase behavior of binary fatty acid mixtures 3. Mixtures of oleic acid with capric acid (decanoic acid) and caprylic acid (octanoic acid). **Chemistry and Physics of Lipids**, v. 132, n. 2, p. 225-234, 2004b.

INOUE, T.; HISATSUGU, Y.; YAMAMOTO, R.; SUZUKI, M. Solid-liquid phase behavior of binary fatty acid mixtures 1. Oleic acid/stearic acid and oleic acid/behenic acid mixtures. **Chemistry and Physics of Lipids**, v. 127, n. 2, p. 143-152, 2004c.

JIANG, Z.; IMRIE, C. T.; HUTCHINSON, J. M. An introduction to temperature modulated differential scanning calorimetry (TMDSC): a relatively non-mathematical approach. **Thermochimica Acta**, v. 387, n. 1, p. 75-93, 2002.

JOHNSON, R. W. Fatty alcohols. In: JOHNSON, R. W. e FRITZ, E. (Ed.). **Fatty acids in industry**. New York: Marcel Dekker, 1988. p.217-231.

KOLODZIEJ, P.; SZYMANSKA-KOLODZIEJ, M.; CHOJNACKA, I.; RYCERZ, L.; GAUNE-ESCARD, M. Phase diagram and electrical conductivity of the AgBr–NdBr3 binary system. **Journal of Alloys and Compounds**, v. 480, n. 2, p. 834-838, 2009.

MÁXIMO, G. J.; CARARETO, N. D. D.; COSTA, M. C.; SANTOS, A. O. D.; CARDOSO, L. P.; KRÄHENBÜHL, M. A.; MEIRELLES, A. J. A. On the solid-liquid equilibrium of binary mixtures of fatty alcohols and fatty acids. **Fluid Phase Equilibria**, in press.

NAYEB-HASHEMI, A. A.; CLARK, J. B. The Mg−Si (Magnesium-Silicon) system. **Bulletin of Alloy Phase Diagrams**, v. 5, n. 6, p. 584-592, 1984/12/01 1984.

NÝVLT, J. **Solid-liquid phase-equilibria**. Amsterdam: Elsevier, 1977.

PRAUSNITZ, J. M.; LICHTENTHALER, R. N.; AZEVEDO, E. G. A. **Molecular thermodynamics of fluid-phase equilibria**. 2. New Jersey: Prentice-Hall, 1986.

PRESS, W. H.; FLANNERY, B. P.; TEULOSKY, S. A.; VETTERLING, W. T. **Numerical Recipes**. The art of scientific computing. Cambridge: Cambridge University Press, 1992.

READING, M.; LUGET, A.; WILSON, R. Modulated differential scanning calorimetry. **Thermochimica Acta**, v. 238, n. 0, p. 295-307, 1994.

SANDOR, M.; BAILEY, N. A.; MATHIOWITZ, E. Characterization of polyanhydride microsphere degradation by DSC. **Polymer**, v. 43, n. 2, p. 279-288, 2002.

SAUER, B. B.; KAMPERT, W. G.; NEAL BLANCHARD, E.; THREEFOOT, S. A.; HSIAO, B. S. Temperature modulated DSC studies of melting and recrystallization in polymers exhibiting multiple endotherms. **Polymer**, v. 41, n. 3, p. 1099-1108, 2000.

SCHAINK, H. M.; VAN MALSSEN, K. F.; MORGADO-ALVES, S.; KALNIN, D.; VAN DER LINDEN, E. Crystal network for edible oil organogels: Possibilities and limitations of the fatty acid and fatty alcohol systems. **Food Research International**, v. 40, n. 9, p. 1185-1193, 2007.

SCHAWE, J. E. K. A comparison of different evaluation methods in modulated temperature DSC. **Thermochimica Acta**, v. 260, n. 0, p. 1-16, 1995.

SCHAWE, J. E. K.; HÖHNE, G. W. H. The analysis of temperature modulated DSC measurements by means of the linear response theory. **Thermochimica Acta**, v. 287, n. 2, p. 213-223, 1996.

SINGH, S.; JALALI, A.; ALDÉN, M. Modulated temperature differential scanning calorimetry for examination of tristearin polymorphism: I. Effect of operational parameters. **Journal of the American Oil Chemists' Society**, v. 76, n. 4, p. 499-505, 1999.

SLAUGHTER, D. W.; DOHERTY, M. F. Calculation of Solid-Liquid Equilibrium and Crystallization Paths for Melt Crystallization Processes. **Chemical Engineering Science**, v. 50, n. 11, p. 1679-1694, 1995.

TIMMS, R. E. Phase behaviour of fats and their mixtures. **Progress in Lipid Research**, v. 23, n. 1, p. 1-38, 1984.

VENTOLA, L.; CALVET, T.; CUEVAS-DIARTE, M. A.; MONDIEIG, D.; OONK, H. A. J. The C19H39OH-C20H41OH system: Experimental phase diagram and thermodynamic modelling. **Physical Chemistry Chemical Physics**, v. 4, n. 10, p. 1953-1956, 2002.

VENTOLA, L.; CALVET, T.; CUEVAS-DIARTE, M. A.; RAMIREZ, M.; OONK, H. A. J.; MONDIEIG, D.; NEGRIER, P. Melting behaviour in the n-alkanol family. Enthalpy-entropy compensation. **Physical Chemistry Chemical Physics**, v. 6, n. 8, p. 1786-1791, 2004.

WHITE, M. A.; PERRY, R. T. Melting Behavior in Binary Compounds: Inclusion Compounds as Examples of Congruent vs Incongruent Melting. **Chemistry of Materials**, v. 6, n. 5, p. 603-610, 1994.

WUNDERLICH, B.; BOLLER, A.; OKAZAKI, I.; ISHIKIRIYAMA, K. Heat-capacity determination by temperature-modulated DSC and its separation from transition effects. **Thermochimica Acta**, v. 304-305, n. 0, p. 125-136, 1997.

ZENG, J. L.; CAO, Z.; YANG, D. W.; XU, F.; SUN, L. X.; ZHANG, L.; ZHANG, X. F. Phase diagram of palmitic acid-tetradecanol mixtures obtained by DSC experiments. **Journal of Thermal Analysis and Calorimetry**, v. 95, n. 2, p. 501-505, 2009.

Capítulo 5. On the solid-liquid phase diagrams of binary mixtures of even saturated fatty alcohols: systems exhibiting peritectic reaction

Natália D. D. Carareto[a], Adenílson O. dos Santos[b], Marlus P. Rolemberg[c], Lisandro P. Cardoso[d], Mariana C. Costa[e], Antonio J. A. Meirelles[a]*

[a] EXTRAE, Department of Food Engineering, Faculty of Food Engineering, University of Campinas, UNICAMP, CEP 13083-862 Campinas, SP, Brazil.
[b] Social Sciences, Health and Technology Center, University of Maranhão, UFMA, CEP 65900-410 Imperatriz, MA, Brazil
[c] DETQI, Department of Chemical Technology, Federal University of Maranhão, UFMA, CEP 65085-580 São Luís, MA, Brazil
[d] Institute of Physics Gleb Wataghin, University of Campinas, UNICAMP, C.P. 6165, CEP 13083-970 Campinas, SP, Brazil
[e] School of Applied Science, University of Campinas, UNICAMP, CEP 13484-350 Limeira, SP, Brazil.

Trabalho a ser submetido na revista **Thermochimica Acta**

Abstract

The solid–liquid phase diagrams of the following binary mixtures of even saturated fatty alcohols are reported in the literature for the first time: 1-octanol (C8OH) + 1-decanol (C10OH), 1-decanol + 1-dodecanol (C12OH), 1-dodecanol + 1-hexadecanol (C16OH) and 1-tetradecanol (C14OH) + 1-octadecanol (C18OH). The phase diagrams were obtained by differential scanning calorimetry (DSC) using a linear heating rate of 1 K min^{-1} and further investigated by using a stepscan DSC method. X-ray diffraction (XRD) and polarized light microscopy were also used to complement the characterization of the phase diagrams which have shown a complex global behavior, presenting not only peritectic and eutectic reactions, but also the metatectic reaction and partial immiscibility on solid state.

Keywords

- Solid-Liquid Equilibrium;
- Fatty alcohols;
- DSC;
- Stepscan DSC.

5.1. Introduction

Fatty alcohols are classified as long chain aliphatic alcohols with a chain length larger than or equal to six carbon atoms (FISK et al., 2009). They are widely used in the cosmetic, chemical, food and pharmaceutic industries with most applications involving their lubricating, emollient, solubilizing or emulsifying properties (GANDOLFO et al., 2004; BELANGER et al., 2009). Fatty alcohols can be obtained from natural sources, either as free components or as degradation products of alcohol-containing compounds present in those sources (BELANGER et al., 2009). In industrial processes fatty alcohols are usually produced in mixtures containing a series of homologues over a range of carbon chain lengths (NOWECK e GRAFAHREND, 2000; FISK et al., 2009).

Crystallization methods for purification of fatty alcohols and other fatty substances, such as fatty acids, are recommended since these compounds can easily suffer thermal decomposition (COUTINHO e RUFFIER-MERAY, 1998; COSTA et al., 2007a). Knowledge of phase equilibria, solid-liquid equilibrium (SLE) in the case of crystallization, is essential to optimize industrial processes and to design the corresponding equipment (JAKSLAND et al., 1995). Furthermore, in order to use fatty components in the formulation of products it is important to understand their role in the final product under consideration as well as to have precise and reliable physicho-chemical data of these compounds. In fact information about SLE of fatty alcohols is required due to their use as structurants in food products (DANIEL e RAJASEKHARAN, 2003; GANDOLFO et al., 2004; SCHAINK et al., 2007). Moreover, some fatty alcohols as C14OH, C16OH and C18OH, which have a high melting point, are studied for applications in energy storage and thermal protection, and they are considered in this case as phase change materials (*PCM*) (VENTOLA et al., 2004b; VENTOLA et al., 2005).

The knowledge of solid-liquid boundaries and behavior of simple fatty systems can be helpful to understand the physical properties of complex lipids and their mixtures, but the literature concerning the SLE of fatty alcohol systems is somewhat limited in contrast with studies on the solid–liquid phase transitions of fatty acid mixtures (BAILEY, 1950;

DOMANSKA e GONZALEZ, 1997; VENTOLA et al., 2002; VENTOLA et al., 2003; INOUE et al., 2004a,b,c; VENTOLA et al., 2004a,b; COSTA et al., 2007b; COSTA et al., 2009a,b,c; CARARETO et al., 2011). Calorimetric methods, such as DSC and differential thermal analysis (DTA), are used for measuring the SLE of organic mixtures (COUTINHO e RUFFIER-MERAY, 1998; BROWN e GALLAGHER, 2008). Both techniques allow the construction of phase diagrams by measuring phase transitions of mixtures even in the case of complex phase diagrams with total or partial miscibility. In fact DSC and DTA analyses provide quantitative and qualitative information about physical and chemical changes that involve endothermic or exothermic processes and changes in heat capacity (COUTINHO e RUFFIER-MERAY, 1998).

The present study is part of a series concerning SLE of binary mixtures formed by saturated fatty alcohols. DSC with a linear heating rate, a well stablished method (COSTA et al., 2007b; COSTA et al., 2009a,b,c; BOROS et al., 2009c; CARARETO et al., 2011; COSTA et al., 2011; COSTA et al., 2012), stepscan DSC, optical microscopy with temperature control and XRD were employed to characterize the solid-liquid behavior of the following mixtures of saturated fatty alcohols: C8OH + C10OH, C10OH + C12OH, C12OH + C16OH and C14OH + C18OH. The solid-liquid phase diagrams for these four binary systems are, as far as we know, published for the first time in the literature.

5.1.1. Differential scanning calorimetry (DSC): Stepscan DSC

The Temperature-modulated DSC (TMDSC) is a technique recently proposed to make possible a better understanding of thermal phase transitions. TMDSC consists of a combination of a linear rate superimposed by a sinusoidal heating sign suggested to allow the deconvolution of reversible and non-reversible transitions (SCHAWE e HÖHNE, 1996; JIANG et al., 2002). A simple version of the TMDSC involving multiple cycles of a linear heating rate in a small temperature range followed by an isothermal hold named stepscan DSC was proposed by Perkin-Elmer. The heat flow response to the heating (or cooling) segment is the thermodynamic component and reflects the reversing changes of the samples, as for example, melting and glass transition.

Both tecniques, TMDSC and stepscan DSC, were especially developed to separate the time dependent and time independent components of a number of transition phenomena. These techniques are mostly applied in the studies with polymers (SAUER et al., 2000; SCHICK, 2002; PIELICHOWSKA e PIELICHOWSKI, 2010; XIVILLÉ et al., 2012), since the effects of material relaxation interfere in the conventional DSC analysis. Basically, the relaxation problem is related to the size of molecules, but the TMDSC and stepcan DSC techniques have also shown good results in the application to materials with comparatively shorter organic chains, such as biodiesel and triacylglycerols (BAICHOO et al., 2006; RAMALHO et al., 2012).

In the stepscan DSC analysis the parameters that have to be adjusted are heating rate, second temperature, isothermal period and criteria of stability (Fig.5.1). The applied linear heating rate (in Fig.5.1 represented by κ = dT/dt) is related to the sensitivity and resolution of a DSC analysis. The sensitivity of any measurement can be improved by heating at a faster rate, whereas in order to increase the transition resolution that occur within a small range of temperature the scan rate must be lowered. So the sensitivity is defined always at the expense of the resolution and vice versa (VERDONCK et al., 1999; JIANG et al., 2002). Other parameter to be adjusted is the second temperature (ΔT in Fig.5.1). It makes reference to the temperature step used in every cycle in the stepscan DSC. Given the fact that fatty systems exhibit a large number of transitions within a small interval of temperatures, as shown in previous works (BOROS et al., 2009a; COSTA et al., 2009a,b; CARARETO et al., 2011), a small ΔT is required to achieve well-defined peaks in the thermal curve (BAICHOO et al., 2006).

The isothermal period (Δt in Fig.5.1) is the main aspect that differentiates the stepscan from the linear heating rate DSC, since, during the isothermal period, the sample is able to reach thermal equilibrium in contrast to the standard method in which the sample is always in a quasi-equilibrium state. The effect of quasi-equilibrium can be minimized using small samples and applying a slow heating rate in the DSC analyses, usually 1-2 K min^{-1}. Considering that materials with a low thermal conductivity, such as fatty compounds, tend to form temperature gradients within the samples, it is recommeded to use small

samples, with weight of 3-5 mg, and an isothermal period that could ensure the sample reachs the thermal equilibrium.

The criterion of stability of the heat flow is other parameter related to the isothermal period of the stepscan DSC. This criterion exists to eventually shorthen the isothermal step and it consists in checking the heat flow to/from the samples during the pre-specified time interval (Δt). When a set of seven consecutive data points falls within the pre-defined heat flow equilibrium criterion the isotherm step ends and the next scanning step (with the linear heating rate) starts. If the criterion of stability is overstimated the isothermal step can be crossed with the sample not reaching thermal equilibrium (BAICHOO et al., 2006).

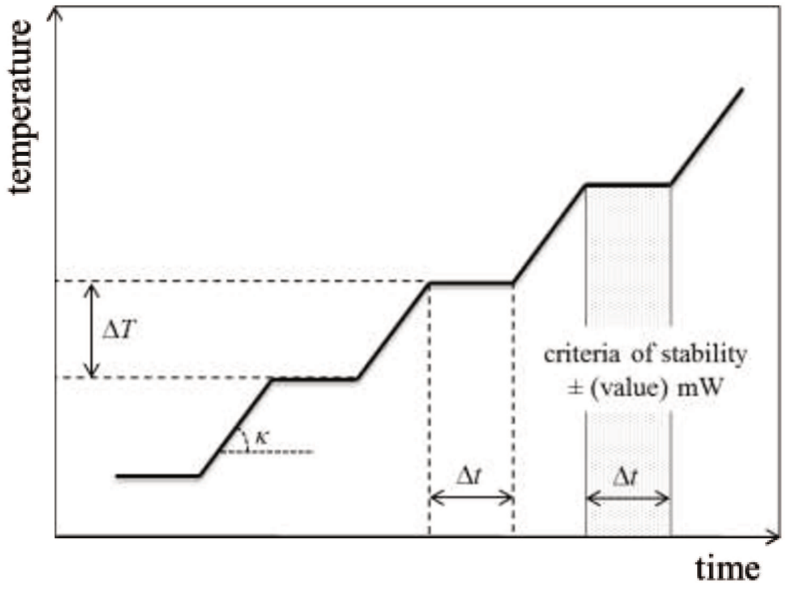

Fig.5. 1. Schematic illustration for temperature response versus time in a stepscan DSC analysis.

5.2. Experimental Section

5.2.1. Preparation of fatty alcohol binary mixtures

The fatty alcohols listed in Table 5.1 were purchased from Sigma-Aldrich and used with no further purification. The binary mixtures were prepared as described in a previous work (CARARETO et al., 2011). Standards materials for DSC calibration were: indium (99.99%) provided by TA Instruments or Perkin-Elmer, cyclohexane (min. 99%) and naphthalene (min. 99%), both from Merck. Commercial nitrogen (used for preparing binary samples) and high purity nitrogen (used in the calorimeters) were supplied by Air Liquide.

Table 5. 1. Melting temperature for pure fatty alcohols using standard and stepscan DSC analyses.

Fatty alcohol	Purity[a]	Melting temperature (K)		Deviation[b] (K)
		Standard	Stepscan	
C8OH	0.995	258.7 ± 0.2	258.3 ± 0.1	0.4
C10OH	0.994	280.6 ± 0.2	279.9 ± 0.1	0.1
C12OH	0.998	297.8 ± 0.3	297.4 ± 0.2	0.4
C14OH	0.984	311.2 ± 0.1	310.9 ± 0.4	0.3
C16OH	0.999	323.3 ± 0.2	323.0 ± 0.3	0.3
C18OH	0.996	331.6 ± 0.1	331.6 ± 0.4	0.1

[a] according to the supplier; [b] ($T_{melt,standard}$-$T_{melt,stepscan}$)

5.2.2. Differential scanning calorimetry – Standard and stepscan DSC

The molar fractions of the binary systems were selected to cover the entire range of composition. To perform all the DSC analyses the samples were placed in hermetic aluminium pans and weighed in a Perkin-Elmer AD-6 microbalance (±0.02 mg).

The binary systems were analysed by using two different DSC methods. The first method, here named as *standard DSC*, was performed using a TA Instruments MDSC 2920 calorimeter with a linear heating rate of 1 K min^{-1} to evaluate the transitions for all samples as described elsewhere (CARARETO et al., 2011). The temperature uncertainty for

standard DSC was estimated to be not larger than 0.3 K. The second DSC method, here named *stepscan DSC*, was carried out with a Perkin-Elmer DSC 8500 calorimeter coupled to a cooling system (Intracooler III) in order to be compared with the standard DSC results for the systems C12OH + C16OH and C14OH + C18OH, as will be discussed.

Several sets of parameters were tested with the aim of determining a reliable procedure for the stepscan DSC method and a brief discussion is made in sequence. The parameters adjusted were heating rate (κ), second temperature (ΔT), isothermal step (Δt) and criteria of stability. A heating rate of 2 K min^{-1} is recommended by the equipment manufacturer and was used in this study. We tested the following ΔT values: 0.1, 0.2 and 0.3 K. In the case of $\Delta T = 0.1\,K$, due to the small temperature step, the relative noise has increased, making difficult to separate the transitions in the thermal curves. When applying a ΔT equal to 0.2 or 0.3 K, no significant difference in the the results for both tempererature step was observed, so $\Delta T = 0.2\,K$ was used, since it shows a good resolution of the thermal curves with insignificant influence upon the noises of the stepcan DSC results.

The isothermal step is a crucial parameter in stepscan DSC. A Δt value of 1 min was insufficient to allow the samples to reach thermal equilibrium and the interpretation of thermal curves was difficult. In this way, a Δt of 2 and 3 min were also tested, resulting in very similar thermal curves. The $\Delta t = 2\,\text{min}$ was selected since the total time of each analysis is smaller. A stability criterion of ± 0.002 mW was used in this work showing a good repeatibility.

Standard deviations for stepscan DSC were estimated by performing repeated experimental runs at least three times with each pure fatty alcohol. The standard deviations of the measurements ranged from 0.03 to 0.4 K. On this basis the uncertainty of the phase equilibrium data measured in the present work with stepscan DSC method was estimated to be not larger than 0.4 K.

5.2.3. Polarized light microscopy

The samples were placed in a temperature controller (Instec STC200) programmed with a heating rate of 0.1 K min^{-1} and a polarized light microscope (Motic BA-200) connected to a digital camera (Moticom 2300) was used to acquire images with a magnification of forty times every 0.5 K.

5.2.4. X-Ray difraction

The X-ray powder diffraction analyses were performed at different temperatures with a Philips diffractometer working in the Bragg-Brentano (θ:2θ) geometry, using Cu-Kα radiation and a secondary graphite monochromator. The X-ray patterns were collected at constant temperature using an Anton PAAR TTK 450 camera, with a heating rate of 1 K min^{-1} and 5 min of stabilization time. The measurements were taken from 273 K until melting. The patterns were scanned with 0.02° in 2θ steps and acquisition time of 2 seconds, with scans of 5 to 40° (2θ scale).

5.3. Results and discussion

In DSC analysis, the transitions that occur in the samples are identified as peaks generated in the thermal curves (heat flow versus temperature). In general, for pure substances, the melting temperatures are commonly presented as the onset temperature of the peak (COSTA et al., 2007b), but in the case of the existence of polymorphic transitions close to the melting temperature the use of peak top temperature is recommended to avoid errors on temperature evaluation (COSTA et al., 2009b,c). Thus, in this study the peak top temperature was considered as the melting temperature or as the temperature of other observed transitions. Pure fatty alcohols melting temperatures obtained by standard and stepscan DSC methods are presented in Table 5.1. The absolute deviation between the temperatures was lower than 0.4 K.

5.3.1. 1-octanol + 1-decanol and 1-decanol + 1-dodecanol systems

Tables 5.2 and 5.3 present the temperatures of the solid-liquid and solid-solid phase transitions obtained with the standard DSC method for systems C8OH + C10OH and C10OH + C12OH, respectively. The SLE phase diagrams are shown in Figs. 5.2 and 5.3. Observe that the C8OH + C10OH system exhibts in the liquidus line two inflection points associated to the eutectic and peritectic reactions. To C10OH + C12OH system an additional inflection point was observed in the liquidus line around $x_{\mathrm{C10OH}} \cong 0.9$, which corresponds to a second peritectic reaction rich in the shorter chain alcohol.

The eutectic point is identifyed as the point in the solid-liquid phase diagram which two solid phases and a liquid solution, saturated with both compounds, are in equilibrium at a defined composition, x_E, and temperature, T_{E} (NÝVLT, 1977). The T_{E} is the lowest temperature in which the liquid phase can be observed. The eutectic reaction occurs along a line at T_{E} and the amount of liquid formed at this temperature varies as a function of the system composition. This means that the eutectic reaction enthalpy also varies as function of the system composition. The relation between system composition and the reaction enthalpy is known as Tamman plot, which makes possible to identify the range of concentration associated with this reaction (CHERNIK, 1995; GUENET, 1996). In fact, the energy required for the eutectic reaction to occur is proportional to the quantitie of liquid formed at T_{E} in the mixture, following the lever rule applied to the mixture´s overal composition. For a simple eutectic system, the Tamman plot must present a maximum at the eutectic point concentration and a minimum at the extremes of the phase diagram (INOUE et al., 2004a; COSTA et al., 2007b; BOROS et al., 2009b). A similar connection between composition and enthalpy is found for peritectic and metatectic reactions.

Table 5. 2. Solid–liquid equilibrium data for the C8OH + C10OH system using standard DSC.

x_{C8OH}	$T_{s\text{-}s}$ (K)	T_{eut} (K)	T_{per} (K)	T_{melt} (K)
0.0000	280.1			280.6
0.1012	247.6		251.2	277.5
0.2084	247.0		253.3	275.0
0.3084	247.4		252.8	272.8
0.4018	247.4		253.3	269.2
0.5036	247.5		253.3	265.0
0.5994	247.1		254.3	259.4
0.6613	248.2	250.1		254.7
0.7450	247.7	249.7		252.4
0.7962	244.5			249.2
0.8964	245.4	249.0		251.6
0.9313	243.3	248.8		253.5
0.9693		249.0		255.6
1.0000	255.5			258.7

$T_{s\text{-}s}$ = solid-solid transition temperature; T_{eut} = eutectic reaction temperature; T_{per} = peritectic reaction temperature and; T_{melt} = melting temperature.

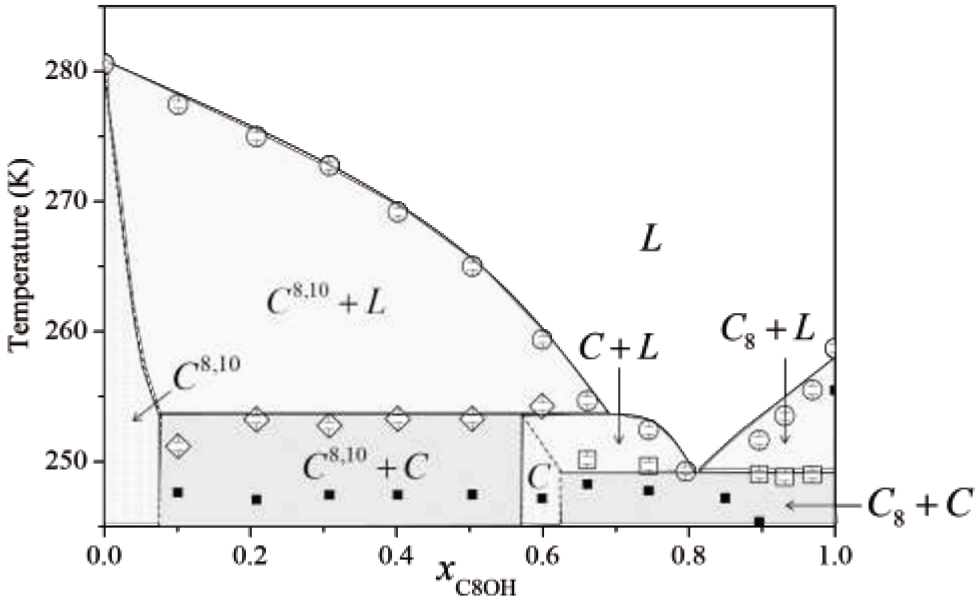

Fig.5. 2. Solid-liquid phase diagram of the C8OH + C10OH system by standard DSC. ○ melting temperature; □ eutectic reaction; ◊ peritectic reaction; ■ solid-solid transition. (---) and (—) are guide to the eyes. *L*: the liquid phase; $C^{8,10}$: solid solution rich in C10OH; C_8: C8OH pure on solid state and; *C*: peritectic compound.

Table 5. 3. Solid–liquid equilibrium data for the C10OH + C12OH system using standard DSC.

x_{C10OH}	$T_{s\text{-}s}$ (K)	$T_{s\text{-}s}$ (K)	$T_{s\text{-}s}$ (K)	T_{eut} (K)	T_{per} (K)	T_{met} (K)	$T_{s\text{-}l}$ (K)	T_{melt} (K)
0.0000			296.6					297.8
0.1042	261.6	264.9						295.6
0.2108	261.7	265.0				278.1		292.9
0.3025	262.0	264.9	271.9		275.2	280.0	285.4	290.6
0.4050			272.0		276.4	280.2		288.1
0.4977	261.6	264.8	272.3		276.3	280.1		282.7
0.5991			272.3					276.4
0.6486				272.4				275.0
0.6981				272.5				274.6
0.7501								272.9
0.8033	262.7							273.1
0.8486				273.0				273.3
0.9018	265.4			273.2				275.2
0.9382					274.2			277.0
0.9696					274.2			279.0
1.0000			280.1					281.1

$T_{s\text{-}l}$ = solid-liquid transition temperature; T_{met} = metatectic reaction temperature.

The Tamman plot for the C8OH + C10OH system is shown in Fig. 5.4a. Note that the eutectic reaction enthalpy increases in function of system's concentration until reach the eutectic point, corresponding to the maximum value of enthalpy obtained at a concentration around $x_{C8OH} \cong 0.81$. An additional transition was observed for compositions smaller than $x_{C8OH} < 0.6$ at temperatures close to the eutectic one (around 247 K), but the corresponding enthalpy values do not fit in the prior linear behavior as observed for the eutectic reaction enthalpy. This additional thermal event corresponds probably to a solid-solid transition. A similar behavior was previously observed for systems formed by saturated fatty acids (COSTA et al., 2009a,b,c). The enthalpy from the transition observed around 253 K were also plotted in the Tamman plot shown in Fig. 4a, being possible to detect that the enthalpy values increase in function of the system composition. This transition was associated to the peritectic reaction. Note that a line drawn between the enthalpy values does not extend to the pure component ($x_{C8OH} = 0.0$). This result confirms the existence of a solid solution

region in the extreme of the phase diagram rich in C10OH and is an indicative that the biphasic region does not exist for compositions smaller than $x_{C8OH} < 0.10$. The liquidus line of the binary diagram can be divided into two regions separated by the eutectic inflection point: the first one extends within a larger concentration range, being easier to characterize due to the higher number of experimental data available; the second region, close to the melting temperature of C8OH, is smaller and the thermal events occur in a narrower range of temperature. From the available experimental data, including the Tamman plot, we propose that in this second region is an eutectic domain, as evidenced in Fig. 5.2.

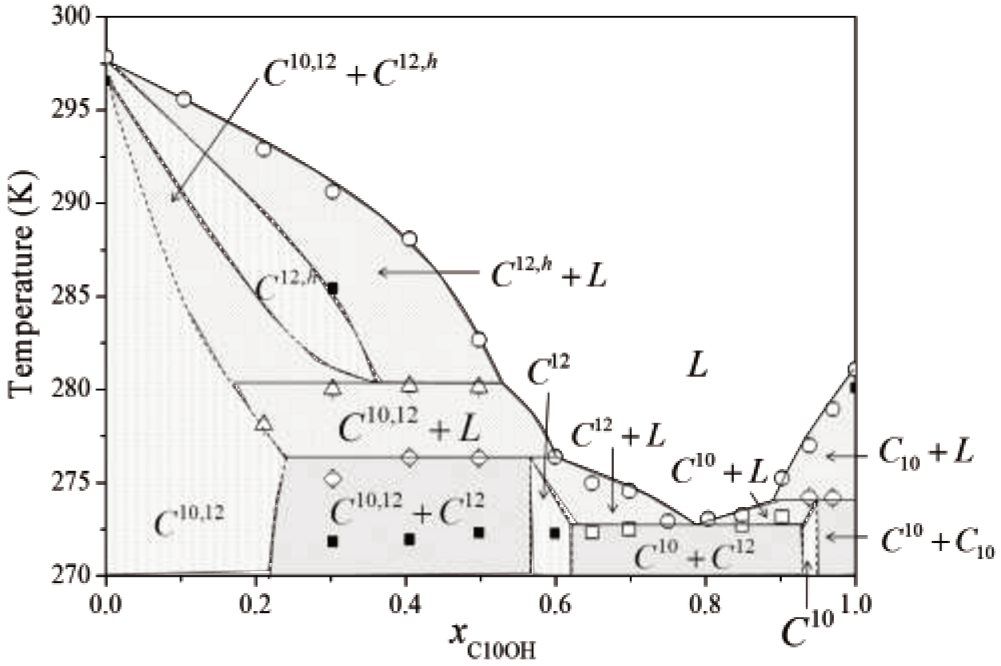

Fig.5. 3. Solid-liquid phase diagram of the C10OH + C12OH system by standard DSC. ○ melting temperature; □ eutectic reaction; ◊ peritectic reaction; Δ metatectic reaction; and ■ solid-solid transition. (---) and (—) are guides to the eyes. *L*: liquid phase; C_{10}: C10OH pure on solid state, $C^{10,12}$: solid solution rich in C12OH; C^{12}: peritectic compound rich in C12OH; C^{10}: peritectic compound rich in C10OH; and $C^{12,h}$: metatectic compound.

The phase diagram for the C8OH + C10OH system is proposed in Fig. 5.2 and the notation used in the division of the phase diagram has the following meaning: $C^{8,10}$

corresponds to a solid solution formed rich in C10OH; C_8 corresponds to the C8OH pure in solid state and the *C* phase is related to the peritectic compound. The following domains are presented in the phase diagram for the C8OH + C10OH system: one homogeneous liquid phase - region (*L*), 2 monophasic solid domains - regions ($C^{8,10}$) and (*C*); 3 biphasic solid-liquid domains - regions ($C^{8,10}$ + *L*), (C_8+ *L*) and (*C* + *L*); and 2 biphasic solid-solid domains – regions (C_8 + *C*) and ($C^{8,10}$ + *C*).

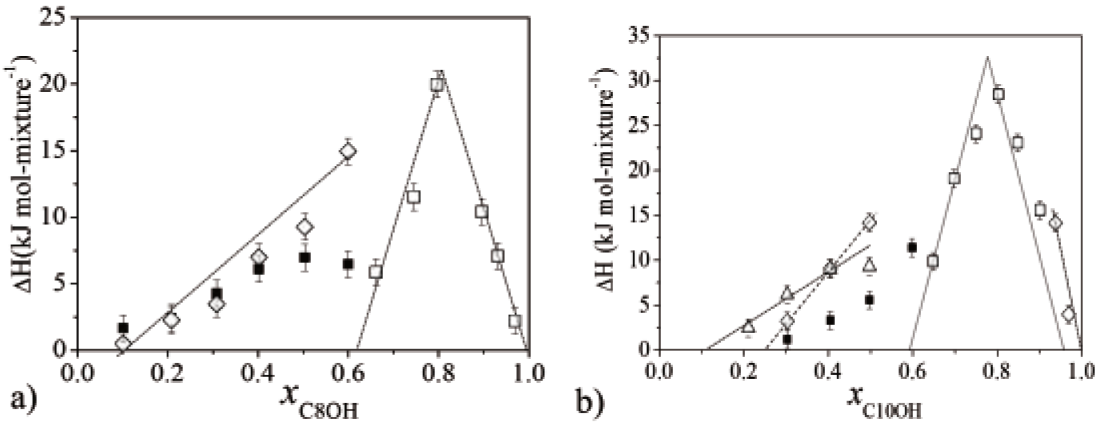

Fig.5. 4. Tamman plots based on standard DSC. a) C8OH + C10OH system and; b) C10OH + C12OH system. □ eutectic reaction; ◊ peritectic reaction; Δ metatectic reaction and; ■ solid-solid transition.

The eutectic and peritectic reactions also occur for the C10OH + C12OH system, as set in the Tamman plot for standard DSC analyses (Fig. 5.4b). In the case of this system, the eutectic point is located between $0.75 < x_{C10OH} < 0.8$. Consequently the DSC result at this region is an unique peak in which the melting and eutectic reaction are built-in and, sometimes, are indistinguishable. In this way, we assumed that the total enthalpy for the peaks around 273 K as the eutectic enthalpy at compositions between $0.75 < x_{C10OH} < 0.8$ for fitting the Tamman plot (Fig.5.4b).

An additional transition observed around 280 K was also identified for some samples (as can be noted in Fig.5.3). In the same way observed for eutectic and peritectic reactions the enthalpy of the mentioned transition increases in function of the system

composition and also presents a significative value of enthalpy. Similar behavior was observed for binary fatty acids systems and it was attributed to a metatectic reaction (COSTA et al., 2009a,b,c). The metatectic reaction is defined as a reversible reaction of a solid mixture phase β into a different solid phase α plus a liquid phase during cooling of a system occuring along the metatectic line characterized by the metatectic temperature (GAMSJAGER et al., 2008).

From the analysis of the DSC results and the Tamman plot (Fig.5.4b), in the region close to the melting temperature of C10OH, a second peritectic reaction was found (as shown in Fig.5.3 and Fig.5.4b through the symbol ◊). As for the C8OH + C10OH system, the temperature range in which the transitions are occuring is relatively small and the available experimental data does not allow a better characterization of the Tamman plot, in this way, we propose that in this region the compounds are immiscible on solid state.

The phase diagram for C10OH + C12OH with the regions of SLE is drawn in Fig.5.3. It is important to notice that some transitions found under T_E and which have a negligible value of enthalpy are related, most probably, to solid-solid transitions that are not interesting in the scope of this study. As the notation used for C8OH + C10OH, the different domains of the phase diagram has the following meaning: $C^{10,12}$ is related to a solid solution rich in C12OH, C^{10} and C^{12} are related to the peritectic compound in the regions rich in C10OH and C12OH, respectively, C_{10} is associated to the C10OH as pure component and the superscript "*h*" was used to indicate that a new crystal structure is formed due to the metatectic reaction. The following domains are presented in the phase diagram for the C10OH + C12OH system: one homogeneous liquid phase - region (*L*), 4 monophasic solid domains - regions ($C^{10,12}$), (C^{10}), (C^{12}) and ($C^{12,h}$); 5 biphasic solid-liquid domains - regions ($C^{10,12} + L$), ($C^{10} + L$), ($C^{12} + L$), ($C_{10} + L$) and ($C^{12,h} + L$); and 4 biphasic solid-solid domains – regions ($C^{10} + C_{10}$), ($C^{10} + C^{12}$), ($C^{10,12} + C^{12}$) and ($C^{10,12} + C^{12,h}$).

5.3.2. 1-dodecanol + 1-hexadecanol and 1-tetradecanol + 1-octadecanol systems

The stepscan DSC method was positively applied to describe the SLE of systems containing fatty acid + fatty alcohols which have present some exothermic transitions during the heating DSC analyses (CARARETO et al., submitted article). In this work we applied the same proposed method in the case of C12OH + C16OH and C14OH + C18OH systems to verify the range of the stepscan method for other fatty systems. As discussed above, the stepscan is a DSC tool which is capable of separating the thermal response into two signals, the first one related to the reversible or thermodynamic component and the other, the irreversible component, associated with kinetic effects of the heating or cooling rate.

Fig.5.5 exhibits the thermal curves of the C14OH + C18OH system, obtained by standard and stepcan DSC for the composition $x_{C14OH} = 0.6012$. The peaks occuring at higher temperatures are atributted to the complete melting of the sample for both methods. Some additional peaks are atributted to other events that occur during the sample heating, such as the eutectic and peritectic reactions that usually present well defined peaks. The other peaks are smaller and spreader and can be related to polymorphic transitions. Note in Fig.5.5 that the peaks representing the samples melting for stepscan and standard DSC have similar shape and intensity (i.e. enthalpy). The melting temperatures for standard and stepscan DSC methods were compared and an average absolute deviation equal to 0.4 K was found.

Also in Fig.5.5, it is possible to note a transition that occurs around 307 K (a arrow is indicating the transition). As we are going to discuss briefly, this transition is related to some solid-solid transition probably associated to kinetic aspects of the analysis. Observe in the standard DSC response that this transition has a high enthalpy value, nevertheless for the stepscan DSC its value is lower. Indeed, we expected that stepscan DSC would remove all transitions related to kinetic aspects, but they were only minimized by the use the stepcan DSC method. Possibly this fact can be attributed to the stability criterion used. Still,

the stepscan DSC provided reliable data, and they were used in this work to discuss the SLE for the C12OH + C16OH and C14OH + C18OH systems.

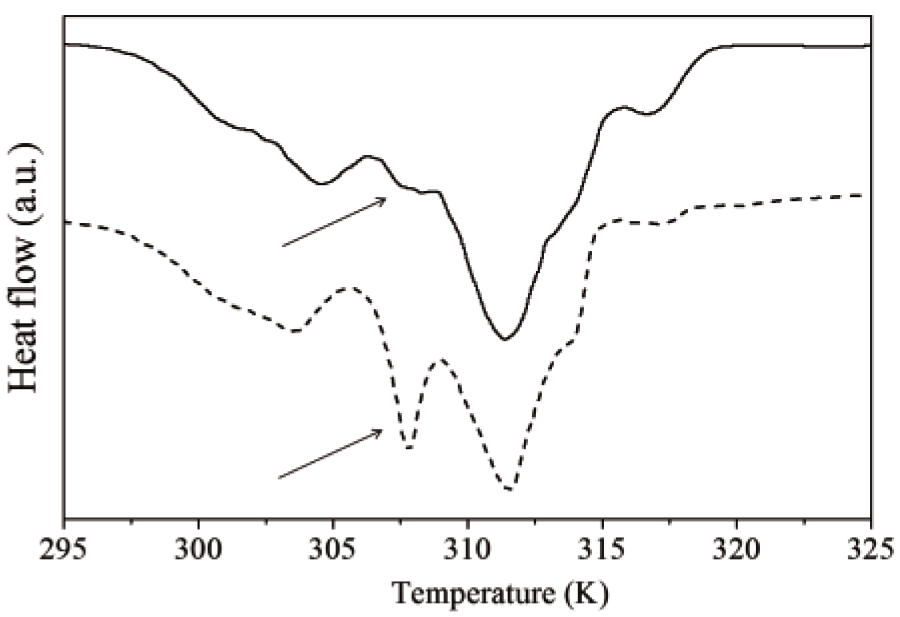

Fig.5. 5. DSC thermal curves of the system C14OH + C18OH for composition $x_{C14OH} = 0.6012$. (---) standard DSC at 1.0 K min^{-1} and; (—) stepscan DSC.

The phase diagrams of both systems are presented in Figs.5.6 and 5.7, obtained from standard DSC (Figs.5.6a and 5.7a) (at 1.0 K min^{-1}), and from stepscan DSC (Figs.5.6b and 5.7b). Note in the phase diagrams for C12OH + C16OH, that some transitions occuring in Fig.5.6a were not found in the case of the phase diagram obtained from stepscan DSC (Fig.5.6b). Also, for the C14OH + C18OH system, in Fig.5.7a the transition observed around 307 K in the region comprised between $0.2 < x_{C14OH} < 0.6$ does not occur in Fig.5.7b.

Tables 5.4 and 5.5 report the solid–liquid equilibrium data for the C12OH + C16OH and C14OH + C18OH systems, respectively, obtained using stepscan DSC. Observing the liquidus line of the phase diagrams presented in Figs.5.6 and 5.7 it is clear the occurrence of two inflection points, the first one at smaller temperatures which can be attributed to the

eutectic reaction and the second one, few degrees above, that can be associated to a peritectic or metatectic reaction as the following discussions. Both systems exhibit other transitions observed at higher temperatures, around 314 K in the case of C12OH + C16OH and around 322 K for the C14OH + C18OH system. In order to investigate these transitions and better set the limits of the SLE regions other experimental techniques were applied. The corresponding results are presented and discussed bellow.

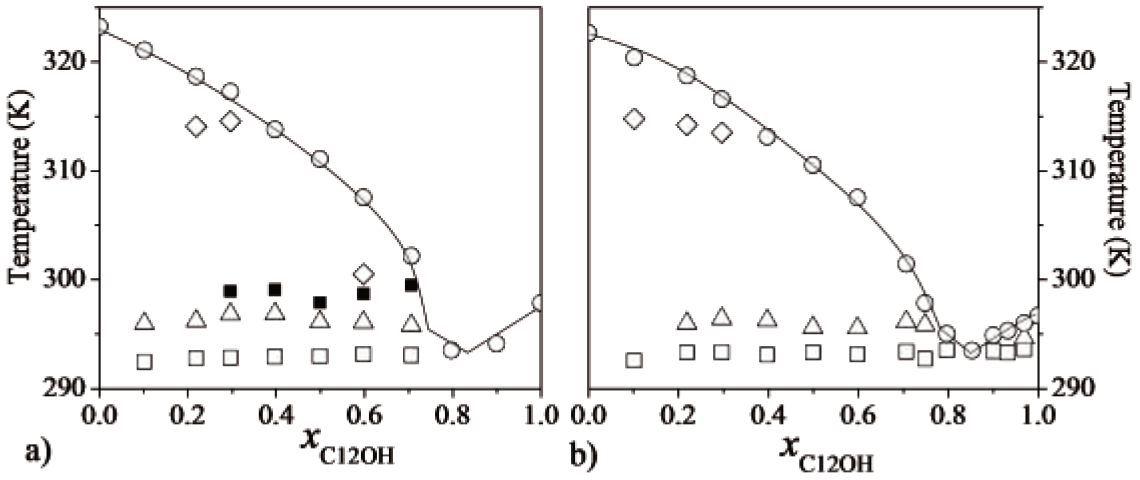

Fig.5. 6. DSC analyses for the C12OH + C16OH system. a) standard DSC results and; b) stepscan DSC results. ○ melting temperature; □ eutectic reaction; ◊ metatectic reaction; ■ solid-solid transition. (—) is a guide to the eye.

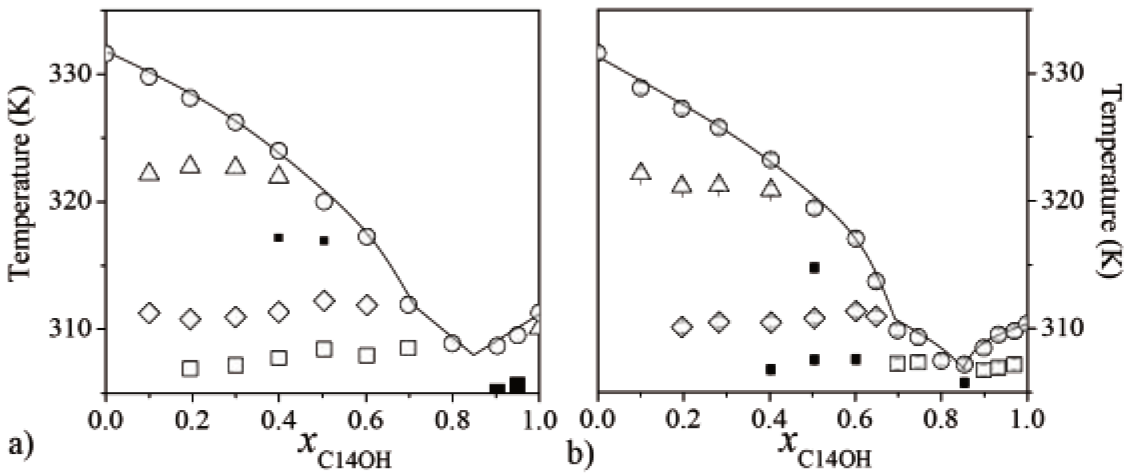

Fig.5. 7. DSC analyses for the C14OH + C18OH system. a) standard DSC results and; b) stepscan DSC results. ○ melting temperature; □ eutectic reaction; ◊ peritectic reaction; ♦ metatectic reaction; ■ solid-solid transition. (—) is a guide to the eye.

Table 5. 4. Solid–liquid equilibrium data for the C12OH + C16OH system using stepscan DSC.

x_{C12OH}	T_{eut} (K)	T_{met} (K)	T_{per} (K)	$T_{s\text{-}s}$ (K)	T_{melt} (K)
0.0000				321.9	322.7
0.1014	292.6		314.8		320.4
0.2187	293.3	296.0	314.2		318.7
0.2964	293.3	296.4	313.5		316.6
0.3972	293.1	296.2			313.1
0.4992	293.3	295.6			310.5
0.5980	293.2	295.5			307.5
0.7066	293.4	296.1			301.4
0.7483	292.7	295.9			297.8
0.7970	293.5				295.0
0.8526					293.5
0.8998	293.4				294.9
0.9324	293.3				295.3
0.9686	293.6				296.0
1.0000				296.6	296.7

- *C14OH + C18OH system*

The transitions enthalpies for the C14OH + C18OH system were plotted versus composition, as can be seen in Fig.5.8a. As discussed for the C8OH + C10OH and C10OH + C12OH systems, the enthalpies of the transitions that happen under liquidus line have presented a linear dependence of the system composition. The transition occuring around 307 K was related to the eutectic reaction, while the transitions found at 310 K and 322 K were associated to the peritectic and metatectic reactions, respectively. From the analyses of the Tamman plot, it was also possible to identify the formation of a solid solution close to the pure C18OH region, meaning that the two compounds are partially miscible in the solid state. On the other hand, the region of SLE rich in C14OH is very small and makes difficult the evaluation of the transitions enthalpies in the thermal curves. The overlapped peaks do not allow a clear identification of the eutectic transition and preclude the confirmation of a possible solid solution in this part of the diagram. In this case, we suggest that in this regions the components of the mixture are immiscible on the solid state.

Table 5. 5. Solid–liquid equilibrium data for the C14OH + C18OH system using stepscan DSC.

x_{C14OH}	$T_{s\text{-}s}$ (K)	$T_{s\text{-}s}$ (K)	T_{eut} (K)	T_{per} (K)	$T_{s\text{-}l}$ (K)	T_{met} (K)	T_{melt} (K)
0.0000		331.3					331.6
0.1006						322.1	328.9
0.1964				310.1		321.2	327.3
0.2826	303.5			310.5		321.2	325.7
0.4036	303.7	306.8		310.5		320.9	323.2
0.5046	304.1	307.6		310.8	314.8		319.4
0.6012	304.5	307.6		311.4			317.0
0.6483	303.7			311.0			313.7
0.6982	304.0		307.2				309.9
0.7469	304.0		307.4				309.3
0.8006	304.6						307.5
0.8540	305.8						307.2
0.8990	304.6		306.8				308.5
0.9335			307.0				309.5
0.9708			307.2				309.8
1.0000		310.1					310.4

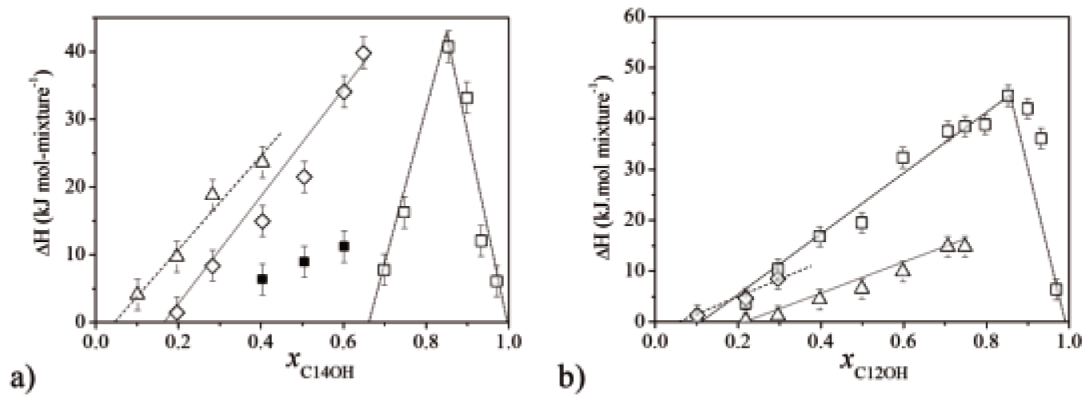

Fig.5. 8. Tamman plots based on stepscan DSC. a) C14OH + C18OH system and; b) C12OH + C16OH system. □ eutectic reaction; ◊ peritectic reaction; Δ metatectic reaction and; ■ solid-solid transition.

Some polarized light microscopy images obtained for the C14OH + C18OH system at a composition $x_{C14OH} = 0.1951$ are presented in Fig.5.9 in a temperature range from 300 to 327 K. At 300 K it is easy to see that the sample is in solid state and the crystals are arranged in thin overlapped layers presenting an irregular shape. In a conventional phase diagram presenting only eutectic and peritectic points a SLE region must exist within the region comprised between the liquidus line and the peritectic temperature (NÝVLT, 1977). According to the lever rule, if we suppose that the C14OH + C18OH system have this type of phase diagram, then at 320 K the amount of liquid present in equilibrium for a sample with the composition $x_{C14OH} = 0.1951$ would be around 40%, which means that almost half of the sample in the coverslip should be in liquid state. But at this temperature it is difficult to observe liquid in the image (see Fig.5.9b). At 325 K, the sample shape changes, becoming round, due to its partial melting, as can be seen in Fig.5.9c. However, at 325 K the amount of liquid on the coverslip does not follow the lever rule as it would be expected for a conventional phase diagram with only eutectic and peritectic points (without any solid solution in the extreme left of the phase diagram or presenting metatectic reaction), in this case the portion of liquid on the coverslip at 325 K should be higher than 50%. An

additional increase of only two degrees, to 327 K (Fig.5.9d), brings the sample to the liquid phase with small quantity of crystals co-existing in equilibrium.

Fig.5.10 shows images of the C14OH + C18OH system at different temperatures and compositions. According to Fig.5.10a, the sample remains in the solid state for both temperatures (308 and 320 K). For this composition (x_{C14OH} = 0.1000), the sample starts melting only at a temperature higher than 323 K, confirming that the event observed by both DSC methods close to this temperature is related to a solid-liquid transition. On the other hand, the images obtained for the composition of x_{C14OH} = 0.2998 at 320 K (Fig.5.10b) show the partial melting of the sample, indicating that the boundary between solid and liquid phases at this temperature starts within the composition range 0.1000 < x_{C14OH} < 0.2998. For a higher molar fraction of C14OH (x_{C14OH} = 0.6022) no liquid is obseved at 308 K, but at 310 K (Fig.5.10c) a SLE domain is reached (observed the transition at temperatures close to 310 K in the phase diagram shown in Fig.5.8b) and liquid is easyly detected on the coverslip. For the composition x_{C14OH} = 0.7992 the mixture is almost completely melted at a temperature of only 308 K (Fig.5.10d), a value close to the eutectic temperature.

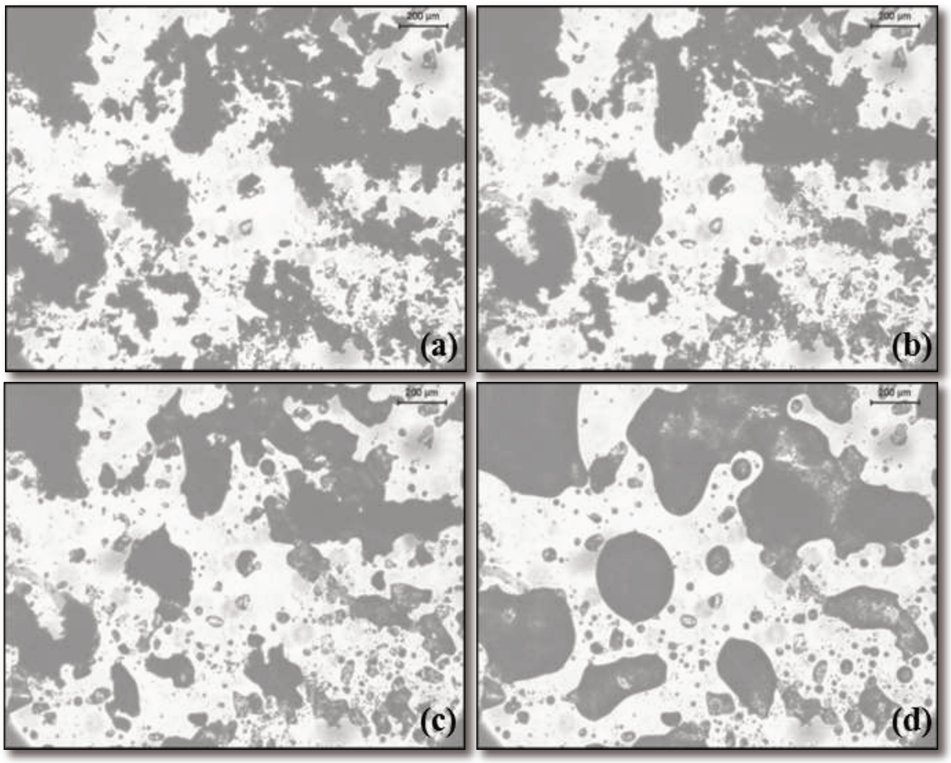

Fig.5. 9. Light microscopy images of the system C14OH + C18OH for $x_{C14OH} = 0.1951$. (a) 300 K; (b) 320 K; (c) 325 K; (d) 327 K.

X-ray diffraction analyses were performed for the pure components C14OH and C18OH and for their mixture at composition $x_{C14OH} = 0.2998$ in order to identify and check the transitions found in the DSC analyses and in the mycroscope images. The effect of the temperature on the diffractograms was evaluated but, unfortunately, most solid phases present very similar powder diffractograms, making difficult to distinguish the solid phases and to observe some transitions present in the phase diagram. Despite this fact it was possible to collect interesting information from them that support the proposed phase diagram.

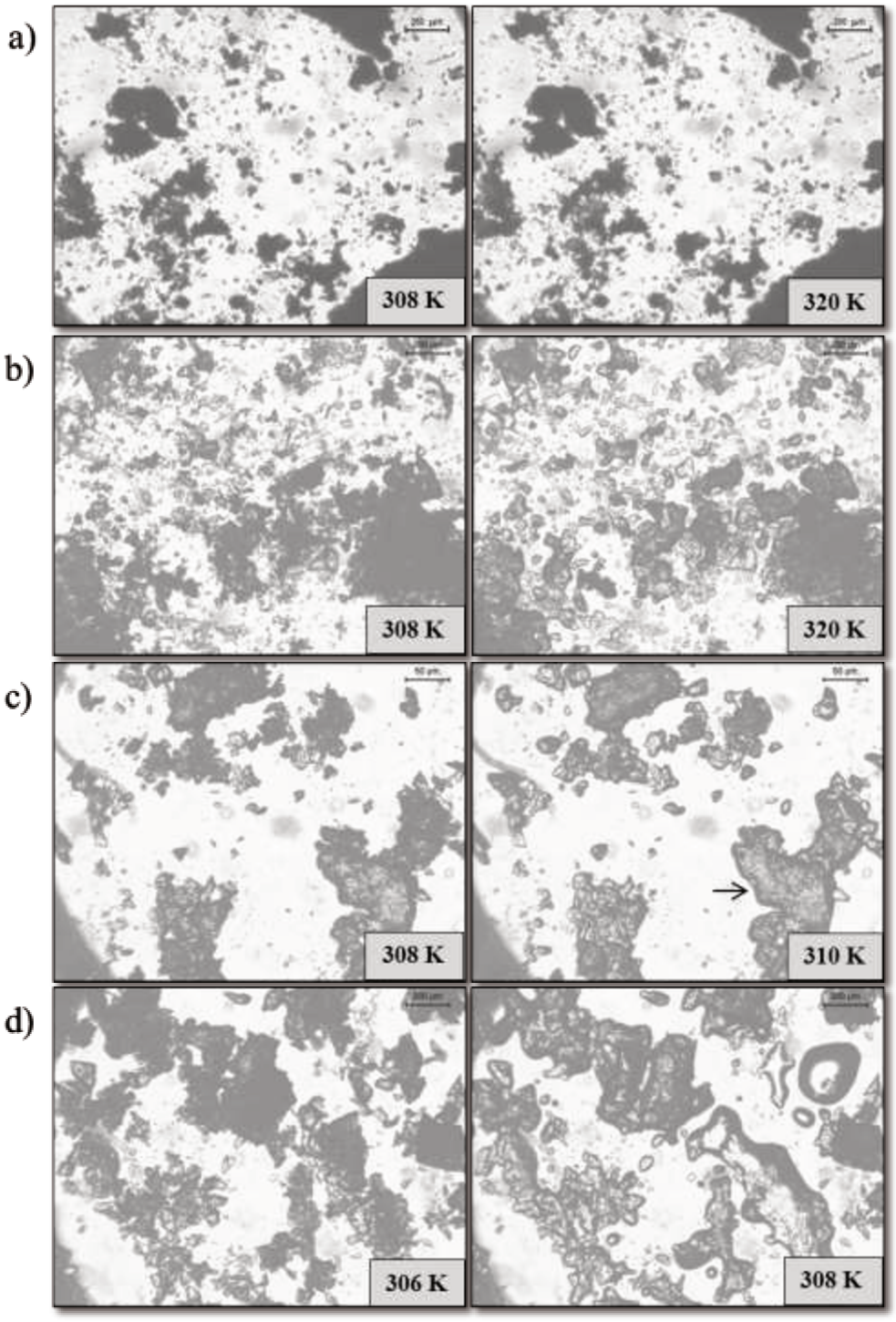

Fig.5. 10. Light microscopy images of the system C14OH + C18OH at different compositions and temperatures. (a) x_{C14OH} = 0.1000; (b) x_{C14OH} = 0.2998; (c) x_{C14OH} = 0.6022; (d) x_{C14OH} = 0.7992.

Fig.5.11a shows the X-ray pattern of the system C14OH + C18OH at $x_{C14OH} = 0.2998$. Within the temperature range from 273 to 318 K no visible change in the X-ray pattern was observed, this means that the crystaline structures of the solid state do not undergo any significant change. On the other hand, at the temperatures of 321 K and 322 some peaks appear/disappear on the diffraction pattern, as indicated by the arrows in Fig.5.11a. This means that the transition observed in thermal curves around 322 K is also detected by another analytical method, confirming the change in the crystaline structure of the solid phase and the occurrence of a metatectic reaction. For temperatures equal to or higher than 323 K the changes in the diffraction pattern are very clear, with some peaks disappearing and the broadening of the remaining ones indicating the presence of a liquid phase.

Fig.5.11b shows the diffraction patterns at T = 303.15 K for the pure components C14OH and C18OH and their mixture at the composition $x_{C14OH} = 0.2998$. The diffraction patterns for the pure components and their mixture are significantly different. A well defined peak for both pure fatty alcohols was observed around $2\theta = 22.5^{\circ}$ and is not present in the diffractogram for the mixture. The absence of this peak in the mixture diffraction pattern confirms that the fatty alcohols have miscibility in the solid state.

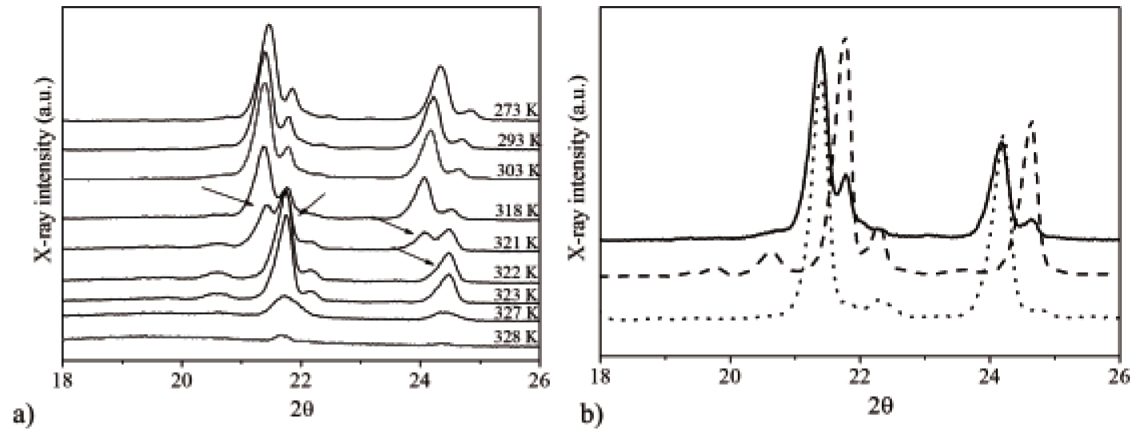

Fig.5. 11. X-ray powder diffraction patterns for the system C14OH + C18OH. a) $x_{C14OH} = 0.2998$ at different temperatures; b) for C14OH (···), C18OH (- -) and $x_{C14OH} = 0.2998$ (—) at T = 303.15 K.

The results obtained by different techniques enable the representation of the phase diagram for the C14OH + C18OH system, as suggested in Fig.5.12 having eutectic, peritectic and metatectic reactions. In Fig.5.12, $C^{14,18}$ states for the solid solution formed rich in C18OH. The peritectic compound formed is characterized by the region identified as "C". The phase diagram could be divided into the following regions: one homogeneous liquid phase - region (L), 3 monophasic solid domains - regions ($C^{14,18}$), ($C^{18,h}$) and (C); 4 biphasic solid-liquid domains - regions ($C^{14,18} + L$), ($C^{18,h} + L$), ($C_{14} + L$) and ($C + L$); and 3 biphasic solid-solid domains – regions ($C_{14} + C$), ($C^{14,18} + C$) and ($C^{14,18} + C^{18,h}$).

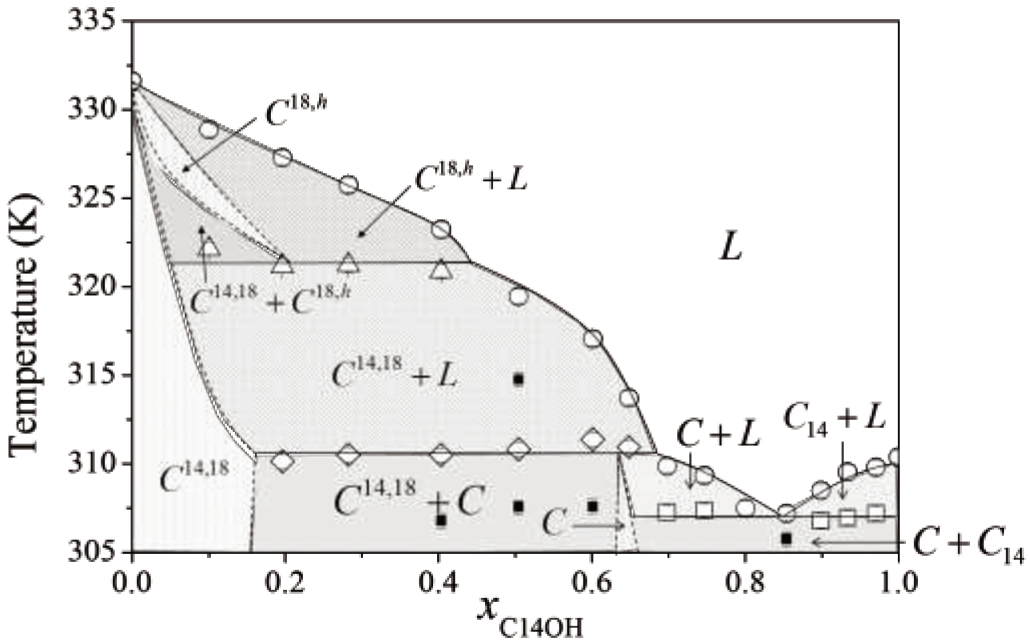

Fig.5. 12. Solid-liquid phase diagram of the C14OH + C18OH system by stepscan DSC. ○ melting temperature; □ eutectic reaction; ◊ peritectic reaction; Δ metatectic reaction; and ■ solid-solid transition. (---) and (—) are guides to the eyes. *L:* liquid phase; C_{14}: C14OH on solid state, $C^{14,18}$: solid solution rich in C18OH; C: peritectic compound; and $C^{18,h}$: metatectic compound.

- *C12OH + C16OH system*

Tamman plot of the transitions observed around 293 and 296 K of the C12OH + C16OH system is shown in Fig.5.8b. As it is expected for eutectic and peritectic transitions the enthalpy values must increase in function of the composition and reach the maximum value when the mixture has the composition corresponding to the transition under analysis, in respect of the lever rule in a biphasic region. The transitions found in the stepscan DSC analyses and their respectives enthapies could be an indication that the C12OH + C16OH has a behavior similar to the C14OH + C18OH system. Nevertheless, according to the Gibbs phase rule a binary phase diagram with peritectic reaction can not undergo an eutectic transition in the entire range of composition, since a solid region must exist at temperatures lower than the peritectic reaction temperature (observe the monophasic region *C* in Fig.5.12). This phase behavior is not usual for systems formed by fatty compounds, nevertheless it is similar to the behavior already observed for decanedioic acid + dodecanedioic acid system (VENTOLA et al., 2008). From the Tamman plot, it is also possible to conclude that the two fatty alcohols are partially miscible in the solid phase, having two regions of solid solutions in the extremes of the phase diagram.

Fig.5.13 shows light microscopy images captured for differents compositions of the C12OH + C16OH system. In Fig.5.13a when the sample of composition of $x_{C12OH} = 0.2187$ is kept at 311 K no liquid can be observed on the coverslip, but increasing the temperature to 318 K a small amount of liquid can be identified in equilibrium with the solid phase, being apparent due to the round shape of the crystals (indicated by arrows in Fig.5.13a). Subsequently, when the temperature is increased to 320 K, the amount of liquid on the coverslip further increases, approaching to the total melting of the sample.

Fig.5.13b presents images at a composition of $x_{C12OH} = 0.3972$ within a temperature range of 295 K to 305 K. At 295 K the sample is into a region comprising two transitions as detected by the DSC analyses (vide Fig.5.6). At 295 K a small amount of liquid was observed in the coverslip, an evidence of the eutectic reaction occurrence. Accordingly to the conventional interpretation of a simple eutectic system, at 300 K and $x_{C12OH} = 0.3972$,

it was expected that approximately half of the mixture should be in the liquid state, however, as can be seen in Fig.5.13b, the sample image at 300 K is very similar to that taken at 295 K. Only around 305 K a significant amount of liquid can be observed on the coverslip, as indicated by the arrow. This behavior suggests that the system C12OH + C16OH has a metatectic transition around 295.5 K, exhibiting a phase diagram similar to that of the system decanedioic acid + dodecanedioic acid (VENTOLA et al., 2008).

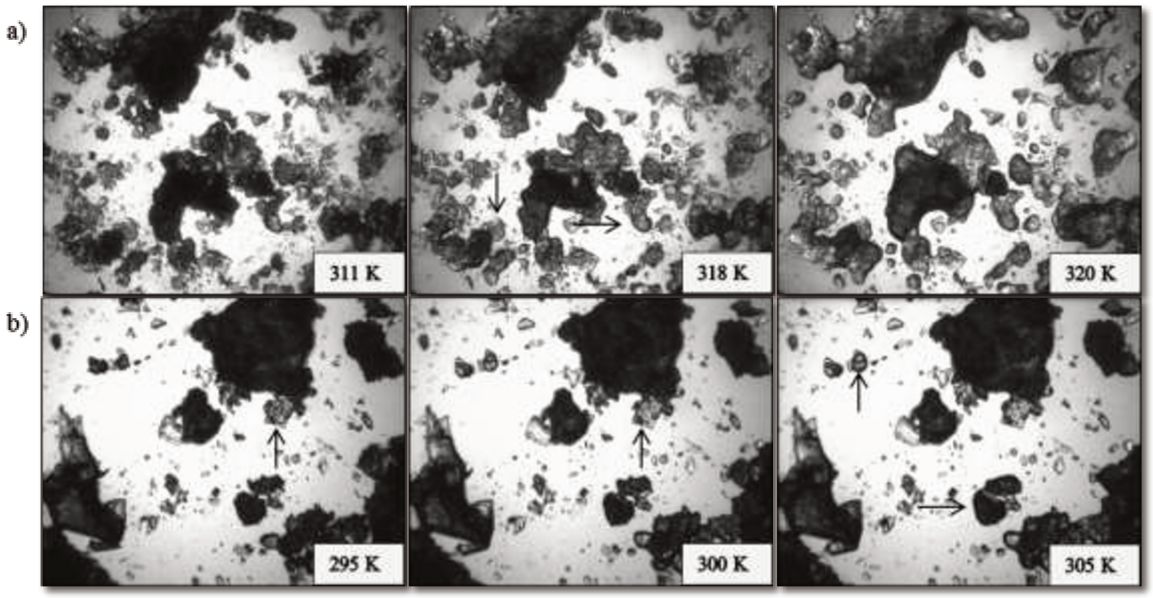

Fig.5. 13. Light microscopy images of the system C12OH + C16OH at different compositions and temperatures. (a) $x_{C12OH} = 0.2187$; (b) $x_{C12OH} = 0.3972$.

The proposed phase diagram of the C12OH + C16OH system can be found in Fig.5.14 and it is divided in the resulting domains: one homogeneous liquid phase - region (L), 2 monophasic solid domains - regions ($C^{12,16}$) and ($C^{16,h}$); 3 biphasic solid-liquid domains - regions (C_{16} + L), ($C^{12,16}$ + L) and ($C^{16,h}$ + L); and 2 biphasic solid-solid domains – regions (C_{16} + $C^{12,16}$) and ($C^{12,16}$ + $C^{16,h}$). In the same way as the notation used for the prior systems, the different domains of the phase diagram has the following meaning: $C^{12,16}$ is related to the solid solution formed rich in C16OH. The SLE region close to the melting temperature of C12OH corresponds to an eutectic domain and showing immiscibility of the compounds on solid state.

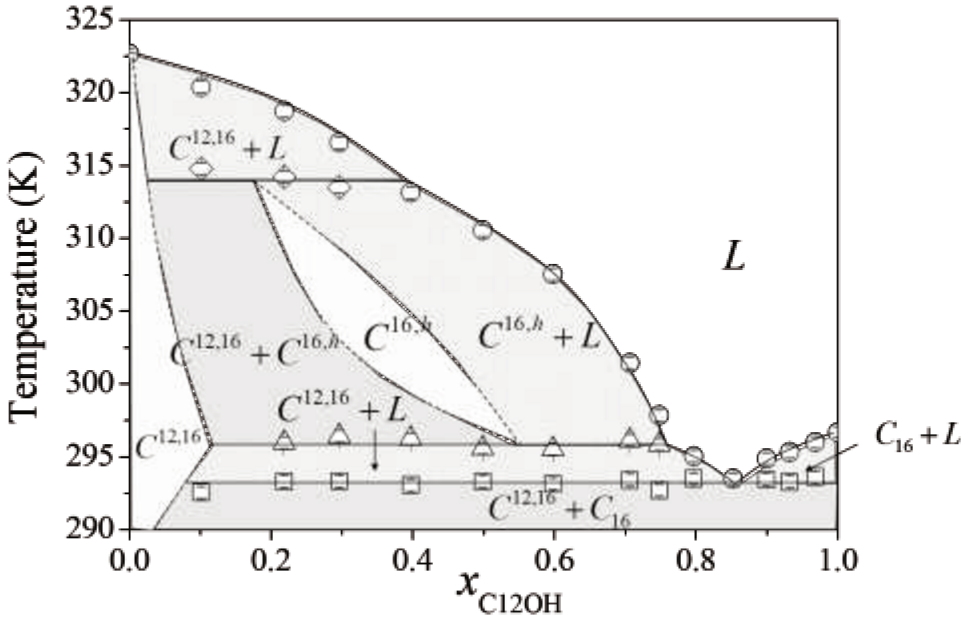

Fig.5. 14. Solid-liquid phase diagram of the C12OH + C16OH system by stepscan DSC. ○ melting temperature; □ eutectic reaction; ◊ peritectic reaction ; Δ metatectic reaction. (---) and (—) are guides to the eyes. *L*: liquid phase; $C^{12,16}$: solid solution rich in C16OH; C_{16}: C16OH on solid state, and $C^{16,h}$: metatectic compound.

5.4. Conclusions

The phase diagrams of four binary mixtures of fatty alcohols were reported in the present study: C8OH + C10OH, C10OH + C12OH, C12OH + C16OH and C14OH + C18OH. Standard and stepscan DSC analyses were used for measuring the phase diagram of the binary systems, X-ray diffraction and polarized light microscopy analyses were used as complementary techniques in the understanding of the observed transitions. The four systems present eutectic and peritectic reactions. A metatectic reaction was also identified for the C10OH + C12OH, C12OH + C16OH and C14OH + C18OH systems. The stepscan DSC method proposed in a previous work (CARARETO et al., submitted article) was applied to measure SLE of fatty alcohols binary systems exhibiting a good repeatability and accuracy. Although the standard DSC methodology keeps being a reliable methodology for measuring SLE of complex systems, as those formed by fatty alcohols, the stepscan

methodology showed be able to improve the understanding of some transitions that occur along the phase diagrams.

Acknowledgments

The authors are grateful to CNPq (483340/2012-0, 304495/2010-7, 552280/2010-0, 142193/2010-0), FAPESP (2007/06162-1, 2008/09502-0, 2008/56258-8), CAPES and FAEPEX/UNICAMP for their financial support and assistantships.

References

BAICHOO, N.; MACNAUGHTAN, W.; MITCHELL, J.; FARHAT, I. A STEPSCAN Differential Scanning Calorimetry Study of the Thermal Behavior of Chocolate. **Food Biophysics,** v. 1, n. 4, p. 169-177, 2006.

BAILEY, A. E. **Melting and solidification of fats**. New York: Interscience publishers, 1950.

BELANGER, S. E.; SANDERSON, H.; FISK, P. R.; SCHÄFERS, C.; MUDGE, S. M.; WILLING, A.; KASAI, Y.; NIELSEN, A. M.; DYER, S. D.; TOY, R. Assessment of the environmental risk of long-chain aliphatic alcohols. **Ecotoxicology and Environmental Safety,** v. 72, n. 4, p. 1006-1015, 2009.

BOROS, L.; BATISTA, M. L. S.; VAZ, R. V.; FIGUEIREDO, B. R.; FERNANDES, V. F. S.; COSTA, M. C.; KRAHENBUHL, M. A.; MEIRELLES, A. J. A.; COUTINHO, J. A. P. Crystallization Behavior of Mixtures of Fatty Acid Ethyl Esters with Ethyl Stearate. **Energy & Fuels,** v. 23, p. 4625-4629, 2009a.

BOROS, L.; BATISTA, M. L. S.; VAZ, R. V.; FIGUEIREDO, B. R.; FERNANDES, V. F. S.; COSTA, M. C.; KRÄHENBÜHL, M. A.; MEIRELLES, A. J. A.; COUTINHO, J. A. P. Crystalization behaviour of mixtures of fatty acid ethyl esters with ethyl stearate. **Energy & Fuels,** v. 23, p. 4625–4629, 2009b.

BOROS, L.; BATISTA, M. L. S.; VAZ, R. V.; FIGUEIREDO, B. R.; FERNANDES, V. F. S.; COSTA, M. C.; KRÄHENBÜHL, M. A.; MEIRELLES, A. J. A.; COUTINHO, J. A. P. Crystallization Behavior of Mixtures of Fatty Acid Ethyl Esters with Ethyl Stearate. **Energy & Fuels,** v. 23, n. 9, p. 4625-4629, 2009c.

BROWN, M. E.; GALLAGHER, P. K. Chapter 1 Introduction to recent advances, techniques and applications of thermal analysis and calorimetry. In: MICHAEL, E. B. e PATRICK, K. G. (Ed.). **Handbook of Thermal Analysis and Calorimetry**: Elsevier Science B.V., v.Volume 5, 2008. p.1-12.

CARARETO, N. D. D.; CASTAGNARO, T.; COSTA, M. C.; MEIRELLES, A. J. A. The binary solid-liquid phase diagrams of caprylic or capric acid + 1-octanol or 1-decanol. **Fluid Phase Equilibria**, submitted article.

CARARETO, N. D. D.; COSTA, M. C.; ROLEMBERG, M. P.; KRÄHENBÜHL, M. A.; MEIRELLES, A. J. A. The solid–liquid phase diagrams of binary mixtures of even saturated fatty alcohols. **Fluid Phase Equilibria,** v. 303, n. 2, p. 191.e1-191.e8, 2011.

CHERNIK, G. G. Phase equilibria in phospholipid water-systems. **Advances in Colloid and Interface Science,** v. 61, p. 65-129, 1995.

COSTA, M. C.; BOROS, L. A. D.; BATISTA, M. L. S.; COUTINHO, J. A. P.; KRÄHENBÜHL, M. A.; MEIRELLES, A. J. A. Phase diagrams of mixtures of ethyl palmitate with fatty acid ethyl esters. **Fuel,** v. 91, n. 1, p. 177-181, 2012.

COSTA, M. C.; BOROS, L. A. D.; COUTINHO, J. O. A. P.; KRÄHENBÜHL, M. A.; MEIRELLES, A. J. A. Low-Temperature Behavior of Biodiesel: Solid–Liquid Phase Diagrams of Binary Mixtures Composed of Fatty Acid Methyl Esters. **Energy & Fuels,** v. 25, n. 7, p. 3244-3250, 2011.

COSTA, M. C.; KRAHENBUHL, M. A.; MEIRELLES, A. J. A.; DARIDON, J. L.; PAULY, J.; COUTINHO, J. A. P. High pressure solid-liquid equilibria of fatty acids. **Fluid Phase Equilibria,** v. 253, n. 2, p. 118-123, 2007a.

COSTA, M. C.; ROLEMBERG, M. P.; BOROS, L. A. D.; KRAHENBUHL, M. A.; DE OLIVEIRA, M. G.; MEIRELLES, A. J. A. Solid-liquid equilibrium of binary fatty acid mixtures. **Journal of Chemical and Engineering Data,** v. 52, n. 1, p. 30-36, 2007b.

COSTA, M. C.; ROLEMBERG, M. P.; MEIRELLES, A. J. A.; COUTINHO, J. A. P.; KRAHENBUHL, M. A. The solid-liquid phase diagrams of binary mixtures of even saturated fatty acids differing by six carbon atoms. **Thermochimica Acta,** v. 496, n. 1-2, p. 30-37, Dec 10 2009a.

COSTA, M. C.; SARDO, M.; ROLEMBERG, M. P.; COUTINHO, J. A. P.; MEIRELLES, A. J. A.; RIBEIRO-CLARO, P.; KRAHENBUHL, M. A. The solid-liquid phase diagrams of binary mixtures of consecutive, even saturated fatty acids. **Chemistry and Physics of Lipids,** v. 160, n. 2, p. 85-97, 2009b.

COSTA, M. C.; SARDO, M.; ROLEMBERG, M. P.; COUTINHO, J. A. P.; MEIRELLES, A. J. A.; RIBEIRO-CLARO, P.; KRÄHENBÜHL, M. A. The solid–liquid phase diagrams of binary mixtures of consecutive, even saturated fatty acids: differing by four carbon atoms. **Chem. Phys. Lip.,** v. *157*, p. 40-50, 2009c.

COUTINHO, J. A. P.; RUFFIER-MERAY, V. A new method for measuring solid-liquid equilibrium phase diagrams using calorimetry. **Fluid Phase Equilibria,** v. 148, p. 147-160, 1998.

DANIEL, J.; RAJASEKHARAN, R. Organogelation of plant oils and hydrocarbons by long-chain saturated FA, fatty alcohols, wax esters, and dicarboxylic acids. **Journal of the American Oil Chemists Society,** v. 80, n. 5, p. 417-421, 2003.

DOMANSKA, U.; GONZALEZ, J. A. Solid-liquid equilibria for systems containing long-chain 1-alkanols .3. Experimental data for 1-tetradecanol, 1-hexadecanol, 1-octadecanol or 1-icosanol plus 1-butanol, 1-hexanol, 1-octanol or 1-decanol mixtures, characterization in terms of DISQUAC. **Fluid Phase Equilibria,** v. 129, n. 1-2, p. 139-163, 1997.

FISK, P. R.; WILDEY, R. J.; GIRLING, A. E.; SANDERSON, H.; BELANGER, S. E.; VEENSTRA, G.; NIELSEN, A.; KASAI, Y.; WILLING, A.; DYER, S. D.; STANTON, K. Environmental properties of long chain alcohols. Part 1: Physicochemical, environmental fate and acute aquatic toxicity properties. **Ecotoxicology and Environmental Safety,** v. 72, n. 4, p. 980-995, 2009.

GAMSJAGER, H.; LORIMER, J. W.; SCHARLIN, P.; SHAW, D. G. Glossary of terms related to solubility. **Pure and Applied Chemistry,** v. 80, n. 2, p. 233-276, 2008.

GANDOLFO, F.; BOT, A.; FLÖTER, E. Structuring of edible oils by long-chain FA, fatty alcohols, and their mixtures. **Journal of the American Oil Chemists' Society,** v. 81, n. 1, p. 1-6, 2004.

GUENET, J.-M. Contributions of phase diagrams to the understanding of organized polymer-solvent systems. **Thermochimica Acta,** v. 284, n. 1, p. 67-83, 1996.

INOUE, T.; HISATSUGU, Y.; ISHIKAWA, R.; SUZUKI, M. Solid-liquid phase behavior of binary fatty acid mixtures 2. Mixtures of oleic acid with lauric acid, myristic acid, and palmitic acid. **Chemistry and Physics of Lipids,** v. 127, n. 2, p. 161-173, 2004a.

INOUE, T.; HISATSUGU, Y.; SUZUKI, M.; WANG, Z. N.; ZHENG, L. Q. Solid-liquid phase behavior of binary fatty acid mixtures 3. Mixtures of oleic acid with capric acid (decanoic acid) and caprylic acid (octanoic acid). **Chemistry and Physics of Lipids,** v. 132, n. 2, p. 225-234, 2004b.

INOUE, T.; HISATSUGU, Y.; YAMAMOTO, R.; SUZUKI, M. Solid-liquid phase behavior of binary fatty acid mixtures 1. Oleic acid/stearic acid and oleic acid/behenic acid mixtures. **Chemistry and Physics of Lipids,** v. 127, n. 2, p. 143-152, 2004c.

JAKSLAND, C. A.; GANI, R.; LIEN, K. M. Separation process design and synthesis based on thermodynamic insights. **Chemical Engineering Science,** v. 50, n. 3, p. 511-530, 1995.

JIANG, Z.; IMRIE, C. T.; HUTCHINSON, J. M. An introduction to temperature modulated differential scanning calorimetry (TMDSC): a relatively non-mathematical approach. **Thermochimica Acta,** v. 387, n. 1, p. 75-93, 2002.

NOWECK, K.; GRAFAHREND, W. Fatty Alcohols. In: (Ed.). **Ullmann's Encyclopedia of Industrial Chemistry**: Wiley-VCH Verlag GmbH & Co. KGaA, 2000.

NÝVLT, J. **Solid-liquid phase-equilibria**. Amsterdam: Elsevier, 1977.

PIELICHOWSKA, K.; PIELICHOWSKI, K. Crystallization behaviour of PEO with carbon-based nanonucleants for thermal energy storage. **Thermochimica Acta,** v. 510, n. 1–2, p. 173-184, 2010.

RAMALHO, E. F. S. M.; CARVALHO FILHO, J. R.; ALBUQUERQUE, A. R.; DE OLIVEIRA, S. F.; CAVALCANTI, E. H. S.; STRAGEVITCH, L.; SANTOS, I. M. G.;

SOUZA, A. G. Low temperature behavior of poultry fat biodiesel:diesel blends. **Fuel,** v. 93, n. 0, p. 601-605, 2012.

SAUER, B. B.; KAMPERT, W. G.; NEAL BLANCHARD, E.; THREEFOOT, S. A.; HSIAO, B. S. Temperature modulated DSC studies of melting and recrystallization in polymers exhibiting multiple endotherms. **Polymer,** v. 41, n. 3, p. 1099-1108, 2000.

SCHAINK, H. M.; VAN MALSSEN, K. F.; MORGADO-ALVES, S.; KALNIN, D.; VAN DER LINDEN, E. Crystal network for edible oil organogels: Possibilities and limitations of the fatty acid and fatty alcohol systems. **Food Research International,** v. 40, n. 9, p. 1185-1193, 2007.

SCHAWE, J. E. K.; HÖHNE, G. W. H. The analysis of temperature modulated DSC measurements by means of the linear response theory. **Thermochimica Acta,** v. 287, n. 2, p. 213-223, 1996.

SCHICK, C. Chapter 16 Temperature modulated differential scanning calorimetry (TMDSC)-basics and applications to polymers. In: STEPHEN, Z. D. C. (Ed.). **Handbook of Thermal Analysis and Calorimetry**: Elsevier Science B.V., v.Volume 3, 2002. p.713-810.

VENTOLA, L.; BAYES, L.; BENAGES, R.; NOVEGIL-ANLEO, F. J.; CUEVAS-DIARTE, M. A.; CALVET, T. Decanedioic acid (C10H18O4)/dodecanedioic acid (C12H22O4) system: Polymorphism of the components and experimental phase diagram. **Helvetica Chimica Acta,** v. 91, n. 7, p. 1286-1298, 2008.

VENTOLA, L.; CALVET, T.; CUEVAS-DIARTE, M. A.; MONDIEIG, D.; OONK, H. A. J. The C19H39OH-C20H41OH system: Experimental phase diagram and thermodynamic modelling. **Physical Chemistry Chemical Physics,** v. 4, n. 10, p. 1953-1956, 2002.

VENTOLA, L.; CALVET, T.; CUEVAS-DIARTE, M. A.; OONK, H. A. J.; MONDIEIG, D. Solid-solid and solid-liquid equilibria in the n-alkanols family: C18H37OH-C20H41OH system. **Physical Chemistry Chemical Physics,** v. 6, n. 13, p. 3726-3731, 2004a.

VENTOLA, L.; CALVET, T.; CUEVAS-DIARTE, M. A.; RAMIREZ, M.; OONK, H. A. J.; MONDIEIG, D.; NEGRIER, P. Melting behaviour in the n-alkanol family. Enthalpy-entropy compensation. **Physical Chemistry Chemical Physics,** v. 6, n. 8, p. 1786-1791, 2004b.

VENTOLA, L.; CALVET, T.; CUEVAS-DIARTE, M. A.; SOLANS, X.; MONDIEIG, D.; NEGRIER, P.; VAN MILTENBURG, J. C. Solid state equilibrium in the n-alkanols family: the stability of binary mixed samples. **Physical Chemistry Chemical Physics,** v. 5, n. 5, p. 947-952, 2003.

VENTOLA, L.; DIARTE, M. A. C.; CALVET, T.; MONDIEIG, D. New materials for thermal protection and energy storage. **Materials Technology,** v. 20, n. 4, p. 207-210, 2005.

VERDONCK, E.; SCHAAP, K.; THOMAS, L. C. A discussion of the principles and applications of Modulated Temperature DSC (MTDSC). **International Journal of Pharmaceutics,** v. 192, n. 1, p. 3-20, 1999.

XIVILLÉ, N. R.; LORENTE, L. T.; KORDIKOWSKI, A. MDSC parameter optimization for the determination of glass transitions using a Design of Experiments approach. **International Journal of Pharmaceutics,** v. 422, n. 1–2, p. 271-279, 2012.

Capítulo 6. High pressure solid–liquid equilibrium of fatty acid ethyl esters binary systems

Natália D. D. Carareto[a,b], *Mariana C. Costa*[c], *Antonio J. A. Meirelles*[a], *J. Pauly*[*b]

[a] EXTRAE, Department of Food Engineering, Faculty of Food Engineering, University of Campinas, UNICAMP, Campinas, Brazil

[b] Laboratoire des Fluides Complexes, Université de Pau, BP 1155, 64013 Pau Cedex, France

[c] FCA, Applied Sciences Faculty, University of Campinas, UNICAMP, Limeira, Brazil

Trabalho a ser submetido na revista **Fluid Phase Equilibria**

Abstract.

The solid–liquid phase diagrams of three binary mixtures of fatty acids ethyl esters (FAEEs), formed by ethyl laurate, ethyl myristate and ethyl palmitate, were measured using high pressure microscopy in the range of 0.1 – 80 MPa. In a first step, the melting temperatures of pure FAEEs have been determined showing a linear dependence from the pressure. The binary phase diagrams are only slightly affected by the pressure, even in very large pressure ranges such as those studied in this work. The modeling of the phase diagrams was attempted using a predictive approach previously developed by one of the authors in the case for n-alkane mixtures. The model was able to provide an accurate description of the high pressure solid–liquid equilibrium of FAEE mixtures. Average absolute deviations between experimental and predicted liquidus curve varied from 0.6 to 2.3 K in the entire interval of pressures.

Keywords.

- Fatty acid ethyl esters
- Solid-liquid equilibrium
- High pressure data

6.1. Introduction

Biodiesel is the reaction product of the transesterification of triacylglycerol with a short chain alcohol in an alkaline medium (BOUAID et al., 2007), resulting in Fatty Acid Methyl Esters (FAMEs) or Fatty Acid Ethyl Esters (FAEEs) when using, respectively, methanol or ethanol. As renewable, the biodiesel possesses low toxicity, having many fuel properties and other characteristics that make it an attractive and environmental friendly alternative to conventional fossil-based diesel since its feedstock of biomass is carbonneutral and has low sulfur content (MEHER et al., 2006; MOSER, 2009).

Bioethanol is a renewable alcohol in contrast to methanol, which is mainly obtained from fossil sources (DA CONCEIÇÃO et al., 2011). However, the production of ethyl biodiesel is not yet sufficiently developed for efficient use on the industrial scale in contrast to the production of methyl biodiesel (CARARETO et al., 2012). Information on the physicochemical properties of ethyl esters and ethyl biodiesel, which are required to improve the ethyl biodiesel production and storage, are still scarce in open literature. Liquid-liquid and vapor-liquid equilibria of mixtures related to the purification and reaction steps of ethyl biodiesel production have only been published recently (FOLLEGATTI-ROMERO et al., 2010; OLIVEIRA et al., 2010; OLIVEIRA et al., 2011).

To select all the process parameters of biodiesel production and transportation is a hard task since its physicochemical properties are function of the raw materials used in the reaction (as vegetable oils or animal fats). The composition of these raw materials varies in function of climatic and agricultural factors. To well-describe physicochemical properties of biodiesel, expressed as function of temperature, pressure and composition, empirical or thermodynamic models are usually applied since it is impracticable to acquire experimental data in all possible conditions (ALLEN et al., 1999; KNOTHE, 2005; RAMOS et al., 2008; CERIANI et al., 2009).

Biodiesels with large concentration of saturated fatty acid esters, as palm oil biodiesel, although with a high oxidation stability and showing a better lubricating and combustion properties, have a tendency to crystallize which affects their flow properties

and storage (COUTINHO et al., 2010; ROBUSTILLO et al., 2013). Potential deposition problems can be avoided if the variables involved in the process, namely cold properties, are known or can be predicted (KNOTHE, 2005). The cloud point (CP), one of the cold properties, is defined as the temperature at which a foggy appearance occurs on a fuel during the cooling due to the process of crystallization (IMAHARA et al., 2006; WANG et al., 2011). Lowering the temperature the crystal particles grow and agglomerate, reducing the capacity of the liquid to flow (WANG et al., 2011). There are some studies concerning the CP and solid-liquid equilibrium (SLE) of methylic or ethylic esters or of biodiesels in the open literature (KNOTHE, 2005; IMAHARA et al., 2006; RAMOS et al., 2008; BOROS et al., 2009; MOSER, 2009; COSTA et al., 2011; WANG et al., 2011; COSTA et al., 2012; ROBUSTILLO et al., 2013). As example, the crystallization phenomenon of biodiesel may occur despite the high pressure gradient in an engine startup which can achieve 150 MPa at the injection of the fuel (KOUAKOU et al., 2013). Although this role in the formation of solid deposits is well known, SLE under high pressure for biodiesel or FAMEs/FAEEs remains much less studied than those of normal alkanes.

The aim of this study is, as part of our research subject, to improve the knowledge from the SLE under pressure for some FAEEs, as pure substances or in binary mixtures. The liquidus lines in a range of pressure going from 0.1 MPa to 80 MPa were measured by means of a high pressure microscopy device for ethyl laurate, ethyl myristate and ethyl palmitate and theirs binary mixtures. The values at atmospheric pressure where compared with the values available from literature (COSTA et al., 2012). The experimental results for the binary systems were compared with those obtained by an adaptation from a model previously proposed to predict wax precipitation in complex mixtures under high pressure (PAULY et al., 2000).

6.2. Experimental Section

High purity reactants were purchased from Sigma-Aldrich and used to prepare the samples with no further purification process. Their purities, CAS registry numbers and melting properties are listed in Table 6. 1. The samples were selected to cover the entire range of composition and were prepared gravimetrically (weighted quantity of 5 g) using a high precision balance (±0.0002 g) with an accuracy of 0.02% in the molar fraction.

Table 6. 1. FAEEs used in this study.

Name (CAS number)	Purity[a]	$T_{melt,i}$ [b] (K)	$\Delta_{melt}H_i$ [b] (kJ mol^{-1})	T_C [c] (K)	P_C [c] (bar)	ω [c]	$\Delta_{vap}H_i$ [c] (kJ mol^{-1})
Ethyl laurate (106-33-2)	> 98%	272.2	38.44	719.13	15.97	0.787	77.6
Ethyl myristate (124-06-1)	99 %	286.4	47.30	744.27	14.02	0.862	87.4
Ethyl palmitate (628-97-7)	> 95%	297.4	55.57	766.41	12.43	0.935	97.2

[a] according to the supplier; [b] measured by μDSC; [c] data from COSTA et al., 2012.

6.2.1. High pressure microscopy

The high pressure SLE of the binary FAEE mixtures was studied using a high pressure cell, as described in previous works (DARIDON et al., 2002; MILHET et al., 2005; KOUAKOU et al., 2013). The experimental apparatus is built around a stainless steel autoclave cell, equipped with two sapphire windows through which the sample could be observed and with an end closed with a moving piston. The piston is able to produce a pressure up to 100 MPa inside the cell. A heat-transducing fluid circulating inside the flow lines built in the metallic thermostat block enables the temperature control of the high pressure cell, which could be maintained between 253 and 353 K and held by a thermostat

bath (Huber, Germany) with a temperature stability of 0.01 K. The temperature was measured with a calibrated platinum resistance inserted inside the cell and connected to a high-precision thermometer (AOIP). The temperature uncertainty was estimated not large than 0.2 K (PAULY et al., 2000; MILHET et al., 2005; KOUAKOU et al., 2013). The pressure was measured by a piezoresistive silicon pressure transducer (Kulite) with a precision of 0.2% and placed inside the cell in order to reduce the dead volume. A polarized light microscope coupled to a video camera was used to observe and annotate the SLE transitions of the samples.

The samples were introduced into the high pressure cell at a temperature higher than the melting temperature of the FAEEs to avoid their crystallization during injection. Then the temperature was decreased 10-15 K below the melting temperature of the sample to allow the sample crystallization and kept at this temperature for 20-30 min. The temperature was increased in small increments (0.1 – 0.5 K) in order to allow an isothermal environment prevailing at each step for 1-3 min until the disappearance of the last crystal was observed, which was annotated as the melting temperature of the sample. Then the pressure of the system was increased and a new temperature cycle was started. All the samples had the melting temperature measured in pressures of 0.1, 20, 40, 60 and 80 MPa.

6.2.2. Micro Differential Scanning Calorimetry (μDSC)

A SETARAM Micro DSC 7 evo calorimeter was used to measure melting enthalpies and temperature for pure FAEEs at atmospheric pressure. The equipment is coupled to an external cooling fluid (water) around a calorimetric block which allows a range of temperature from 228.15 to 393.15 K. Nitrogen was used as purge gas (purity ≥ 99.995% from Linde group). The results from μDSC (temperature and enthalpy) were collected and analyzed by the Calisto SETARAM softwares, respectively Data Acquisition and Processing. The standard batch vessel was used (6.4 mm internal diameter, useful height of 19.5 mm, volume of 1 cm^3). The μDSC calibration was performed with naphthalene following the recommended procedure of the manufacturer.

A pre-treatment procedure was made before the experimental analyses in which the samples were kept 15 K above their melting point and maintained at this temperature during 30 min. The samples were then cooled 20 K below the melting point at 1.2 K min^{-1} and kept during 30 min. Afterward the solid samples were heated at a rate of 0.01 K min^{-1} until the melting of the samples was reached. The temperatures were determined with an accuracy of 0.2 K. The melting enthalpies were obtained from the surface area using a linear baseline between the onset and the end of the peaks (Fig.6. 1) with a relative accuracy of 1% determined by calibration with naphthalene and n-heptacosane (molar purities ≥ 99%).

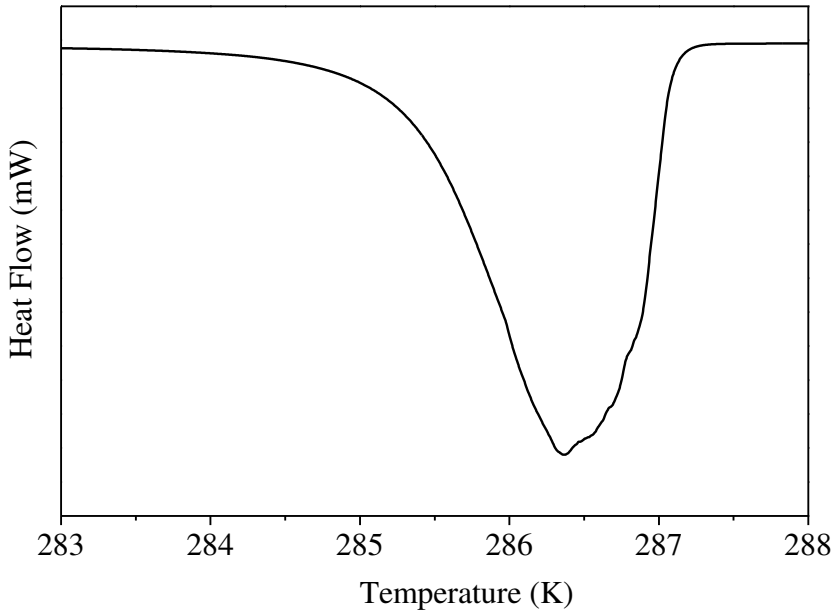

Fig.6. 1. Thermogram of ethyl myristate from μDSC analysis using a heating rate of 0.01 K min^{-1}.

6.3. Results and discussion

6.3.1. Effect of pressure on the melting temperature of pure fatty acid ethyl esters (FAEEs)

The melting temperature and respectives melting enthalpies from μDSC analyses can be found in Table 6.2. In DSC analyses, the peaks relative to the FAEEs melting in the thermograms are usually overlapped due to the presence of polymorphic transitions. Consequently the onset temperature can be incorrectly determined producing a high deviation in DSC results. As already justified in previous works (COSTA et al., 2007; CARARETO et al., 2011; COSTA et al., 2011; KOUAKOU et al., 2013), the peak temperature was chosen to represent the melting temperature for pure FAEEs according to the DSC results.

The μDSC technique was used in order to compare the results from the microscope apparatus at atmospheric pressure. Melting temperatures from both methods and data from literature are presented in Table 6. 2. The AAD_1 between the melting temperatures from μDSC and high pressure microscope are low as well as the AAD_2 between μDSC and from literature. Ethyl myristate was the compound with the largest AAD and it can be propably caused by the presence of the metastable phase close to the melting temperature, as noted in the thermogram from Fig.6. 1. A metastable phase is normally found for organic compounds as, for example, fatty acids (INOUE et al., 2004a; INOUE et al., 2004b; INOUE et al., 2004c), fatty alcohols (VENTOLA et al., 2002; CARARETO et al., 2011) or FAMEs (KOUAKOU et al., 2013). This behavior is characteristic from the compounds but can also occur due to the presence of even small amount of impurities in the samples (KOBAYASHI et al., 1986). On the other hand, most AAD values are low, indicating a good agreement between data measured by different techniques.

Table 6. 2. Average absolute deviation (AAD) between $T_{melt,i}$ at atmospheric pressure from μDSC and microscope (AAD_1) and from μDSC and literature (AAD_2).

	$T_{melt,i}$ (K)				
FAEE	μDSC	Microscopy	From (COSTA et al., 2012)	AAD_1	AAD_2
Ethyl laurate	272.2	272.3	272.6	0.1	0.4
Ethyl myristate	286.4	285.8	287.4	0.6	1.0
Ethyl palmitate	297.4	297.6	297.7	0.2	0.3

The melting temperatures from FAEEs were then measured in the high pressure microscope within a pressure range of 0.1 – 80 MPa. The results are listed in Table 6. 3. From the experimental data, the solid-liquid transition temperatures in the (*T*,*P*) diagram could be plotted for the FAEE (Fig.6. 2). They reveal a linear relationship between melting temperature and pressure as represented by the R^2 from the curves (varying from 0.9987 to 0.9997). This dependence was calculated by means of the average slope of each curve (see Table 6. 4) as follows and the uncertainty has been estimated at 2.5 % by earlier studies (DARIDON et al., 2002):

$$\frac{\Delta T}{\Delta P} = \frac{T_{melt}\left(P_{\max}\right) - T_{melt}\left(P_{atm}\right)}{P_{\max} - P_{atm}}$$

Eq.6. 1

where P_{atm} is the atmospheric pressure and $P_{\max}$ the maximum pressure measured for each compound (in this case 80 MPa). The slope value permits to calculate the molar volume change through the Clapeyron equation, providing an important information concerning the solid-liquid phase equilibria of multicomponent systems, as biodiesel, for example.

Table 6. 3. Melting temperatures of the FAEEs as a function of pressure P measured by the high pressure microscopy apparatus.

P (MPa)	$T_{melt,i}$ (K)		
	ethyl laurate	ethyl myristate	ethyl palmitate
0.1	272.3	285.8	297.6
20	276.4	289.9	302.0
40	280.3	294.1	306.4
60	284.0	298.0	310.3
80	287.4	301.9	314.3

Table 6. 4. Average slope of the solid-liquid transition curve for each FAEE.

	ethyl laurate	ethyl myristate	ethyl palmitate
Average slope (K MPa^{-1})	0.1890	0.2015	0.2090

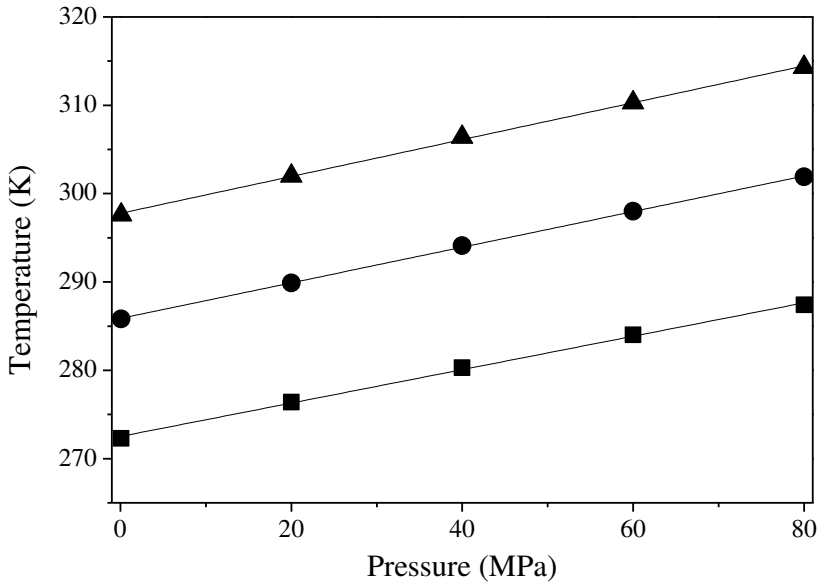

Fig.6. 2. Melting temperatures from the FAEEs as function of pressure. ■ ethyl laurate ($R^2 = 0.9987$); ● ethyl myristate ($R^2 = 0.9997$) and; ▲ ethyl palmitate ($R^2 = 0.9992$).

6.3.2. High pressure solid-liquid equilibrium from FAEEs binary mixtures

Measurements were performed in the microscope apparatus from 0.1 until 80 MPa for different compositions at every 20 MPa for ethyl laurate, ethyl myristate and ethyl palmitate binary systems. The results are presented in Tables 6. 5-7.

The SLE data for the systems ethyl laurate + ethyl palmitate and ethyl myristate + ethyl palmitate have been already reported in literature at atmospheric pressure obtained using the DSC technique (COSTA et al., 2012). A comparison between the set of data was made and presented as deviations in Fig.6. 3. In general, the different sets of experimental data presented a good agreement with AAD values of 0.4 and 0.2 K for the systems ethyl laurate + ethyl palmitate and ethyl myristate + ethyl palmitate, respectively.

Table 6. 5. Solid-liquid equilibrium data for the system ethyl laurate + ethyl myristate.

$x_{laurate}$	T (K)				
	0.1 MPa	20 MPa	40 MPa	60 MPa	80 MPa
0.0000	285.8	289.9	294.1	298.0	301.9
0.2018	284.2	288.5	292.9	297.5	301.5
0.4013	280.2	284.2	288.3	292.4	296.2
0.6000	274.2	277.8	282.0	286.0	289.9
0.7011	271.0	274.3	279.3	283.3	287.9
0.7437	267.9	271.9	275.5	279.0	282.5
0.8008	269.0	273.1	277.0	280.6	284.2
0.8476	269.5	273.3	277.1	281.1	284.1
0.8972	269.3	273.0	278.0	281.6	285.4
1.0000	272.3	276.4	280.3	284.0	287.4

Table 6. 6. Solid-liquid equilibrium data for the system ethyl laurate + ethyl palmitate.

$x_{laurate}$	T (K)				
	0.1 MPa	20 MPa	40 MPa	60 MPa	80 MPa
0.0000	297.6	302.0	306.4	310.3	314.3
0.2002	295.7	300.5	304.9	308.5	312.7
0.4013	293.4	297.6	302.0	306.5	311.1
0.6004	288.5	292.4	296.6	300.9	305.3
0.6979	284.6	289.9	293.7	297.5	301.8
0.8003	279.1	284.0	288.5	292.0	295.1
0.8478	275.3	279.4	282.8	286.7	290.9
0.9003	269.8	273.9	277.8	281.8	285.6
1.0000	272.3	276.4	280.3	284.0	287.4

Table 6. 7. Solid-liquid equilibrium data for the system ethyl myristate + ethyl palmitate.

$x_{myristate}$	T (K)				
	0.1 MPa	20 MPa	40 MPa	60 MPa	80 MPa
0.0000	297.6	302.0	306.4	310.3	314.3
0.2009	294.6	299.3	303.7	307.8	311.8
0.3993	291.3	296.2	301.1	305.4	309.2
0.5006	288.8	293.3	298.0	302.4	306.3
0.5992	285.1	289.2	293.9	297.9	301.5
0.6981	283.4	287.7	292.1	295.8	299.1
0.7489	282.6	286.8	290.8	294.5	298.5
0.7996	282.8	287.1	291.3	295.2	298.9
0.8997	284.2	288.6	292.2	296.0	299.5
1.0000	285.8	289.9	294.1	298.0	301.9

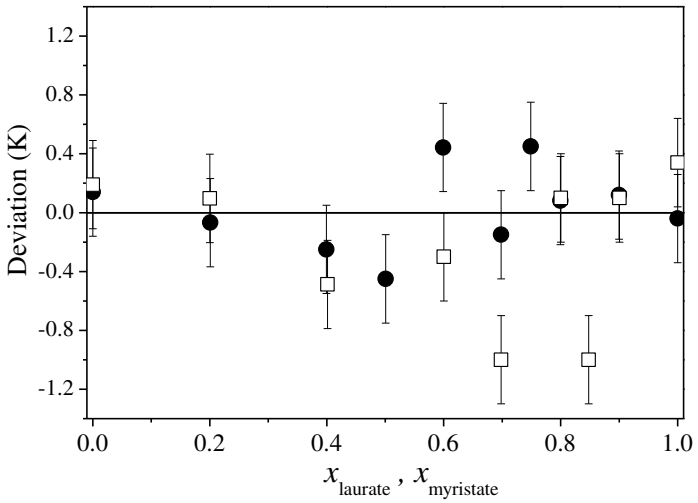

Fig.6. 3. Deviations between liquidus temperatures from FAEE binary mixtures reported in the literature (Costa et al., 2012) and the corresponding values measured in the present work. □ ethyl laurate + ethyl palmitate and; ● ethyl myristate + ethyl palmitate.

The liquidus lines in function of the composition for the three binary systems are presented in Figs.6.4-6. Plotting T in function of P for all samples, the results show that liquidus line has a linear dependence from the pressure (R^2 from the linear fit varying from 0.9903 to 0.9997), as well as found for the pure FAEEs.

An inflection on the liquidus line related to the eutectic point was observed for ethyl laurate + ethyl myristate and ethyl myristate + ethyl palmitate systems around a 0.75 molar fraction from the lighter FAEE, and for the system ethyl laurate + ethyl palmitate around a 0.90 molar fraction of ethyl laurate. The eutectic point was observed over the entire pressure range studied, as shown in Figs.6.4-6, and its composition does not seem to be affected by the pressure's increase. The average slope for all measured samples was calculated and the values have fluctuate around the values from the pure FAEE. The dependence from pressure is an important parameter to predict the crystallization behavior in multicomponent mixtures as in the case of methylic and ethylic biodiesels.

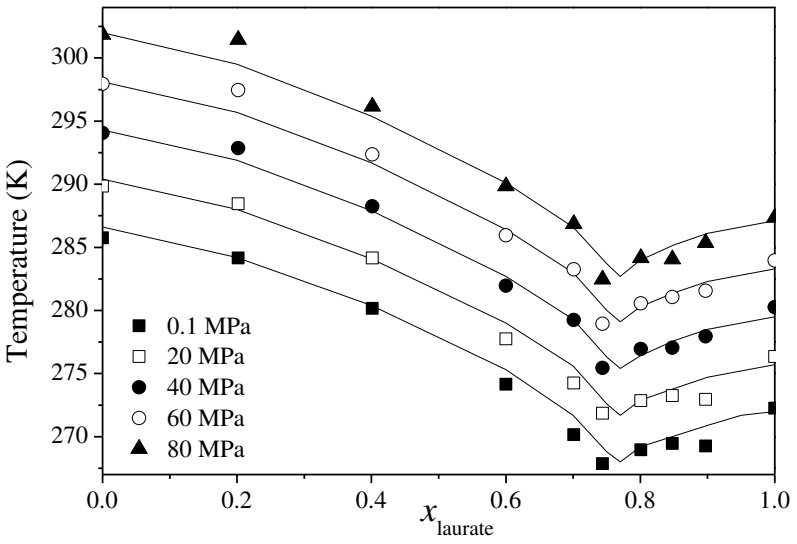

Fig.6. 4. Liquidus curves of the ethyl laurate + ethyl myristate system as a function of pressure. (—) modeling results in the respective pressures (from bottom to the top): 0.1; 20; 40; 60 and 80 MPa.

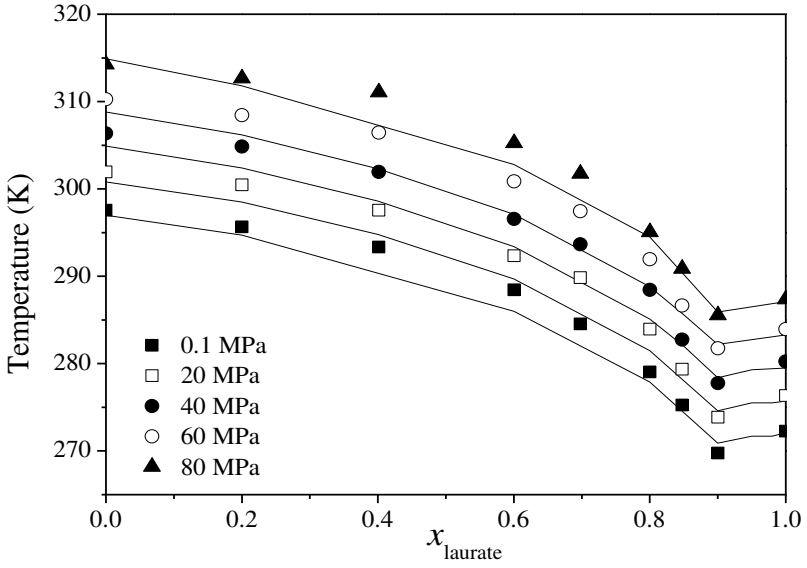

Fig.6. 5. Liquidus curves of the ethyl laurate + ethyl palmitate system as a function of pressure. (—) modeling results in the respective pressures (from bottom to the top): 0.1; 20; 40; 60 and 80 MPa.

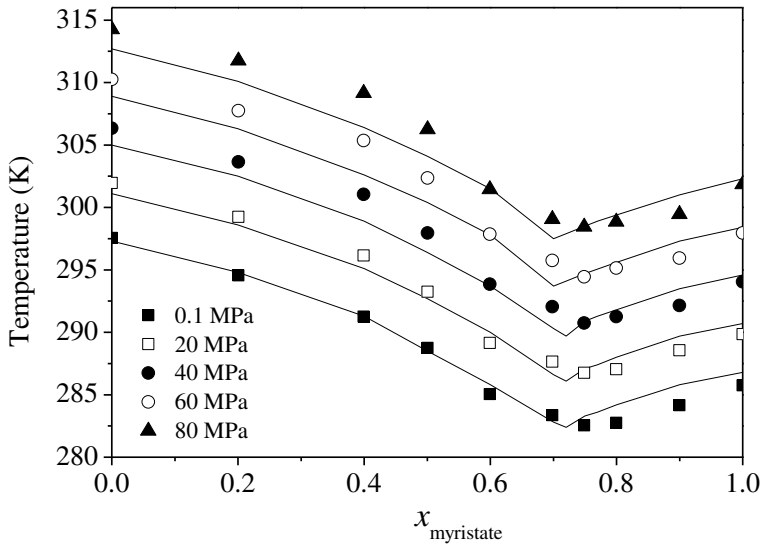

Fig.6. 6. Liquidus curves of the ethyl myristate + ethyl palmitate system as a function of pressure. (—) modeling results in the respective pressures (from bottom to the top): 0.1; 20; 40; 60 and 80 MPa.

6.3.3. Modeling

The thermodynamic modeling has been developed as a powerful tool to describe the behavior of matter, either pure or in complex mixtures, as function of pressure and/or temperature. From relatively simple equations the behavior of many natural and industrial processes could be developed and improved. However, there are still many aspects that need to be improved in the proposed models. Most part of the SLE studies in the literature are focused on experimental data and modeling at atmospheric pressure. Here, the SLE could be described in function of the system pressure. The modeling of the high pressure phase equilibrium from the binary mixtures of FAEE was carried using an approach previously proposed for alkane mixtures (DARIDON et al., 2002; PAULY et al., 2005) and also successfully extended to fatty acids binary systems (COSTA et al., 2007).

The SLE state is defined from the equality of fugacity of each component in the liquid and solid phase, as represented in Eq.6. 2.

$$f_i^L\left(T,P,x_i^L\right)=f_i^S\left(T,P,x_i^S\right)$$

Eq.6. 2

The liquid phase fugacities can be written in terms of the fugacity coefficient, ϕ_i^L, as:

$$f_i^L\left(T,P,x_i^L\right)=Px_i^L\phi_i^L$$

Eq.6. 3

The fugacity coefficient, ϕ_i^L can be calculated from equations of state (EOS), and in this study it was applied the Soave-Redlich-Kwong EOS (SOAVE, 1972), with the LCVM mixing rules (BOUKOUVALAS et al., 1994; BOUKOUVALAS et al., 1997). The volumetric properties calculated by the cubic EOS were corrected using the volume translation proposed by Peneloux et al. (1982).

For the solid phase, the fugacity at a pressure *P* for component *i* is obtained by the Eq.6.4:

$$\ln f_i^S\left(P\right)=\ln f_i^S\left(P_0\right)+\frac{1}{RT}\int_{P_0}^{P}\overline{V}_i^S dP$$

Eq.6. 4

where the fugacity of component *i* in the solid phase at pressure P_0 is given from its fugacity in subcooled liquid state at the same temperature *T*:

$$f_i^S\left(P_0\right)=x_i^S\gamma_i^S\left(P_0\right)f_i^{0,L}\left(P_0\right)\exp\left[-\frac{\Delta_{melt}H_i}{RT}\left(1-\frac{T}{T_{melt,i}}\right)\right]$$

Eq.6. 5

where $T_{melt,i}$ and $\Delta_{melt}H_i$ are, respectively, the melting temperature and enthalpy of the pure component *i*, γ_i^S represents the activity coefficient of *i* in the solid phase.

The Poynting correction term of Eq.6. 4 can be simplified by the assumption that the partial molar volume of each component is proportional to the subcooled liquid molar volume:

$$\overline{V}_i^S = V_i^{0,S} = \beta V_i^{0,L}$$

Eq.6. 6

where β is a constante assumed to be pressure independent and having the same value for both compounds in the mixture. In this study, a value of $\beta = 0.88$ was used for describing the relation between the molar volumes from liquid and solid phases of the FAEEs. Thus the Eq.6. 4 can be rewritten as proposed by Pauly et al. (2000):

$$f_i^S(T,P,x_i^S) = x_i^S \gamma_i^S \left[f_i^{0,L}(T,P_0)\right]^{1-\beta} \left[f_i^{0,L}(T,P)\right]^{\beta} \exp\left[-\frac{\Delta_{melt}H_i}{RT}\left(1-\frac{T}{T_{melt,i}}\right)\right]$$

Eq.6. 7

The activity coefficients, γ_i^S, were described by means of a new Predictive UNIQUAC model proposed by (COUTINHO et al., 2006) which is defined by:

$$\frac{g^E}{RT} = \sum_{i=1}^{n} x_i \ln\left(\frac{\Phi_i}{x_i}\right) + \frac{Z}{2}\sum_{i=1}^{n} q_i x_i \ln\frac{\theta_i}{\Phi_i} - \sum_{i=1}^{n} q_i x_i \ln\left[\sum_{j=1}^{n}\theta_j \exp\left(-\frac{\lambda_{ij}-\lambda_{ii}}{q_i RT}\right)\right]$$

Eq.6. 8

with

$$\Phi_i = \frac{x_i r_i}{\sum_j x_j r_j} \qquad \text{and} \qquad \theta_i = \frac{x_i q_i}{\sum_j x_j q_j}$$

Eq.6. 9

The interaction energy, λ_{ij}, can be estimated by means of the local composition concept proposed by the predictive UNIQUAC equation (COUTINHO et al., 1996; COUTINHO et al., 2006). The interaction energies between two identical molecules can be

estimated from the enthalpy of sublimation of an orthorhombic crystal of the pure component as:

$$\lambda_{ii} = -\frac{2}{Z}\left(\Delta_{sub}H_i - RT\right)$$

Eq.6. 10

where Z is the coordination number, and $Z = 10$ will be used for UNIQUAC. The enthalpy of sublimation ($\Delta_{sub}H_i = \Delta_{vap}H_i + \Delta_{melt}H_i$) is calculated at the melting temperature of the pure component. All the thermophysical properties for the pure compounds used for the modeling are reported in Table 6. 1.

The interaction energy between two non-identical molecules is given by:

$$\lambda_{ij} = \lambda_{ji} = \lambda_{jj}\left(1 - \alpha_{ij}\right)$$

Eq.6. 11

where j is the compound with the shorter alkyl chain of the pair ij. As reported in previous work (COUTINHO *et al.*, 1996), it was found that generally a very small interaction parameter α_{ij} is required, usually varying from 0.03 to 0.05 for alkanes (MILHET *et al.*, 2005) and fatty acids (COSTA *et al.*, 2007) systems. In this study, the best fitting was found when using α_{ij} equal to 0.05.

From the approach, the high pressure solid–liquid equilibrium model is consequently a predictive model that enables the calculation of the phase behavior from the pure component properties with the possibility of fine adjustment of the experimental data. Using a flash calculation, the modeling was carried out on the basis of this approach to predict the solid–liquid phase diagrams for the studied systems. The UNIQUAC model predicted an eutectic system for the three binary mixtures. A good description of the liquidus line was obtained within the entire pressure range, as shown in Figs.6. 4-6. The AAD between the preditive model and the experimental data ranged from 0.6 K to 2.3 K (Table 6. 8).

Table 6. 8. AAD between modeling and experimental data from the liquidus lines for ethyl laurate + ethyl myristate, ethyl laurate + ethyl palmitate and ethyl myristate + ethyl palmitate systems under different pressures.

Pressure (MPa)	AAD (K)		
	ethyl laurate + ethyl myristate	ethyl laurate + ethyl palmitate	ethyl myristate + ethyl palmitate
0.1	0.8	1.1	0.8
20	0.8	1.8	0.8
40	0.6	2.1	1.0
60	0.6	2.3	1.8
80	0.7	1.5	1.1

6.4. Conclusions

Liquidus lines of three binary systems formed by FAEEs were determined for the first time at high pressure using a high pressure microscope described in the first part of this work. It was observed a translation of the liquidus line with the increase of the pressure. This translation in the liquidus line results from a change of the melting points of both, pure compounds and mixtures.

A predictive model, previously applied to alkanes, was used in this work to describe the phase behavior of these systems under high pressure. The results obtained show that this approach can be extended with success to other compounds than alkanes. The model can provide a good description of the phase behavior over large pressure ranges.

Acknowledgments

The authors are grateful to CNPq (304495/2010-7, 480992/2009-6, 552280/2010-0, 142193/2010-0), FAPESP (2008/09502-0, 2008/56258-8, 2012/05027-1), CAPES and FAEPEX/UNICAMP for their financial support and assistantships. We would like to

thanks Assamoi Cédric Kouakou from University of Pau (France) due to his contribution to this work.

References

ALLEN, C. A. W.; WATTS, K. C.; ACKMAN, R. G.; PEGG, M. J. Predicting the viscosity of biodiesel fuels from their fatty acid ester composition. **Fuel**, v. 78, p. 1319-1326, 1999.

BOROS, L.; BATISTA, M. L. S.; VAZ, R. V.; FIGUEIREDO, B. R.; FERNANDES, V. F. S.; COSTA, M. C.; KRÄHENBÜHL, M. A.; MEIRELLES, A. J. A.; COUTINHO, J. A. P. Crystallization Behavior of Mixtures of Fatty Acid Ethyl Esters with Ethyl Stearate. **Energy & Fuels**, v. 23, n. 9, p. 4625-4629, 2009.

BOUAID, A.; MARTINEZ, M.; ARACIL, J. A comparative study of the production of ethyl esters from vegetable oils as a biodiesel fuel optimization by factorial design. **Chemical Engineering Journal**, v. 134, n. 1, p. 93-99, 2007.

BOUKOUVALAS, C.; SPILIOTIS, N.; COUTSIKOS, P.; TZOUVARAS, N.; TASSIOS, D. Prediction of vapor-liquid equilibrium with the LCVM model: a linear combination of the Vidal and Michelsen mixing rules coupled with the original UNIF. **Fluid Phase Equilibria**, v. 92, n. 0, p. 75-106, 1994.

BOUKOUVALAS, C. J.; MAGOULAS, K. G.; STAMATAKI, S. K.; TASSIOS, D. P. Prediction of Vapor−Liquid Equilibria with the LCVM Model: Systems Containing Light Gases with Medium and High Molecular Weight Compounds. **Industrial & Engineering Chemistry Research**, v. 36, n. 12, p. 5454-5460, 1997.

CARARETO, N. D. D.; COSTA, M. C.; ROLEMBERG, M. P.; KRÄHENBÜHL, M. A.; MEIRELLES, A. J. A. The solid–liquid phase diagrams of binary mixtures of even saturated fatty alcohols. **Fluid Phase Equilibria**, v. 303, n. 2, p. 191.e1-191.e8, 2011.

CARARETO, N. D. D.; KIMURA, C. Y. C. S.; OLIVEIRA, E. C.; COSTA, M. C.; MEIRELLES, A. J. A. Flash points of mixtures containing ethyl esters or ethylic biodiesel and ethanol. **Fuel**, v. 96, n. 0, p. 319-326, 2012.

CERIANI, R.; GANI, R.; MEIRELLES, A. J. A. Prediction of heat capacities and heats of vaporization of organic liquids by group contribution methods. **Fluid Phase Equilibria**, v. 283, n. 1-2, p. 49-55, 2009.

COSTA, M. C.; BOROS, L. A. D.; BATISTA, M. L. S.; COUTINHO, J. A. P.; KRÄHENBÜHL, M. A.; MEIRELLES, A. J. A. Phase diagrams of mixtures of ethyl palmitate with fatty acid ethyl esters. **Fuel**, v. 91, n. 1, p. 177-181, 2012.

COSTA, M. C.; BOROS, L. A. D.; COUTINHO, J. O. A. P.; KRÄHENBÜHL, M. A.; MEIRELLES, A. J. A. Low-Temperature Behavior of Biodiesel: Solid–Liquid Phase Diagrams of Binary Mixtures Composed of Fatty Acid Methyl Esters. **Energy & Fuels**, v. 25, n. 7, p. 3244-3250, 2011.

COSTA, M. C.; ROLEMBERG, M. P.; BOROS, L. A. D.; KRAHENBUHL, M. A.; DE OLIVEIRA, M. G.; MEIRELLES, A. J. A. Solid-liquid equilibrium of binary fatty acid mixtures. **Journal of Chemical and Engineering Data**, v. 52, n. 1, p. 30-36, 2007.

COUTINHO, J. A. P.; GONÇALVES, M.; PRATAS, M. J.; BATISTA, M. L. S.; FERNANDES, V. F. S.; PAULY, J.; DARIDON, J. L. Measurement and modeling of biodiesel cold-flow properties. **Energy & Fuels**, v. 24, n. 4, p. 2667-2674, 2010.

COUTINHO, J. A. P.; KNUDSEN, K.; ANDERSEN, S. I.; STENBY, E. H. A Local Composition Model For Paraffinic Solid Solutions. **Chemical Engineering Science**, v. 51, p. 3273, 1996.

COUTINHO, J. A. P.; MIRANTE, F.; PAULY, J. A new predictive UNIQUAC for modeling of wax formation in hydrocarbon fluids. **Fluid Phase Equilibria**, v. 247, n. 1–2, p. 8-17, 2006.

DA CONCEIÇÃO, L. R. V.; DA COSTA, C. E. F.; DA ROCHA FILHO, G. N.; ZAMIAN, J. R. Obtaining and characterization of biodiesel from jupati (Raphia taedigera Mart.) oil. **Fuel**, v. 90, n. 9, p. 2945-2949, 2011.

DARIDON, J. L.; PAULY, J.; MILHET, M. High pressure solid-liquid phase equilibria in synthetic waxes. **Physical Chemistry Chemical Physics**, v. 4, n. 18, p. 4458-4461, 2002.

FOLLEGATTI-ROMERO, L. A.; LANZA, M.; BATISTA, F. R. M.; BATISTA, E. A. C.; OLIVEIRA, M. B.; COUTINHO, J. O. A. P.; MEIRELLES, A. J. A. Liquid−Liquid Equilibrium for Ternary Systems Containing Ethyl Esters, Anhydrous Ethanol and Water at 298.15, 313.15, and 333.15 K. **Industrial & Engineering Chemistry Research**, v. 49, n. 24, p. 12613-12619, 2010.

IMAHARA, H.; MINAMI, E.; SAKA, S. Thermodynamic study on cloud point of biodiesel with its fatty acid composition. **Fuel**, v. 85, n. 12-13, p. 1666-1670, 2006.

INOUE, T.; HISATSUGU, Y.; ISHIKAWA, R.; SUZUKI, M. Solid-liquid phase behavior of binary fatty acid mixtures 2. Mixtures of oleic acid with lauric acid, myristic acid, and palmitic acid. **Chemistry and Physics of Lipids**, v. 127, n. 2, p. 161-173, 2004a.

INOUE, T.; HISATSUGU, Y.; SUZUKI, M.; WANG, Z. N.; ZHENG, L. Q. Solid-liquid phase behavior of binary fatty acid mixtures 3. Mixtures of oleic acid with capric acid (decanoic acid) and caprylic acid (octanoic acid). **Chemistry and Physics of Lipids**, v. 132, n. 2, p. 225-234, 2004b.

INOUE, T.; HISATSUGU, Y.; YAMAMOTO, R.; SUZUKI, M. Solid-liquid phase behavior of binary fatty acid mixtures 1. Oleic acid/stearic acid and oleic acid/behenic acid mixtures. **Chemistry and Physics of Lipids**, v. 127, n. 2, p. 143-152, 2004c.

KNOTHE, G. Dependence of biodiesel fuel properties on the structure of fatty acid alkyl esters. **Fuel Processing Technology**, v. 86, n. 10, p. 1059-1070, 2005.

KOBAYASHI, M.; KANEKO, F.; SATO, K.; SUZUKI, M. Vibrational spectroscopic study on polymorphism and order-disorder phase transition in oleic acid. **The Journal of Physical Chemistry**, v. 90, n. 23, p. 6371-6378, 1986.

KOUAKOU, A. C.; MAPIHAN, K. L.; PAULY, J. Solid-liquid equilibria under high pressure of pure fatty acid methyl esters. **Fuel**, v. 109, p. 297-302, 2013.

MEHER, L. C.; SAGAR, D. V.; NAIK, S. N. Technical aspects of biodiesel production by transesterification — a review. **Renewable and Sustainable Energy Reviews**, v. 10, p. 248-268, 2006

MILHET, M.; PAULY, J.; COUTINHO, J. A. P.; DIRAND, M.; DARIDON, J. L. Liquid–solid equilibria under high pressure of tetradecane + pentadecane and tetradecane + hexadecane binary systems. **Fluid Phase Equilibria**, v. 235, n. 2, p. 173-181, 2005.

MOSER, B. R. Biodiesel production, properties, and feedstocks. **In Vitro Cellular & Developmental Biology** — Plant, v. 45, p. 229-266, 2009.

OLIVEIRA, M. B.; BARBEDO, S.; SOLETTI, J. I.; CARVALHO, S. H. V.; QUEIMADA, A. J.; COUTINHO, J. A. P. Liquid-liquid equilibria for the canola oil biodiesel + ethanol + glycerol system. **Fuel**, v. 90, n. 8, p. 2738-2745, 2011.

OLIVEIRA, M. B.; MIGUEL, S. I.; QUEIMADA, A. N. J.; COUTINHO, J. O. A. P. Phase Equilibria of Ester + Alcohol Systems and Their Description with the Cubic-Plus-Association Equation of State. **Industrial & Engineering Chemistry Research**, v. 49, n. 7, p. 3452-3458, 2010.

PAULY, J.; DARIDON, J.-L.; COUTINHO, J. A. P.; LINDELOFF, N.; ANDERSEN, S. I. Prediction of solid–fluid phase diagrams of light gases–heavy paraffin systems up to 200 MPa using an equation of state–GE model**. Fluid Phase Equilibria**, v. 167, n. 2, p. 145-159, 2000.

PAULY, J.; DARIDON, J. L.; COUTINHO, J. A. P.; DIRAND, M. Crystallisation of a multiparaffinic wax in normal tetradecane under high pressure. **Fuel**, v. 84, n. 4, p. 453-459, 2005.

PÉNELOUX, A.; RAUZY, E.; FRÉZE, R. A consistent correction for Redlich-Kwong-Soave volumes. **Fluid Phase Equilibria**, v. 8, n. 1, p. 7-23, 1982.

RAMOS, M. J.; FERNÁNDEZ, C. M.; CASAS, A.; RODRÍGUEZ, L.; PÉREZ, A. Influence of fatty acid composition of raw materials on biodiesel properties. **Bioresource Technology**, v. 100, n. 1, p. 261-268, 2008.

ROBUSTILLO, M. D.; BARBOSA, D. F.; MEIRELLES, A. J. D. A.; FILHO, P. D. A. P. Solid–liquid equilibrium in ternary mixtures of ethyl oleate, ethyl laurate and ethyl palmitate. **Fluid Phase Equilibria**, v. 339, n. 0, p. 58-66, 2013.

SOAVE, G. Equilibrium constants from a modified Redlich-Kwong equation of state. **Chemical Engineering Science**, v. 27, n. 6, p. 1197-1203, 1972.

VENTOLA, L.; RAMIREZ, M.; CALVET, T.; SOLANS, X.; CUEVAS-DIARTE, M. A.; NEGRIER, P.; MONDIEIG, D.; VAN MILTENBURG, J. C.; OONK, H. A. J. Polymorphism of N-alkanols: 1-heptadecanol, 1-octadecanol, 1-nonadecanol, and 1-eicosanol. **Chemistry of Materials**, v. 14, n. 2, p. 508-517, 2002.

WANG, P. S.; THOMPSON, J.; VAN GERPEN, J. Minimizing the cost of biodiesel blends for specified cloud points. **Journal of the American Oil Chemists' Society**, v. 88, n. 4, p. 563-572, 2011.

Capítulo 7. High pressure solid-liquid equilibrium of fatty alcohols binary systems

Natália D. D. Carareto[a,b], *Mariana C. Costa*[c], *Antonio J. A. Meirelles*[a], *J. Pauly*[*b]

[a] EXTRAE, Department of Food Engineering, Faculty of Food Engineering, University of Campinas, UNICAMP, Campinas, Brazil

[b] Laboratoire des Fluides Complexes, Université de Pau, BP 1155, 64013 Pau Cedex, France

[c] FCA, Applied Sciences Faculty, University of Campinas, UNICAMP, Limeira, Brazil

Trabalho a ser submetido na revista **Fluid Phase Equilibria.**

Abstract.

The melting temperatures of four fatty alcohols, 1-dodecanol, 1-tetradecanol, 1-hexadecanol and 1-octadecanol, have been measured at atmospheric pressure using a μDSC calorimeter and at high pressures (up to 80 MPa) thanks to a dedicated microscope. The solid–liquid phase diagrams of six binary mixtures formed by these saturated fatty alcohols, namely 1-dodecanol + 1-tetradecanol, 1-dodecanol + 1-hexadecanol, 1-dodecanol + 1-octadecanol, 1-tetradecanol + 1-hexadecanol, 1-tetradecanol + 1-octadecanol and 1-hexadecanol + 1-octadecanol systems, were also measured using high pressure microscopy within the range of 0.1–80 MPa. In addition, the phase diagrams of the 1-dodecanol + 1-tetradecanol, 1-tetradecanol + 1-hexadecanol and 1-hexadecanol + 1-octadecanol systems were also measured by DSC in order to compare the results obtained from both techniques. Based on the experimental data, it could be concluded that the behavior of the phase diagrams is slightly affected by the pressure, even within very large pressure ranges, such as the ones studied in this work.

Keywords.

- Fatty alcohols;
- Solid-liquid equilibrium;
- High pressure data
- DSC

7.1. Introduction

Fatty alcohols have a potential of usage in the pharmaceutical, food or chemical industries since they are natural derivatives of plants or animal oils and fats and are considered as a class of compounds which can be used as structurants in the lipid phase present in a wide range of products (DANIEL e RAJASEKHARAN, 2003; GANDOLFO et al., 2004; SCHAINK et al., 2007). The solid-liquid boundaries and behavior of simple fatty systems can be helpful to understand the physical properties of complex lipids and their mixtures. They are also important for developing purification and fractionation processes of lipid mixtures. For example, the controlled precipitation of solid phases is widely applied in pharmaceutical, cosmetic and food industries as a separation process. In other areas like petroleum engineering, the wax crystallization is a problem for the storage, exploitation and transportations of fossil oils (MILHET et al., 2005).

In the case of fatty mixtures, solid-liquid equilibrium (SLE) data measured under high pressure are very rare. For this reason the modeling approach commonly used in the literature does not take into account the influence of pressure. However, recently we can find an increasing interest for experimental data and development of models for solid-liquid equilibrium under high pressure. Important aspects to be investigated in the melting of mixtures under high pressure are the modification to higher temperatures of the liquidus curve due to the pressure increase, the potential change of the eutectic composition and of the structure of the different solid phases.

Solid-liquid equilibrium data of systems containing fatty alcohols were investigated by different research groups. Yamamoto et al. (1990) measured the phase diagram of a binary system formed by 1-heptadecanol + 1-octadecanol, with a detailed description of the solid-solid transitions. Ventola et al. (VENTOLA et al., 2002; VENTOLA et al., 2003; VENTOLA et al., 2004a; VENTOLA et al., 2004b) have presented the phase behavior of fatty alcohol systems showing different polymorphic behaviors. Domańska and Gonzalez (DOMANSKA e GONZALEZ, 1996a; b; 1997) studied the solid–liquid equilibrium of a

series of fatty alcohol binary mixtures, using a dynamic method with visual detection of the melting temperatures.

This work is part of a series of studies regarding the SLE of binary systems composed of saturated fatty alcohols. In a previous work, we have reported the phase diagrams of fatty alcohols mixtures measured by DSC in which the systems present either a simple eutectic behavior (CARARETO et al., 2011) or, in case of more complex mixtures, peritectic and metatectic reactions (CARARETO et al., submitted work-b). The aim of the present work was to investigate the liquidus curves of six saturated fatty alcohols binary mixtures, namely 1-dodecanol (C12OH) + 1-tetradecanol (C14OH), C12OH + 1-hexadecanol (C16OH), C12OH + 1-octadecanol (C18OH), C14OH + C16OH, C14OH + C18OH and C16OH + C18OH, by means of a cross polar microscopy device that allows the study of phase equilibrium up to 80 MPa. In addition, the DSC technique using a linear heating rate of 1.0 K min^{-1} was applied in order to improve the understanding of the SLE of the following systems: C12OH + C14OH, C14OH + C16OH and C16OH + C18OH. As far as we know, the systems C12OH + C14OH and C14OH + C16OH have not been previously reported in the literature, even at ambient pressure, and none of them has been investigated at higher pressures.

7.2. Experimental Section

High purity reactants (Sigma-Aldrich) with no further purification process were used to prepare the samples (Table 7. 1). All the binary mixtures were prepared gravimetrically using a high precision balance with an accuracy of ± 0.2 mg.

7.2.1. Micro Differential Scanning Calorimetry (μDSC)

The μDSC analyses were used to measure the melting temperatures of the pure fatty alcohols and they were carried out using a SETARAM Micro DSC 7 evo calorimeter using

nitrogen as purge gas (purity ≥ 99.995% from Linde group), as described in previous works (KOUAKOU et al., 2013; CARARETO et al., submitted work-a). Each sample was analyzed in a heating run, at a heating rate of 0.01 K min^{-1}. Peak top temperatures for the thermal curves were selected to represent the melting temperature for pure fatty alcohols, since the onset temperature can be incorrectly determinated due to the presence of polimorphics transitions close to the melting point (COSTA et al., 2007; CARARETO et al., 2011; KOUAKOU et al., 2013). The uncertainty of the temperature was estimated as 0.2 K.

Table 7. 1. Melting temperature (T_{melt}) at 0.1 MPa for the fatty alcohols used in this work, and absolute deviation (AD) between $T_{melt,i}$ at atmospheric pressure from μDSC and microscope (AD_1) and from μDSC and literature (AD_2).

Reactant (CAS number)	Purity[a] (*w*/*w*)	T_{melt} at 0.1 MPa			Deviation (K)	
		$T_{melt,HP}$ (K)	$T_{melt,DSC}$ (K)	$T_{melt,lit}$[b] (K)	AD_1	AD_2
C12OH (112-53-8)	0.98	296.9	297.1	297.8	0.2	0.7
C14OH (112-72-1)	0.97	310.6	310.9	311.2	0.4	0.3
C16OH (36653-82-4)	0.99	322.2	322.8	323.3	0.6	0.5
C18OH (112-92-5)	0.99	330.9	331.3	331.6	0.5	0.3

$T_{melt,HP}$: melting temperature at atmospheric pressure using the high pressure cell

$T_{melt,DSC}$: melting temperature at atmospheric pressure using μDSC analyses

[a] according to the supplier. [b] from (CARARETO et al., 2011)

7.2.2. Differential Scanning Calorimetry (DSC)

The DSC analyses were applied in order to evaluate the phase diagrams at atmospheric pressure for the folowing bynary systems: C12OH + C14OH, C14OH +

C16OH and C16OH + C18OH. A TA Instruments calorimeter (model MDSC 2920) equipped with a refrigerated cooling system was used in the DSC analyses. Samples of each mixture (3 to 5 mg) were weighed in a microanalytical balance (Perkin Elmer AD6) with 0.005 mg accuracy and put in sealed aluminum pans. An empty pan was used as reference in the analyses. A pre-treatment was applied as follows: the samples were kept isothermally for 20 min at 15 K above the melting temperature of the heavier component of the mixture and subsequently cooled to 45 K below the melting point of the lightest component at a cooling rate of 1.0 $K \cdot min^{-1}$ and kept in isothermal state during 30 min. After this pre-treatment, the samples were then analyzed by a heating run with a rate of 1.0 K min^{-1}. As well as for μDSC analyses, peak temperatures were selected to represent the melting and other transitions temperatures of the mixtures. The uncertainty of the phase equilibrium data is estimated to be less than 0.3 K, as reported in the preceding works (CARARETO et al., 2011; CARARETO et al., submitted work-b).

7.2.3. High pressure microscopy

The melting temperature of the pure fatty alcohols and the SLE of their binary mixtures were studied in a high pressure microscope. The apparatus has been successfully used in previous works for measuring the liquidus line for waxes, alkanes, fatty acids and methylic or ethylic esters (DARIDON et al., 2002; MILHET et al., 2005; COSTA et al., 2007; KOUAKOU et al., 2013; CARARETO et al., submitted work-a). The samples were injected in a stainless steel autoclave cell equipped with two sapphire windows through which the sample can be observed and with an end closed with a moving piston which was able to produce a pressure up to 100 MPa inside the cell (as described in Fig. 7. 1). The temperature control in the high pressure cell was made by flowing a heat-transducing fluid in flow lines in the metallic thermostat block, which could be maintained between 253 and 353 K, and carried out by a thermostat bath (Huber, Germany) with a temperature stability of 0.01 K. The samples temperatures were measured with a calibrated platinum resistance inserted inside the cell and connected to a high-precision thermometer (AOIP). The temperature uncertainty was estimated not large then 0.2 K (MILHET et al., 2005). The

pressure inside the cell was measured by a piezoresistive silicon pressure transducer (Kulite), placed inside the cell in order to reduce the dead volume, with a precision of 0.2%. A polarized light microscope coupled to a video camera was used to observe and registrate the SLE transitions.

The samples were inserted into the high pressure cell at a temperature higher than the melting temperature of the fatty alcohols to avoid the crystallization. Then the temperature was decreased 10-15 K below the melting temperature and kept at this temperature for 20-30 min. The temperature was increased in small steps (0.1 – 0.5 K) and allowed isothermally about 1-3 min at each step, until the disappearance of the last crystal was observed, and which was annotated as the melting temperature of the sample. Then the pressure of the system was increased and a new temperature cycle was started. All the samples had the melting temperature measured in pressures of 0.1, 20, 40, 60 and 80 MPa.

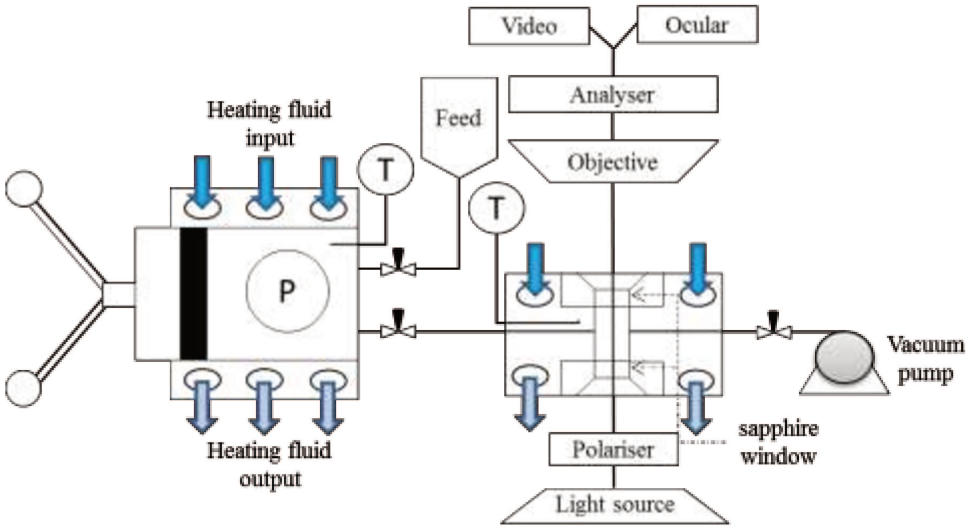

Fig. 7. 1. Scheme of the high pressure microscopy apparatus.

7.3. Results and discussion

7.3.1. Effect of pressure on the melting temperature of pure fatty alcohols

The melting temperature at atmospheric pressure of pure fatty alcohols measured using the high pressure cell and μDSC are presented in Table 7. 1. The absolute deviations between these melting temperatures (AD_1) ranged from 0.2 to 0.5 K. Considering the uncertainty of each experimental technique, both sets of data showed a good agreement. A comparison between the melting temperatures from the μDSC and from literature (CARARETO et al., 2011) was made and the absolute deviations (AD_2) ranged from 0.3 to 0.7 K, also showing a good agreement between both set of data.

The effect of pressure on the melting temperatures of pure fatty alcohols are presented in Table 7. 2. The corresponding curves are shown in Fig. 7. 2 and they indicate that the fatty alcohols melting temperatures have a quasilinear dependence with the pressure's increasing. The coefficients of determination (R^2) for the (T,P) curves have varied from 0.9978 to 0.9999. The (T,P) dependence can be calculated by means of the average slope of each curve as follows (see Table 7. 2):

$$\frac{\Delta T}{\Delta P} = \frac{T_{melt}\left(P_{\max}\right) - T_{melt}\left(P_0\right)}{P_{\max} - P_0}$$

Eq.7. 1

For comparison purposes and in order to reduce the uncertainty of the calculated slopes, P_{max} was set as 80 MPa and P_0 corresponds to atmospheric pressure for all compositions. The uncertainty of the (T,P) slope has been estimated as 2.5 % (MILHET et al., 2005).

Table 7. 2. Melting temperatures (T_{melt}) as a function of pressure and average slope of the solid-liquid transition of the pure fatty alcohols.

	Pressure					Average slope
Fatty alcohol	0.1 MPa	20 MPa	40 MPa	60 MPa	80 MPa	(K MPa^{-1})
C12OH	296.9	300.5	304.6	308.4	311.7	0.1852
C14OH	310.6	314.2	319.0	323.8	327.8	0.2153
C16OH	322.2	327.3	332.4	337.6	342.7	0.2566
C18OH	330.9	335.8	340.9	345.9	350.6	0.2466

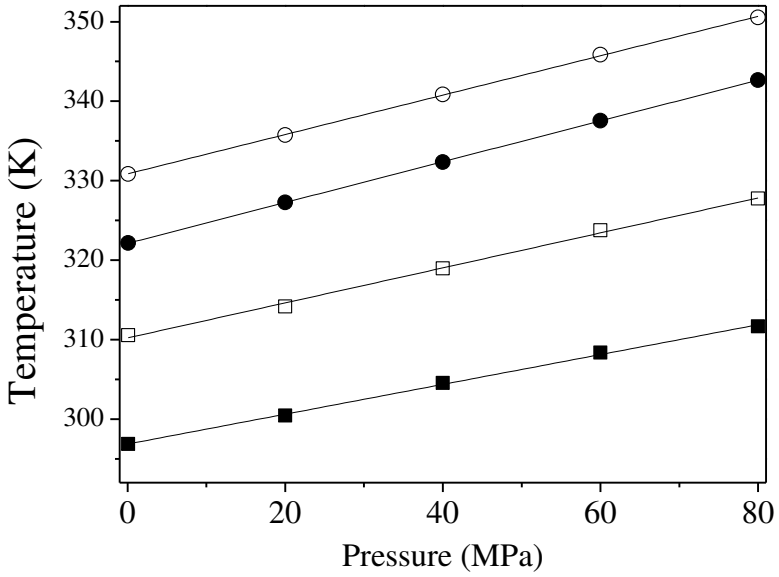

Fig. 7. 2. Melting temperature from the fatty alcohols as a function of pressure. ■ C12OH ($R^2 = 0.9988$); □ C14OH ($R^2 = 0.9978$); ● C16OH ($R^2 = 0.9999$) and; ○ C18OH ($R^2 = 0.9998$).

7.3.2. High pressure solid-liquid equilibrium for fatty alcohols binary mixtures

The effect of pressure on the solid–liquid phase equilibrium has been measured for each binary system at various constant compositions. The high-pressure apparatus used allows liquid–solid equilibrium studies from atmospheric pressure up to 80 MPa. The melting temperatures were measured for differents pressures and selected compositions. The experimental results are summarized in Tables 7. 3-8.

The SLE data for the systems C12OH + C18OH, C12OH + C16OH and C14OH + C18OH have been already reported at atmospheric pressure and were obtained by using the DSC technique at a heating rate of 1.0 K min^{-1} (CARARETO et al., 2011; CARARETO et al., submitted work-b). In general, the systems measured by the different techniques presented a good agreement with an average absolute deviation (AAD given by Eq.7.2) of 0.8, 0.5 and 0.5 K for the systems C12OH + C18OH, C12OH + C16OH and C14OH + C18OH, respectively. A comparison of the liquidus lines between the different sets of data is presented as deviations in Fig.7.3. As can be noted, the higher deviations occur in the regions close to the eutectic and peritectic points. The deviations may be explained by the appearance of a metastable phase close to the melting of the samples and by kinetic considerations, since the heating rates are different. In general, the deviations were negatives meaning that the temperatures measured in the microscope are higher than the values from the DSC, as already observed when comparing data from both experimental tecniques for fatty acids or n-alkanes binary systems (MILHET et al., 2005; COSTA et al., 2007).

$$\mathrm{AAD} = \frac{1}{n}\sum_{i=1}^{n}\left(\left|T_{i,lit} - T_{i,\exp}\right|\right)$$

Eq.7. 2

Table 7. 3. SLE data for the system C12OH + C18OH from microscope device.

	T_{melt} (K)				
x_{C12OH}	0.1 MPa	20 MPa	40 MPa	60 MPa	80 MPa
0.0000	330.9	335.8	340.9	345.9	350.6
0.2987	326.1	330.9	335.4	340.0	344.5
0.5043	321.7	326.5	331.8	336.8	341.4
0.7034	315.4	320.4	325.6	330.1	334.4
0.8000	310.0	314.9	319.7	323.2	327.3
0.8530	304.6	309.8	314.0	318.1	322.1
0.9007	297.5	302.3	307.3	311.1	315.4
0.9533	295.9	300.4	304.5	308.5	312.2
1.0000	296.9	300.5	304.6	308.4	311.7

Table 7. 4. SEL data for the system C12OH + C16OH from microscope device.

	T_{melt} (K)				
x_{C12OH}	0.1 MPa	20 MPa	40 MPa	60 MPa	80 MPa
0.0000	322.2	327.3	332.4	337.6	342.7
0.2033	319.5	324.0	328.4	333.3	337.5
0.3995	315.2	320.0	324.5	328.3	332.7
0.6002	308.3	313.0	317.8	322.0	326.7
0.6986	304.0	308.5	313.2	317.7	321.9
0.7501	299.8	304.2	308.7	313.0	316.9
0.7997	296.5	300.6	305.0	309.1	312.5
0.8494	293.7	298.0	301.9	306.1	309.4
0.8992	293.9	298.2	302.5	306.7	310.2
1.0000	296.9	300.5	304.6	308.4	311.7

Table 7. 5. SLE data for the system C14OH + C18OH from microscope device.

	T_{melt} (K)				
x_{C14OH}	0.1 MPa	20 MPa	40 MPa	60 MPa	80 MPa
0.0000	330.9	335.8	340.9	345.9	350.6
0.1994	327.2	331.8	336.2	340.8	345.3
0.3951	324.5	329.2	333.9	338.0	342.6
0.5981	318.2	323.0	327.6	333.3	337.6
0.6992	311.7	316.6	321.5	325.9	329.8
0.8008	308.3	313.1	317.8	322.6	326.7
0.8500	307.4	312.3	316.9	321.3	325.8
0.8994	308.2	312.8	317.4	321.4	325.9
1.0000	310.6	314.2	319.0	323.8	327.8

Table 7. 6. SLE data for the system C12OH + C14OH from microscope device.

	T_{melt} (K)				
x_{C12OH}	0.1 MPa	20 MPa	40 MPa	60 MPa	80 MPa
0.0000	310.6	314.2	319.0	323.8	327.8
0.2021	306.5	311.3	316.3	320.8	325.0
0.3992	301.3	306.5	311.7	316.2	320.3
0.5346	298.1	303.0	308.0	312.8	316.6
0.7004	294.8	299.6	304.2	308.4	312.4
0.8003	293.4	298.1	302.6	306.9	311.2
0.9003	294.7	298.9	302.7	306.5	310.8
1.0000	296.9	300.5	304.6	308.4	311.7

Table 7. 7. SLE data for the system C14OH + C16OH from microscope device.

	T_{melt} (K)				
x_{C14OH}	0.1 MPa	20 MPa	40 MPa	60 MPa	80 MPa
0.0000	322.2	327.3	332.4	337.6	342.7
0.2691	317.9	322.9	327.7	332.5	337.7
0.4023	315.3	320.2	325.1	329.9	334.2
0.6046	312.2	317.1	321.7	326.0	330.3
0.7045	311.0	315.9	320.5	324.9	329.2
0.8031	310.1	315.2	320.0	324.7	328.4
0.9033	310.0	315.1	319.8	324.5	328.8
1.0000	310.6	314.2	319.0	323.8	327.8

Table 7. 8. SLE data for the system C16OH + C18OH from microscope device.

	T_{melt} (K)				
x_{C16OH}	0.1 MPa	20 MPa	40 MPa	60 MPa	80 MPa
0.0000	330.9	335.8	340.9	345.9	350.6
0.1996	328.0	333.2	338.0	343.0	347.5
0.3981	325.6	330.4	335.3	340.1	344.4
0.5987	323.3	328.3	333.0	337.2	341.7
0.7952	321.3	326.3	331.2	335.6	339.9
0.8848	321.3	326.3	331.2	335.8	340.2
1.0000	322.2	327.3	332.4	337.6	342.7

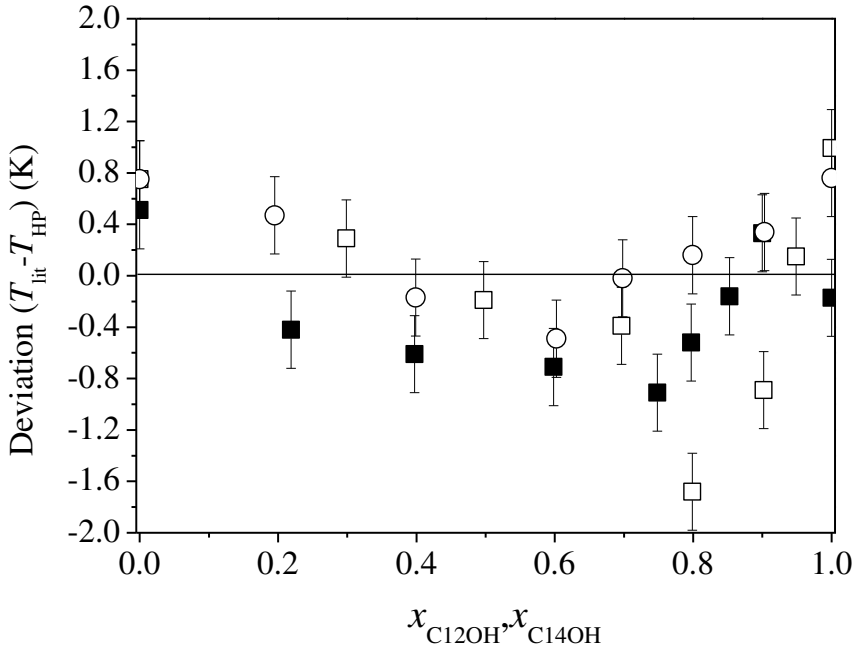

Fig. 7. 3. Liquidus line deviation between microscope experimental data and literature. □ C12OH + C18OH from (CARARETO et al., 2011); ■ C12OH + C16OH from (CARARETO et al., submitted work-b) and; ○ C14OH + C18OH from (CARARETO et al., submitted work-b).

In previous work (CARARETO et al., 2011), the C12OH + C18OH system was classified as a simple eutectic one, with the eutectic point at atmospheric pressure occurring around $x_{C12OH} = 0.93$. The same behavior was observed in the set of data obtained by means of the high pressure microscope as can be noted in Fig.7.4. It is possible to note that the general behavior of the liquidus curve shape, including the eutectic point, is not affected by the pressure increase, although the melting temperature values increase in a quasilinear way as already observed for the pure components.

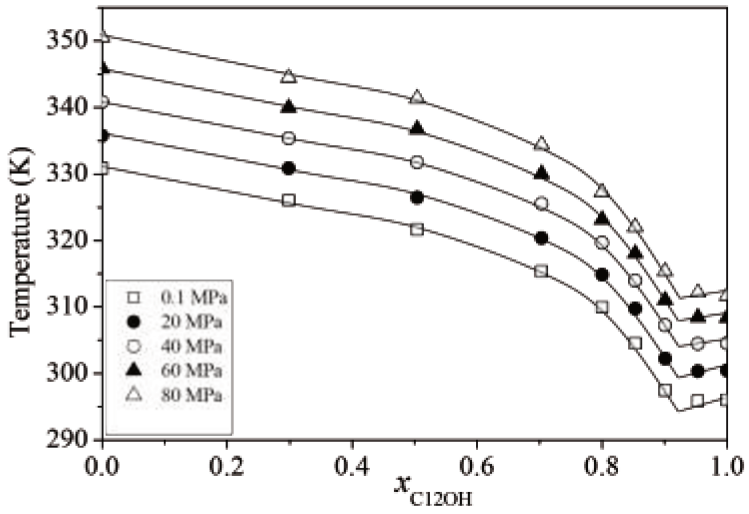

Fig. 7. 4. Liquidus curve of the C12OH + C18OH binary system at atmospheric and higher pressures. Liquidus curve at: □ 0.1 MPa, ● 20 MPa, ○ 40 MPa, ▲ 60 MPa and, Δ 80 MPa; (—) is a guide to the eye.

Both C12OH + C16OH and C14OH + C18OH systems have presented an eutectic point close to the 0.85 molar concentration of the ligher component, as can be noted in Figs.7.5 and 7.6. In a previous work the solid-liquid phase diagrams were presented having more complex behavior (CARARETO et al., submitted work-b), with a inflection in the liquidus curve related to the peritectic point. Since the microscopy is a visual method of measuring phase diagrams, with the technique it is only possible to determine the liquidus line. The solidus curves, which is the line that separates the SLE region from the completely solid state region, and other solid-liquid transitions can not be easily determined by the microscopy analyses, but still the inflection point related to the peritectic reaction can be noted in the Figs.7.5 and 7.6 (the line representing the trend of the liquidus curve makes easier the identification of the peritectic inflection point in Figs. 7.5 and 7.6). Comparing the liquidus line for the different pressures it is possible to note that the increasing of pressure did not affect the eutectic and peritectic points for both binary systems.

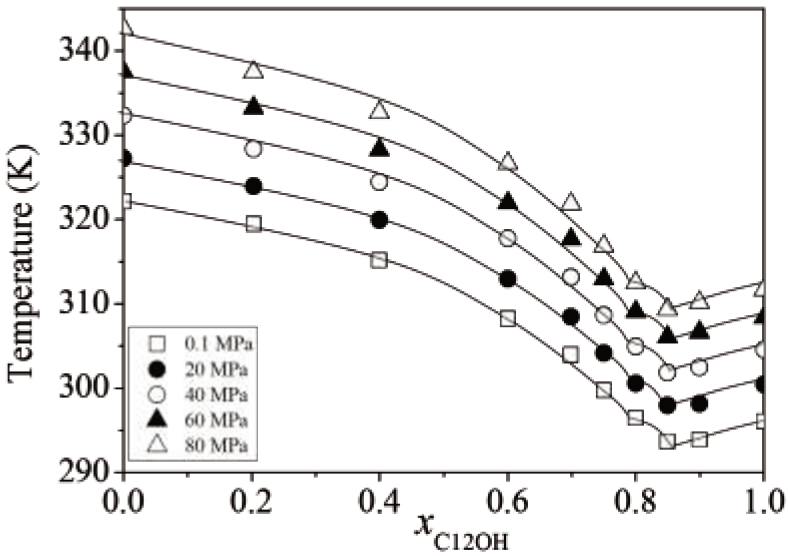

Fig. 7. 5. Liquidus curve at atmospheric and higher pressures for the C12OH + C16OH system. Liquidus curve at: □ 0.1 MPa, ● 20 MPa, ○ 40 MPa, ▲ 60 MPa and, Δ 80 MPa; (—) is a guide to the eye.

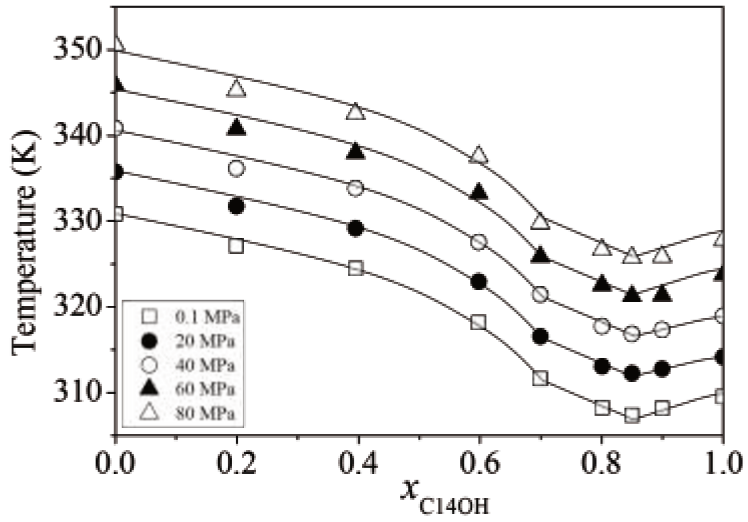

Fig. 7. 6. Liquidus curve at atmospheric and higher pressures for the C14OH + C18OH system. Liquidus curve at: □ 0.1 MPa, ● 20 MPa, ○ 40 MPa, ▲ 60 MPa and, Δ 80 MPa; (—) is a guide to the eye.

The DSC results for the C12OH + C14OH, C14OH + C16OH and C16OH + C18OH systems are summarized in Tables 7.9 to 7.11 and shown in Figs. 7.7a, 7.8a and

7.9a, respectively. For these three systems, a point of minimum temperature is observed around a molar fraction of 0.8 of the lower melting point component. Nevertheless, this point can not be associated to an eutectic transition, since the compounds have a large miscibility region on the solid state and solid-liquid domains is very narrow in comparison with others fatty alcohol systems, as already reported by Smith (1931) and Ventolà et al. (2004b) for the C16OH + C18OH system. A similar behavior was reported in the literature for binary mixtures of n-alkanes (COUTINHO et al., 1996; HE et al., 2003); these n-alkane systems were also characterized by a high miscibility on the solid phase. So, the minimum point on the liquidus curve of these binary systems correponds to a transition of a liquid phase *l* in equilibrium with a single solid phase associated to the formed solid solution. In contrast, the definition of the eutectic point is an invariant point in which a liquid phase *l* is in equilibrium with two different solid phases α and β at the eutectic temperature and composition (GAMSJAGER et al., 2008).

Based on the results for other fatty systems (COSTA et al., 2009a; COSTA et al., 2009b; COSTA et al., 2009c; CARARETO et al., 2011; CARARETO et al., submitted work-b) it is possible to conclude that mixtures with eutectic or even peritectic transitions exihibit a relatively large range of temperatures in the solid liquid equilibrium region, i.e. the temperature difference between the solidus and liquidus line is large, making easier to separate the beginning and end of the mixture´s melting by the microscopy analysis. However, for the C12OH + C14OH, C14OH + C16OH and C16OH + C18OH systems, a small SLE range of temperatures was observed for all analyzed samples along the entire concentration range.

Concerning the pressure effect, the progress of the melting temperature for all samples displayed a quasilinear function of the incresing pressure (see Figs. 7.7b, 7.8b and 7.9b). Plotting these slope values in function of composition for the three system - C12OH + C14OH, C14OH + C16OH and C16OH + C18OH - (Fig. 7.10) shows that the average slope of the liquidus curves in the (T, P) diagram is similar for the three different systems. In fact, in the case of the C12OH + C14OH, the average slope is equal to (0.22 ± 0.01) K

MPa^{-1}, for C14OH + C16OH it is equal to (0.234 ± 0.008) K MPa^{-1} and for C16OH + C18OH the average slope is equal to (0.240 ± 0.009) K MPa^{-1} excluding the slope values for the pure fatty alcohols. Comparing with the average slope of the pure reactants the values are slightly different, which may imply that the mixtures have some differences in the crystal forms when compared with the original compounds. This difference on the slope values may give an additional support to the hypothesis that these systems have miscibility in the solid state. A better characterization of the transitions observed under the liquidus curve can be performed using X-ray analysis.

When compared with the data obtained by using differential scanning calorimetry (DSC), the microscope results shows a relatively good agreement (deviations ranging from 0.1 K to 2.6 K). The visual microscopy is known to give different temperatures in comparison to other techniques (ROENNINGSEN et al., 1991; JI et al., 2004). The onsets temperature measured by DSC for mixtures that crystallize in a rotator form seem to give a underestimated result for some compositions and should correspond to the melting point of the metastable phase. Since the kinetics of transformation for the stable form for some compositions is very slow, the stable phase can take many hours after the rotator one and might be easily missed (MILHET et al., 2005). But the experimental apparatus used in this work for the microscope analyses allows to increase the system's pressure by a fast raising, then the phase change is almost instantaneous. In the work of Milhet et al. (2005), it was verified that this fast raising in the system's pressure can induce the crystallization of the stable form and may be the reason for the temperatures deviations of for the two analytical techniques.

Table 7. 9. SLE data for the system C12OH + C14OH from DSC.

x_{C12OH}	$T_{trans,1}$ (K)	$T_{trans,2}$ (K)	$T_{trans,3}$ (K)	$T_{trans,4}$ (K)	T_{melt}
0.0000					311.3
0.1010			306.0		309.0
0.1956		287.3	301.5		307.3
0.3102		288.6	294.2		304.9
0.3984		289.0	291.7	296.2	302.4
0.4983	288.4	289.1		296.8	300.6
0.5939	286.1	289.8		296.6	297.9
0.6955	285.2	288.8		295.6	297.3
0.8028	286.6				295.5
0.8982	288.1				296.3
1.0000					297.8

Table 7. 10. SLE data for the system C14OH + C16OH from DSC.

x_{C14OH}	$T_{trans,1}$ (K)	$T_{trans,2}$ (K)	$T_{trans,3}$ (K)	T_{melt}
0.0000				323.3
0.1017			316.0	321.2
0.2047			310.6	319.8
0.2967	295.6	299.2	305.1	318.6
0.3991	295.6			317.5
0.5024	294.3	298.2		315.8
0.5990		296.8		314.5
0.7014	294.0	297.4		312.2
0.7988	293.3	297.8		311.0
0.9019		299.8		311.6
1.0000				311.3

Table 7. 11. SLE data for the system C16OH + C18OH from DSC.

x_{C16OH}	$T_{trans,1}$ (K)	$T_{trans,2}$ (K)	$T_{trans,3}$ (K)	T_{melt}
0.0000				331.6
0.0996		324.0	325.8	330.0
0.1977	301.9		319.0	328.5
0.2989	304.0	309.8	313.1	327.2
0.4003	304.8	310.4		326.1
0.5004	304.2	310.0		324.7
0.6004	304.6	310.1		323.9
0.7003	302.1	307.9		323.0
0.7998	300.7	308.0		322.4
0.9008	305.9	308.4		322.2
1.0000				323.3

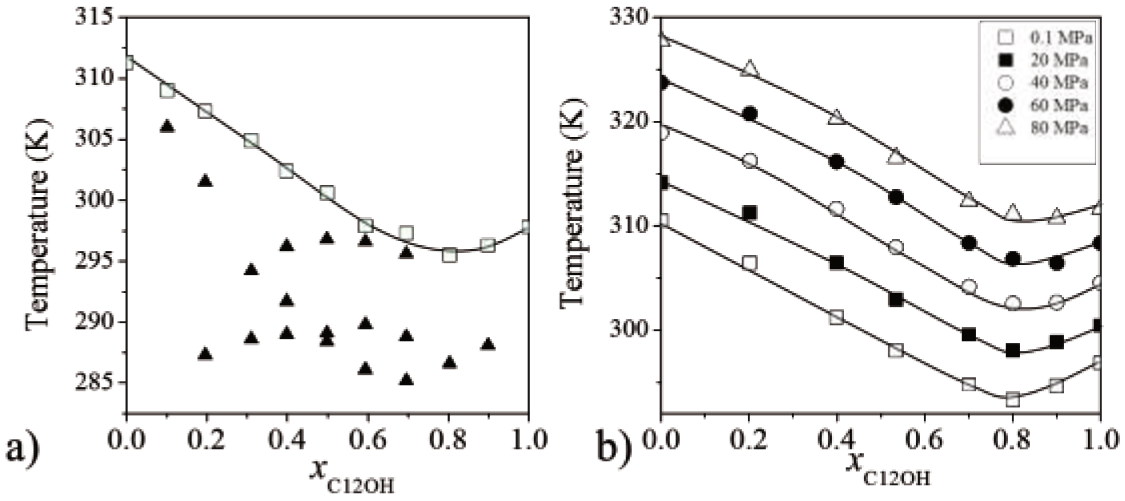

Fig. 7. 7. SLE curves for the C12OH + C14OH system. a) data from DSC and; b) data from high pressure microscopy. Liquidus curve at: □ 0.1 MPa, ■ 20 MPa, ○ 40 MPa, ● 60 MPa and, Δ 80 MPa; ▲ solid-solid transition; (—) is a guide to the eye.

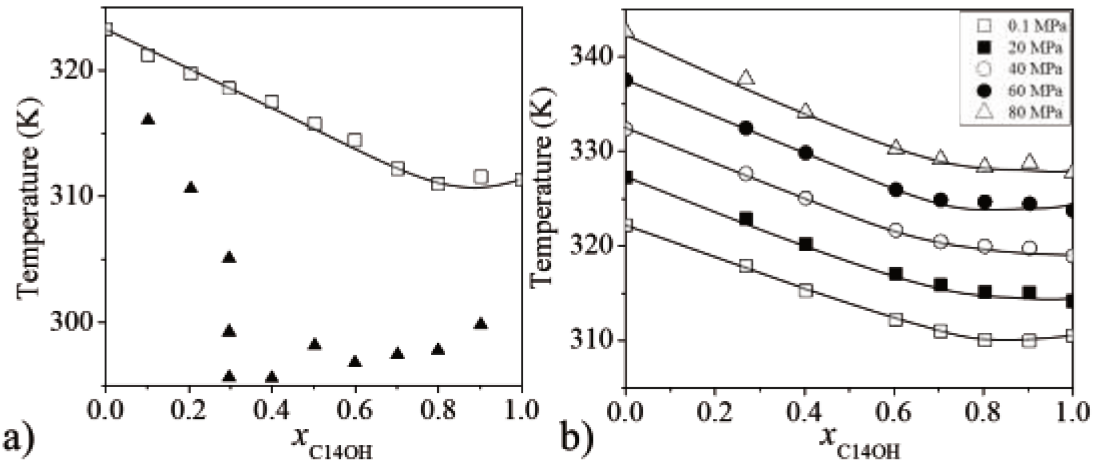

Fig. 7. 8. SLE curves for the C14OH + C16OH system. a) data from DSC and; b) data from high pressure microscopy. Liquidus curve at: □ 0.1 MPa, ■ 20 MPa, ○ 40 MPa, ● 60 MPa and, Δ 80 MPa; ▲ solid-solid transition; (—) is a guide to the eye.

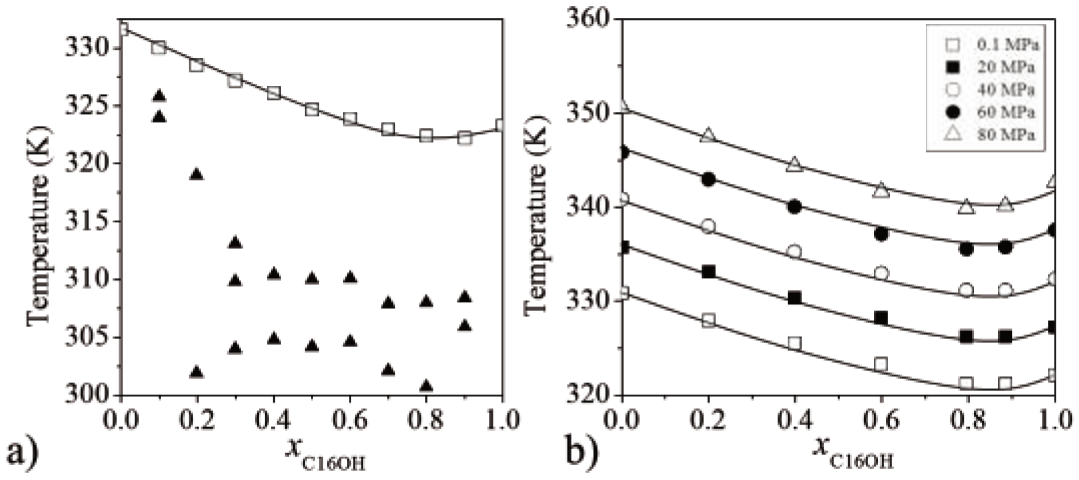

Fig. 7. 9. SLE curves for the C14OH + C16OH system. a) data from DSC and; b) data from high pressure microscopy. Liquidus curve at: □ 0.1 MPa, ■ 20 MPa, ○ 40 MPa, ● 60 MPa and, Δ 80 MPa; ▲ solid-solid transition; (—) is a guide to the eye.

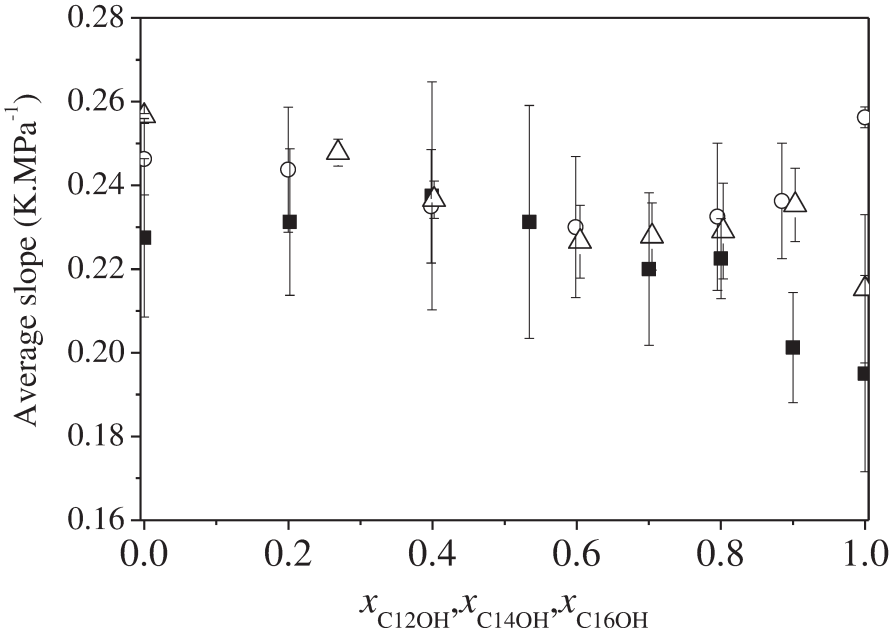

Fig. 7. 10. Average slopes *ΔT/ΔP* of the liquidus curves in the (*T, P*) diagram calculated for each solid phase as a function of composition for C12OH + C14OH (■), C14OH + C16OH (Δ) and C16OH + C18OH (○) systems.

7.4. Conclusions

The SLE of six saturated fatty alcohol binary systems was studied with a high pressure microscopy device up to 80MPa. As this technique allows visual monitoring of the samples, it is possible to measure their melting point in function of system's pressure. The microscope liquidus curves for the binary systems at atmospheric pressure were compared with the DSC results, showing a good agreement between both sets of data. It is also shown that the behavior of the liquidus line is only slightly affected by the pressure, i.e., the SLE curves preserve the same tendency for all measured pressures, confirming the presence of eutectic and peritectic points, if the case, or the solubility of the fatty alcohols in the solid domain, when the case, even with the increase of system pressure.

Acknowledgments

The authors are grateful to CNPq (304495/2010-7, 480992/2009-6, 552280/2010-0, 142193/2010-0, 201896/2011-7), FAPESP (2008/09502-0, 2008/56258-8), CAPES and FAEPEX/UNICAMP for their financial support and assistantships.

References

CARARETO, N. D. D.; COSTA, M. C.; MEIRELLES, A. J. A.; PAULY, J. High pressure solid–liquid equilibrium of fatty acid ethyl esters binary systems. **Fluid Phase Equilibria**, submitted work-a.

CARARETO, N. D. D.; COSTA, M. C.; ROLEMBERG, M. P.; KRÄHENBÜHL, M. A.; MEIRELLES, A. J. A. The solid-liquid phase diagrams of binary mixtures of even saturated fatty alcohols. **Fluid Phase Equilibria,** v. 303, n. 2, p. 191.e1-191.e8, 2011.

CARARETO, N. D. D.; SANTOS, A. O. D.; ROLEMBERG, M. P.; CARDOSO, L. P.; COSTA, M. C.; MEIRELLES, A. J. A. On the solid-liquid phase diagrams of binary

mixtures of even saturated fatty alcohols: systems exhibiting peritectic reaction. **Fluid Phase Equilib.**, submitted work-b.

COSTA, M. C.; ROLEMBERG, M. P.; BOROS, L. A. D.; KRAHENBUHL, M. A.; DE OLIVEIRA, M. G.; MEIRELLES, A. J. A. Solid-liquid equilibrium of binary fatty acid mixtures. **Journal of Chemical and Engineering Data,** v. 52, n. 1, p. 30-36, 2007.

COSTA, M. C.; ROLEMBERG, M. P.; MEIRELLES, A. J. A.; COUTINHO, J. A. P.; KRÄHENBÜHL, M. A. The solid-liquid phase diagrams of binary mixtures of even saturated fatty acids differing by six carbon atoms. **Thermochimica Acta,** v. 496, n. 1-2, p. 30-37, 2009a.

COSTA, M. C.; SARDO, M.; ROLEMBERG, M. P.; COUTINHO, J. A. P.; MEIRELLES, A. J. A.; RIBEIRO-CLARO, P.; KRAHENBUHL, M. A. The solid-liquid phase diagrams of binary mixtures of consecutive, even saturated fatty acids. **Chemistry and Physics of Lipids,** v. 160, n. 2, p. 85-97, 2009b.

COSTA, M. C.; SARDO, M.; ROLEMBERG, M. P.; RIBEIRO-CLARO, P.; MEIRELLES, A. J. A.; COUTINHO, J. A. P.; KRAHENBUHL, M. A. The solid-liquid phase diagrams of binary mixtures of consecutive, even saturated fatty acids: differing by four carbon atoms. **Chemistry and Physics of Lipids,** v. 157, n. 1, p. 40-50, 2009c.

COUTINHO, J. A. P.; KNUDSEN, K.; ANDERSEN, S. I.; STENBY, E. H. A Local Composition Model For Paraffinic Solid Solutions. **Chemical Engineering Science,** v. 51, p. 3273, 1996.

DANIEL, J.; RAJASEKHARAN, R. Organogelation of plant oils and hydrocarbons by long-chain saturated FA, fatty alcohols, wax esters, and dicarboxylic acids. **Journal of the American Oil Chemists Society,** v. 80, n. 5, p. 417-421, May 2003.

DARIDON, J. L.; PAULY, J.; MILHET, M. High pressure solid-liquid phase equilibria in synthetic waxes. **Physical Chemistry Chemical Physics,** v. 4, n. 18, p. 4458-4461, 2002.

DOMANSKA, U.; GONZALEZ, J. A. Solid-liquid equilibria for systems containing long-chain 1-alkanols .1. Experimental data for 1-dodecanol, 1-tetradecanol, 1-hexadecanol, 1-octadecanol or 1-icosanol-benzene or -toluene mixtures. Characterization in terms of DISQUAC. **Fluid Phase Equilibria,** v. 119, n. 1-2, p. 131-151, 1996a.

DOMANSKA, U.; GONZALEZ, J. A. Solid-liquid equilibria for systems containing long-chain 1-alkanols .2. Experimental data for 1-dodecanol, 1-tetradecanol, 1-hexadecanol, 1-octadecanol or 1-eicosanol plus CCl4 or plus cyclohexane mixtures. Characterization in terms of DISQUAC. **Fluid Phase Equilibria,** v. 123, n. 1-2, p. 167-187, 1996b.

DOMANSKA, U.; GONZALEZ, J. A. Solid-liquid equilibria for systems containing long-chain 1-alkanols .3. Experimental data for 1-tetradecanol, 1-hexadecanol, 1-octadecanol or 1-icosanol plus 1-butanol, 1-hexanol, 1-octanol or 1-decanol mixtures, characterization in terms of DISQUAC. **Fluid Phase Equilibria,** v. 129, n. 1-2, p. 139-163, 1997.

GAMSJAGER, H.; LORIMER, J. W.; SCHARLIN, P.; SHAW, D. G. Glossary of terms related to solubility. **Pure and Applied Chemistry,** v. 80, n. 2, p. 233-276, 2008.

GANDOLFO, F.; BOT, A.; FLÖTER, E. Structuring of edible oils by long-chain FA, fatty alcohols, and their mixtures. **Journal of the American Oil Chemists' Society,** v. 81, n. 1, p. 1-6, 2004.

HE, B.; MARTIN, V.; SETTERWALL, F. Liquid–solid phase equilibrium study of tetradecane and hexadecane binary mixtures as phase change materials (PCMs) for comfort cooling storage. **Fluid Phase Equilibria,** v. 212, n. 1–2, p. 97-109, 2003.

JI, H.-Y.; TOHIDI, B.; DANESH, A.; TODD, A. C. Wax phase equilibria: developing a thermodynamic model using a systematic approach. **Fluid Phase Equilibria,** v. 216, n. 2, p. 201-217, 2004.

KOUAKOU, A. C.; MAPIHAN, K. L.; PAULY, J. Solid-liquid equilibria under high pressure of pure fatty acid methyl esters. **Fuel,** v. 109, p. 297-302, 2013.

MILHET, M.; PAULY, J.; COUTINHO, J. A. P.; DIRAND, M.; DARIDON, J. L. Liquid–solid equilibria under high pressure of tetradecane + pentadecane and tetradecane + hexadecane binary systems. **Fluid Phase Equilibria,** v. 235, n. 2, p. 173-181, 2005.

ROENNINGSEN, H. P.; BJOERNDAL, B.; BALTZER HANSEN, A.; BATSBERG PEDERSEN, W. Wax precipitation from North Sea crude oils: 1. Crystallization and dissolution temperatures, and Newtonian and non-Newtonian flow properties. **Energy & Fuels,** v. 5, n. 6, p. 895-908, 1991.

SCHAINK, H. M.; VAN MALSSEN, K. F.; MORGADO-ALVES, S.; KALNIN, D.; VAN DER LINDEN, E. Crystal network for edible oil organogels: Possibilities and limitations of the fatty acid and fatty alcohol systems. **Food Research International,** v. 40, n. 9, p. 1185-1193, 2007.

SMITH, J. C. Higher aliphatic compounds Part I The systems ethyl palmitate-ethyl stearate and hexadecyl alcohol-octadecyl alcohol. **Journal of the Chemical Society**, p. 802-807, 1931.

VENTOLA, L.; CALVET, T.; CUEVAS-DIARTE, M. A.; MONDIEIG, D.; OONK, H. A. J. The C19H39OH-C20H41OH system: Experimental phase diagram and thermodynamic modelling. **Physical Chemistry Chemical Physics,** v. 4, n. 10, p. 1953-1956, 2002.

VENTOLA, L.; CALVET, T.; CUEVAS-DIARTE, M. A.; OONK, H. A. J.; MONDIEIG, D. Solid-solid and solid-liquid equilibria in the n-alkanols family: C18H37OH-C20H41OH system. **Physical Chemistry Chemical Physics,** v. 6, n. 13, p. 3726-3731, Jul 7 2004a.

VENTOLA, L.; CALVET, T.; CUEVAS-DIARTE, M. A.; RAMIREZ, M.; OONK, H. A. J.; MONDIEIG, D.; NEGRIER, P. Melting behaviour in the n-alkanol family. Enthalpy-entropy compensation. **Physical Chemistry Chemical Physics,** v. 6, n. 8, p. 1786-1791, 2004b.

VENTOLA, L.; CALVET, T.; CUEVAS-DIARTE, M. A.; SOLANS, X.; MONDIEIG, D.; NEGRIER, P.; VAN MILTENBURG, J. C. Solid state equilibrium in the n-alkanols family: the stability of binary mixed samples. **Physical Chemistry Chemical Physics,** v. 5, n. 5, p. 947-952, 2003.

YAMAMOTO, T.; NOZAKI, K.; HARA, T. X-ray and thermal studies on the rotator phases of normal higher alcohols C17H35OH, C18H37OH, and their mixtures. **Journal of Chemical Physics,** v. 92, n. 1, p. 631-641, 1990.

Capítulo 8. Conclusões Gerais

Este trabalho de tese foi elaborado de forma a cumprir cinco objetivos principais:

i. Aprofundar o conhecimento sobre o comportamento do ponto de fulgor de biodiesel etílico, em função da presença de etanol na mistura e em função da composição em ésteres etílicos do mesmo;
ii. Investigar o ESL de misturas de ácidos graxos + álcoois graxos utilizando a técnica de DSC;
iii. Utilizar diferentes técnicas experimentais, DSC, difração de raios-X e microscopia óptica com controle de temperatura, para caracterizar o ELS de sistemas binários de álcoois graxos saturados que apresentaram reação eutética e peritética;
iv. Examinar a influência da pressão no ESL de misturas de ésteres etílicos utilizando um microscópio que opera a altas pressões (até 80 MPa) e aplicar um modelo termodinâmico preditivo para caracterização do ESL em diferentes pressões e;
v. Examinar a influência da pressão na temperatura de fusão de álcoois graxos saturados e no ESL de suas misturas utilizando um microscópio que opera a altas pressões (até 80 MPa).

Na primeira parte deste trabalho, os pontos de fulgor dos ésteres etílicos foram medidos experimentalmente e um modelo empírico foi proposto para expressar estes valores como função do número de átomos de carbono e de ligações duplas do radical do ácido graxo. Para isso, foram medidos os pontos de fulgor de misturas binárias e multicomponentes contendo ésteres etílicos e etanol. Os parâmetros de interação da equação NRTL entre ésteres etílicos e etanol puderam ser estimados a partir dos dados de ponto de fulgor utilizando a equação de equilíbrio líquido-vapor associada à termodinâmica do ponto de fulgor (Eq.3.4). Os parâmetros de interação ésteres-etanol também foram expressos como uma função do número de átomos de carbono e ligações duplas do radical do ácido graxo. A equação proposta para o cálculo dos parâmetros de interação foi testada comparando-se valores calculados e experimentais de ponto de fulgor para um sistema contendo biodiesel de óleo de palma + etanol. O desvio quadrático médio entre os valores

experimentais e calculados foi inferior a 6,5 K para os ésteres etílicos puros, igual a 5,7 K para as misturas de ésteres etílicos + etanol e igual a 3,4 K para as misturas de biodiesel de óleo de palma + etanol.

A outra parte do trabalho estava focada no ESL de misturas de compostos graxos. No primeiro artigo foram apresentados quatro diagramas de fases de misturas binárias de ácidos graxos + álcoois graxos. As análises de DSC mostraram que os sistemas apresentam reações eutéticas e peritéticas. A técnica de *stepscan* DSC foi proposta como uma ferramenta para avaliar o ESL com uma boa repetibilidade e precisão, com desvio experimental de 0.4 K, sendo este valor semelhante aos desvios experimentais para o DSC com taxa de aquecimento linear. O *stepscan* DSC mostrou ser uma boa técnica para analisar o ESL de misturas complexas, tais como sistemas graxos, uma vez que permite separar os efeitos cinéticos das transições termodinâmicas. Vale a pena ressaltar que, tendo em conta que existem muitos parâmetros a serem ajustados nas análises *stepscan* DSC, possivelmente outros métodos além do apresentado neste trabalho podem conseguir bons resultados na avaliação do ESL. Além de realizar as análises experimentais, neste artigo utilizou-se a abordagem proposta por Slaughter e Doherty[1] (1997) na modelagem termodinâmica do ESL para sistemas com reação peritética. Os parâmetros dos modelos de Margules 2 e 3 sufixos e NRTL foram ajustados aos dados experimentais e permitiram um bom ajuste da linha liquidus para os sistemas investigados. O desvio quadrático médio (RMSD) variou de 0,3 a 1,3 K, sendo que o melhor ajuste dos dados foi obtido quando utilizado o modelo de Margules 3 sufixos.

No terceiro artigo foram apresentados os diagramas de fases de quatro misturas binárias de álcoois graxos: 1-octanol + 1-decanol, 1-decanol + 1-dodecanol, 1-dodecanol + 1-hexadecanol e 1-tetradecanol + 1-octadecanol. Análises de DSC foram utilizadas para determinar as transições que ocorreram para cada sistema binário. O método de *stepscan* DSC proposto para os sistemas de ácidos graxos + álcoois graxos foi utilizado para avaliar-se estes diagramas e comparar com os resultados das análises de standard DSC no caso dos sistemas 1-dodecanol + 1-hexadecanol e 1-tetradecanol + 1-octadecanol. A metodologia de

[1] SLAUGHTER, D. W.; DOHERTY, M. F. Calculation of Solid-Liquid Equilibrium and Crystallization Paths for Melt Crystallization Processes. **Chemical Engineering Science,** v. 50, n. 11, p. 1679-1694, 1995.

stepscan DSC mostrou ser uma boa ferramenta para se compreender algumas transições que ocorrem para sistemas complexos como os formados por álcoois graxos, mas de qualquer forma não descaracterizou o uso das técnicas de DSC com taxa de aquecimento linear já usualmente aplicadas nas análises de ESL. Para complementar a discussão dos resultados também foram feitas análises microscopia de luz polarizada para os sistemas 1-dodecanol + 1-hexadecanol e 1-tetradecanol + 1-octadecanol. Difração de raios-X foram feitas para o sistema 1-tetradecanol + 1-octadecanol. Os quatro sistemas apresentam reação eutética e peritética. Reação metatética foi identificada nos sistemas 1-decanol + 1-dodecanol, 1-dodecanol + 1-hexadecanol e 1-tetradecanol + 1-octadecanol.

No quarto artigo apresentado, os diagramas de fases de três sistemas binários de ésteres etílicos, laurato de etila, miristato de etila e palmitato de etila, foram determinados por análise visual em função da pressão utilizando-se um microscópio de alta pressão nas seguintes condições de pressão do sistema: 0,1; 20; 40; 60 e 80 MPa. Observou-se o aumento linear da temperatura de fusão dos ésteres etílicos puros assim como da linha liquidus dos três sistemas com o aumento da pressão. Um modelo termodinâmico preditivo, previamente aplicado a alcanos, foi utilizado neste trabalho para descrever o comportamento de fase dos sistemas sobre alta pressão, e os resultados obtidos mostram que esta abordagem pode ser estendida com sucesso a outros tipos de compostos além dos alcanos, fornecendo uma boa descrição do comportamento de fase em grandes faixas de pressão. O desvio quadrático médio variou em 0,8 a 2,3 K, e embora estes possam ser desvios expressivos quando comparados com os resultados de outros modelos termodinâmicos, como se trata de uma abordagem totalmente preditiva estes valores devem ser considerados como uma boa aproximação dos resultados.

No último artigo apresentado, os resultados obtidos a partir de análises de DSC e de microscopia ótica foram comparados para seis sistemas binários de álcoois graxos, 1-dodecanol + 1-octadecanol, 1-dodecanol + 1-hexadecanol, 1-tetradecanol + 1-octadecanol, 1-dodecanol + 1-tetradecanol, 1-tetradecanol + 1-hexadecanol e 1-hexadecanol + 1-octadecanol e apresentaram valores de RMSD entre 0,5 e 0,8 K. As temperaturas de fusão

dos álcoois puros e também linhas liquidus para os seis sistemas foram medidas em função da pressão no microscópio e mostraram uma dependência quase linear da mesma.

Em suma, este trabalho permitiu um avanço no estudo das propriedades físico-químicas de substâncias graxas. Introduziu novos conceitos para o ponto de fulgor de biodieseis etílicos, propriedade ainda pouco estudada. Apresentou um avanço significativo no estudo dos diagramas de fases de misturas binárias de compostos graxos confirmando a complexidade e variedade destes sistemas, que além dos pontos eutético, peritético, metatético e formação de soluções na fase sólida, também dão origem a diagramas com forte miscibilidade na fase sólida nos quais nenhum dos pontos invariantes mencionados anteriormente pode ser detectado.

8.1. Sugestões para Trabalhos Futuros

- Determinação do ponto de fulgor de misturas formadas por ésteres etílicos para se melhorar a predição do ponto de fulgor de biodiesel etílico a partir da sua composição e assim considerar os desvios da idealidade em misturas de ésteres que foram desconsiderados no modelo proposto no Capítulo 3;
- Determinação do ponto de fulgor de misturas de ésteres metílicos e também suas misturas com metanol, a fim de se obter um modelo capaz de predizer o comportamento de biodiesel metílico;
- Estudo de diagramas multicomponentes de álcoois graxos;
- Estudo do equilíbrio sólido-líquido sobre altas pressões de misturas ternárias de compostos graxos;
- Aplicação da técnica de *stepscan* DSC para outros sistemas graxos para se verificar se a metodologia proposta neste trabalho também pode ser estendida a outros sistemas de interesse;
- Estudar o equilíbrio líquido-vapor de misturas de álcoois graxos com o aprimoramento da calorimetria exploratória diferencial para medição de tais dados.

Chapitre 8. Conclusions

Cette thèse a été préparée afin de répondre à cinq objectifs principaux:

i. Approfondir les connaissances sur le comportement du point d'éclair des mélanges de biodiesels éthyliques et d'éthanol, en fonction de leur composition en esters éthyliques;
ii. Etudier l'ESL des mélanges d'acides gras et d'alcools gras en utilisant la technique de DSC;
iii. Caractériser les ELS de systèmes binaires d'alcools gras saturés en utilisant différentes techniques expérimentales telles que la DSC, la diffraction des rayons X et la microscopie optique avec contrôle de température;
iv. Examiner l'influence de la pression sur l'ESL des mélanges des esters éthyliques, en utilisant un microscope à des pressions élevées (jusqu'à 80 MPa) et en appliquant un modèle prédictif thermodynamique pour caractériser l'ESL à différentes pressions;
v. Examiner l'influence de la pression sur les températures de fusion des alcools gras saturés et de leur mélange, en utilisant un microscope qui fonctionne à des pressions élevées (jusqu'à 80 MPa).

Dans la première partie de ce travail, les points d'éclair d'esters éthyliques ont été mesurés expérimentalement et un modèle empirique a été proposé pour représenter ces valeurs en fonction du nombre d'atomes de carbone et de doubles liaisons dans le radical de l'acide gras. Pour cela, nous avons mesuré les points d'éclair de mélanges binaires et de multi-composants contenant des esters éthyliques et de l'éthanol. Les paramètres d'interaction de l'équation NRTL entre les esters éthyliques et l'éthanol peuvent alors être estimés à partir des données du point d'éclair. Nous avons utilisé l'équation thermodynamique d'équilibre vapeur-liquide associée au point d'éclair (Eq. 3.4), exprimée en fonction du nombre d'atomes de carbone et de doubles liaisons dans le radical d'acide gras. L'équation proposée pour le calcul des paramètres d'interaction a été testée en comparant les valeurs de points d'éclair d'un système contenant du biodiesel éthylique d'huile de palme + éthanol. L'écart quadratique entre les valeurs expérimentales et calculées

est inférieur à 6,5 K pour les esters éthyliques purs, égal à 5,7 K pour les mélanges d'esters éthyliques + éthanol et égal à 3,4 K pour les mélanges de biodiesel d'huile de palme + éthanol.

Les quatre autres parties de l'étude ont porté sur l'ESL des mélanges de composés gras. Quatre diagrammes de phase de mélanges binaires d'acides gras + alcools gras ont été présentés dans le premier article. L'analyse par DSC a montré que les systèmes présentent des réactions eutectiques et péritectiques. La technique de Stepscan DSC a été proposée comme un outil pour évaluer l'ESL avec une bonne reproductibilité et une précision expérimentale de 0,4 K, ce qui est comparable aux déviations expérimentales obtenues à partir d'une mesure DSC avec vitesse de chauffe linéaire. Le stepscan DSC s'est avéré une bonne technique d'analyse de l'ELS des mélanges de systèmes gras complexes, car il permet de séparer les effets cinétiques des transitions thermodynamiques. On remarque que, face à la grande quantité de paramètres à ajuster pour les analyses Stepscan DSC, d'autres méthodes non présentées dans ce travail peuvent, éventuellement, conduire à de bons résultats dans l'évaluation de l'ESL. En plus d'effectuer l'analyse expérimentale, cet article a utilisé l'approche proposée par Slaughter et Doherty[1] (1997) pour la modélisation thermodynamique en ESL des systèmes à réaction péritectique. Les paramètres des modèles Margules et NRTL ont été ajustés aux données expérimentales et ont permis une bonne représentation de la ligne de liquidus pour les systèmes étudiés. L'écart quadratique moyen (RMSD) varie entre 0,3 et 1,3 K, et on constate que le meilleur ajustement des données a été obtenu en utilisant le modèle de Margules 3-suffixes.

Les diagrammes de phase des quatre mélanges binaires d'alcools gras ont été présentés dans le troisième article: 1-octanol + 1-décanol , 1-décanol + 1-dodécanol, 1-dodécanol + 1-hexadécanol et 1-tétradécanol + 1-octadécanol. Des analyses de DSC ont été utilisées pour déterminer les transitions qui se produisent pour chaque système binaire. La méthode de Stepscan DSC proposée dans le cadre du Chapitre 4 pour les systèmes acides gras + alcools gras a été utilisée pour mesurer et comparer les résultats d'analyses de DSC des systèmes 1-dodécanol + 1-hexadécanol et 1-tétradécanol + 1-octadécanol. La

[1] SLAUGHTER, D. W.; DOHERTY, M. F. Calculation of Solid-Liquid Equilibrium and Crystallization Paths for Melt Crystallization Processes. **Chemical Engineering Science,** v. 50, n. 11, p. 1679-1694, 1995.

méthodologie Stepscan DSC s'est avérée un bon outil pour comprendre certaines transitions qui se produisent pour des systèmes complexes, tels que ceux constitués d'alcools gras. Néanmoins, l'utilisation des techniques de DSC à vitesse de chauffe linéaire, normalement appliquées à l'analyse de ESL permet tout de même d'obtenir de bons résultats. Des mesures microscopiques ont été également effectuées pour les systèmes 1-dodécanol + 1-hexadécanol et 1-tétradécanol + 1-octadécanol et des mesures de diffraction des rayons X ont été réalisées pour le système 1-tétradécanol + 1-octadécanol. Les quatre systèmes présentent une réaction eutectique et péritectique alors que les systèmes 1-décanol + 1-dodécanol, 1-dodécanol + 1-hexadécanol et 1-tétradécanol + 1-octadécanol exhibent une réaction métathétique.

Dans le quatrième article présenté, les trois diagrammes de phase des systèmes binaires des esters éthyliques, ethyl laurate, ethyl myristate et ethyl palmitate, ont été déterminés pour différentes pressions du système par analyse visuelle à l'aide d'un microscope à haute pression. Les pression du système utilisées étaient 0,1, 20, 40, 60 et 80 MPa. Une augmentation de la température de fusion des esters éthyliques purs, ainsi que de la ligne de liquidus des trois systèmes, a été observée lorsqu'on procède à une élévation de la pression. Un modèle thermodynamique prédictif appliqué auparavant à des n-alcanes, a été utilisé dans ce travail pour décrire le comportement de phase du système à haute pression. Les résultats obtenus montrent que cette approche peut être étendue avec succès, fournissant une bonne description des phases même à grandes échelles de pression. L'écart quadratique moyen varie entre 0,8 et 2,3 K, et, bien que ces valeurs puissent présenter des écarts importants par rapport aux résultats d'autres modèles thermodynamiques, cela peut être considéré comme une bonne approximation des résultats, puisqu'il s'agit d'une approche totalement prédictive de ces valeurs.

Le dernier article présente les résultats obtenus à partir d'analyse DSC et de microscopie optique pour six systèmes binaires d'alcools gras, 1-dodécanol + 1-octadécanol, 1-dodécanol + 1-hexadécanol, 1-tétradécanol + 1-octadécanol, 1-dodécanol + 1-tétradécanol, 1-tétradécanol + 1-hexadécanol et 1-hexadécanol + 1-octadécanol. Ils montrent un écart quadratique moyen entre 0,5 et 0,8 K. La température de fusion des

alcools gras purs mais également les courbes de liquidus pour les six systèmes ont été mesurées en fonction de la pression par l'intermédiaire du microscope. Une dépendance quasi linéaire a été observée.

Pour conclure, ce travail représente une percée dans l'étude des propriétés physico-chimiques des substances grasses. Il introduit de nouveaux concepts pour la description du point d'éclair des biodiesels éthyliques, propriétés encore peu étudiées. Il représente également un progrès significatif dans l'étude des diagrammes de phase des mélanges binaires de composés gras. Il permet, entre autre, de confirmer la complexité de tels systèmes qui, outre la présence de points eutectique, péritectique et la formation de solutions dans la phase solide, mènent à des diagrammes avec une forte miscibilité en phase solide, où aucun des points invariants ne peut être détecté.

8.1. Suggestions pour Travaux Futurs

- Détermination du point d'éclair de mélanges constitués d'esters éthyliques pour améliorer la prédiction du point d'éclair de biodiesels éthyliques à partir de sa composition. Cela permettrait de prendre en compte les énergies d'interaction entre les esters qui sont négligées dans le modèle du Chapitre 3;
- Détermination du point d'éclair de mélanges d'esters méthyliques, ainsi que de leur mélange avec de l'éthanol, afin de développer un modèle capable de prédire le comportement de biodiesel méthylique;
- Etude de diagrammes de phase multi-composant d'alcools gras;
- Etude de l'équilibre liquide-solide à haute pression de mélanges ternaires de composés gras;
- Application de la technique de *Stepscan* DSC pour d'autres systèmes gras, afin de vérifier la possibilité d'élargir le domaine de validité de la méthodologie proposée dans ce travail;
- Etudier l'équilibre liquide-vapeur de mélanges d'alcools gras en améliorant la DSC pour la mesure de telles données.